

Critical Dynamics of Magnets

By E. FREY and F. SCHWABL

Technische Universität München,

Institut für Theoretische Physik,

D-85747 Garching, Germany

(April 1, 2018)

Abstract

We review our current understanding of the critical dynamics of magnets above and below the transition temperature with focus on the effects due to the dipole–dipole interaction present in all real magnets. Significant progress in our understanding of real ferromagnets in the vicinity of the critical point has been made in the last decade through improved experimental techniques and theoretical advances in taking into account realistic spin-spin interactions. We start our review with a discussion of the theoretical results for the critical dynamics based on recent renormalization group, mode coupling and spin wave theories. A detailed comparison is made of the theory with experimental results obtained by different measuring techniques, such as neutron scattering, hyperfine interaction, muon–spin–resonance, electron–spin–resonance, and magnetic relaxation, in various materials. Furthermore we discuss the effects of dipolar interaction on the critical dynamics of three–dimensional isotropic antiferromagnets and uniaxial ferromagnets. Special attention is also paid to a discussion of the consequences of dipolar anisotropies on the existence of magnetic order and the spin–wave spectrum in two–dimensional ferromagnets and antiferromagnets. We close our review with a formulation of critical dynamics in terms of nonlinear Langevin equations.

Contents

I	INTRODUCTION	4
II	ISOTROPIC FERROMAGNETS	9
	A Dynamical Scaling and Hydrodynamics	9
	B Mode Coupling Theory	11
	1 Paramagnetic Phase	14
	2 Ferromagnetic Phase	19
	C Renormalization Group Theory	25
	1 Paramagnetic Phase	26
	2 Ferromagnetic Phase	30
III	DIPOLAR FERROMAGNETS	43
	A The Model–Hamiltonian	43
	B Mode Coupling Theory for the Paramagnetic Phase	46
	1 General Mode Coupling Equations	47
	2 Lorentzian Approximation	53
	3 Selected Results of the Complete Mode Coupling Equations	55
	C Spin Wave Theory in the Ferromagnetic Phase	57
	D Renormalization Group Theory of Time–Dependent Ginzburg–Landau Models in the Ferromagnetic Phase	62
IV	APPLICATION TO EXPERIMENTS	81
	A Neutron scattering	82
	1 Shape crossover	83
	2 Line width crossover	87
	3 Constant energy scans	90
	B Electron spin resonance and magnetic relaxation	92

C	Hyperfine Interactions	97
D	Muon Spin Relaxation (μ SR)	102
V	OTHER DIPOLAR SYSTEMS	137
A	Dipolar Antiferromagnets	137
1	Hamiltonian and equation of Motion	137
2	Critical Behavior of 3D Dipolar Antiferromagnets	139
B	Uniaxial Dipolar Ferromagnets	142
C	Two-dimensional Systems	144
1	Ferromagnets	145
2	Antiferromagnets	147
VI	STOCHASTIC THEORY	157
A	Classical field theory and dynamic functional	157
B	Self consistent one loop theory	165
1	Self consistent determination of the line width in Lorentzian approximation	166
2	Self consistent equation for the Kubo relaxation function	168
VII	CONCLUSIONS AND OUTLOOK	174
	APPENDIXES	180
A	Fluctuation-dissipation relations	180
B	Derivation of non-linear Langevin equations	182
C	Validity of mode coupling theory, higher orders in perturbation theory	186

I. INTRODUCTION

Remarkable progress has been achieved in our qualitative and quantitative understanding of the critical dynamics of magnetic materials. This is partly due to the advances and new developments in experimental techniques such as neutron scattering, electron spin resonance and hyperfine interaction probes. Simultaneously, on the theoretical side, important developments were provided by dynamical scaling theory, mode coupling theory and the renormalization group theory. The theoretical progress has been mainly promoted by including effects of magnetic interactions, such as dipole–dipole and spin–orbit interaction, on top of the exchange interaction. These interactions, which are present in all real magnetic materials, were found to change the critical dynamics quite drastically. Around 1986 the experimental situation was quite puzzling showing both quite excellent agreement but also large discrepancies with the theories existing at that time. Motivated by this seemingly contradictory situation anewed theoretical interest on the subject of critical dynamics was promoted.

In this review we shall mostly be interested in the effects of the dipole–dipole interaction on the critical dynamics of isotropic ferromagnetic materials in three dimensions. The static properties are reviewed only in as much as they are needed for the dynamics or if they emerge naturally together with the dynamical results. We will also discuss other dipolar systems, such as dipolar antiferromagnets and uniaxial ferromagnets in three dimensions, as well as the consequences of dipolar interactions in two–dimensional magnets. We do not consider pure dipolar systems such as the nuclear magnets *Cu*, *Ag*, and *Au*. We aim at giving an up-to-date account of the situation in the field, where we try to give attention to the theoretical as well as the experimental progress. In order to make the discussion as self-contained as possible we give brief discussions of the various theoretical concepts where needed.

Ferromagnets have always played a special role in the field of critical phenomena. Several simplified models, such as the Ising [126], Heisenberg [106], and Hubbard [120] model have

been developed in order to understand the fundamental questions of the statistical behavior of magnetically ordered systems. The attraction of these models resides in the simplicity of their form and complexity of behavior they are capable to describe. Over the last two decades various approaches to study the above models have been intensively developed, which lead to a profound understanding of the statistical mechanics of magnetic systems on the basis of the above simplified models. However, one has to keep in mind that for a more realistic description of magnetic materials it is not sufficient to consider solely the electrostatic interaction between the electrons in the partly filled shells leading in conjunction with the Pauli principle to the exchange interaction. There are magnetic interactions, such as the mutual interaction of the electron spins (dipole–dipole interaction) and the interaction of the spin and orbital moments of electrons (spin–orbit interaction) which may lead to magneto-crystalline anisotropies.

The exchange interaction is responsible for the phenomenon of magnetic ordering itself (at least above two dimensions). The characteristic feature of the exchange forces is their isotropic and short–range nature. They do not impose any definite orientation of the magnetic moments with respect to the crystallographic axis. Magneto-crystalline anisotropies are due to relativistic or magnetic forces (spin–spin dipole, quadrupole, etc.; spin–orbital, orbital–orbital). Microscopic models of various magnetic interactions have shown that, in the majority of cases, the spin–orbital interaction is the basic one responsible for the magneto-crystalline anisotropy (see e.g. Ref. [256,200]). It relates the directions of the spin magnetic moments of atoms through their orbital states with the crystallographic axes. Irrespective of the microscopic nature of the magnetic anisotropy forces, their macroscopic manifestation in a crystal seems to be determined mainly by the type of symmetry of the lattice. A special role among the magnetic forces is played by the dipole–dipole interaction between the magnetic moments of the electrons, because it is of long range and in cubic crystals leads to an anisotropy with respect to the wave vector but to leading order not to the crystallographic axes.

A Hamiltonian which takes into account exchange interaction as well as dipole–dipole

interaction between the magnetic moments of the electrons has first been given and studied by Holstein and Primakoff [115]. The dipolar interaction is usually two to three orders of magnitude weaker than the exchange interaction, and it can therefore (in many cases) be considered to be a small perturbation. However, because of its long-range nature, the effects of the dipole-dipole interaction become significant at least very close to the critical temperature T_c and for small wave vectors \mathbf{q} , as will become clear in this review. Note, that in particular it leads to the appearance of the demagnetization factors. Using renormalization group theory it has been shown by Fisher and Aharony [74,4,5] that the dipolar interaction is a relevant perturbation with respect to the Heisenberg model. They find that the short-range Heisenberg fixed point of the renormalization group is unstable against perturbations resulting from the dipolar interaction, and the asymptotic critical behavior is characterized by a new dipolar critical fixed point. Furthermore, the long-range nature of the dipolar interaction reflects itself in the Fourier transform containing a contribution of the singular direction dependent form $q^\alpha q^\beta / q^2$. An immediate consequence is the fact that longitudinal fluctuations are reduced in comparison to the two transverse ones and do not have a divergent susceptibility any more at T_c . Here, by longitudinal and transverse we refer to the direction of the wave vector \mathbf{q} . A consequence of this reduction of the number of effective order parameter components is a change in the static critical indices. Hence in a system with dominating exchange interaction there is a crossover from Heisenberg critical behavior to dipolar critical behavior. For instance the effective temperature dependent critical exponent of the static susceptibility γ approaches the Heisenberg value then goes through a minimum until finally it ends up at the dipolar limiting value.

In general the long-range dipolar interaction is of importance whenever fluctuations get large. This is the case in the vicinity of critical points and in systems of reduced dimensionality. In the vicinity of critical points longitudinal fluctuations are suppressed and rotational invariance is destroyed. This leads to modified static critical behavior and to drastic changes in the dynamics. In systems of reduced dimensionality which on the basis of short-range interactions would not have a phase transition at a finite temperature due

to the large fluctuations destroying the order parameter, the dipolar interaction suppresses these fluctuations and thereby allows a finite order parameter. With the detection of high- T_c superconductors and their fascinating magnetic properties, the study of mechanisms which lead to phase transitions in such quasi-two-dimensional systems (inter-plane interaction, anisotropy, dipolar interaction, etc.) is of prime importance.

In this paper we review the critical dynamics of magnetic systems. As a reference and a simpler situation to start with we treat in chapter 2 first isotropic ferromagnets without dipolar interaction. This allows us to introduce the main theoretical concepts such as dynamic scaling, mode coupling and dynamic renormalization group theory in a quite elementary and hopefully pedagogical way.

In chapter 3 we describe the theoretical results on the dynamics of dipolar ferromagnets with an emphasis on the mode coupling theory for the paramagnetic phase. A detailed analysis of the consequences of the dipolar interaction on the functional form of the dynamic scaling laws, critical exponents and the line shape and line width crossover will be given. For the ferromagnetic phase we give some results based on spin-wave theory and we also comment on some recent theoretical approaches, which go beyond the linearized spin-wave theory.

In chapter 4 the theoretical results are then compared with the findings from a variety of experimental techniques. They include neutron scattering, electron spin resonance and magnetic relaxation, hyperfine techniques and muon spin resonance experiments.

Whereas the main part of the review concentrates on dipolar effects in isotropic ferromagnets, chapter 5 concerns dipolar effects in other magnetic systems. These include three-dimensional isotropic antiferromagnets, bulk uniaxial ferromagnets and two-dimensional systems. In the latter case the dipolar interaction leads to long-range order, which would not be possible for the isotropic Heisenberg model in two dimensions.

Finally, in chapter 6, we discuss alternative derivations of the mode coupling theory via the generalized Langevin equations of Zwanzig and Mori. These methods allow for a systematic derivation of the mode coupling theory in the framework of a diagrammatic

analysis. Also, some systematic improvements are possible. We conclude with a summary and an outlook in chapter 7. Some technical details and important conceptual background material is collected in the appendices.

II. ISOTROPIC FERROMAGNETS

Our main concern in this review is the immediate vicinity of the critical point and the influence of the dipolar interaction on the critical dynamics. As a reference and a simpler situation to start with we treat first isotropic ferromagnets without dipolar interaction. This allows us to introduce the basic concepts and results of the different theoretical approaches and compare them with the experimental situation.

A. Dynamical Scaling and Hydrodynamics

In systems where a continuous symmetry is broken, hydrodynamics together with dynamical scaling allows one to obtain definite conclusions about the dynamic critical behavior.

To start with, we remind the reader of the structure of the hydrodynamic modes in isotropic ferromagnets. In an isotropic ferromagnet magnetization is conserved giving rise to three hydrodynamic equations for the magnetization vector $\mathbf{M}(\mathbf{x})$. In the paramagnetic phase, i.e. for temperatures above the Curie temperature T_c and in zero magnetic field \mathbf{H} , ($T > T_c$, $\mathbf{H} = 0$) the magnetization obeys a diffusion equation,

$$\frac{\partial \mathbf{M}}{\partial t} = D \nabla^2 \mathbf{M}, \quad (2.1)$$

with a diffusion constant D . Hence the long wave length excitations are diffusive

$$\omega(q) = -iDq^2. \quad (2.2)$$

In the ferromagnetic phase the magnetization \mathbf{M} is finite and the spin fluctuations which are perpendicular to the mean magnetization obey spin-wave equations of motion. The spin-wave frequency is according to hydrodynamics given by

$$\omega(q) = \frac{M}{\chi^T(q)} - iq^4 \Lambda. \quad (2.3)$$

Here $\chi^T(q)$ is the transverse susceptibility, M the magnetization, and Λ a damping constant. The real part of the frequency is related to static critical quantities. For the imaginary part,

the damping, hydrodynamics predicts a decay rate proportional to the fourth power of the wave number ¹.

Dynamical scaling states that the critical frequency is of the homogeneous form

$$\omega(q, \xi) = q^z \Omega(q\xi), \quad (2.4)$$

where z is the dynamic critical exponent and $\xi \propto |T - T_c|^{-\nu}$ the correlation length with the static critical exponent ν . Using the scaling behavior of the static quantities [175] in the hydrodynamic region ($M \sim \xi^{-\beta/\nu}$, and $\chi^T(q) \sim q^{-2}\xi^{-\eta}$) and the scaling relations between the static exponents ($\gamma = \nu(2 - \eta)$, $2\beta = (d - 2 + \eta)\nu$) one finds for the spin-wave frequency in the hydrodynamic region

$$\text{Re} \{ \omega(q, \xi) \} = M/\chi^T(q) \propto q^2 \xi^{(2-d+\eta)/2} = q^{(d+2-\eta)/2} (q\xi)^{(2-d+\eta)/2}. \quad (2.5)$$

Here d is the spatial dimension of the system. One thus finds as a result of the dynamic scaling law, Eq. (2.4) and the hydrodynamic behavior of the static quantities an exact relation for the dynamic exponent

$$z = \frac{d + 2 - \eta}{2}. \quad (2.6)$$

Using again Eqs. (2.5) and (2.6) the damping coefficient Λ of the spin-waves and the spin diffusion coefficient D in the paramagnetic phase are

$$\Lambda \sim \xi^{(6-d+\eta)/2}, \quad \text{and} \quad D \sim \xi^{(2-d+\eta)/2}. \quad (2.7)$$

The spin diffusion coefficient D goes to zero at the critical temperature, a phenomenon known as *critical slowing down*. Thus hydrodynamics and dynamical scaling allow one to determine the main critical dependencies of the transport coefficients. The picture emerging from Eqs. (2.2)–(2.7) is summarized in Fig. 2.1.

¹Indeed the microscopic theory of the Heisenberg model predicts a spin-wave decay rate of the form $q^4 (c_2(\ln q)^2 + c_1 \ln q + c_0)$ [65,133,102,257].

The critical frequency is a function of the wave number and the inverse correlation length. The hydrodynamic region is given by $q \ll \xi^{-1}$, whereas the non hydrodynamic critical region by $q \gg \xi^{-1}$. Of course the critical region is limited to $q \ll a^{-1}$ and $\xi \gg a$, where a is a microscopic length scale (e.g. the lattice spacing).

We close this subsection by giving the hydrodynamic equations of the low temperature phase [244,112]

$$\begin{aligned}\frac{d}{dt}M_{\mathbf{q}}^x &= \frac{M}{\chi^T(q)}M_{\mathbf{q}}^y - \Lambda q^4 M_{\mathbf{q}}^x, \\ \frac{d}{dt}M_{\mathbf{q}}^y &= -\frac{M}{\chi^T(q)}M_{\mathbf{q}}^x - \Lambda q^4 M_{\mathbf{q}}^y, \\ \frac{d}{dt}M_{\mathbf{q}}^z &= -\Gamma(q)M_{\mathbf{q}}^z,\end{aligned}$$

the excitations of which were the basis of our discussion. Here we assumed that the magnetization is oriented along the z -direction. In addition to the transverse equation the magnetization component along the order parameter obeys a diffusion equation in three dimensions $\Gamma(q) = D_M q^2$.

B. Mode Coupling Theory

One of the most successful theoretical approaches in critical dynamics are mode coupling theories. The first such theory was proposed by Fixman [75], and then put on a more rigorous basis by Kadanoff and Swift [130], and especially Kawasaki [137,138,140]. In this section we exemplify the mode coupling theory for the critical dynamics of an isotropic ferromagnet, where the spins are coupled only by short range isotropic exchange interaction. The Hamiltonian for such a spin system is given by

$$H = \int_{\mathbf{q}} J(\mathbf{q}) \mathbf{S}_{\mathbf{q}} \cdot \mathbf{S}_{-\mathbf{q}}, \quad (2.8)$$

Here we have introduced the notation $\int_{\mathbf{q}} = v_a \int \frac{d^3q}{(2\pi)^3}$, where v_a is the volume of the primitive cell of the Bravais lattice. Upon introducing the cube edge length a of the corresponding cubic unit cell, the dimensionless quantity $b = \sqrt{a^3/v_a}$ characterizes the lattice structure.

The Fourier transforms of the Cartesian components $S^i(\mathbf{x})$ of the spin operator are defined by

$$S_{\mathbf{q}}^i = \int d^3x e^{i\mathbf{q}\cdot\mathbf{x}} S^i(\mathbf{x}), \quad (2.9)$$

and $J(\mathbf{q}) = -J_0 + Jq^2a^2$ characterizes the exchange interaction. We are retaining only terms up to second order in the wave vector \mathbf{q} and have supposed that the exchange interaction extends up to the second nearest neighbors. For *bcc* and *fcc* lattices we have $J = J_1 + J_2$, where J_1 and J_2 are, respectively, the values of the exchange parameters between the nearest and next-nearest neighbors. For a simple cubic (*sc*) crystal the relation is $J = J_1 + 4J_2$. The parameter J_0 does not enter the equations of motion. It is convenient to introduce the ladder operators

$$S_{\mathbf{q}}^{\pm} = S_{\mathbf{q}}^x \pm iS_{\mathbf{q}}^y, \quad (2.10)$$

and $S_{\mathbf{q}}^z$ instead of the Cartesian components of the spin operator. Then, using the commutation relation for spin operators one finds for the Hamiltonian (2.8) the following set of equations of motion (we take $\hbar = 1$)

$$\frac{d}{dt} S_{\mathbf{q}}^z = -i \int_{\mathbf{k}} [J(\mathbf{k}) - J(\mathbf{q} - \mathbf{k})] S_{\mathbf{q}-\mathbf{k}}^+ S_{\mathbf{k}}^-, \quad (2.11)$$

$$\frac{d}{dt} S_{\mathbf{q}}^{\pm} = \pm 2i \int_{\mathbf{k}} [J(\mathbf{k}) - J(\mathbf{q} - \mathbf{k})] S_{\mathbf{q}-\mathbf{k}}^{\pm} S_{\mathbf{k}}^z. \quad (2.12)$$

The equations of motion (2.11) and (2.12) exhibit explicitly the vanishing of $dS_{\mathbf{q}}^i/dt$ at $\mathbf{q} = 0$, i.e., the order parameter itself is a constant of motion. Starting from these microscopic equations of motion there are a variety of different schemes for deriving the mode coupling equations for the spin correlation functions [19,262,232,233,137,118,119].

The quantity of interest is the Kubo relaxation matrix for a set of dynamical variables $\{X^{\alpha}(\mathbf{x})\}$, which is defined by

$$\Phi^{\alpha\beta}(\mathbf{q}, t) = i \lim_{\epsilon \rightarrow 0} \int_t^{\infty} d\tau e^{-\epsilon\tau} \langle [X^{\alpha}(\mathbf{q}, \tau), X^{\beta}(\mathbf{q}, 0)^{\dagger}] \rangle, \quad (2.13)$$

where $\langle \dots \rangle$ denotes the thermal average. The dynamical variables are normalized such that

$$(X^\alpha, X^\beta) := \Phi^{\alpha\beta}(\mathbf{q}, t = 0) = \delta^{\alpha\beta}, \quad (2.14)$$

i.e., we use normalized spin variables $X_{\mathbf{q}}^\alpha(t) = S_{\mathbf{q}}^\alpha(t)/\sqrt{\chi^\alpha(\mathbf{q})}$, where $\chi^\alpha(\mathbf{q})$ are the static susceptibilities.

One of the most concise ways of deducing mode coupling equations utilizes the projection operator technique, originally introduced by Mori [197] and Zwanzig [276]. The main idea is that one can separate the set of dynamical variables into two classes, one slowly and one fast varying class. With the aid of this projection operator method the fast variables are eliminated and one can derive generalized Langevin equations for the dynamic variables or equivalently for the correlation functions [199,198,139] (see also chapter VI, and appendix B). The corresponding equations for the Kubo relaxation function is

$$\frac{\partial \Phi^{\alpha\beta}(\mathbf{q}, t)}{\partial t} = i\omega^{\alpha\gamma}(\mathbf{q})\Phi^{\gamma\beta}(\mathbf{q}, t) - \int_0^t d\tau \Gamma^{\alpha\gamma}(\mathbf{q}, t - \tau)\Phi^{\gamma\beta}(\mathbf{q}, \tau), \quad (2.15)$$

and for its half-sided Fourier transform

$$\Phi^{\alpha\beta}(\mathbf{q}, \omega) = \int_0^\infty dt \Phi^{\alpha\beta}(\mathbf{q}, t)e^{i\omega t}, \quad (2.16)$$

one obtains

$$\Phi(\mathbf{q}, \omega) = i[\omega \mathbf{1} + \boldsymbol{\omega}(\mathbf{q}) + i\boldsymbol{\Gamma}(\mathbf{q}, \omega)]^{-1}. \quad (2.17)$$

The frequency matrix $\omega^{\alpha\beta}(\mathbf{q})$ is given by

$$i\omega^{\alpha\beta}(\mathbf{q}) = (\dot{X}_{\mathbf{q}}^\alpha, X_{\mathbf{q}}^\beta) = -i\langle [X_{\mathbf{q}}^\alpha, X_{-\mathbf{q}}^\beta] \rangle, \quad (2.18)$$

where we have used the Kubo identity $(\dot{A}, B) = -i\langle [A, B^\dagger] \rangle$ [157]. The non-linear aspects of the spin dynamics are contained in the matrix of the transport coefficients (memory matrix) $\boldsymbol{\Gamma}$. As a result of the projection operator technique these can be written in terms of the Kubo relaxation matrix [138,140]

$$\Gamma^{\alpha\beta}(\mathbf{q}, t) = (\delta\dot{X}_{\mathbf{q}}^\alpha(t), \delta\dot{X}_{\mathbf{q}}^\beta(t)) \quad (2.19)$$

of the non conserved parts of the currents²

$$\delta\dot{X}_{\mathbf{q}}^{\alpha} = \dot{X}_{\mathbf{q}}^{\alpha} - i\omega^{\alpha\beta}(\mathbf{q})X_{\mathbf{q}}^{\beta}. \quad (2.20)$$

The simplest approximation which can be made at this stage is to consider only two mode decay processes, which in technical terms amounts to a factorization of the Kubo formulas (2.19) after insertion of the equations of motion. Frequently one makes additionally an approximation for the line shape (i.e. frequency dependence) of the relaxation matrix, e.g. a Lorentzian approximation. In principal, however, one can solve directly the set of self consistent equations for the shape functions resulting from the decoupling approximation only. For the isotropic ferromagnet this was first achieved by Wegner [262] and Hubbard [118] in the paramagnetic phase. For most practical purposes an excellent approximation for the line width can be obtained from the mode coupling equations simplified by the Lorentzian approximation.

1. Paramagnetic Phase

In the paramagnetic phase the order parameter is zero $\langle \mathbf{S}_{\mathbf{q}} \rangle|_{\mathbf{q}=0} = 0$ implying that the frequency matrix $\omega^{\alpha\beta}$ vanishes. Upon using the above decoupling procedure one obtains the following set of coupled integro-differential equations for the Kubo relaxation function

$$\frac{\partial\Phi(\mathbf{q}, t)}{\partial t} = - \int_0^t d\tau \Gamma(\mathbf{q}, t - \tau)\Phi(\mathbf{q}, \tau), \quad (2.21)$$

and the transport coefficients

$$\Gamma(\mathbf{q}, t) = 4k_B T \int_{\mathbf{k}} v(\mathbf{k}, \mathbf{q}) \frac{\chi(\mathbf{q} - \mathbf{k})\chi(\mathbf{k})}{\chi(\mathbf{q})} \Phi(\mathbf{k}, t)\Phi(\mathbf{q} - \mathbf{k}, t), \quad (2.22)$$

²Here we have chosen a linear projection operator $\mathcal{P}X = (X, X^{\alpha})X^{\alpha}$. Then the random forces can be written in terms of the projection operator as $\delta\dot{X}_{\mathbf{q}} = \exp[i(1 - \mathcal{P})\mathcal{L}t](1 - \mathcal{P})\dot{X}_{\mathbf{q}}$, where \mathcal{L} is the Liouville operator. Neglecting the projection operator in the time development one gets Eq. (2.20); see also Appendix B.

with the vertex function ($\hbar = 1$)

$$v(\mathbf{k}, \mathbf{q}) = (J(\mathbf{k}) - J(\mathbf{q} - \mathbf{k}))^2 = \left(2Jq^2 a^2 \left[\frac{\mathbf{q} \cdot \mathbf{k}}{q^2} - \frac{1}{2} \right] \right)^2. \quad (2.23)$$

Essentially the same equations have been derived by numerous authors [19,262,232,233], [137,140], [118,119] using different approaches. The temperature dependence enters the equations only implicitly via the correlation length

$$\xi = \xi_0 \left(\frac{T - T_c}{T_c} \right)^{-\nu}. \quad (2.24)$$

The equations for the Kubo relaxation function must in general be solved numerically. However, in the critical region one can deduce certain important properties of the solution analytically. Upon inserting the static scaling law [269]

$$\chi(q, \xi) = \frac{1}{2Ja^2} q^{-2+\eta} \hat{\chi}(x), \quad (2.25)$$

with the scaling variable $x = 1/q\xi$ one can show by inspection that the solution of Eqs. (2.21) and (2.22) fulfills dynamic scaling

$$\Phi(q, \xi, \omega) = (\Lambda q^z)^{-1} \phi(x, \nu), \quad (2.26)$$

$$\Gamma(q, \xi, \omega) = \Lambda q^z \gamma(x, \nu), \quad (2.27)$$

with the scaling variable $\nu = \omega/\Lambda q^z$ and the non universal constant

$$\Lambda = \frac{a^{5/2}}{b} \sqrt{\frac{2Jk_B T_c}{4\pi^4}}, \quad (2.28)$$

where b is a dimensionless parameter which depends on the crystal structure (see Table I). Note that in Eqs. (2.25)–(2.27) we have explicitly incorporated the correlation length ξ into the list of arguments of the correlation functions in order to indicate the reduction of arguments accomplished by the dynamic scaling form. In order to simplify notation this temperature dependence is in most of the remaining text not written out explicitly.

The above mode coupling equations give a dynamic critical exponent $z = (5 + \eta)/2$ instead of the correct expression $z = (5 - \eta)/2$ [99,174,127,17]. This inconsistency of the

conventional derivation of the mode coupling equations is fortunately not a very serious problem since η is very small in the case of 3D ferromagnets, $\eta \approx 0.05$ [189]. In order to be consistent one has to take for the scaling functions an Ornstein-Zernike form

$$\hat{\chi}(x) = \frac{1}{1+x^2}, \quad (2.29)$$

neglecting the exponent η . In chapter VI we will give a derivation of modified mode coupling equations based on a path integral formulation of the stochastic equations of motion. There we will show how the above inconsistency can be resolved by taking into account certain kinds of vertex corrections which are neglected in the conventional derivation of mode coupling equations.

The scaling relations (2.26) and (2.27) for the Fourier transformed quantities imply for their time dependent counterparts

$$\Phi(q, \xi, t) = \phi(x, \tau), \quad (2.30)$$

$$\Gamma(q, \xi, t) = (\Lambda q^z)^2 \gamma(x, \tau), \quad (2.31)$$

with the scaled time variable

$$\tau = \Lambda q^z t. \quad (2.32)$$

The mode coupling equations for the corresponding scaling functions are

$$\frac{\partial \phi(x, \tau)}{\partial \tau} = - \int_0^\tau d\tau' \gamma(x, \tau - \tau') \phi(x, \tau'), \quad (2.33)$$

and

$$\gamma(x, \tau) = 2\pi^2 \int_{-1}^{+1} d\eta \int_0^\infty d\rho \rho_-^2 \hat{v}(\rho, \eta) \frac{\hat{\chi}(x/\rho) \hat{\chi}(x/\rho_-)}{\hat{\chi}(x)} \phi(x/\rho, \tau \rho^z) \phi(x/\rho_-, \tau \rho_-^z). \quad (2.34)$$

The scaled vertex function reads

$$\hat{v}(\rho, \eta) = 2 (\rho\eta - 1/2)^2, \quad (2.35)$$

where we have defined $\rho = k/q$, $\rho_- = |\mathbf{k} - \mathbf{q}|/q$, and $\eta = \cos(\mathbf{k}, \mathbf{q})$.

Before turning to the numerical solution of the mode-coupling equations, let us quote some results which can be obtained analytically. For temperatures not too close to T_c one can infer from Eqs. (2.22) and (2.23) that in the limit $q \rightarrow 0$ (hydrodynamic limit) the vertex factor $v(\mathbf{k}, \mathbf{q})$ and hence the memory kernel $\Gamma(q, t)$ becomes small. Hence one could argue that the relaxation function $\Phi(q, t)$ varies very slowly and the solution of Eq. (2.21) becomes an exponential [118]

$$\Phi(q, t) = \exp \left\{ -Dq^2t \right\} , \quad (2.36)$$

where the diffusion constant is given by

$$D = \lim_{q \rightarrow 0} \frac{1}{q^2} \int_0^\infty \Gamma(q, t) dt = \lim_{q \rightarrow 0} \frac{1}{q^2} \Gamma(q, \omega = 0) . \quad (2.37)$$

A scaling analysis of the right hand side gives for the temperature dependence of the diffusion coefficient $D \sim \xi^{-1/2}$ in agreement with the scaling result by Halperin and Hohenberg [99].

The above argument leading to the spin diffusion behavior has been questioned by Månson [180]. Starting from a relaxation function which is of spin diffusion type (see Eq. (2.36)) Månson [180] showed that the memory kernel becomes of the form

$$\Gamma(q, t) \propto t^{-5/2} e^{-Dq^2t/2} \quad (2.38)$$

for asymptotic times and small q . Therefrom Månson [180] concludes that the spin diffusion type of behavior can not be the correct form of the relaxation function at asymptotic times, which would raise some questions on the validity of the mode coupling theory (since it invalidates the results obtained from a hydrodynamic theory based on the conservation of the magnetization). The above argument leading to an exponentially decaying relaxation function becomes invalid also close to T_c because the static susceptibilities in the expression for the memory matrix diverge and therefore the relaxation function no longer varies slowly. A shape crossover from a Lorentzian to a different critical shape takes place by approaching the critical temperature [118]. Nevertheless, a Lorentzian approximation for the line shape still gives reasonable an approximation for the line width, since the latter is not so sensitive to the precise form of the line shape.

In the Lorentzian approximation the mode coupling equations reduce to a single integral equation for the line width $\Gamma_{\text{lor}}(q) = \Lambda q^z \gamma_{\text{lor}}(x)$

$$\gamma_{\text{lor}}(x) = \frac{2\pi^2}{\hat{\chi}(x)} \int_{-1}^{+1} d\eta \int_0^\infty d\rho \rho_-^2 \hat{v}(\rho, \eta) \frac{\hat{\chi}(x/\rho) \hat{\chi}(x/\rho_-)}{\rho^{5/2} \gamma_{\text{lor}}(x/\rho) + \rho_-^{5/2} \gamma_{\text{lor}}(x/\rho_-)}. \quad (2.39)$$

Therefrom one can deduce the asymptotic behavior of the typical line width analytically

$$\gamma_{\text{lor}}(x) \sim \begin{cases} 1 & \text{for } x \ll 1 \quad , \\ \sqrt{x} & \text{for } x \gg 1 \quad , \end{cases} \quad (2.40)$$

implying $\Gamma(q) \sim q^{5/2}$ right at $T = T_c$ and $\Gamma(q) \sim q^2 \xi^{-1/2}$ in the hydrodynamic limit $q\xi \ll 1$, i.e the temperature dependence of the diffusion constant is given by $D \sim \xi^{-1/2}$ [137] as we have already deduced from scaling arguments. The full scaling function resulting from Eq. (2.39) is shown in Fig. 2.2. It is usually called Resibois–Piette scaling function [231] since Resibois and Piette did the first numerical solution of the mode coupling equations in Lorentzian approximation.

In order to find the complete behavior of the relaxation function $\Phi(q, t)$ one has to solve Eqs. (2.33) and (2.34) numerically. This was done by Wegner [262] at T_c and extended to temperatures above T_c by Hubbard [118,119]. The results are shown in Fig. 2.3. It is found that for small wave vectors (not too close to the zone boundary) there is a shape crossover from a Lorentzian (see Eq. (2.36)) to a more Gaussian like shape by approaching the critical temperature. The critical shape at T_c is essentially the same as the one obtained from RG–theory [61,21] (see also section II C 1)

Recently, this shape crossover has been reexamined by Aberger and Folk [1] and Frey et al. [85] in detail with emphasis on constant energy scans. Their results, shown in Figs. 2.4.a and 2.4.b for the scaling function of the spin relaxation function versus time and frequency, respectively, confirm the shape crossover from a Lorentzian to a critical shape first found by Hubbard [118,119]. In addition, strongly over-damped oscillations in the time-dependent spin relaxation function at T_c are found. These oscillations, however, do not lead to an observable structure in the Fourier transform apart from a flatter decrease at small frequencies. With increasing temperature these oscillations practically disappear. Presently it is

not clear, whether these oscillations are an artifact of the mode coupling approximation and go away when higher order terms are included. A RG analysis does not show these oscillations [61,21,123].

Hubbard [118] also discusses the shape function for cubic ferromagnets with nearest-neighbor interaction for wave vectors close to the Brillouin zone boundary: $J(\mathbf{q}) \sim J[\cos(q_x a) + \cos(q_y a) + \cos(q_z a)]$. He finds that there is a tendency of the shapes to become more squarer than a Lorentzian and as the wave vectors come close to the zone boundary one observes the formation of small shoulders. Recently Cuccoli et al. [54] have studied the shape of the correlation function at the zone boundary for *EuO* and *EuS* with a face-centered-cubic lattice taking into account nearest- and next-nearest-neighbour exchange interaction. The numerical solution of the mode coupling equations give, as in the simple cubic case with nearest-neighbor interaction considered by Hubbard [118], inelastic shoulders at the zone boundary, but less intense than seen in the experiment [26,29].

2. Ferromagnetic Phase

In this section we review the mode coupling equations for isotropic ferromagnets below the Curie point [245,81]. Assuming that the spontaneous magnetization points along the z -axis the frequency matrix is given by

$$\omega^{\alpha\beta}(q) = \omega(q) \begin{pmatrix} 0 & 0 & 0 \\ 0 & -1 & 0 \\ 0 & 0 & +1 \end{pmatrix}, \quad (2.41)$$

where $\alpha, \beta = z, +, -$. The frequency of the transverse modes is

$$\omega(q) = \frac{M}{\chi^T(q)}, \quad (2.42)$$

where $M = \langle S_{q=0}^z \rangle$ denotes the magnetization and $\chi^T(q)$ the static transverse susceptibility. Due to the rotational symmetry of the Hamiltonian the Kubo relaxation matrix $\Phi^{\alpha\beta}(q, \omega)$ is diagonal

$$\Phi^{zz}(q, \omega) = \frac{i}{\omega + i\Gamma^{zz}(q, \omega)}, \quad (2.43)$$

$$\Phi^{\pm\pm}(q, \omega) = \frac{2i}{\omega \mp \omega(q) + i\Gamma^{\pm\pm}(q, \omega)}. \quad (2.44)$$

The mode coupling approximation for the transport coefficients

$$\Gamma^{zz}(q, t) = (\dot{S}_{\mathbf{q}}^z(t), \dot{S}_{\mathbf{q}}^z(0))/\chi^L(q) \equiv \Gamma(q, t), \quad (2.45)$$

$$\Gamma^{\pm\pm}(q, t) = (\dot{S}_{\mathbf{q}}^{\pm}(t) \pm i\omega(q)S_{\mathbf{q}}^{\pm}(t), \dot{S}_{\mathbf{q}}^{\pm}(0) \pm i\omega(q)S_{\mathbf{q}}^{\pm}(0))/2\chi^T(q) \equiv \Lambda^{\pm}(q, t), \quad (2.46)$$

where $\chi^L(q)$ is the longitudinal susceptibility, results in the following set of integral equations [245]

$$\Gamma(\mathbf{q}, \omega) = k_{\text{B}}T \int_{\nu} \int_{\mathbf{k}} v(\mathbf{k}, \mathbf{q}) \frac{\chi^T(\mathbf{q} - \mathbf{k})\chi^T(\mathbf{k})}{\chi^L(\mathbf{q})} \Phi^{++}(\mathbf{q} - \mathbf{k}, \omega - \nu)\Phi^{--}(\mathbf{k}, \nu), \quad (2.47)$$

$$\Lambda^{\pm}(\mathbf{q}, \omega) = 2k_{\text{B}}T \int_{\nu} \int_{\mathbf{k}} v(\mathbf{k}, \mathbf{q}) \frac{\chi^T(\mathbf{q} - \mathbf{k})\chi^L(\mathbf{k})}{\chi^T(\mathbf{q})} \Phi^{\pm\pm}(\mathbf{q} - \mathbf{k}, \omega - \nu)\Phi^{zz}(\mathbf{k}, \nu). \quad (2.48)$$

Here we have used the notation $\int_{\nu} = \int \frac{d\nu}{2\pi}$. Eqs. (2.43), (2.44) together with (2.47), (2.48) constitute a complete set of self consistent integral equations for the Kubo relaxation functions $\Phi^{\alpha\alpha}(q, \omega)$, which in principal could be solved numerically. For $M = 0$ and $\chi^L = \chi^T$ Eqs. (2.47), (2.48) reduce to the mode coupling equations for the paramagnetic phase, Eqs. (2.22).

The above mode coupling equations have been analyzed in the Lorentzian approximation for the relaxation functions

$$\Phi^{zz}(q, \omega) = \frac{i}{\omega + i\Gamma(q)}, \quad \Phi^{\pm\pm}(q, \omega) = \frac{2i}{\omega \mp \omega(q) + i\Lambda^{\pm}(q)}, \quad (2.49)$$

with

$$\Gamma(q) = \Gamma(q, \omega = 0), \quad \Lambda(q) \equiv \Lambda^{+}(q) = \Lambda^{-}(q)^{*} = \Lambda^{+}(q, \omega(q)). \quad (2.50)$$

The frequency integrals can now be carried out readily and one finds the following set of coupled integral equations for the line widths

$$\Gamma(\mathbf{q}) = \frac{4ik_B T}{\chi^L(\mathbf{q})} \int_{\mathbf{k}} v(\mathbf{k}, \mathbf{q}) \frac{\chi^T(\mathbf{q} - \mathbf{k})\chi^T(\mathbf{k})}{\omega(\mathbf{k}) - \omega(\mathbf{q} - \mathbf{k}) + i\Lambda(\mathbf{q} - \mathbf{k}) + i\Lambda^*(\mathbf{k})}, \quad (2.51)$$

$$\Lambda(\mathbf{q}) = \frac{4ik_B T}{\chi^T(\mathbf{q})} \int_{\mathbf{k}} v(\mathbf{k}, \mathbf{q}) \frac{\chi^T(\mathbf{q} - \mathbf{k})\chi^L(\mathbf{k})}{\omega(\mathbf{q}) - \omega(\mathbf{q} - \mathbf{k}) + i\Lambda(\mathbf{q} - \mathbf{k}) + i\Gamma(\mathbf{k})}. \quad (2.52)$$

As is easily seen $\Gamma(q)$ is real, but $\Lambda(q)$ in general is complex. The imaginary part of the transverse damping function $\Lambda(q)$ leads to a shift of the frequency of the transverse spin-waves, which however is a negligible correction in comparison to the frequency matrix (2.41) as will be seen later.

In the hydrodynamic regime the Eqs. (2.51), (2.52) can be solved analytically with the result

$$\Gamma(q) \propto \frac{q}{\chi^L(q)}, \quad \text{and} \quad \Lambda(q) \propto q^4 \left[c_1 \ln \left(\frac{1}{q\xi} \right) + c_0 \right], \quad (2.53)$$

where c_0 and c_1 are constants³. With the well known scaling properties of the static susceptibilities neglecting the Fisher exponent η

$$\chi^{L,T}(q) = \frac{1}{2Jq^2a^2} \hat{\chi}^{L,T}(x), \quad (2.54)$$

Eq. (2.41) gives

$$\omega(q) = \Lambda q^z \hat{\omega}(x), \quad (2.55)$$

where the dynamical critical exponent z equals 5/2 as in the paramagnetic phase.

The scaling function for the bare frequency of the transverse modes following from Eq.(2.42) can be written as

$$\hat{\omega}(x) = \begin{cases} f\sqrt{x} & \text{for } T \leq T_c \quad , \\ 0 & \text{for } T \geq T_c \quad . \end{cases} \quad (2.56)$$

³The low-temperature spin-wave theory of Dyson [65] gives in addition a term $q^4 (\ln(1/q\xi))^2$ [133,102,257]. This will probably come out from a mode coupling theory where decays of the transverse mode into three transverse modes are included.

Analyzing the scaling properties of the mode coupling equations and combining this with the static and dynamic scaling law it was shown [240,241] that the amplitude f for the scaling function of the spin-wave frequency is a universal quantity and determined by other universal amplitude ratios

$$f = \left(\frac{\hat{c}}{2}\right)^{1/2} \left(\frac{R_c}{(R_\xi^+)^d}\right)^{1/2} \left(\frac{\xi_0}{\xi_0^T}\right)^{d-2} \left(\frac{\xi_-}{\xi_+}\right)^{z-2}. \quad (2.57)$$

Here \hat{c} is an arbitrary normalization constant for the scaling functions. If one chooses the value of the scaling functions at criticality to be $\gamma(0) = 5.1326$, \hat{c} becomes $\hat{c} = 8\pi^4$ [241]. The quantities R_c and R_ξ^+ are universal amplitude ratios as defined in the review article by Privman et al. [226], ξ_0^T is a transverse correlation length below T_c [226], and ξ_+ , ξ_- are longitudinal correlation lengths above and below T_c , respectively.

The amplitude f for the spin-wave frequency can be determined from RPA-arguments (see e.g. Ref. [245]), which gives $f = \pi^{3/2}$. This value has been used in consecutive applications of mode coupling theory on magnets [81] below T_c . Upon using the known values for the static amplitude ratios [226] it is found [240,241]

$$f = 9.5 \pm 1.8. \quad (2.58)$$

This amplitude can also be determined from the available experimental data in Refs. [29,26,30,34,220], and references cited therein. The results are summarized in Table II [240,241], where depending on which experiment [29,26,30,34,220] one analyzes one gets slightly different values for f .

Hence Eqs. (2.51), (2.52) can be solved by using an dynamic scaling Ansatz

$$\Gamma(q) = \Lambda q^z \gamma(x), \quad \Lambda(q) = \Lambda q^z \lambda(x), \quad (2.59)$$

where the dynamical scaling functions $\gamma(x)$ and $\lambda(x)$ obey the following set of coupled integral equations

$$\gamma(x) = 2\pi^2 i \int_{-1}^{+1} d\eta \int_0^\infty d\rho \rho_-^{-2} \hat{v}(\rho, \eta) \frac{\hat{\chi}^T(x/\rho_-) \hat{\chi}^T(x/\rho)}{\hat{\chi}^L(x)}$$

$$\times \frac{1}{-\rho^z \hat{\omega}(x/\rho) + \rho^z \hat{\omega}(x/\rho_-) + i\rho^z \lambda(x/\rho) + i\rho^z \lambda^*(x/\rho_-)}, \quad (2.60)$$

$$\lambda(x) = 2\pi^2 i \int_{-1}^{+1} d\eta \int_0^\infty d\rho \rho_-^{-2} \hat{v}(\rho, \eta) \frac{\hat{\chi}^L(x/\rho_-) \hat{\chi}^T(x/\rho)}{\hat{\chi}^T(x)}$$

$$\times \frac{1}{\hat{\omega}(x) - \rho^z \hat{\omega}(x/\rho) + i\rho^z \lambda(x/\rho) + i\rho^z \gamma(x/\rho_-)}. \quad (2.61)$$

Here we have used the same notation as in section II B 1.

In order to solve those mode coupling equations one has to know the static susceptibilities. In the ferromagnetic phase the global continuous rotation symmetry is spontaneously broken. Although one of the equivalent directions of the order parameter is selected, no free energy is required for an infinitesimal quasi-static rotation of the magnetization vector, which in turn leads to a diverging transverse correlation length. This physical effect is mathematically expressed by the Goldstone theorem [92], stating that there is exactly one massless mode for each generator of the broken-symmetry group. In the context of a ferromagnet below T_c this implies that the transverse susceptibility is given by

$$\chi^T(q) = \frac{1}{2Jq^2 a^2}. \quad (2.62)$$

The longitudinal correlation functions entering these integral equations has been computed by Mazenko [184] to first order in $\epsilon = 4 - d$ using Wilson's matching technique

$$\frac{1}{\chi^L(q)} = 2Jq^2 a^2 \left[1 - \frac{9\epsilon}{n+8} x^2 \left(1 + \sqrt{1+4x^2} \ln \left(\frac{\sqrt{1+4x^2}-1}{2x} \right) \right) + x^2 \left(\frac{n+8+(5-\frac{n}{2})\epsilon}{9+(n-1)x^\epsilon} \right) \right], \quad (2.63)$$

where n is the number of spin components. The last term in $\chi^L(q)$ results from the presence of Goldstone modes below T_c , and it implies that also the longitudinal susceptibility diverges in the limit $q \rightarrow 0$ for any temperature below T_c .

The resulting numerical solution of the mode coupling equations (2.60), (2.61) have been achieved in Ref. [81,240,241]. The results are shown in Fig. 2.5 for three different values of the frequency amplitude f .

One recognizes that the scaling function $Im\lambda(x)$ for the frequency shift of the transverse modes is very small compared to $\hat{\omega}(x)$. In the critical region $Im\lambda(x)$ starts at the critical

point with infinite slope and is negative in the hydrodynamical region. The scaling functions for the longitudinal and transverse line widths split off linearly at the critical temperature and differ by orders of magnitude in the hydrodynamic region. This linear split-off of the longitudinal and transverse widths and the infinite slope of the frequency shift at the critical temperature below T_c is an immediate consequence of the presence of Goldstone modes below T_c . This feature can be derived analytically from Eqs. (2.51), (2.52). The sign of the slope of the longitudinal line width depends on the magnitude of the amplitude f for the frequency of the spin-waves. For values of f close to the RPA-value the slope is positive. If this value is increased towards the universal value determined in Ref. [240,241] the slope becomes negative and one gets a minimum in the longitudinal scaling function γ . This minimum has been observed in a recent experiment by Böni et al. [34] (see below). Above T_c the scaling function for the line width starts quadratically in agreement with a renormalization group calculation by Iro [123], but in contrast to the numerically found infinite slope of Hubbard [118]. It disagrees also with a computation of Bhattacharjee and Ferrell [22], who predict, using Ward identities, a linear dependence on $1/q\xi$.

The numerical data can be fitted in the limits $x \gg 1$ (hydrodynamical region) and $x \ll 1$ (critical region) by simple approximants as summarized in Table III (note that all functions are given in units of the value at criticality $\gamma(0) = Re\lambda(0) \cong 5.1326$)

In unpolarized neutron scattering experiments on *Fe* [48], *Ni* [194], and *EuO* [210] no quasi-elastic peak from spin diffusion, as predicted by the mode coupling theory [81], was discernible. Only the side-peaks originating from the transverse spin waves were observed. This is plausible in the light of the mode coupling results in Ref. [81]. In the hydrodynamical region ($x = 1/q\xi \gg 1$) the width of the longitudinal peak is much wider than the separation of the transverse peaks [245]. Moreover, its intensity is smaller than that of the transverse magnons, which altogether implies that it may be very difficult to distinguish the longitudinal peak from the background. In the critical region the line widths are of the same order of magnitude. In this limit however the frequency of the transverse modes tends to zero. Using unpolarized neutrons one can only observe a superposition of the peaks. Lacking a theory

for the line width in the critical region below T_c it was impossible up to recently to resolve the longitudinal and transverse peaks.

The first observation of the longitudinal peak was reported by Mitchell et al. [195] using polarized neutrons. This study shows in agreement with the theory that the width of the quasi-elastic longitudinal peak becomes comparable with the spin-wave energy explaining why this peak was not observed by neutron scattering experiments with unpolarized neutrons. However, there are not enough data as yet to permit a quantitative comparison with the theoretical predictions. Furthermore, the material is disordered (palladium with 10% iron) which makes it not an ideal system [34]. Very recently, Böni et al. [34] have investigated the spin dynamics of a *Ni* single crystal by means of polarized neutron scattering. They observe that the longitudinal fluctuations are quasi-elastic in agreement with our theoretical predictions [245,81] and RG calculations [174]. In Fig. 2.6 we show a quantitative comparison of the longitudinal line width, obtained from solving the mode coupling equations in Lorentzian approximation [274,240,241], with the experiment [34]. The light dashed line represents the result of the mode coupling equations with an amplitude $f = \pi^{3/2}$, taken from RPA-arguments. The solid line and the dot-dashed line represent the results of solving the mode coupling equations with an amplitude of $f = 5.1326 \times 1.49$ and $f = 5.1326 \times 1.60$, respectively. The agreement between theory and experiment is quite well for an appropriate choice of the universal amplitude. One should especially note, that the scaling function of the longitudinal line width shows a minimum in accord with the experimental data.

Finally we note that the above analysis does not take into account effects from the dipole-dipole interaction. Those effects have up to now not been studied quantitatively in the ferromagnetic phase, but, one may expect similar effects as above T_c , which we are going to describe in the next chapter.

C. Renormalization Group Theory

1. Paramagnetic Phase

Renormalization group calculations of the critical dynamics of ferromagnets start from a stochastic equation of motion for the spin density $\mathbf{S}(\mathbf{x}, t)$

$$\frac{\partial \mathbf{S}(\mathbf{x}, t)}{\partial t} = \lambda f \mathbf{S} \times \frac{\delta \mathcal{H}}{\delta \mathbf{S}} + \lambda \nabla^2 \frac{\delta \mathcal{H}}{\delta \mathbf{S}} + \boldsymbol{\zeta}, \quad (2.64)$$

where $\boldsymbol{\zeta}(\mathbf{x}, t)$ is a random force with a Gaussian probability distribution with zero mean and variance

$$\langle \zeta^i(\mathbf{x}, t) \zeta^j(\mathbf{x}', t') \rangle = 2\Gamma k_B T \delta^{(3)}(\mathbf{x} - \mathbf{x}') \delta(t - t') \delta^{ij}. \quad (2.65)$$

The effective Landau-Ginzburg-Wilson free energy functional is given by

$$\mathcal{H} = \int d^d x \left[\frac{1}{2} (r \mathbf{S}^2 + (\nabla \mathbf{S})^2) + \frac{u}{4!} (\mathbf{S}^2)^2 \right]. \quad (2.66)$$

These equations can be derived [198,139,199] using a Mori-Zwanzig projection operator formalism [197,276] (see also chapter VI). An exhaustive discussion of these semi-phenomenological equation of motion can be found in the article by Ma and Mazenko [174]. The first term in Eq. (2.64) describes the Larmor precession of the spins in the local magnetic field, $\delta \mathcal{H} / \delta \mathbf{S}$, and the second term characterizes the damping of the conserved order parameter. The precession term of the spins in the local magnetic field plays a major role in the dynamics. From the RG analysis in Refs. [174,17] one can infer that its effect can be ignored above the upper critical dimension $d_c = 6$, and can be treated by perturbation theory in $\epsilon = 6 - d^4$.

The RG-theory proves [174,17] the dynamical scaling hypothesis [70,99] and shows that the spin correlation function fulfills the dynamical scaling form near the fixed point

⁴The upper critical dimension for the corresponding static problem (see Hamiltonian in Eq. (2.65)) is $d_c = 4$. Since the precessional term is of second order in the equations of motion corresponding to third order in the Lagrangian the upper critical dimension is shifted to $d_c = 6$.

$$C(q, \xi, \omega) = \chi(q, \xi) \frac{1}{\omega_c(q, \xi)} \phi(x, \nu), \quad (2.67)$$

with the scaling variables $x = 1/q\xi$ and

$$\nu = \frac{\omega}{\omega_c(q, \xi)}, \quad (2.68)$$

where the characteristic frequency has itself the scaling form

$$\omega_c(q, \xi) = \Lambda q^z \Omega(x). \quad (2.69)$$

The dynamic critical exponent z is known exactly from RG theory [174,127,17]

$$z = \frac{d + 2 - \eta}{2}, \quad (2.70)$$

in accord with the general dynamic scaling considerations of section II A. Here η is the Fisher exponent from the static scaling law

$$\chi(q, \xi) = q^{-2+\eta} \hat{\chi}(x). \quad (2.71)$$

The Fourier transform of the spin correlation function can be written in the form

$$C(q, \xi, \omega) = \chi(q, \xi) \frac{1}{\lambda q^z} \text{Re} \frac{2}{-i\hat{\omega} + [\hat{\chi}(x)\Pi(x, \hat{\omega})]^{-1}}, \quad (2.72)$$

where $\Pi(x, \hat{\omega})$ is the self-energy of the dynamic susceptibility and we have defined $\hat{\omega} = \omega/\lambda q^z$.

The asymptotic behavior of the self-energy is known exactly from a RG-analysis [17,61]

$$\Pi(x, \hat{\omega}) \sim \begin{cases} \hat{\omega}^{(4-z)/z} & \text{for } \hat{\omega} \rightarrow \infty, \\ x^{4-z} & \text{for } x \rightarrow \infty. \end{cases} \quad (2.73)$$

One-loop RG-calculations give to order $O(\epsilon)$

$$\Pi(x, \hat{\omega}) = 1 - \epsilon [F(x, i\hat{\omega}) + \frac{1}{2} \ln 2] + O(\epsilon^2), \quad (2.74)$$

with [61,123]

$$F(0, i\hat{\omega}) = \begin{cases} -\frac{1}{8} \ln(-i\hat{\omega}) - \frac{3}{8} \ln 2 + O(\hat{\omega}^{-1/2}) & \text{for } \hat{\omega} \gg 1, \\ -(\pi + \frac{1}{3})/8 + 3(2 + 2 \ln 2 - \pi) \frac{i\hat{\omega}}{8} & \text{for } \hat{\omega} \ll 1, \end{cases} \quad (2.75)$$

and [174,123]

$$F(x, 0) = \begin{cases} -\frac{1}{2} \ln x - (\ln 2 + \frac{3}{4})/2 - \frac{13}{128}x^{-2} & \text{for } x \gg 1 \quad , \\ -(\pi + \frac{1}{3})/8 - (3\pi - \frac{25}{8} - 3 \ln 4)\frac{x^2}{4} & \text{for } x \ll 1 \quad . \end{cases} \quad (2.76)$$

In an ϵ -expansion with respect to the upper critical dimension $d_c = 6$ the ϕ^4 -term is irrelevant for $4 < d$, hence the static critical behavior is classical. This is no more the case for $d < 4$, a fact which has to be kept in mind if one extends the results of the RG ϵ -expansion to $\epsilon = 3$. The explicit form of $F(x, i\hat{\omega})$ to order $O(\epsilon)$ can be found in Ref. [123]. The logarithms in the limits ($x \rightarrow 0, \nu \rightarrow \infty$) and ($x \rightarrow \infty, \nu \rightarrow 0$) are the $O(\epsilon)$ -contributions of the power law behavior in Eqs. (2.73) which are known exactly for any dimension d . Exponentiating these logarithms in such a way that the exactly known asymptotic behavior Eqs. (2.73) is matched one obtains [21,124,125] the two-parameter interpolation formula

$$\Pi(x, \hat{\omega}) = \left[(1 + bx^2)^{2-\epsilon/4} - ai\hat{\omega} \right]^{\epsilon/(8-\epsilon)}, \quad (2.77)$$

with $a = 0.46$ ($a = \frac{z}{4}(6 + 6 \ln 2 - 3\pi)$) and $b = 3.16$ for $\epsilon = 3$. This reasoning for exponentiating the leading logarithms of a first order ϵ -expansion to match the exactly known asymptotic results is due to Bhattacharjee and Ferrell [21]. One should note, however, that this exponentiation procedure is not unique. To test the validity of the exponentiated expression one would have to calculate contributions to order $O(\epsilon^2)$ which would be quite cumbersome a task.

The shape function

$$\phi(x, \hat{\omega}) = 2Re \frac{1}{-i\hat{\omega} + [\hat{\chi}(x)\Pi(x, \hat{\omega})]^{-1}} \quad (2.78)$$

shows the crossover from the critical shape at $x = 0$ to a Lorentzian at $x = \infty$ in agreement with the mode coupling results by Hubbard [118] and a more recent reanalysis by Aberger and Folk [1]. From Eqs. (2.72) one can also determine the half width at half maximum ω_c defined by

$$C(q, \xi, \omega_c) = \frac{1}{2}C(q, \xi, 0). \quad (2.79)$$

In Fig. 2.7 the scaling function $\omega_c(x)$ resulting from Eqs. (2.72) and (2.79) is compared with mode coupling results [231,1]. Whereas the MC–result in Lorentzian approximation [231] shows large deviations from the RG–result in the hydrodynamic limit, the complete MC–result abandoning the Lorentzian approximation [1] follows closely the RG scaling function. One should note, however, that if all scaling functions are rescaled in such a way that they coincide in the hydrodynamic limit the differences between the scaling functions appear much less pronounced.

Let us now compare the theoretical predictions with the experiment. In early neutron scattering experiments almost all data have been fitted by a Lorentzian shape function. Recently, however, with the advances in neutron scattering techniques leading to higher intensities and better resolution, deviations of the measured spectra from a Lorentzian have been observed. By comparing the RG–result at T_c [61,21] with constant energy scans on *Fe* [264,171,172] it has been shown [77] that theory was in accord with the data in the observed experimental wave vector and frequency window. As has been demonstrated in Ref. [29] the peak positions as well as the peak profile in constant–energy scans of *EuO* could be explained on the basis of RG–theory, taking into account short range exchange interaction only, for wave vectors in the range $0.15\text{\AA}^{-1} \leq q \leq 0.3\text{\AA}^{-1}$ and energies $0.2\text{meV} \leq \omega \leq 0.4\text{meV}$.

If a model based on the exchange coupling between neighboring spins is the correct description of the critical behavior of real ferromagnets, one would have expected that the results from RG and MC theories would become even closer to the experimental data as one comes close to the critical temperature or/and for very large wavelength. It came as a completely unexpected surprise, when Mezei [190] found in spin echo experiments on *EuO* that the observed shape at even smaller wave vectors $q = 0.024\text{\AA}^{-1}$ clearly resembled a Lorentzian shape in disagreement with the predictions of RG theory for the dynamics of an isotropic Heisenberg ferromagnet, which would give a bell shaped decay.

As we will explain in chapter III this ultimate crossover to a Lorentzian can be explained by taking into account the long–range dipolar interaction. Further evidence of dipolar effects have been found in *EuS*, where it was observed that the peak positions (in constant-E scans)

do not scale [31].

Concerning the line width the experimental situation is as follows. Right at the critical temperature there is almost perfect agreement of the wave vector dependence of the line width with $\Gamma \sim q^{5/2}$ in *EuS* [30], *EuO* [57,28,189], *Fe* [48,188,264] and *Ni* [194,34]. In early experimental studies on *Fe* it seemed that the experimental data [208,209] are in reasonable agreement with the theoretically predicted scaling function of Resibois and Piette [231]. Recent neutron scattering experiments, however, showed large deviations from the Resibois-Piette scaling function in *Fe* [188,189], *EuO* [193,192] and *EuS* [33]. This puzzling situation can only be resolved by additionally taking into account the dipolar interaction, which is the subject of chapters III and IV.

2. Ferromagnetic Phase

The critical dynamics below the transition temperature has been studied also by renormalization group methods. Ma and Mazenko [174] calculated the transport coefficient for the longitudinal magnetization for small wave vectors in an ϵ -expansion ($\epsilon = 6 - d$). Their result was

$$\Gamma(q) = \frac{\hat{\Gamma}(q)}{\chi^L(q)} q^2, \quad (2.80)$$

with

$$\hat{\Gamma} \propto q^{\frac{d-6}{6}}. \quad (2.81)$$

With $\chi^L(q) \propto \frac{1}{q}$ in $d = 3$ dimensions this would give $\Gamma(q) \propto q^{\frac{5}{2}}$ in contradiction to the mode coupling result for small q (i.e. in the hydrodynamical limit [231]). However, Sasvári's [237] reanalysis of Ma and Mazenko's [174] exponentiation method showed, that taking into account the regular parts of $\hat{\Gamma}(q)$ results in

$$\hat{\Gamma}(q) \propto q^{\frac{d-6}{3}}. \quad (2.82)$$

This leads to $\Gamma(q) \propto q^2$ for $d = 3$ dimensions, in agreement with the mode coupling result in Table III. The q^4 -dependence of the transverse transport coefficient in the hydrodynamical limit is also confirmed by the renormalization group calculations [174].

A thorough renormalization group study of the critical dynamics of a Heisenberg ferromagnet below T_c is still lacking. Such a study would have to take into account all the peculiarities resulting from the presence of the Goldstone modes below T_c . As a first step towards this end, there is a recent study [250] of the critical dynamics of the $O(n)$ -symmetric relaxational models with either non-conserved (model A) or conserved order parameter (model B) below the transition temperature (see also chapter V).

TABLES

TABLE I. Crystal structure dependent parameters of cubic Bravais lattices. c counts the number of next nearest neighbors to a given lattice site. The parameter b is defined as $b = (a^3/v_a)^{1/2}$, and characterizes the lattice structure. δ is the distance between nearest neighbors ions and v_a the volume of the Bravais lattice primitive cell. a is the cube edge.

	sc	bcc	fcc
c	6	8	12
b	1	$\sqrt{2}$	2
δ/a	1	$\sqrt{3}/2$	$\sqrt{2}/2$
v_a/a^3	1	1/2	1/4

TABLE II. Experimental values for the spin-wave amplitude $\hat{b} = f/5.1326$.

	Fe	Ni	Co	EuO	EuS
\hat{b}	1.5(1)	1.5(1)	1.6(2)	1.3(2)	1.4(2)
	1.8(1)	2.1(1)			1.9(3)

Data are collected from Refs. [29,26,30,34,220], and references cited therein.

TABLE III. Asymptotic behavior of the scaling functions below the critical temperature in units of the value at criticality $\gamma(0)$.

	$\gamma(x)/\gamma(0)$	$\Gamma(q)$	$\frac{Re\lambda(x)}{\gamma(0)}$	$\frac{Im\lambda(x)}{\gamma(0)}$	$Im\Lambda(q); Re\Lambda(q)$
$x \gg 1$	$1.37 + 0.37 \frac{x^{-1/2}}{\chi^L(x)}$	$q^2 \xi^{-1/2}$	$0.16x^{-3/2} \ln(x)$	$-0.07x^{-3/2} \ln(x)$	$q^4 \xi^{3/2} \ln\left(\frac{1}{q\xi}\right)$
$x \ll 1$	$1.0 + 0.55x$	$q^{5/2}$	$1.0 - 1.34x$	$0.77x^{1/2}$	$q^2 \xi^{-1/2}; q^{5/2}$

Figure Captions:

Figure 2.1:

The macroscopic domain of wave vector q and correlation length ξ . In the three shaded regions the correlation functions have different characteristic behaviors. (a) Hydrodynamic regions: $q\xi \ll 1$, $T > T_c$, and $T < T_c$, (b) critical region: $q\xi \gg 1$, $T \approx T_c$. There is a change-over from under-damped spin-waves to spin diffusion when the temperature is raised from below T_c to above T_c , as schematically indicated in the diagram.

Figure 2.2:

The Resibois–Piette scaling function versus $x = 1/q\xi$, resulting from the numerical solution [231] of the mode coupling equations in Lorentzian approximation for a Heisenberg ferromagnet in the paramagnetic phase.

Figure 2.3:

The universal function $\phi(\omega/\sigma q^{5/2}, 1/q\xi)$ for several values of $1/q\xi$: A) $1/q\xi = 0.$, B) $1/q\xi = 0.2$, C) $1/q\xi = 1.04$. Taken from Ref. [118]. The scale σ is defined in Ref. [118].

Figure 2.4a:

The spin relaxation function $\phi(\Lambda q^{5/2}t, 1/q\xi)$ for several values of $1/q\xi$ indicated in the graph.

Figure 2.4b:

The scaling function $\phi(\omega/\Lambda q^{5/2}, 1/q\xi)$ for the spin relaxation function $\Phi(q, \omega) = \phi(\omega/\Lambda q^{5/2}, 1/q\xi)/\Lambda q^{5/2}$ for several values of $1/q\xi$ indicated in the graph, showing the shape crossover to a Lorentzian shape for $1/q\xi \geq 1$.

Figure 2.5:

Dynamic scaling function for ferromagnets with short range exchange interaction only versus $1/q\xi$ below T_c for three different amplitudes of the spin-wave frequency: $f = \pi^{3/2}$ (solid), $f = 7.65$ (dashed), and $f = 8.20$ (point-dashed). Taken from Ref. [241,242].

Figure 2.6:

Comparison of the longitudinal line width with the polarized neutron scattering experiments on *Ni* [34]. All line widths are normalized to 1 at criticality. The result of mode coupling theory is shown for two different values of the spin-wave frequency amplitude $f = \pi^{3/2}$ (solid), $f = 7.65$ (dashed), and $f = 8.20$ (point-dashed). Taken from Ref. [240,241].

Figure 2.7:

Comparison of the line width obtained from mode coupling and renormalization group analysis. Taken from Ref. [125].

FIGURES

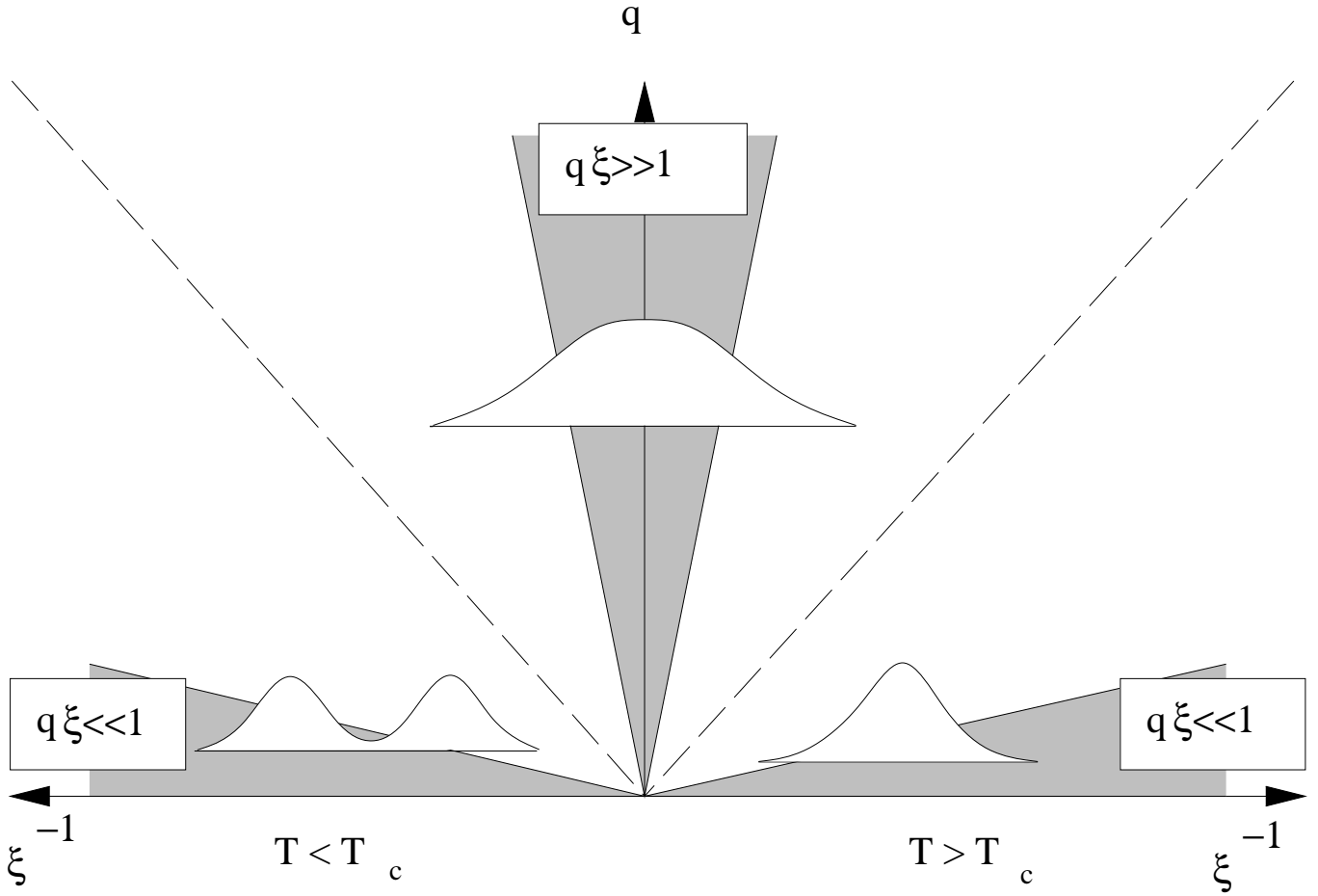


Figure 2.1: The macroscopic domain of wave vector q and correlation length ξ . In the three shaded regions the correlation functions have different characteristic behaviors. (a) Hydrodynamic region: $q\xi \ll 1$, $T > T_c$, and $T < T_c$, (b) critical region: $q\xi \gg 1$, $T \approx T_c$. There is a change-over from under-damped spin-waves to spin diffusion when the temperature is raised from below T_c to above T_c , as schematically indicated in the diagram.

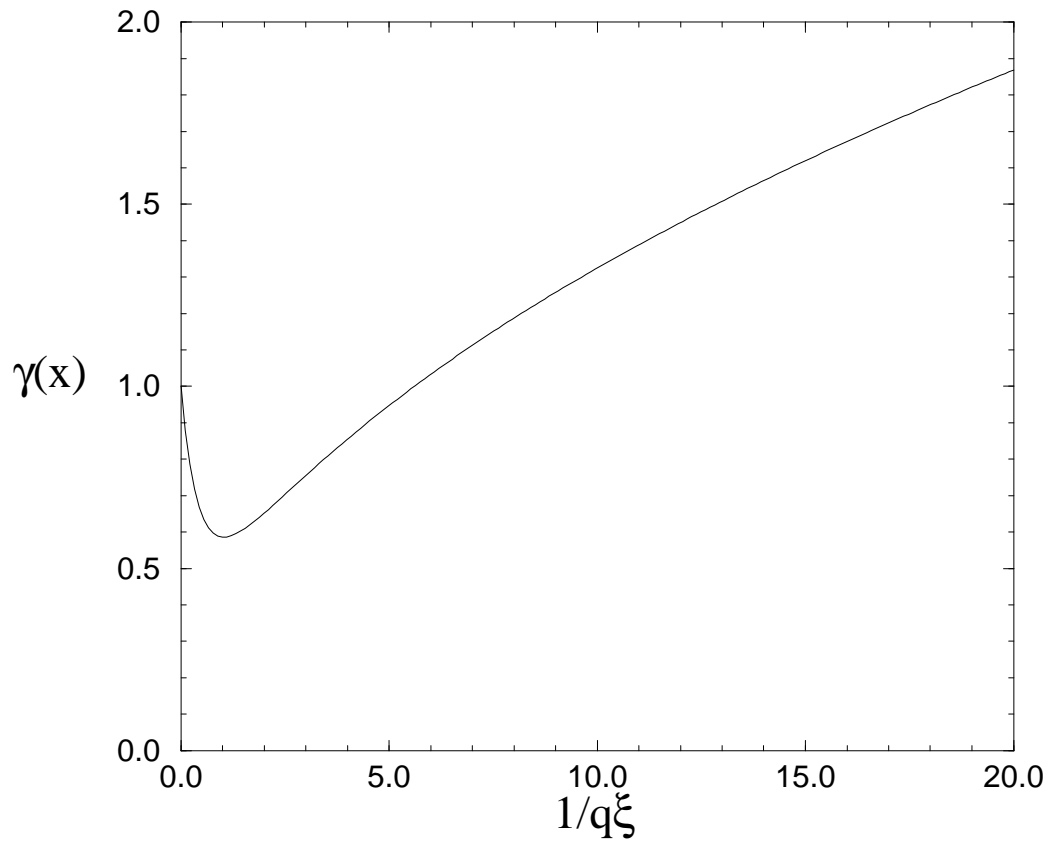


Figure 2.2: The Resibois–Piette scaling function versus $x = 1/q\xi$, resulting from the numerical solution [231] of the mode coupling equations in Lorentzian approximation for a Heisenberg ferromagnet in the paramagnetic phase.

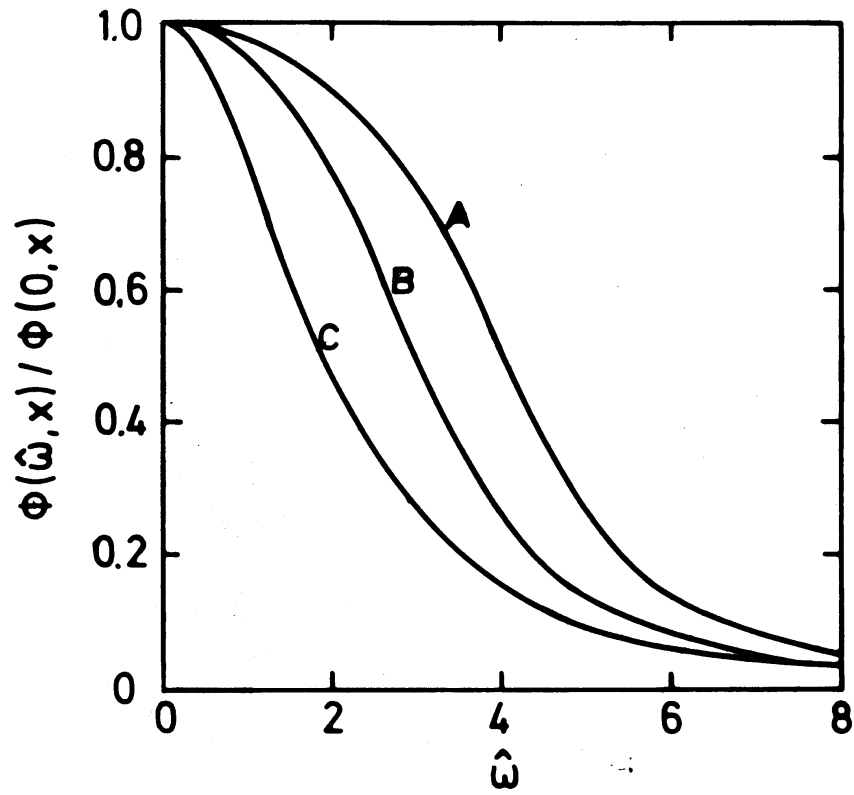


Figure 2.3: The universal function $\phi(\omega/\sigma q^{5/2}, 1/q\xi)$ for several values of $1/q\xi$: A) $1/q\xi = 0.$, B) $1/q\xi = 0.2$, C) $1/q\xi = 1.04$. Taken from Ref. [118]. The scale σ is defined in Ref. [118].

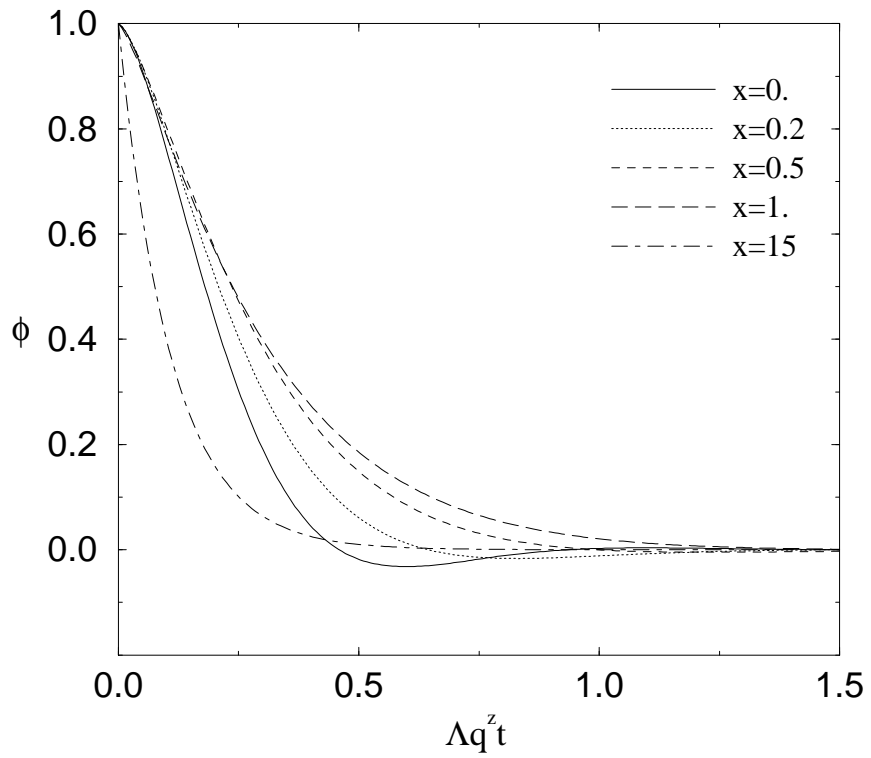


Figure 2.4.a: The spin relaxation function $\phi(\Lambda q^{5/2}t, 1/q\xi)$ for several values of $1/q\xi$ indicated in the graph.

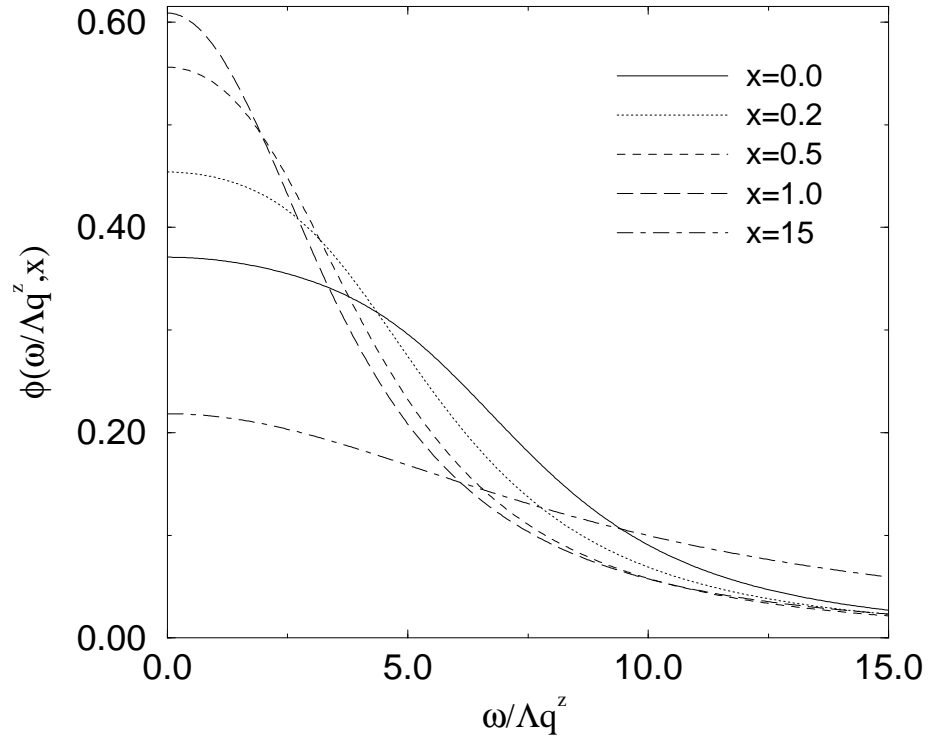


Figure 2.4.b: The scaling function $\phi(\omega/\Lambda q^{5/2}, 1/q\xi)$ for the spin relaxation function $\Phi(q, \omega) = \phi(\omega/\Lambda q^{5/2}, 1/q\xi)/\Lambda q^{5/2}$ for several values of $1/q\xi$ indicated in the graph, showing the shape crossover to a Lorentzian shape for $1/q\xi \geq 1$.

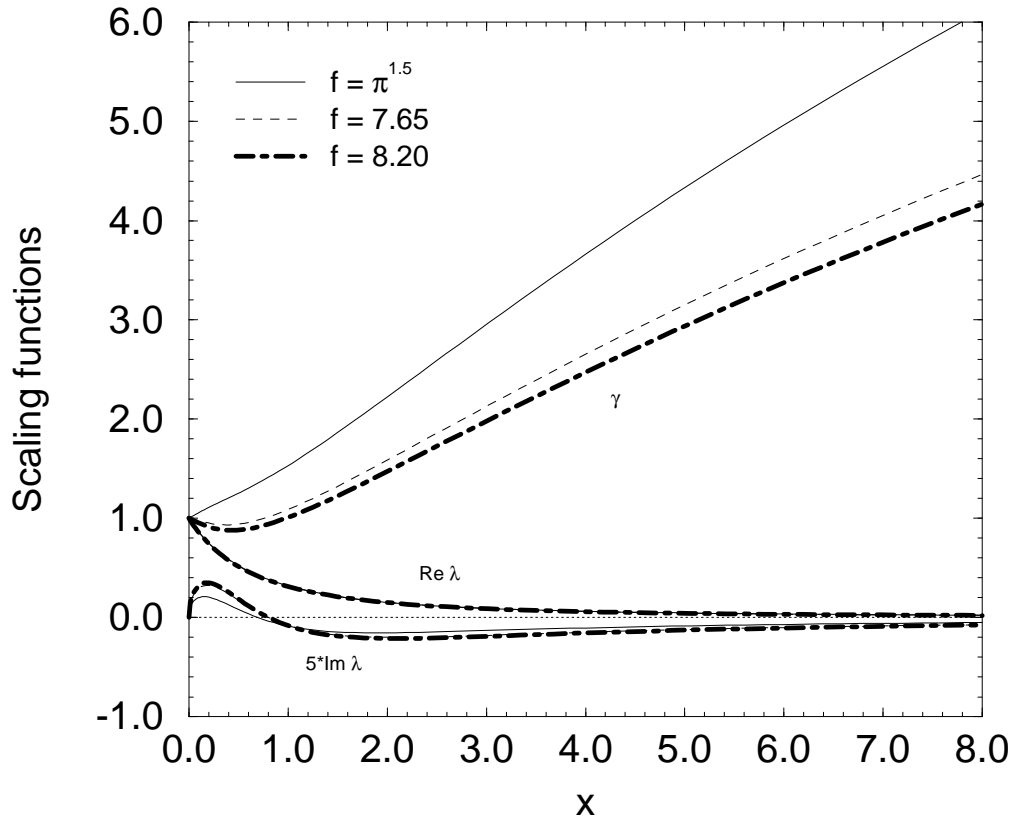


Figure 2.5: Dynamic scaling function for ferromagnets with short range exchange interaction only versus $1/q\xi$ below T_c for three different amplitudes of the spin-wave frequency: $f = \pi^{3/2}$ (solid), $f = 7.65$ (dashed), and $f = 8.20$ (point-dashed). Taken from Ref. [241,242].

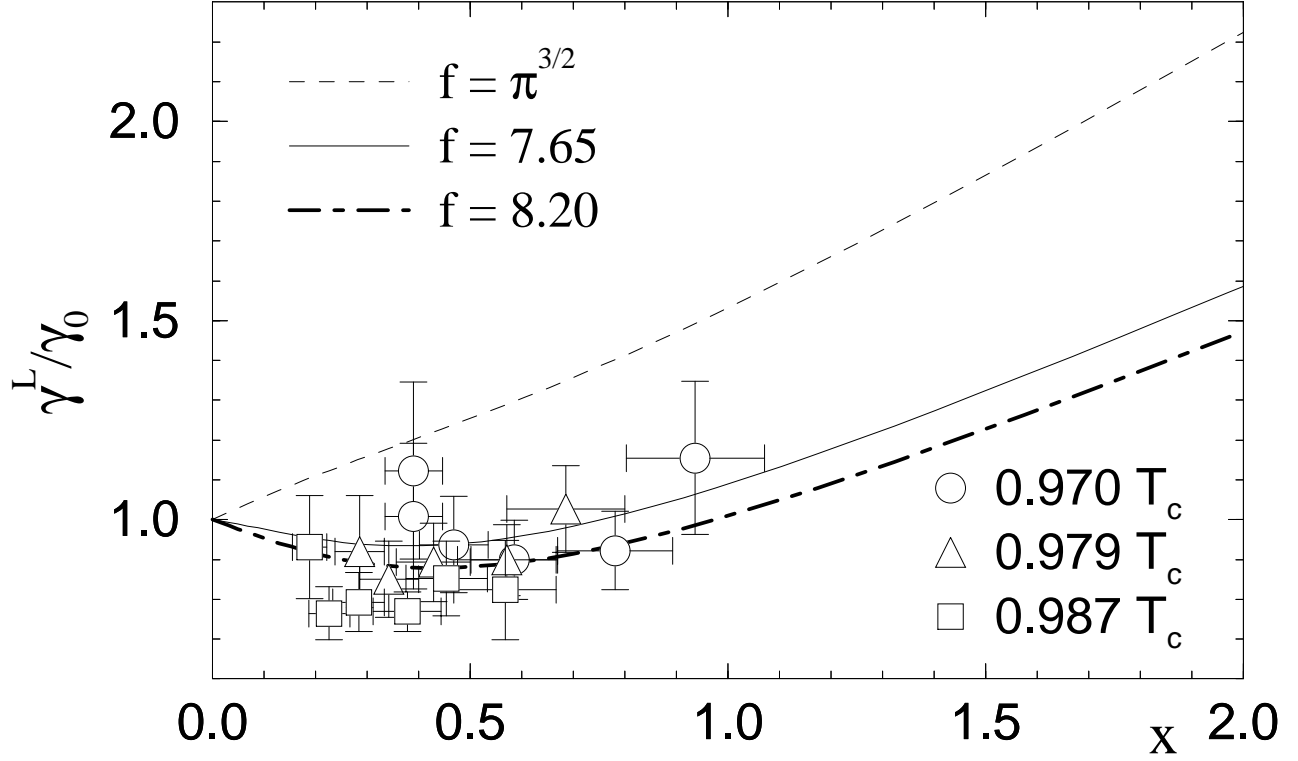


Figure 2.6: Comparison of the longitudinal line width with the polarized neutron scattering experiments on *Ni* [34]. All line widths are normalized to 1 at criticality. The result of mode coupling theory is shown for two different values of the spin-wave frequency amplitude $f = \pi^{3/2}$ (solid), $f = 7.65$ (dashed), and $f = 8.20$ (point-dashed). Taken from Ref. [240,241].

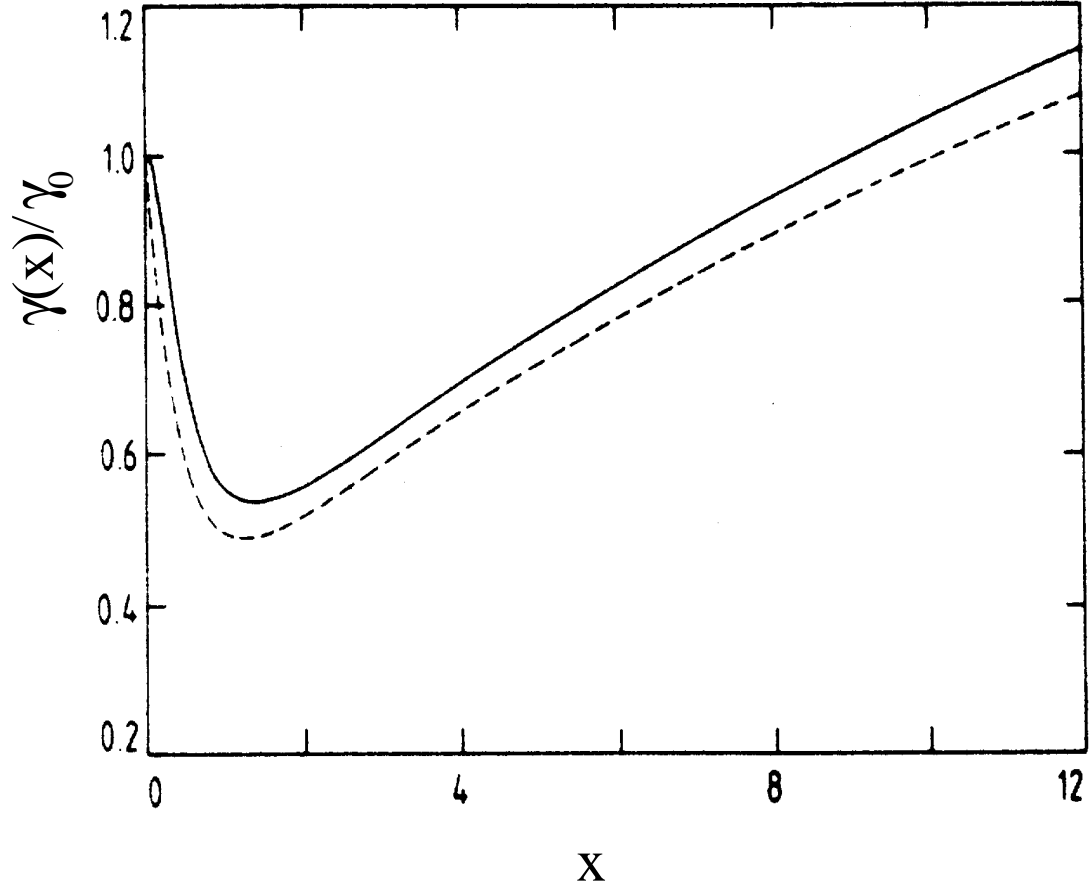


Figure 2.7: Comparison of the line width obtained from mode coupling and renormalization group analysis. Taken from Ref. [125].

III. DIPOLAR FERROMAGNETS

In this chapter we review the static and dynamic critical behavior of dipolar ferromagnets, i.e., spin systems with both short-range exchange and long-range dipole-dipole interaction. Special emphasis is put on the discussion of the mode coupling theory in the paramagnetic phase.

But, before turning to the detailed analysis we would like to emphasize the following characteristic features of the dipole-dipole interaction, which have important implications on the critical dynamics. (1) In contrast to the short range exchange interaction the dipolar interaction is long-ranged and thus dominates the asymptotic critical behavior of ferromagnets. (2) It introduces an anisotropy of the spin fluctuations longitudinal and transverse to the wave vector \mathbf{q} . This implies that the longitudinal static susceptibility remains finite for $\mathbf{q} \rightarrow 0$ and $T \rightarrow T_c$ [4]. (3) The order parameter no longer is conserved as can be inferred from the equations of motion. (4) The strength of the dipolar interaction introduces, besides the correlation length ξ , a second length scale q_D^{-1} , where q_D is the so called dipolar wave vector defined below. This leads to generalized scaling laws for the relaxation functions and the line widths.

A. The Model-Hamiltonian

Our starting point is a Hamiltonian for a spin system including both isotropic short-range exchange and long-range dipolar interactions

$$H = - \sum_{l \neq l'} [J_{ll'} \delta^{\alpha\beta} + A_{ll'}^{\alpha\beta}] S_l^\alpha S_{l'}^\beta, \quad (3.1)$$

where $J_{ll'}$ denotes the short range exchange interaction, usually restricted to nearest or next nearest neighbors, and $A_{ll'}^{\alpha\beta}$ is the dipolar interaction tensor given by

$$A_{ll'}^{\alpha\beta} = -\frac{1}{2}(g_L \mu_B)^2 \left(\frac{\delta^{\alpha\beta}}{|\mathbf{x}_l - \mathbf{x}_{l'}|^3} - \frac{3(x_l - x_{l'})^\alpha (x_l - x_{l'})^\beta}{|\mathbf{x}_l - \mathbf{x}_{l'}|^5} \right). \quad (3.2)$$

Here g_L is the Landé factor, μ_B the Bohr magneton. As shown by Cohen and Keffer [47] the lattice sums

$$A_{\mathbf{q}}^{\alpha\beta} = \sum_{l \neq 0} A_{l0}^{\alpha\beta} e^{i\mathbf{q} \cdot \mathbf{x}_l} \quad (3.3)$$

can be evaluated by using Ewald's method [68], and one finds for infinite three-dimensional cubic lattices [47,4,5]

$$A_{\mathbf{q}}^{\alpha\beta} v_a = \frac{1}{2} (g_L \mu_B)^2 \left\{ \frac{4\pi}{3} \left(\delta^{\alpha\beta} - \frac{3q^\alpha q^\beta}{q^2} \right) + \alpha_1 q^\alpha q^\beta + \left[\alpha_2 q^2 - \alpha_3 (q^\alpha)^2 \right] \delta^{\alpha\beta} + \mathcal{O}(q^4, (q^\alpha)^4, (q^\alpha)^2 (q^\beta)^2) \right\}, \quad (3.4)$$

where v_a is the volume of the primitive unit cell with lattice constant a , and α_i are constants, which depend on the lattice structure (see Table IV). Upon expanding the exchange interaction,

$$J_{\mathbf{q}} = \sum'_l J_{l0} e^{i\mathbf{q} \cdot \mathbf{x}_l} \approx J_0 - Jq^2 a^2 + \mathcal{O}(q^4), \quad (3.5)$$

and keeping only those terms, which are relevant in the sense of renormalization-group theory this results in the following effective Hamiltonian for dipolar ferromagnets

$$H = \sum_{\mathbf{q}} \left[-J_0 + Jq^2 a^2 + Jg \frac{q^\alpha q^\beta}{q^2} \right] S_{-\mathbf{q}}^\alpha S_{\mathbf{q}}^\beta, \quad (3.6)$$

where the Fourier-transform of the spin variables is defined by

$$S_{\mathbf{q}}^\alpha = \frac{1}{\sqrt{N}} \sum_l S_l^\alpha e^{i\mathbf{q} \cdot \mathbf{x}_l}. \quad (3.7)$$

Here we have defined a dimensionless quantity g as the ratio of the dipolar energy $(g_L \mu_B)^2 / a^3$ and exchange energy $2J$, multiplied by a factor $4\pi a^3 / v_a$, which depends on the lattice structure.

$$g = \frac{4\pi a^3}{v_a} \frac{(g_L \mu_B)^2 / a^3}{2J} \propto \frac{\text{Dipolar Energy}}{\text{Exchange Energy}}. \quad (3.8)$$

Strictly speaking there are dipolar corrections of order $\mathcal{O}(q^2)$ to the exchange coupling. But, those can be neglected, since the strength of the dipolar interaction is small compared with the exchange interaction.

The dipolar interaction induces an anisotropy of the static as well as the dynamic spin-spin correlation function with respect to the wave vector \mathbf{q} . It was shown by Aharony and Fisher [4], that the static transverse susceptibility diverges with the dipolar critical exponent γ as the critical temperature is approached, whereas the longitudinal susceptibility remains finite. The finite value is inversely proportional to the strength of the dipolar interaction g . The dipolar anisotropy becomes substantial when $q^2 + \xi^{-2} \leq q_D^2$, where the dipolar wave vector is defined as $g = (q_D a)^2$. The strong suppression of the longitudinal fluctuations have been observed in *EuS* and *EuO* by polarized neutron scattering experiments [153].

The matrix of the static susceptibility is given by

$$\chi^{\alpha\beta}(g, \mathbf{q}) = \chi^T(g, q) \left(\delta^{\alpha\beta} - \frac{q^\alpha q^\beta}{q^2} \right) + \chi^L(g, q) \frac{q^\alpha q^\beta}{q^2}, \quad (3.9)$$

where one often uses the Ornstein-Zernike forms for the longitudinal and transverse susceptibilities

$$\chi^T(g, q) = \frac{\Upsilon}{q^2 + \xi^{-2}}, \quad (3.10)$$

$$\chi^L(g, q) = \frac{\Upsilon}{q^2 + q_D^2 + \xi^{-2}}, \quad (3.11)$$

with the non-universal static amplitude

$$\Upsilon = \frac{(g_L \mu_B)^2}{2J a^2}. \quad (3.12)$$

Conventional mode coupling theory does not account for effects of the critical exponent η , which will be neglected in the following⁵. Here $\xi = \xi_0 \left(\frac{T-T_c}{T_c} \right)^{-\nu}$ is the correlation length. The static crossover from Heisenberg to dipolar critical behavior is partly contained in ξ through the effective temperature dependent exponent [41,84,89] $\nu \cong \gamma_{\text{eff}}/2$. The full dipolar crossover in the static critical behavior has been studied in Refs. [201,41,42,84,89].

⁵For a refined version of mode coupling theory which allows for a consistent treatment of the Fisher exponent η see chapter VI.

The tensorial structure of the static susceptibility suggests a decomposition of the spin operator $\mathbf{S}_{\mathbf{q}}$ into one longitudinal and two transverse components with respect to the wave vector \mathbf{q} , i.e.,

$$\mathbf{S}_{\mathbf{q}} = S_{\mathbf{q}}^L \hat{\mathbf{q}} + S_{\mathbf{q}}^{T_1} \hat{\mathbf{t}}^1(\hat{\mathbf{q}}) + S_{\mathbf{q}}^{T_2} \hat{\mathbf{t}}^2(\hat{\mathbf{q}}), \quad (3.13)$$

where the orthonormal set of unit vectors is defined by

$$\hat{\mathbf{q}} = \frac{\mathbf{q}}{q}, \quad \hat{\mathbf{t}}^1(\hat{\mathbf{q}}) = \frac{\mathbf{q} \times \mathbf{e}_3}{(q_1^2 + q_2^2)^{1/2}}, \quad \hat{\mathbf{t}}^2(\hat{\mathbf{q}}) = \hat{\mathbf{q}} \times \hat{\mathbf{t}}^1(\hat{\mathbf{q}}). \quad (3.14)$$

For vanishing components of \mathbf{q} the limits are taken in the order of increasing Cartesian components.

From the Hamiltonian, Eq. (3.6), one deduces the following microscopic Heisenberg equations of motion [79,80]

$$\begin{aligned} \frac{d}{dt} S_{\mathbf{q}}^L &= Ja^2 \int \frac{v_a d^3 k}{(2\pi)^3} \frac{1}{k} \left\{ \mathbf{q} \cdot (2\mathbf{k} - \mathbf{q}) \left(\sqrt{k_1^2 + k_2^2} \{S_{\mathbf{q}-\mathbf{k}}^{T_1}, S_{\mathbf{k}}^L\} + k_3 \{S_{\mathbf{q}-\mathbf{k}}^{T_1}, S_{\mathbf{k}}^{T_2}\} \right) \right. \\ &\quad \left. + g \sqrt{k_1^2 + k_2^2} \{S_{\mathbf{q}-\mathbf{k}}^{T_1}, S_{\mathbf{k}}^L\} \right\}, \end{aligned} \quad (3.15)$$

$$\begin{aligned} \frac{d}{dt} S_{\mathbf{q}}^{T_1} &= -Ja^2 \int \frac{v_a d^3 k}{(2\pi)^3} \frac{1}{k} \left\{ \mathbf{q} \cdot (2\mathbf{k} - \mathbf{q}) \left[\frac{-k_1 k_3}{\sqrt{k_1^2 + k_2^2}} \{S_{\mathbf{q}-\mathbf{k}}^{T_1}, S_{\mathbf{k}}^L\} + k_1 \{S_{\mathbf{q}-\mathbf{k}}^{T_1}, S_{\mathbf{k}}^{T_2}\} \right. \right. \\ &\quad \left. \left. + \frac{k_2(k_3 q - k^2)}{|\mathbf{q} - \mathbf{k}| \sqrt{k_1^2 + k_2^2}} \{S_{\mathbf{q}-\mathbf{k}}^{T_2}, S_{\mathbf{k}}^L\} + \frac{1}{2} \frac{k_2 q}{|\mathbf{q} - \mathbf{k}|} \left(\{S_{\mathbf{q}-\mathbf{k}}^L, S_{\mathbf{k}}^L\} - \{S_{\mathbf{q}-\mathbf{k}}^{T_2}, S_{\mathbf{k}}^{T_2}\} \right) \right] \right. \\ &\quad \left. + g \left[\frac{-k_1 k_3}{\sqrt{k_1^2 + k_2^2}} \{S_{\mathbf{q}-\mathbf{k}}^{T_1}, S_{\mathbf{k}}^L\} + \frac{k_2(k_3 q - k^2)}{|\mathbf{q} - \mathbf{k}| \sqrt{k_1^2 + k_2^2}} \{S_{\mathbf{q}-\mathbf{k}}^{T_2}, S_{\mathbf{k}}^L\} \right] \right\}, \end{aligned} \quad (3.16)$$

and for $S_{\mathbf{q}}^{T_2}$ correspondingly, where $\{, \}$ denotes the anticommutator. The terms proportional to g , resulting from the dipolar term in the Hamiltonian remain finite as the wave vector \mathbf{q} tends to zero, whereas all the other terms vanish in this limit. This is responsible for the fact that the dipolar forces lead to a relaxational dynamics in the limit of long wavelengths, i.e., the order parameter is no longer a conserved quantity.

B. Mode Coupling Theory for the Paramagnetic Phase

1. General Mode Coupling Equations

As we have explained in chapter II, mode coupling theory amounts in an factorization approximation for the transport coefficients

$$\Gamma^L(q, g, t) = \frac{(g_L \mu_B)^2}{\chi^L(q, g)} (\dot{S}^L(\mathbf{q}, t), \dot{S}^L(\mathbf{q}, 0)), \quad (3.17)$$

$$\begin{aligned} \Gamma^T(q, g, t) &= \frac{(g_L \mu_B)^2}{\chi^T(q, g)} (\dot{S}^{T_1}(\mathbf{q}, t), \dot{S}^{T_1}(\mathbf{q}, 0)) = \\ &= \frac{(g_L \mu_B)^2}{\chi^T(q, g)} (\dot{S}^{T_2}(\mathbf{q}, t), \dot{S}^{T_2}(\mathbf{q}, 0)). \end{aligned} \quad (3.18)$$

The mode coupling equations resulting from considering two-mode decay processes have been derived in Refs. [79,80] ($\alpha = L, T$) and are given by

$$\begin{aligned} \Gamma^\alpha(q, g, t) &= 2(2Ja^2)^2 \frac{k_B T}{(g_L \mu_B)^2} \int \frac{v_a d^3 k}{(2\pi)^3} \sum_{\beta, \sigma} v_{\beta\sigma}^\alpha(k, q, g, \theta) (\delta^{\sigma, T} + \delta^{\alpha, T} \delta^{\beta, L} \delta^{\sigma, L}) \\ &\times \frac{\chi^\beta(\mathbf{k}, g) \chi^\sigma(\mathbf{q} - \mathbf{k}, g)}{\chi^\alpha(\mathbf{q}, g)} \Phi^\beta(\mathbf{k}, g, t) \Phi^\sigma(\mathbf{q} - \mathbf{k}, g, t). \end{aligned} \quad (3.19)$$

Here the k -integration runs over the first Brillouin zone (BZ). The vertex functions $v_{\beta\sigma}^\alpha$ for the decay of the mode α into the modes β and σ are given by [80]

$$v_{TT}^L(k, q, g, \eta) = 2q^4 \cos^2 \theta \left[\frac{k \cos \theta}{q} - \frac{1}{2} \right]^2, \quad (3.20)$$

$$v_{LT}^L(k, q, g, \eta) = 2q^4 \sin^2 \theta \left[\frac{k \cos \theta}{q} - \frac{1}{2} + \frac{g}{2q^2} \right]^2, \quad (3.21)$$

$$v_{TT}^T(k, q, g, \eta) = q^4 \sin^2 \theta \left[\frac{k \cos \theta}{q} - \frac{1}{2} \right]^2 \left(1 + \frac{q^2}{2|\mathbf{q} - \mathbf{k}|^2} \right), \quad (3.22)$$

$$v_{LT}^T(k, q, g, \eta) = q^4 \left[\frac{k \cos \theta}{q} - \frac{1}{2} + \frac{g}{2q^2} \right]^2 \left(2 - \left(1 + \frac{q^2}{|\mathbf{q} - \mathbf{k}|^2} \right) \sin^2 \theta \right), \quad (3.23)$$

$$v_{LL}^T(k, q, g, \eta) = q^4 \sin^2 \theta \left[\frac{k \cos \theta}{q} - \frac{1}{2} \right]^2 \frac{q^2}{2|\mathbf{q} - \mathbf{k}|^2}, \quad (3.24)$$

with $\eta = \cos \theta$. In passing we note that there were certain attempts to develop a mode coupling theory already twenty years ago, although nobody succeeded to derive the appropriate mode coupling equations. A type of mode coupling calculation was used by Huber [122] to determine the uniform spin relaxation for temperatures larger than the dipolar crossover temperature. This analysis was extended by Finger [72], who put forward certain scaling estimates and computed the uniform spin relaxation in the strong dipolar region. An attempt to construct a mode coupling theory was launched by Borckmans et al. [27], using an incomplete basis and ending up with equations containing undetermined vertices. The theoretical and experimental situation was rather controversial and no explanation was available for the apparent contradictions [151,191]. Only in 1986 a complete self-consistent mode coupling theory was developed by the authors [79,80] and its various properties and consequences were studied in detail [81,82,84,85]. Some of the results were confirmed numerically by Aberger and Folk [2,3], and by Kalashnikov and Tret'jakov [131,132] using analytic approximants.

The mode coupling result for the transport coefficients, Eqs. (3.19), together with the relation

$$\frac{\partial}{\partial t} \Phi^\alpha(q, g, t) = - \int_0^t d\tau \Gamma^\alpha(q, g, t - \tau) \Phi^\alpha(q, g, \tau) \quad (3.25)$$

for the Kubo relaxation functions constitute, as in chapter II, a complete set of self consistent equations.

As emphasized before, the dipolar interaction introduces a second length scale q_D^{-1} besides the correlation length ξ . This entails the following extension of the static scaling law for the spin susceptibilities

$$\chi^\alpha(q, \xi, g) = \Upsilon q^{-2} \hat{\chi}^\alpha(x, y), \quad (3.26)$$

with the scaling variables

$$x = \frac{1}{q\xi} \quad \text{and} \quad y = \frac{q_D}{q}. \quad (3.27)$$

Note, that here and in the remainder of this section we have explicitly indicated the dependence of the susceptibility on the correlation length. In all other parts of this review we

suppress this dependence for notational convenience. Since the vertex functions $v_{\beta\sigma}^\alpha$ are proportional to the fourth power of the wave number, $v_{\beta\sigma}^\alpha \propto q^4$ and because of the homogeneity of Eq. (3.26), the relaxation functions and line widths derived from Eqs. (3.19)-(3.25) obey the dynamical scaling laws

$$\Phi^\alpha(ql, gl^2, \omega l^z) = l^{-z} \Phi^\alpha(q, \xi, g, \omega), \quad (3.28)$$

and

$$\Gamma^\alpha(ql, gl^2, \omega l^z) = l^z \Gamma^\alpha(q, \xi, g, \omega), \quad (3.29)$$

with $z = 5/2$ and a scaling parameter l . We emphasize that despite of z assuming the isotropic value $5/2$, there is a crossover to dipolar critical behavior contained in the functional form of the correlation functions, as will become clear below.

An immediate consequence of Eq. (3.29) is the following scaling property of the characteristic longitudinal and transverse frequencies $\omega_c^\alpha(q, \xi, g)$

$$\omega_c^\alpha(q, \xi, g) = \Lambda q^z \Omega^\alpha(x, y), \quad (3.30)$$

where Λ is a non universal coefficient.

Now there are various ways to rewrite the scaling laws Eqs. (3.28) and (3.29) by appropriate choices of the scaling parameter l . If one sets $l = q^{-1}$ one finds

$$\Phi^\alpha(q, \xi, g, \omega) = q^{-z} \hat{\Phi}^\alpha\left(\frac{1}{q\xi}, \frac{g}{q^2}, \frac{\omega}{q^z}\right), \quad (3.31)$$

and

$$\Gamma^\alpha(q, \xi, g, \omega) = q^z \hat{\Gamma}^\alpha\left(\frac{1}{q\xi}, \frac{g}{q^2}, \frac{\omega}{q^z}\right). \quad (3.32)$$

A disadvantage of the representation given in Eqs. (3.31,3.32) is that both the crossover of the time scales and of the shapes of the correlation functions are intermixed in $\hat{\Phi}^\alpha$. Since the time scales for the isotropic and dipolar critical and hydrodynamic behavior differ quite drastically, it is more natural to measure frequencies in units of the characteristic frequencies. Hence we fix the scaling parameter by the condition

$$l^z = \frac{1}{\Lambda q^z \Omega^\alpha(x, y)}, \quad (3.33)$$

and find from Eqs. (3.31,3.32) the scaling forms

$$\Phi^\alpha(q, \xi, g, \omega) = \frac{1}{\Lambda q^z \Omega^\alpha(x, y)} \phi^\alpha(x, y, \nu_\alpha), \quad (3.34)$$

and

$$\Gamma^\alpha(q, \xi, g, \omega) = \Lambda q^z \Omega^\alpha(x, y) \gamma^\alpha(x, y, \nu_\alpha), \quad (3.35)$$

with the scaling variable for the frequency

$$\nu_\alpha = \frac{\omega}{\Lambda q^z \Omega^\alpha(x, y)}. \quad (3.36)$$

With Eq. (3.33) one has separated the crossover of the frequency scales and the crossover of the shapes of the correlation functions. The former mainly is contained in $\Omega^\alpha(x, y)$ the latter in $\phi^\alpha(x, y, \nu_\alpha)$.

There is still some freedom in the choice of the characteristic frequencies ω_c^α in Eq. (3.33); for instance, one could take the half width at half maximum (HWHM) of the frequency dependent Kubo functions. This, however, would require to solve Eqs. (3.19) and (3.25) simultaneously for the time scales and the shapes of the correlation functions. Therefore, in the following we will use as characteristic frequencies the half widths resulting from the Lorentzian approximation for the line shape (see section 3.3). The Lorentzian line widths qualitatively obey the same scaling laws as the HWHM and have the same asymptotic (hydrodynamic, dipolar, isotropic) properties. Thus this choice for the characteristic frequencies solely is a matter of numerical convenience and does not introduce any approximations in the final result. From the final result one can obtain the HWHM and rewrite the scaling functions in terms of these new variables.

Eqs. (3.34), (3.35) and (3.36) imply for the Laplace transformed quantities the scaling laws

$$\Phi^\alpha(q, \xi, g, t) = \phi^\alpha(x, y, \tau_\alpha), \quad (3.37)$$

and

$$\Gamma^\alpha(q, \xi, g, t) = [\Lambda q^z \Omega^\alpha(x, y)]^2 \gamma^\alpha(x, y, \tau_\alpha), \quad (3.38)$$

where the scaled time variables τ_α are given by

$$\tau_\alpha = \Lambda q^z \Omega^\alpha(x, y) t. \quad (3.39)$$

One should note that the characteristic time scales $1/[\Lambda q^z \Omega^\alpha(x, y)]$ are different for the longitudinal and transverse modes. This is mainly due to the non critical longitudinal static susceptibility implying that the longitudinal characteristic frequency $\Lambda q^z \Omega^L(x, y)$ shows no critical slowing down asymptotically. In other words for $T = T_c$ and $q \rightarrow 0$ the longitudinal characteristic frequency does not tend to zero, which implies an effective longitudinal dynamical critical exponent $z_{\text{eff}}^L = 0$ for the wave vector dependence in the limit $q \rightarrow 0$. In comparison, the effective exponent for the transverse characteristic frequency at T_c shows a crossover from $z_{\text{eff}}^T = 5/2$ to $z_{\text{eff}}^T = 2$ (see also the following section). This mode coupling result disagrees with a calculation based on nonlinear spin wave theory, where $z_{\text{eff}}^T = 1$ is found in the dipolar region [176].

Inserting Eqs. (3.37,3.38) together with the static scaling law (3.26) into Eqs. (3.19) and (3.25) we find the following coupled integro-differential equations

$$\begin{aligned} \gamma^\alpha(x, y, \tau_\alpha) = & 2 \left(\frac{\pi}{\Omega^\alpha(x, y)} \right)^2 \int_{-1}^{+1} d\eta \int_0^{\rho_{\text{cut}}} d\rho \rho_-^{-2} \sum_{\beta, \sigma} \hat{v}_{\beta\sigma}^\alpha(y, \rho, \eta) \left(\delta^{\sigma, T} + \delta^{\alpha, T} \delta^{\beta, L} \delta^{\sigma, L} \right) \\ & \times \frac{\hat{\chi}^\beta \left(\frac{x}{\rho}, \frac{y}{\rho} \right) \hat{\chi}^\sigma \left(\frac{x}{\rho_-}, \frac{y}{\rho_-} \right)}{\hat{\chi}^\alpha(x, y)} \phi^\beta \left(\frac{x}{\rho}, \frac{y}{\rho}, \tau_{\alpha\beta}(x, y, \rho) \right) \phi^\sigma \left(\frac{x}{\rho_-}, \frac{y}{\rho_-}, \tau_{\alpha\sigma}(x, y, \rho_-) \right), \quad (3.40) \end{aligned}$$

and

$$\frac{\partial}{\partial \tau_\alpha} \phi^\alpha(x, y, \tau_\alpha) = - \int_0^{\tau_\alpha} d\tau \gamma^\alpha(x, y, \tau_\alpha - \tau) \phi^\alpha(x, y, \tau), \quad (3.41)$$

connecting the scaling functions for the transport coefficients with the scaling functions for the Kubo relaxation functions. In Eq. (3.40) we introduced the notations $\rho = k/q$, $\rho_- = |\mathbf{q} - \mathbf{k}|/q$, $\eta = \cos(\mathbf{q}, \mathbf{k})$ and $\tau_{\alpha\beta}(x, y, \mu) = \tau_\alpha \mu^z \Omega^\beta(x/\mu, y/\mu) / \Omega^\alpha(x, y)$.

The non universal frequency scale resulting from the transformation of Eq. (3.19) in Eq. (3.40) is

$$\Lambda = \frac{a^{5/2}}{b} \sqrt{\frac{2Jk_B T}{4\pi^4}}. \quad (3.42)$$

The apparent critical dynamic exponent contained in Eq. (3.40) equals $z = 5/2$. However, as noted before, the crossover to dipolar behavior is contained in the scaling functions for the transport coefficients $\gamma^\alpha(x, y, \tau_\alpha)$, the scaling functions for the Kubo relaxation functions $\phi^\alpha(x, y, \tau_\alpha)$ and the scaling functions of the characteristic frequencies $\Omega^\alpha(x, y)$.

The scaled vertex functions appearing in Eq. (3.40) read [80]

$$\hat{v}_{\beta\beta}^\alpha = \left[2\eta^2 \delta^{\alpha,L} + (1 - \eta^2) \left(\delta^{\beta,T} + \frac{1}{2\rho_-^2} \right) \delta^{\alpha,T} \right] \left(\rho\eta - \frac{1}{2} \right)^2, \quad (3.43)$$

$$\hat{v}_{LT}^\alpha = \left[2 \left(1 - \eta^2 \delta^{\alpha,L} \right) - (1 - \eta^2) \left(1 + \frac{1}{\rho_-^2} \right) \delta^{\alpha,T} \right] \left(\rho\eta - \frac{1}{2} + \frac{y^2}{2} \right)^2, \quad (3.44)$$

which are related to the vertex functions $v_{\beta\sigma}^\alpha$ of Eqs. (3.20-3.24) by $v_{\beta\sigma}^\alpha = q^4 \hat{v}_{\beta\sigma}^\alpha$. For both longitudinal and transverse modes, the dipolar interaction enters only in vertices involving decays into a longitudinal and a transverse mode, since the dipolar interaction enters the Hamiltonian only through the longitudinal modes.

Because the k -integration is restricted to the Brillouin zone the ρ -integration of Eq. (3.40) contains the cutoff

$$\rho_{\text{cut}} = \frac{q_{BZ}}{q} = \frac{q_{BZ}}{q_D} y, \quad (3.45)$$

where q_{BZ} denotes the boundary of the first Brillouin zone. All other material dependent parameters are contained in the frequency scale Λ . The cutoff is important for small times, because the integrand of Eq. (3.40) is of order 1 for $t = 0$ and $\rho \gg 1$. Hence for small times also wave vectors near the zone boundary contribute to the relaxation mechanism.

As explained before, in the numerical solution of the MC-equations one has taken [82,85] for the characteristic frequencies the line widths resulting from the Lorentzian approximation of the MC equations, i.e.,

$$\Omega^\alpha(x, y) = \gamma_{\text{lor}}^\alpha(x, y). \quad (3.46)$$

Using as input the solution of the mode coupling equations in the Lorentzian approximation one can solve the complete set of MC-equations for different values of q_{BZ} . Because there are three scaling variables (x , y and ν_α) it is impossible to present here all numerical results. Instead, in chapter IV, we will concentrate on a limited number of temperatures and wave vectors motivated by the available experiments on the substances of primary interest *EuS*, *EuO* and *Fe*.

2. Lorentzian Approximation

For later reference we want to close this section with quoting the results from the so called Lorentzian approximation [80,81]. The results of the numerical solution of the full mode coupling equations will be discussed in chapter IV in conjunction with the experimental data.

If the transport coefficients vary only slowly with ω we may approximate the relaxation functions by Lorentzians, i.e., we replace the transport coefficients by their values at $\omega = 0$

$$\Gamma_{\text{lor}}^L(q, \xi, g) = \Gamma^L(q, \xi, g, \omega = 0), \quad \Gamma_{\text{lor}}^T(q, \xi, g) = \Gamma^T(q, \xi, g, \omega = 0). \quad (3.47)$$

Despite a Lorentzian being not the correct shape of the correlation function for all values of the scaling variables, the resulting line widths obtained in the Lorentzian approximation already capture most of the crossover in the time scale.

The Lorentzian line widths obey the scaling law

$$\Gamma_{\text{lor}}^\alpha(q, \xi, g) = \Lambda q^z \gamma_{\text{lor}}^\alpha(x, y). \quad (3.48)$$

From Eq. (3.20) it is then easily inferred that the scaling functions of the Lorentzian line widths $\gamma_{\text{lor}}^\alpha(x, y)$ are determined by the coupled integral equations

$$\gamma_{\text{lor}}^\alpha(x, y) = \frac{2\pi^2}{\hat{\chi}^\alpha(x, y)} \int_{-1}^{+1} d\eta \int_0^\infty d\rho \rho^{-2} \sum_\beta \sum_\sigma \hat{v}_{\beta\sigma}^\alpha(y, \rho, \eta)$$

$$\left(\delta^{\sigma,T} + \delta^{\alpha,T} \delta^{\beta,L} \delta^{\sigma,L}\right) \frac{\hat{\chi}^{\beta}\left(\frac{x}{\rho}, \frac{y}{\rho}\right) \hat{\chi}^{\sigma}\left(\frac{x}{\rho_-}, \frac{y}{\rho_-}\right)}{\rho^{5/2} \gamma_{\text{lor}}^{\beta}\left(\frac{x}{\rho}, \frac{y}{\rho}\right) + \rho_-^{5/2} \gamma_{\text{lor}}^{\sigma}\left(\frac{x}{\rho_-}, \frac{y}{\rho_-}\right)}. \quad (3.49)$$

As summarized in Table 3.1 the mode coupling equations (3.49) can be solved analytically in the dipolar (D) and isotropic (I) critical (C) and hydrodynamic (H) limiting regions. These are defined by DC: $y \gg 1$, $x \ll 1$; IC: $y \ll 1$, $x \ll 1$; DH: $y \gg x$, $x \gg 1$; IH: $y \ll x$, $x \gg 1$.

Concerning the critical dynamical exponent one finds for the longitudinal line width a crossover from $z = 5/2$ in the isotropic critical region to $z = 0$ in the dipolar critical region, whereas for the transverse line width the crossover is from $z = 5/2$ to $z = 2$. The precise position of this crossover can only be determined numerically.

The numerical solution [79,80] of Eq. (3.49) shows that the dynamic crossover for the transverse width is shifted to smaller wave vectors by almost one order of magnitude with respect to the static crossover, whereas the crossover for the longitudinal width occurs at the static crossover. For the numerical solution of the mode coupling equations it is convenient to introduce polar coordinates

$$r = \sqrt{x^2 + y^2}, \quad \text{and} \quad \varphi = \arctan(y/x).$$

The transverse and longitudinal scaling functions $\gamma^T(r, \varphi)$ and $\gamma^L(r, \varphi)$ are shown in Figs. 3.1 and 3.2 as a function of the radial scaling variables r and φ . A different representation of the results can be given by plotting the linewidth versus the single scaling variable x for several values of φ . This is shown in Figs. 3.3-5, where we have drawn the two-parameter scaling functions $\gamma_{\text{lor}}^{L,T}(x, y)$ in units of the value at criticality $\gamma_0 = \gamma_{\text{lor}}^{L(T)}(0, 0) \cong 5.1326$. The physical content of the two parameter scaling surfaces is illustrated best by considering cuts for fixed q_D and various temperatures. In Figs. 3.3,4 the scaling functions versus $x = 1/q\xi$ are displayed for different values of $\varphi = \arctan(q_D \xi) = N\pi/20$ with $N = 0, 1, \dots, 9$. For $\varphi = 0$, corresponding to vanishing dipolar coupling g , the scaling functions coincide with the Resibois-Piette scaling function. If the strength of the dipolar interaction q_D is finite, the curves approach the Resibois-Piette scaling function for small values of the scaling variable x and deviate therefrom with increasing x . For a given material, q_D is fixed and the

parametrisation by φ corresponds to a parametrisation in terms of the reduced temperature $(T - T_c)/T_c$.

To examine the dipolar crossover precisely at the Curie point, Fig. 3.5 displays the scaling function for the transverse and longitudinal width at $T = T_c$ versus the wave number, i.e., $y^{-1} = q/q_D$. This graph shows that the crossover from the isotropic Heisenberg to dipolar critical dynamics in the transverse line width occurs at a wave number, which is almost one order of magnitude smaller than the static crossover wave vector q_D . The crossover of the longitudinal width, from $z = 2.5$ to $z = 0$, is more pronounced and occurs in the intermediate vicinity of q_D . The reason for the different location of the dynamic crossover is mainly due to the fact that it is primarily the longitudinal static susceptibility which shows a crossover due to the dipolar interaction. Since the change in the static critical exponents is numerically small the transverse static susceptibility is nearly the same as for ferromagnets without dipolar interaction [4]. Hence the crossover in the transverse width is purely a dynamical crossover, whereas the crossover of the longitudinal width being proportional to the inverse static longitudinal susceptibility is enhanced by the static crossover. In order to substantiate these arguments we have plotted in the inset of Fig. 3.5 the scaling functions of the Onsager coefficients $\hat{\chi}^\alpha \gamma^\alpha$ at the critical temperature versus q/q_D , showing only the dynamical crossover.

3. Selected Results of the Complete Mode Coupling Equations

All the scaling functions for the dipolar ferromagnet depend on the three scaling variables $x = 1/q\xi$, $y = q_D/q$ and $\nu_\alpha = \omega/\Lambda q^z \Omega^\alpha(x, y)$. Therefore it is impossible to present all the results obtained from the numerical solution of the complete mode coupling equations. In this section we intend to review the most important features of the shape and line width crossover reported in Refs. [82,85]. Further results and discussion will be presented in the next chapter in conjunction with a comparison with experimental data.

The results from the Lorentzian approximation show that the dipolar line width crossover

in the transverse line width sets in at a wave vector almost one order of magnitude smaller than the dipolar wave vector q_D . In order to get information about the line shape, one has to dismiss this approximation and solve the complete set of mode coupling equations, Eqs. (3.40) and (3.41). This has been achieved in Ref. [82,85], and one finds the following crossover scenario. First of all, the crossover in the line shape sets in at wave vectors of the order of the dipolar wave vector.

Let us first consider the case of temperatures very close to $T = T_c$. Fig. 3.6 and 3.7 show the transverse and longitudinal scaling functions $\phi^\alpha(r, \varphi, \tau_\alpha)$ versus the scaling variables r and τ_α for $\varphi = 1.49$. Referring to EuO , characterized by the (non universal) parameters $q_D = 0.147\text{\AA}^{-1}$, $T_c = 69.1K$ and $\xi_0 = 1.57\text{\AA}$, this corresponds to a temperature $T \approx (1 + 0.003)T_c$. The line shapes of the longitudinal and transverse relaxation function agree in the isotropic Heisenberg limit, i.e., for $r \rightarrow 0$ corresponding to large values of the wave vector q ($q \gg q_D$). In this limit the dipolar interaction becomes negligible and the shape is of the Hubbard-Wegner type as discussed in section II. Upon increasing the value of the scaling variable r the line shape of the transverse and longitudinal relaxation function become drastically different. Whereas the transverse relaxation function shows a nearly exponential decay, pronounced over-damped oscillations show up for the transverse relaxation function. The shape crossover is also shown in Fig. 3.8, where the transverse and longitudinal relaxation functions are plotted versus the scaling variable τ_α for three different values of the scaling variable $r = \sqrt{x^2 + y^2}$ ($r = 0$, $r = 1$, and $r = 10$).

For temperatures well separated from T_c , i.e. $q_D\xi \ll 1$, the dipolar interaction becomes negligible. Hence, the difference in the shape crossover of the longitudinal and transverse relaxation function diminishes with decreasing $q_D\xi$. For $q_D\xi \ll 1$ the shape crossover as a function of r corresponds to the crossover from the critical (Hubbard-Wegner) shape to the hydrodynamic shape as discussed in section II (Note that for $q_D\xi \ll 1$, the scaling variable r reduces to $x = 1/q\xi$). Figs. 3.9 and 3.10 show the shape crossover for $q_D\xi = 3.52$ ($\varphi = 1.294$) for the transverse and longitudinal relaxation function, respectively. Figs. 3.11 and 3.12 display the corresponding crossover for $q_D\xi = 1.46$ ($\varphi = 0.97$). In the latter

case the shape crossover of the transverse and longitudinal relaxation function are already quite similar and almost identical to the shape crossover found for the isotropic Heisenberg ferromagnet without dipolar interaction. The various crossover scenarios can also be read off from Fig. 3.8.

Finally let us add a comment on how the line shape crossover affects the line width crossover. It has been shown [82,85] (see Section IV) that there are only slight changes of the line width crossover, when the line width is determined from the full solution of the mode coupling equations, as compared to the widths obtained from the Lorentzian approximation. Roughly speaking, the overall effect of taking into account the correct line shape is approximately a shift by a constant factor. For details we refer the reader to section IV.

C. Spin Wave Theory in the Ferromagnetic Phase

Holstein and Primakoff [115] have investigated the dynamics of dipolar ferromagnets far below T_c using linear spin-wave theory. Upon neglecting fluctuations in the longitudinal component, $S_i^z \approx S$, they get the following equations of motion for the transverse spin fluctuations (see also Ref. [168])

$$i\frac{d}{dt}S_{\mathbf{k}}^+ = A_{\mathbf{k}}S_{\mathbf{k}}^+ + B_{\mathbf{k}}^*S_{-\mathbf{q}}^-, \quad (3.50)$$

$$i\frac{d}{dt}S_{\mathbf{k}}^- = A_{\mathbf{k}}^*S_{-\mathbf{q}}^- + B_{\mathbf{k}}S_{\mathbf{k}}^+, \quad (3.51)$$

in terms of the raising and lowering operators $S_i^\pm = S_i^x \pm iS_i^y$. From these equations of motion the spin-wave dispersion follows (see also Ref. [141])

$$\epsilon_{\mathbf{k}} = \sqrt{A_{\mathbf{k}} + |B_{\mathbf{k}}|} \sqrt{A_{\mathbf{k}} - |B_{\mathbf{k}}|}. \quad (3.52)$$

The coefficients $A_{\mathbf{k}}$ and $B_{\mathbf{k}}$ are given in terms of the exchange interaction $J_{\mathbf{k}} = 2S \sum_m J_{lm} e^{i\mathbf{k}\cdot(\mathbf{x}_l - \mathbf{x}_m)}$ and the dipolar interaction tensor $A_{\mathbf{k}}^{\alpha\beta}$ (see Eq. (3.3))

$$A_{\mathbf{k}} = g_L \mu_B H_0 + (J_0 - J_{\mathbf{k}}) + (2E_0 + E_{\mathbf{k}}), \quad (3.53)$$

$$E_{\mathbf{k}} = SA_{\mathbf{k}}^{zz}, \quad (3.54)$$

$$B_{\mathbf{k}} = -S(A_{\mathbf{k}}^{xx} - A_{\mathbf{k}}^{yy} - 2iA_{\mathbf{k}}^{xy}) = S\sqrt{(A_{\mathbf{k}}^{xx} - A_{\mathbf{k}}^{yy})^2 + 4A_{\mathbf{k}}^{xy2}}e^{-2i\varphi_{\mathbf{k}}}. \quad (3.55)$$

For crystals with cubic symmetry the dipolar tensor $A_{\mathbf{k}}^{\alpha\beta}$ is given by $A_{\mathbf{k}}^{\alpha\beta} \approx \frac{1}{2}(g_L\mu_B)^2\frac{4\pi}{3}\left(\delta^{\alpha\beta} - \frac{k^\alpha k^\beta}{k^2}\right)$ near the zone center $ka \ll 1$, plus small structure dependent terms proportional to k^2 (see Section III.1). Note however that the dipolar tensor becomes severely structure dependent (requiring numerical evaluation, see Ref. [47]) as \mathbf{k} approaches the zone boundary.

Hence, for $ka \ll 1$ one finds for crystals with cubic symmetry (for more details we refer to the review by Keffer [141])

$$A_{\mathbf{k}} = g_L\mu_B H_0 + (J_0 - J_{\mathbf{k}}) + \frac{1}{2}g_L\mu_B M_0 \left[4\pi - 4\pi(k^z/k)^2\right], \quad (3.56)$$

$$B_{\mathbf{k}} = \frac{1}{2}g_L\mu_B M_0 \left[4\pi \frac{(k^x)^2 - i(k^y)^2}{k^2}\right] = 2\pi g_L\mu_B M_0 \sin^2 \Theta_{\mathbf{k}} \exp(-2i\varphi_{\mathbf{k}}), \quad (3.57)$$

where $\Theta_{\mathbf{k}}$ and $\varphi_{\mathbf{k}}$ define the orientation of the wave vector \mathbf{k} with respect to the z -axis; M_0 is the saturation magnetization. Note, that the latter equations are strictly valid for long thin samples only. Otherwise, one has to take into account demagnetization effects, which amount in an additional magnetic field $H_0 \rightarrow H_0 - N^z M_0$, where N^z is a demagnetization factor ([141], see also Ref. [14]).

Using the formalism of Holstein and Primakoff [115] the influence of the dipole-dipole interaction on the inelastic scattering of neutrons has been investigated by Elliott and Lowde [67] (see also [170]).

The neutron scattering cross section is proportional to the correlation function corresponding to the spin fluctuations (see e.g. Ref. [166,50]). If one considers N identical atoms with fixed positions one finds for the magnetic partial differential cross section for unpolarized neutrons in forward direction

$$\begin{aligned} \frac{d^2\sigma}{d\Omega dE'} &= \frac{k'}{k} \frac{N}{\hbar} r_0^2 |F(\mathbf{Q})|^2 \frac{1}{N} \sum_{l'l''} e^{i\mathbf{Q}\cdot(\mathbf{x}_l - \mathbf{x}_{l''})} \int_{-\infty}^{+\infty} \frac{dt}{2\pi} e^{-i\omega t} \langle S_l^T(t) S_{l''}^T(0) \rangle \\ &= \frac{k'}{k} \frac{N}{\hbar} r_0^2 |F(\mathbf{Q})|^2 S^T(\mathbf{Q}, \omega), \end{aligned} \quad (3.58)$$

where $S_l^\perp(t)$ is the component of the spin density perpendicular to the momentum transfer (scattering vector) $\mathbf{Q} = \mathbf{k} - \mathbf{k}'$, and $\hbar\omega$ is the neutron energy transfer. The length $r_0 = -5.391\text{fm}$ is analogous to the nuclear scattering length (see also chapter IV), and $F(\mathbf{Q})$ the magnetic form factor. We have also defined the transverse magnetic scattering function $S^T(\mathbf{Q}, \omega)$ by

$$S^T(\mathbf{Q}, \omega) = \left(\delta^{\alpha\beta} - \frac{Q^\alpha Q^\beta}{Q^2} \right) \int_{-\infty}^{+\infty} \frac{dt}{2\pi} e^{-i\omega t} \langle S_{-\mathbf{q}}^\alpha(t) S_{\mathbf{q}}^\beta(0) \rangle, \quad (3.59)$$

where $\mathbf{Q} = \mathbf{q} + \boldsymbol{\tau}$ with \mathbf{q} the wave vector of the magnon and $\boldsymbol{\tau}$ a reciprocal lattice vector.

The equations of motion, Eqs. 3.50 and 3.51, are diagonalized in terms of the Bose operators a and a^\dagger that satisfy

$$[a_{\mathbf{q}}, a_{\mathbf{q}'}^\dagger] = \delta_{\mathbf{q}\mathbf{q}'} \quad (3.60)$$

with

$$S_{\mathbf{q}}^+ = u_{\mathbf{q}} a_{\mathbf{q}} + v_{\mathbf{q}} a_{-\mathbf{q}}^\dagger. \quad (3.61)$$

A convenient choice for the coefficients $u_{\mathbf{q}}$ and $v_{\mathbf{q}}$ is [141,168]⁶.

$$u_{\mathbf{q}}^2 = (2SN)(A_{\mathbf{q}} + \epsilon_{\mathbf{q}})/2\epsilon_{\mathbf{q}} \quad (3.62)$$

$$v_{\mathbf{q}} = -u_{\mathbf{q}} B_{\mathbf{q}}^*/(A_{\mathbf{q}} + \epsilon_{\mathbf{q}}). \quad (3.63)$$

The contributions from single-spin-wave events to the dynamic structure factor was calculated by Elliot and Lowde [67,170]

$$S^T(\mathbf{Q}, \omega) = \frac{S}{2}(n_{\mathbf{q}} + 1) \left[\left(1 + \frac{(Q^z)^2}{Q^2} \right) \frac{A_{\mathbf{q}}}{\epsilon_{\mathbf{q}}} + \left(1 - \frac{(Q^z)^2}{Q^2} \right) \frac{|B_{\mathbf{q}}|}{\epsilon_{\mathbf{q}}} \cos[2(\varphi_{\mathbf{Q}} - \varphi_{\mathbf{q}})] \right] \delta(\omega + \epsilon_{\mathbf{q}}), \quad (3.64)$$

⁶Holstein and Primakoff [115] have ignored the phase relationship between $u_{\mathbf{q}}$ and $v_{\mathbf{q}}$, without which an incorrect expression for the scattering cross section between spin-waves and neutrons would be obtained. This error has been corrected by Lowde [67,170,141].

where $n_{\mathbf{q}}$ is the occupation number of the magnon oscillator with wave vector \mathbf{q} . The second term in the dynamic structure factor is due to the dipolar interaction. For zero dipolar interaction or for wave vectors larger than the dipolar wave vector q_D the dynamic structure factor reduces to a simple angular distribution proportional to $1 + (Q^z/Q)^2$. When dipolar effects become of importance, the angular dependence of the scattered intensity gets quite complicated.

More recently Lovesey et al. [168,254] have extended Lowde's analysis to scattering of polarized neutrons, and a discussion of the longitudinal cross section $\langle S_i^z S_{i'}^z \rangle$, which contains two-spin-wave scattering events. Furthermore, they analyze the static susceptibilities in the framework of linear spin-wave theory, correcting work by Toh and Gehring [252] who used the incorrect expressions for the coefficients $u_{\mathbf{q}}$ and $v_{\mathbf{q}}$ from Ref. [115].

As a first step beyond the spin-wave theories described above, Toperverg, and Yashenkin [253] have used the perturbation approach developed by Vaks, Larkin and Pikin [257], to investigate the frequency dependence of the uniform transverse and longitudinal susceptibilities ⁷. The applicability of their results is mainly restricted to low and intermediate temperatures. Their perturbation approach for the dipolar interaction breaks down not only close to the critical temperature, but also at any temperature for low frequencies. For this parameter regime a non perturbative approach like mode coupling theory is needed to account for the strong fluctuations. A first attempt towards such a theory has been made some time ago by Raghavan and Huber [227]. There are, however, several shortcomings in their approach. First of all, the static susceptibilities used in their analysis do not account for the coexistence anomalies and dipolar crossover properly. Instead the longitudinal susceptibility is taken of Ornstein-Zernike form $\chi_L \propto 1/(q^2 + \xi^{-2})$, which neglects dipolar crossover effects as well as the by now well known coexistence anomaly

⁷An excellent review on the theoretical and experimental work prior to 1984 was given by Maleev [179], with a particular emphasis on Green's function techniques.

$\chi_L \propto 1/q$ in the limit $q \rightarrow 0$. The expression used for the transverse susceptibility is valid in certain limits only. Furthermore, in the presence of dipolar interaction, for a general angle between the wave vector and the direction of the spontaneous magnetization, there are three and not just two non degenerate eigenvalues for the static susceptibility matrix. This fact has been neglected completely. Also, they didn't evaluate the complete functional form of the relaxation functions, but used instead a parametrisation, which is strictly valid in the hydrodynamic regime only, and calculated the corresponding parameters. Nevertheless, the theory seems to give a quite reasonable description of the data obtained by a neutron scattering study on *EuO* [207] in the range $q\xi \leq 1$ and $q_D\xi \leq 1$ for not too small values of the wave vector q . Beyond this range the approximate treatment of the dipolar interaction in Ref. [227] breaks down.

More recently Lovesey [169] reported on an approximative mode coupling approach for dipolar ferromagnets below T_c . Similar to Raghavan and Huber the spin wave dispersion relation used by Lovesey is applicable for not too small wave vectors only. The analysis in Ref. [169] is restricted to the exchange region $q_D\xi \leq 1$. This is due to the assumption made in Ref. [169], that the only non vanishing relaxation kernels are those for the spin fluctuations longitudinal and transverse to the direction of the spontaneous magnetization. Neglecting off-diagonal matrix elements excludes the applicability of the theory to the dipolar region. Note, that in the dipolar region close to T_c the memory function and the relaxation functions become – similar to the situation above T_c – diagonal in terms of the spin fluctuations longitudinal and transverse with respect to the wave vector and not to the spontaneous magnetization. Furthermore, the analysis in Ref. [169] is restricted to very small wave vectors. In this limit, however, the expressions for the static susceptibility and the spin-wave dispersion relation used in Ref. [169] are not valid, since they do not account for the presence of the subtle combined effects of Goldstone modes and dipolar anisotropy. Also, no self-consistent solution but only a first iteration of the mode coupling equations, based on neglecting the damping, is performed. In summary, a thorough mode coupling analysis of the effects of the dipolar interactions in the ferromagnetic phase is still a very challenging

theoretical problem and the topic of ongoing research [241].

D. Renormalization Group Theory of Time-Dependent Ginzburg-Landau Models in the Ferromagnetic Phase

The spin-wave theory, reviewed in the preceding section, is only a first step towards a more rigorous theory of the critical dynamics of dipolar ferromagnets below the Curie temperature. For a thorough understanding of the dynamics in the ferromagnetic phase a renormalization group theory or a mode coupling approach analogous to section III.B, which takes into account the effects of the critical fluctuations, would be necessary. A detailed analysis requires a treatment of a modified model J [112] appropriate for the dynamics of isotropic ferromagnets, where dipolar forces are included.

Recently, the effects of the dipolar interaction on the critical dynamics of the n -component time-dependent Ginzburg-Landau models (model A [112]) below the critical temperature have been studied within a generalized minimal subtraction scheme [251]. The corresponding Langevin equation of motion reads (Model A: $a = 0$; Model B: $a = 2$)

$$\frac{\partial \mathbf{S}(\mathbf{x}, t)}{\partial t} = -\lambda (i\nabla)^a \frac{\delta H[\{S^\alpha\}]}{\delta \mathbf{S}(\mathbf{x}, t)} + \zeta(\mathbf{x}, t), \quad (3.65)$$

where the stochastic forces are characterized by a Gaussian probability distribution function with zero mean and variance

$$\langle \zeta^\alpha(\mathbf{x}, t) \zeta^\beta(\mathbf{x}', t') \rangle = 2\lambda k_B T (i\nabla)^a \delta^{(3)}(\mathbf{x} - \mathbf{x}') \delta(t - t') \delta^{\alpha\beta}. \quad (3.66)$$

The Ginzburg-Landau effective free energy functional reads

$$H[\{S^\alpha\}] = \frac{1}{2} \int_q \left[\sum_{\alpha, \beta=1}^{\min(d, n)} \left[(r + q^2) P_{\alpha\beta}^T + (r + g + q^2) P_{\alpha\beta}^L \right] S^\alpha(\mathbf{q}) S^\beta(-\mathbf{q}) + \sum_{\alpha=\min(d, n)+1}^n S^\alpha(\mathbf{q}) S^\alpha(-\mathbf{q}) \right], \quad (3.67)$$

where the general situation $n \neq d$ is considered. Here $P_{\alpha\beta}^T = \delta^{\alpha\beta} - q^\alpha q^\beta / q^2$ and $P_{\alpha\beta}^L = q^\alpha q^\beta / q^2$ denote the transverse and longitudinal projection operator.

Those relaxational models neglect mode coupling terms resulting from the reversible motion of the spins in the local magnetic field. It is expected [251], however, that most of the conclusions based on the relaxational models will also hold for models with mode coupling terms.

As a consequence of the spontaneously broken symmetry there are $n - 1$ massless Goldstone modes in the ordered phase of ideally isotropic systems. These massless modes lead to infrared singularities (coexistence singularities) in certain correlation functions for *all* temperatures below T_c . Based on the analysis of the effects of the critical and Goldstone fluctuations for the $O(n)$ -symmetric time-dependent Ginzburg-Landau models [250], it has been investigated [251] how the coexistence anomalies are modified when dipolar forces or weak anisotropies are included. For later reference the coexistence anomalies of the isotropic relaxational models are collected in Table VI.

The analysis in Ref. [251] shows that the influence of the dipolar interaction on the coexistence singularities is quite subtle. Although the model explicitly breaks the $O(n)$ -symmetry, not all transverse modes lose their Goldstone character, but only their effective number is reduced by one. Hence, while for $n = 2$ a crossover to an asymptotically uncritical theory takes place, for $n \geq 3$ coexistence anomalies persist, governed by a dipolar coexistence fixed point [251].

Below T_c there are two preferred axes, the axis defined by the direction of the spontaneous magnetization and the axis defined by the wave vector \mathbf{q} . This leads to a complex structure of the correlation functions already on the harmonic level. It is quite remarkable, however, that a one-loop theory for the two-point cumulants becomes an exact representation in the ordered phase in the coexistence limit ($\mathbf{q} \rightarrow 0$ and $\omega \rightarrow 0$) [251].

For $n = d \geq 3$ it is found [251], that the power laws characteristic of the coexistence anomalies are *not* changed by the presence of the dipolar interaction. Hence the same power laws as in Table VI apply to the dipolar case also. It is also interesting to note that there is the following exact amplitude ratio of the longitudinal response function in the dipolar and the isotropic case:

$$\frac{\chi_L(\mathbf{q}, \omega)_{\text{dipolar}}}{\chi_L(\mathbf{q}, \omega)_{\text{isotropic}}} = \frac{n-2}{n-1}. \quad (3.68)$$

For $n = 3$ this universal amplitude ratio is $1/2$, in accord with the results of Pokrovsky [222] and Toh and Gehring [252], obtained in the framework of a spin-wave theory.

As is apparent from the value of the dipolar coexistence fixed point $u_{CD}^* = 6(4-d)/(n-2)$, the situation $n = 2$ requires a separate discussion. In this case there are no massless modes left, since the dipolar interaction reduces the number of Goldstone modes from $n-1$ to $n-2$. As a consequence the crossover below T_c is from a critical theory at T_c to a Gaussian theory, i.e. the fluctuations die out on leaving the critical region. A qualitative summary of the various crossover scenarios is given in Table VII [251].

TABLE IV. Coefficients in the Taylor expansion of $A_{\mathbf{q}}^{\alpha\beta}$ for three-dimensional cubic lattices, taken from [Aharony73a,Aharony73b]. c denotes the coordination number, v_a the volume of the primitive unit cell and α_i are lengths characterizing the dipolar interaction.

Lattice	sc	bcc	fcc
c	6	8	12
$v_a[a^3]$	1	$4/3\sqrt{3}$	$1/\sqrt{2}$
$\alpha_1[a]$	1.2755	1.7420	2.8313
$\alpha_2[a]$	0.1649	-0.321	-0.335
$\alpha_3[a]$	1.7700	0.8210	1.823

TABLE V. Asymptotic behavior of the scaling functions for the longitudinal and transverse Lorentzian line width in the paramagnetic phase. The different regions dipolar critical (DC), isotropic critical (IC), dipolar hydrodynamic (DH), and isotropic hydrodynamic (IH) are defined by DC: $y \gg 1, x \ll 1$; IC: $y \ll 1, x \ll 1$; DH: $y \gg x, x \gg 1$; IH: $y \ll x, x \gg 1$.

	γ^T	γ^L
DC	$y^{1/2}$	$y^{5/2}$
IC	1	1
DH	$y^{1/2}x^2$	$y^{5/2}$
IH	$x^{1/2}$	$x^{1/2}$

TABLE VI. Coexistence anomalies of the isotropic relaxational models for the longitudinal dynamic susceptibility $\chi_L(\mathbf{q}, \omega)$ and correlation function $G_L(\mathbf{q}, \omega)$.

	Model A	Model B
a	0	2
$\chi_L(\mathbf{q}, 0)$	$\propto q^{d-4}$	$\propto q^{d-4}$
$Re[\chi_L(0, \omega/q^a)]$	$\propto \omega^{(d-4)/2}$	$\propto (\omega/q^2)^{(d-4)/2}$
$G_L(0, \omega/q^a)$	$\propto \omega^{d/2-3}$	$\propto (\omega/q^2)^{d-4}$

TABLE VII. The influence of the dipolar interaction on the coexistence anomalies. The table summarizes the various crossover scenarios possible if the number of components n and the dimensionality d of space is varied.

	$d = 2 \quad d = 3$	$d = 4$
$n = 1$	Crossover to a Gaussian theory	as for $g = 0$
$n = 2$	Crossover to a Gaussian theory	no anomalies
$n \geq 3$	$u_{CD}^* = \frac{6(4-d)}{n-2} \rightarrow$ anomalies	logarithmic corrections

Figures captions:

Figure 3.1: Scaling function γ^T for the transverse width in Lorentzian approximation versus $r = 1/q\xi(1 + (q_D\xi)^2)^{1/2}$ and $\varphi = \arctan(q_D\xi)$.

Figure 3.2: Scaling function γ^L for the transverse width in Lorentzian approximation versus $r = 1/q\xi(1 + (q_D\xi)^2)^{1/2}$ and $\varphi = \arctan(q_D\xi)$.

Figure 3.3: Scaling function γ^T for the transverse width in Lorentzian approximation versus $1/q\xi$ for values of $\varphi = N\pi/20$ with N indicated in the graph.

Figure 3.4: Scaling function γ^L for the longitudinal width in Lorentzian approximation versus $1/q\xi$ for values of $\varphi = N\pi/20$ with N indicated in the graph.

Figure 3.5: Scaling functions for the transverse (solid) and the longitudinal (point-dashed) widths versus q/q_D in Lorentzian approximation at the critical temperature. **Inset:** Scaling functions for the transverse (solid) and the longitudinal (point-dashed) Onsager coefficients versus q/q_D at the critical temperature.

Figure 3.6: Scaling function of the transverse Kubo relaxation function $\phi^T(r, \varphi, \tau_T)$ at $\varphi = 1.49$ (close to the critical temperature) versus τ_T and $r = \sqrt{(q_D/q)^2 + (1/q\xi)^2}$.

Figure 3.7: Scaling function of the longitudinal Kubo relaxation function $\phi^L(r, \varphi, \tau_L)$ at $\varphi = 1.49$ (close to the critical temperature) versus τ_L and $r = \sqrt{(q_D/q)^2 + (1/q\xi)^2}$.

Figure 3.8: Scaling function of the longitudinal and transverse Kubo relaxation function $\phi^\alpha(r, \varphi, \tau_\alpha)$ versus τ_α for three different values of φ ($\varphi = 1.49, 1.294, 0.97$). In each graph the scaling function is shown for $r = 0$ (solid), $r = 1$ (dashed), and $r = 10$ (dot-dashed).

Figure 3.9: Scaling function of the transverse Kubo relaxation function $\phi^T(r, \varphi, \tau_T)$ at

$\varphi = 1.294$ versus τ_T and $r = \sqrt{(q_D/q)^2 + (1/q\xi)^2}$.

Figure 3.10: Scaling function of the longitudinal Kubo relaxation function $\phi^L(r, \varphi, \tau_L)$ at

$\varphi = 1.294$ versus τ_L and $r = \sqrt{(q_D/q)^2 + (1/q\xi)^2}$.

Figure 3.11: Scaling function of the transverse Kubo relaxation function $\phi^T(r, \varphi, \tau_T)$ at

$\varphi = 0.97$ versus τ_T and $r = \sqrt{(q_D/q)^2 + (1/q\xi)^2}$.

Figure 3.12: Scaling function of the longitudinal Kubo relaxation function $\phi^L(r, \varphi, \tau_L)$ at

$\varphi = 0.97$ versus τ_L and $r = \sqrt{(q_D/q)^2 + (1/q\xi)^2}$.

Figure 3.1: Scaling function γ^T for the transverse width in Lorentzian approximation versus $r = 1/q\xi(1 + (q_D\xi)^2)^{1/2}$ and $\varphi = \arctan(q_D\xi)$.

Figure 3.2: Scaling function γ^L for the transverse width in Lorentzian approximation versus $r = 1/q\xi(1 + (q_D\xi)^2)^{1/2}$ and $\varphi = \arctan(q_D\xi)$.

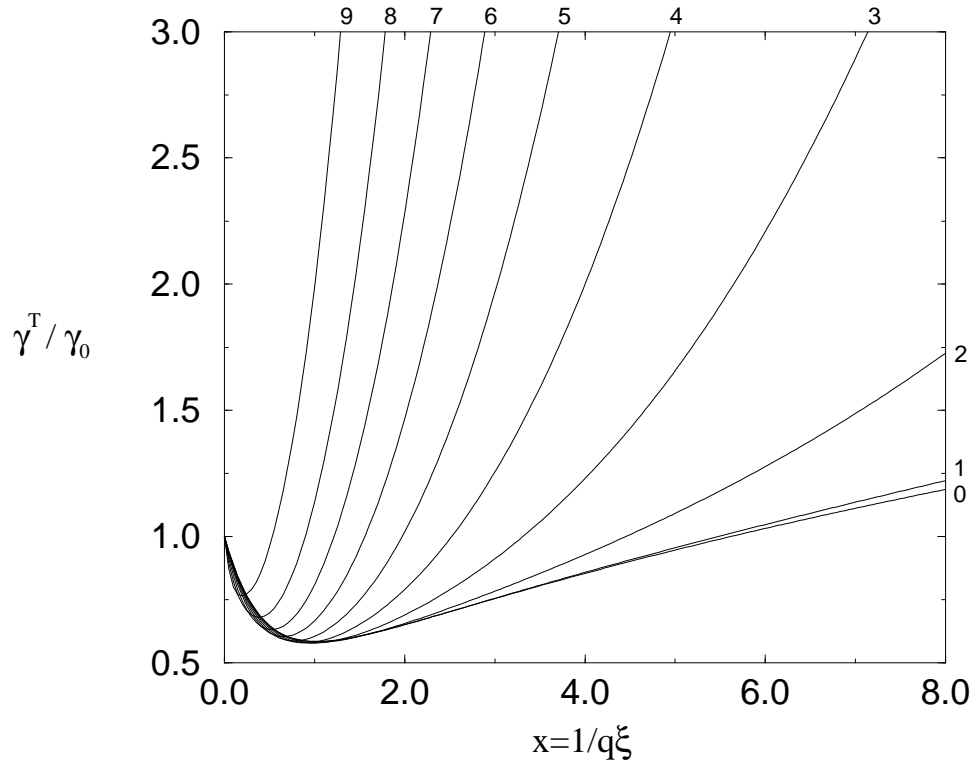


Figure 3.3: Scaling function γ^T for the transverse width in Lorentzian approximation versus $1/q\xi$ for values of $\varphi = N\pi/20$ with N indicated in the graph.

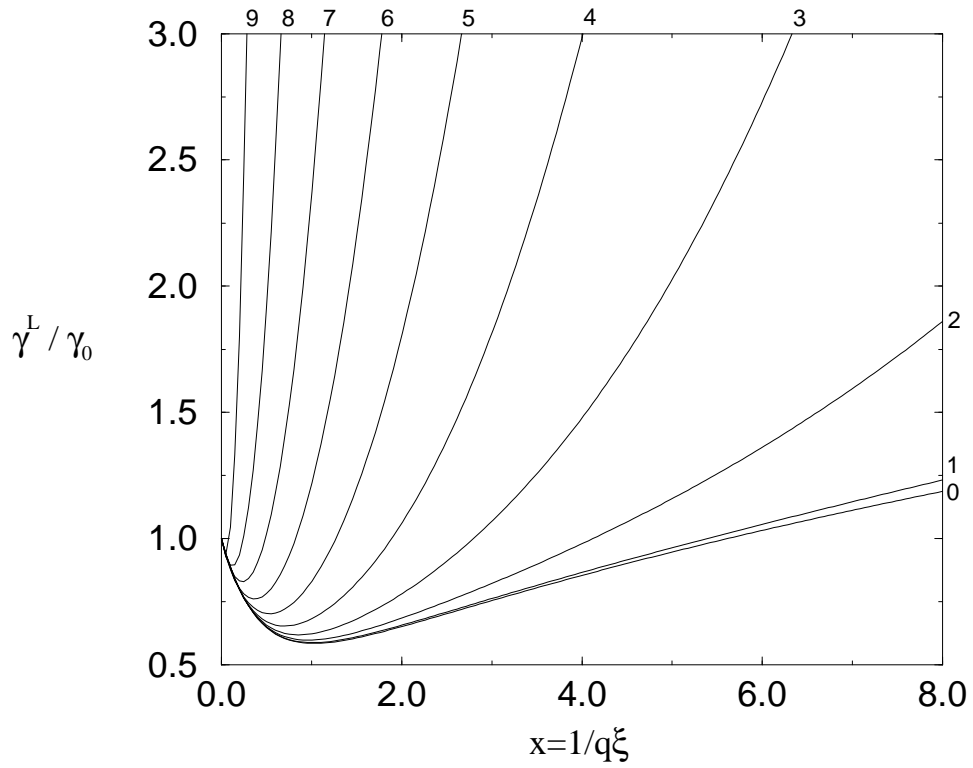


Figure 3.4: Scaling function γ^L for the longitudinal width in Lorentzian approximation versus $1/q\xi$ for values of $\varphi = N\pi/20$ with N indicated in the graph.

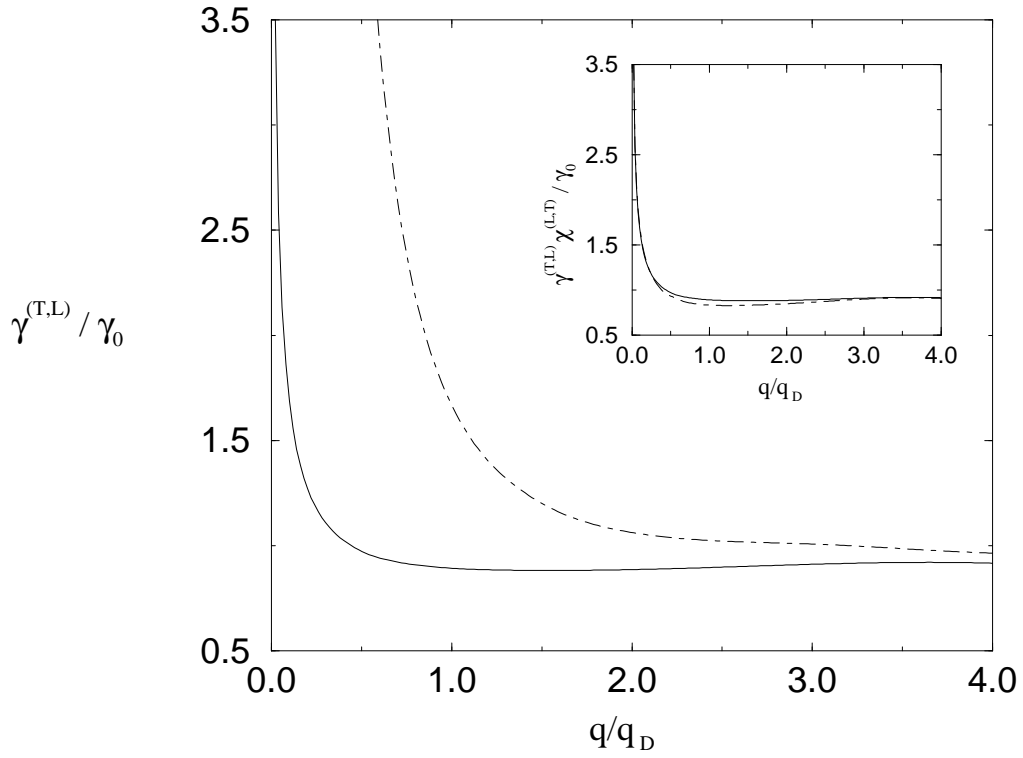


Figure 3.5: Scaling functions for the transverse (solid) and the longitudinal (point-dashed) widths versus q/q_D in Lorentzian approximation at the critical temperature. **Inset:** Scaling functions for the transverse (solid) and the longitudinal (point-dashed) Onsager coefficients versus q/q_D at the critical temperature.

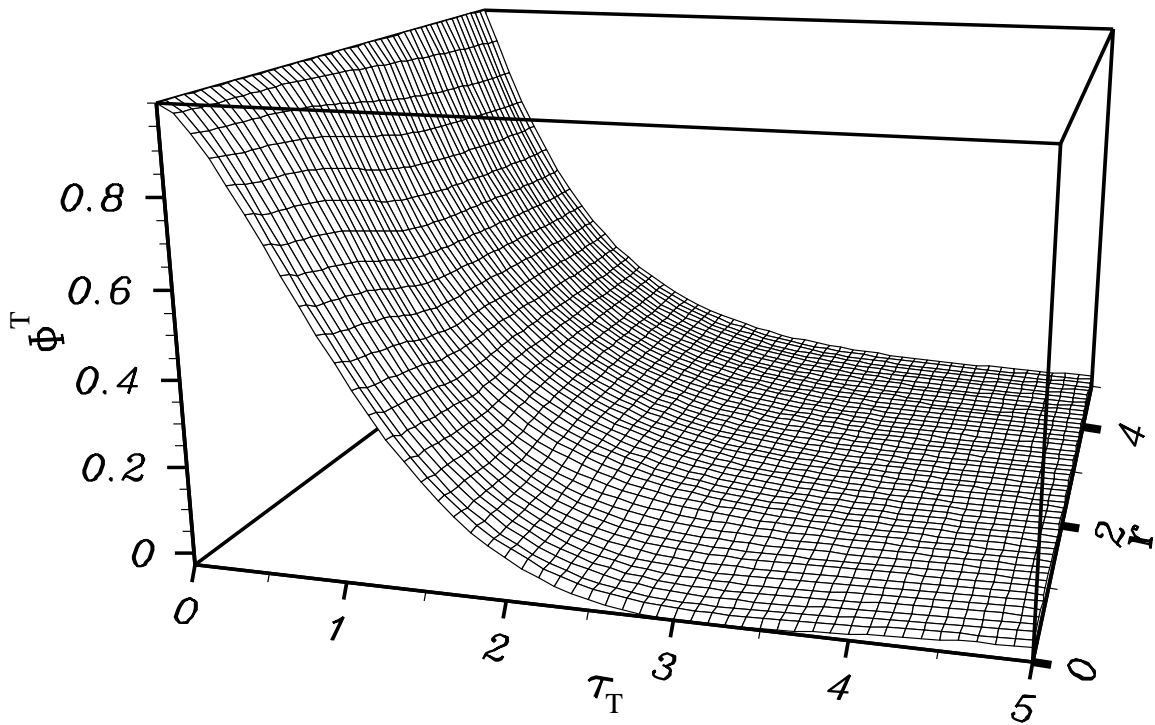


Figure 3.6: Scaling function of the transverse Kubo relaxation function $\phi^T(r, \varphi, \tau_T)$ at $\varphi = 1.49$ (close to the critical temperature) versus τ_T and $r = \sqrt{(q_D/q)^2 + (1/q\xi)^2}$.

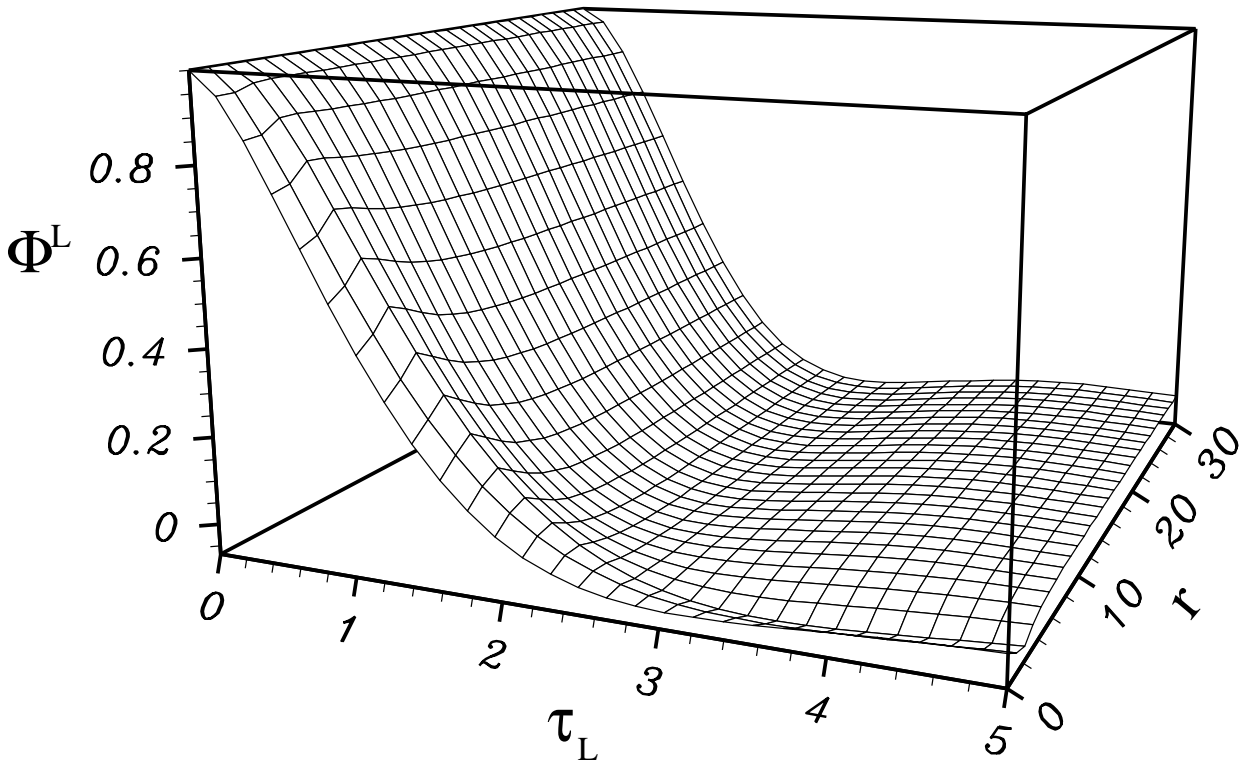


Figure 3.7: Scaling function of the longitudinal Kubo relaxation function $\phi^L(r, \varphi, \tau_L)$ at $\varphi = 1.49$ (close to the critical temperature) versus τ_L and $r = \sqrt{(q_D/q)^2 + (1/q\xi)^2}$.

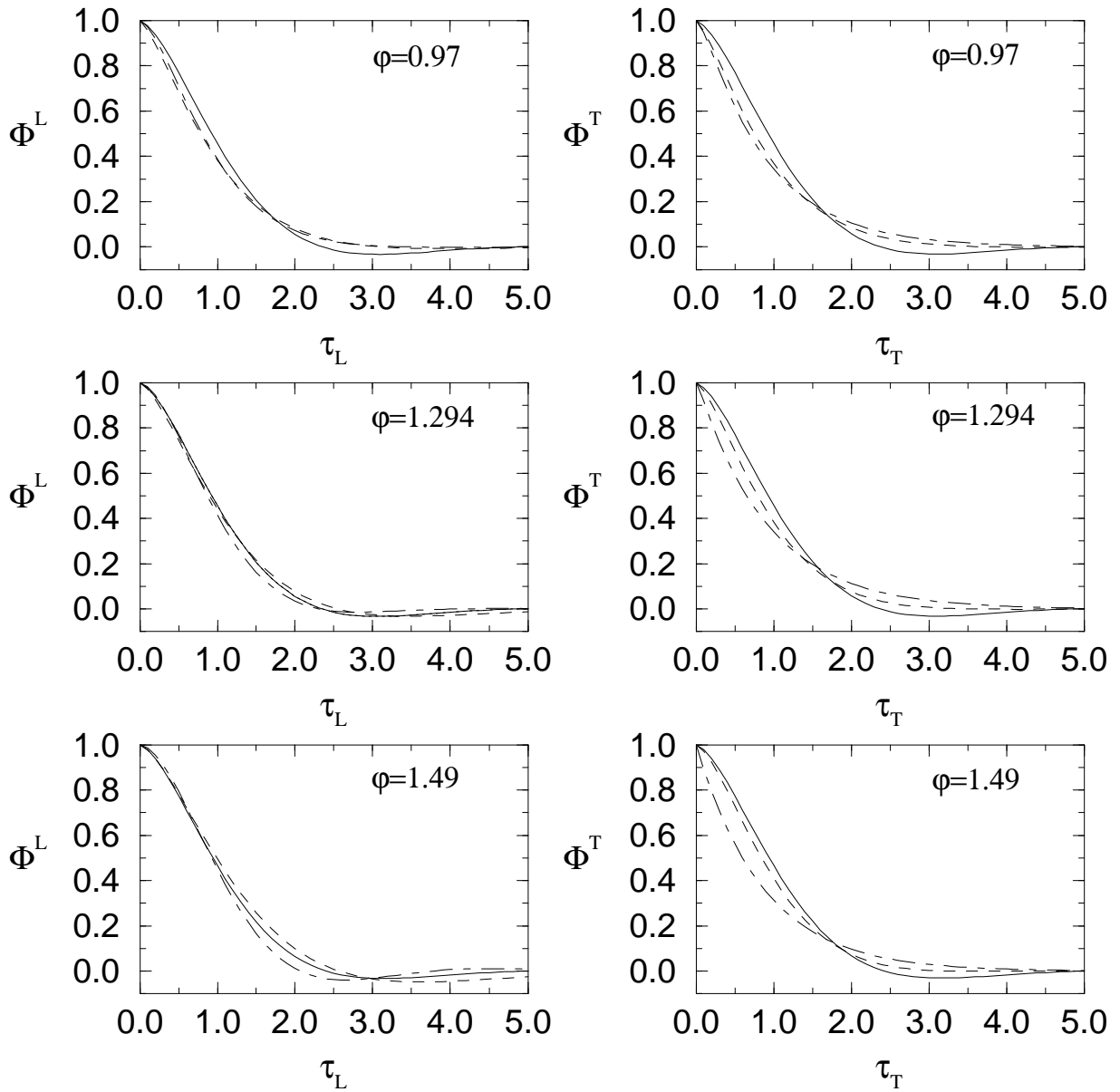


Figure 3.8: Scaling function of the longitudinal and transverse Kubo relaxation function $\phi^\alpha(r, \varphi, \tau_\alpha)$ versus τ_α for three different values of φ ($\varphi = 1.49, 1.294, 0.97$). In each graph the scaling function is shown for $r = 0$ (solid), $r = 1$ (dashed), and $r = 10$ (dot-dashed).

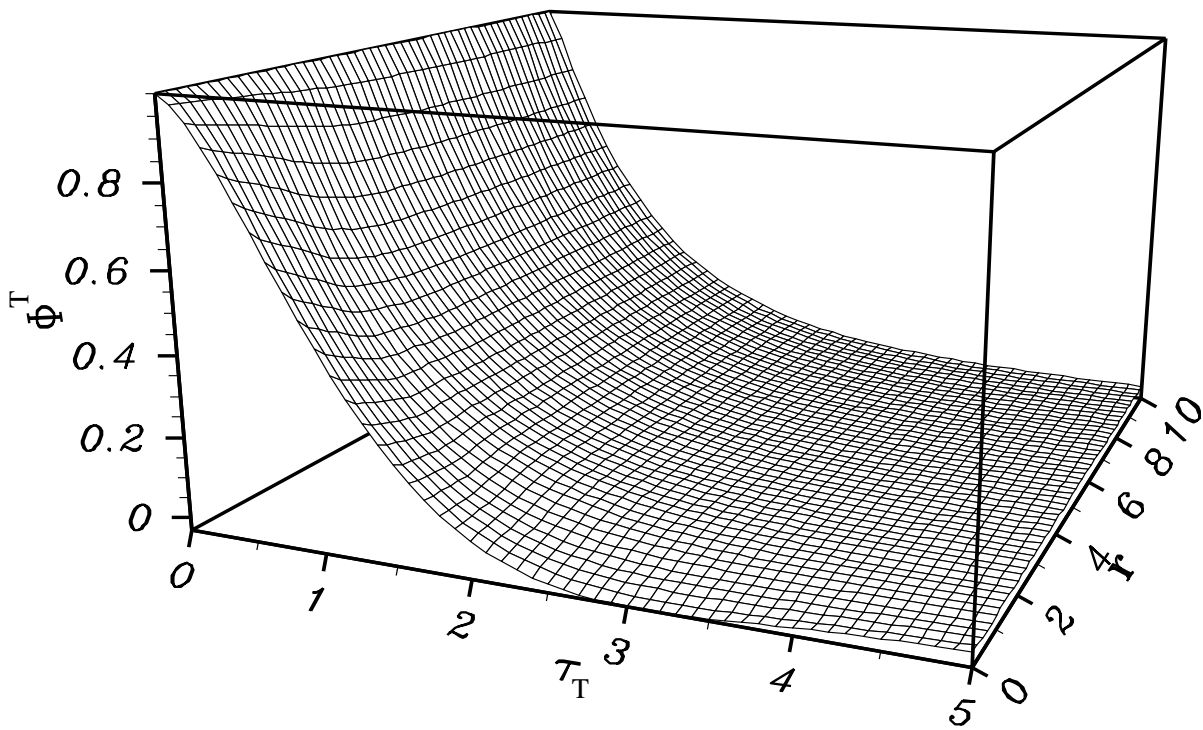


Figure 3.9: Scaling function of the transverse Kubo relaxation function $\phi^T(r, \varphi, \tau_T)$ at $\varphi = 1.294$ versus τ_T and $r = \sqrt{(q_D/q)^2 + (1/q\xi)^2}$.

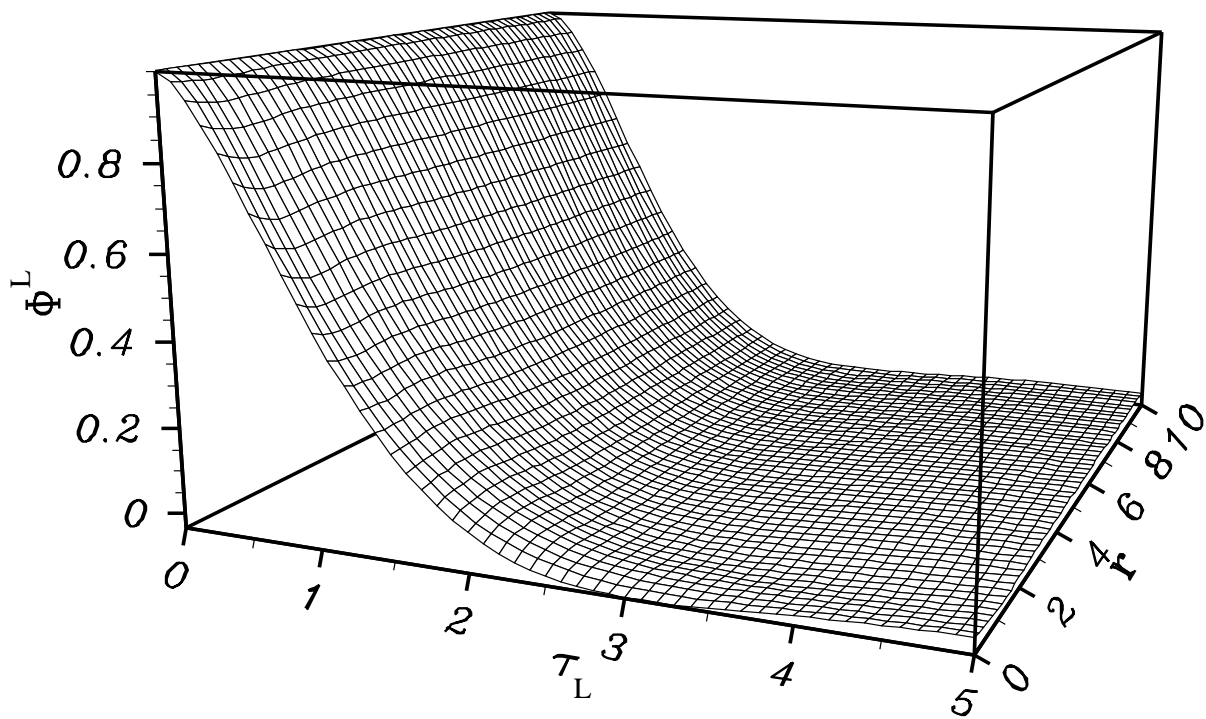


Figure 3.10: Scaling function of the longitudinal Kubo relaxation function $\phi^L(r, \varphi, \tau_L)$ at $\varphi = 1.294$ versus τ_L and $r = \sqrt{(q_D/q)^2 + (1/q\xi)^2}$.

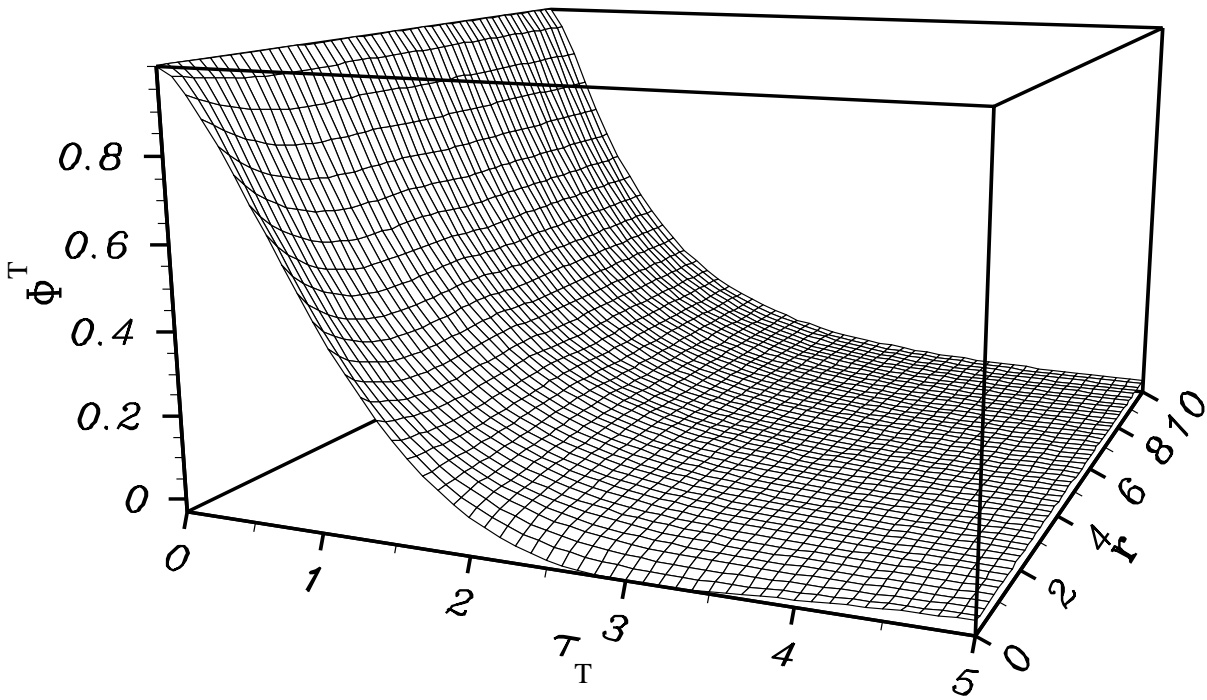


Figure 3.11: Scaling function of the transverse Kubo relaxation function $\phi^T(r, \varphi, \tau_T)$ at $\varphi = 0.97$ versus τ_T and $r = \sqrt{(q_D/q)^2 + (1/q\xi)^2}$.

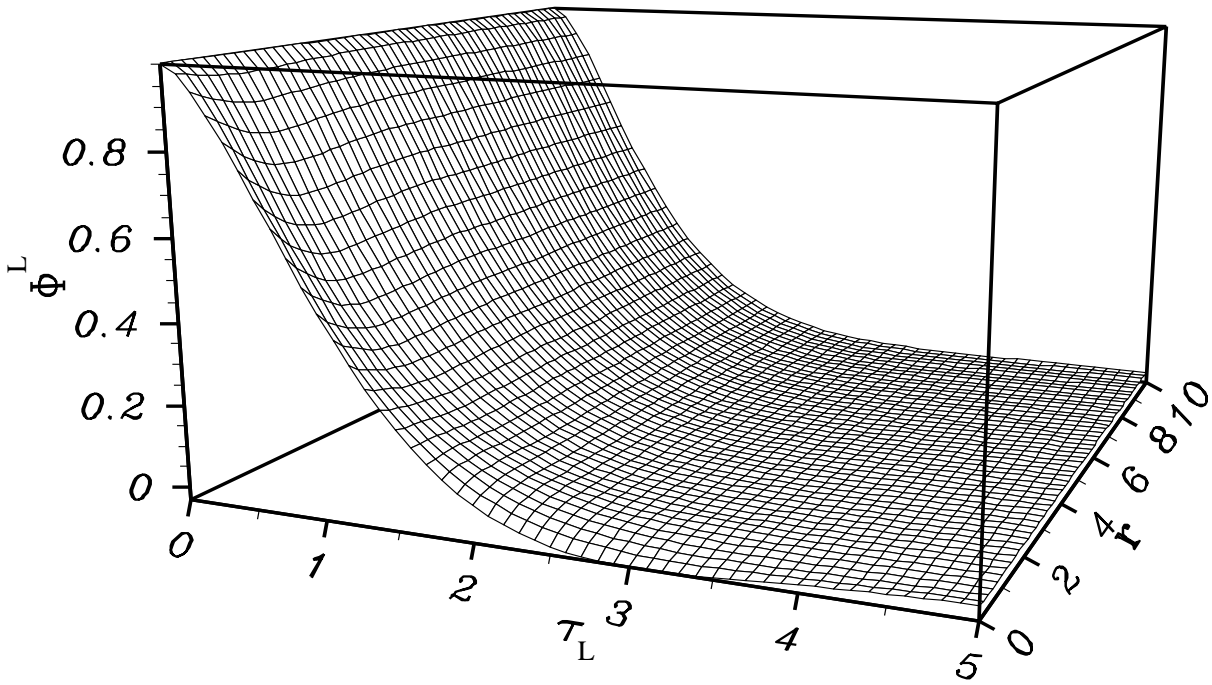


Figure 3.12: Scaling function of the longitudinal Kubo relaxation function $\phi^L(r, \varphi, \tau_L)$ at $\varphi = 0.97$ versus τ_L and $r = \sqrt{(q_D/q)^2 + (1/q\xi)^2}$.

IV. APPLICATION TO EXPERIMENTS

In this chapter we review the results from the numerical solution of the mode coupling equations for dipolar ferromagnets above the transition temperature and compare them with experiments. Furthermore we give a short account of the experimental data recorded below T_c and future theoretical developments.

There are several experimental techniques like neutron scattering (NS), electron spin resonance (ESR), magnetic relaxation (MR), hyperfine interaction (HFI) and muon spin resonance (μ SR) with various complementary characteristics: different wave vector range, short-range point-like probes in real space (HFI, μ SR) vs. probes in reciprocal space (NS, ESR, MR). The critical dynamics of isotropic ferromagnets such as *EuO*, *EuS*, *Fe*, *Ni* and many other materials have been studied by one or several of the above methods.

To emphasize the decisive role of the dipolar interaction we note that the experimental situation prior to the theoretical work in Refs. [79–81] was, however, puzzling in many ways. On the one hand, in hyperfine interaction experiments on *Fe* and *Ni* one observed a crossover in the dynamical critical exponent from $z = 5/2$ to $z = 2$ [228,95,113,114], i.e., a crossover to a dynamics with a non conserved order parameter. This was confirmed by electron spin resonance and magnetic relaxation experiments [147–150,64,152], where a non vanishing Onsager coefficient at zero wave vector was found. These results indicated that the critical dynamics of isotropic ferromagnets cannot be explained solely on the basis of the short range exchange interaction, which would lead to an exponent $z = 5/2$ for the whole wave vector range. However, on the other hand a critical exponent $z = 5/2$ was deduced from the wave vector dependence of the line width observed in neutron scattering experiments right at the critical temperature by three different experimental groups in Refs. [48,57], [188–192] and [264,28–30]. Nevertheless and even more puzzling, the data for the line widths above the transition temperature [188,189,31] could not be described by the Resibois-Piette scaling function resulting from a mode coupling (MC) theory [231] and a renormalization group (RG) theory [174,123], which take into account the short range exchange interaction only

(see chapter II).

Those apparent experimental discrepancies could be resolved by the mode coupling theory [79–81] described in chapter III, which on top of the exchange interaction takes into account the dipole-dipole interaction present in all real ferromagnets. The results of this theory are reviewed in the following and compared with the experimental data.

A. Neutron scattering

Inelastic neutron scattering has been used since decades to investigate the spin dynamics of magnetic systems providing information about the spin correlation function [48,194,208–210,57]. It has become one of the most important experimental techniques for studying the properties of condensed matter systems.

The cross section for magnetic inelastic scattering of polarized neutrons (with polarization \mathbf{P}) is given by [181,166]

$$\begin{aligned} \frac{d^2\sigma}{d\Omega dE'} &= r_0^2 \frac{k'}{k} \sum_{l,d} \sum_{l',d'} e^{i\mathbf{Q}\cdot(\mathbf{R}_{l,d}-\mathbf{R}_{l',d'})} \frac{1}{2} g_d F_d^*(\mathbf{Q}) \frac{1}{2} g_{d'} F_{d'}^*(\mathbf{Q}) \\ &\times \frac{1}{2\pi\hbar} \int_{-\infty}^{\infty} dt e^{-i\omega t} \left[\langle \mathbf{S}_{l,d}^\perp \cdot \mathbf{S}_{l',d'}^\perp(t) \rangle + i\mathbf{P} \cdot \langle \mathbf{S}_{l,d}^\perp \times \mathbf{S}_{l',d'}^\perp(t) \rangle \right], \end{aligned} \quad (4.1)$$

where the spin fluctuations transverse to the neutron wave vector transfer (scattering vector) $\mathbf{Q} = \mathbf{k} - \mathbf{k}'$ are defined by $\mathbf{S}_{l,d}^\perp = \mathbf{Q} \times [\mathbf{S}_{l,d} \times \mathbf{Q}] / Q^2$. $\mathbf{R}_{l,d} = \mathbf{l} + \mathbf{d}$ denotes the position vector of a nucleus in a rigid lattice, where \mathbf{d} is the site of the nucleus (with a gyromagnetic ratio g_d and a form factor $F_d(\mathbf{Q})$ within the unit cell \mathbf{l}). The quantity $r_0 = -0.5391 \text{ fm}$ is a useful unit for the magnetic scattering length.

In neutron scattering experiments using unpolarized neutrons one measures the transverse scattering function $S^T(\mathbf{Q}, \omega)$

$$S^T(\mathbf{Q}, \omega) \propto \left(\delta^{\alpha\beta} - \frac{Q^\alpha Q^\beta}{Q^2} \right) \langle S_{\mathbf{q}}^\alpha(\omega) S_{-\mathbf{q}}^\beta(-\omega) \rangle, \quad (4.2)$$

where \mathbf{q} denotes the neutron wave vector transfer with respect to the nearest reciprocal lattice vector $\boldsymbol{\tau}$, i.e. the scattering vector reads $\mathbf{Q} = \mathbf{q} + \boldsymbol{\tau}$. Eq. (4.2) implies that only spin

fluctuations transverse to the neutron wave vector transfer \mathbf{q} can be measured in the forward direction, where $\boldsymbol{\tau} = \mathbf{0}$. In order to measure the longitudinal fluctuations one has to go to a finite Bragg peak $\boldsymbol{\tau}$ with \mathbf{q} perpendicular to $\mathbf{Q} \approx \boldsymbol{\tau}$. The separation of the longitudinal and transverse spin fluctuations can be achieved by using a polarized neutron beam. A typical scattering geometry is shown in Fig. 4.1, where the polarization \mathbf{P} is defined by a small guide field \mathbf{H}_v . For more details on neutron scattering using polarized neutrons we refer the reader to the books by Marshall and Lovesey [181], Williams [268] and Lovesey [166].

Recent advances in high resolution neutron scattering techniques, like e.g. the Neutron Spin Echo (NSE) technique [187], have allowed to extend the early studies to critical fluctuations of substantially larger wavelengths and even made it possible to distinguish between different line shapes [190].

In this subsection we compare the results of mode coupling theory with neutron scattering data on *EuO*, *EuS* and *Fe*. For a quantitative comparison we need several material parameters (non-universal quantities) like the magnitude of the Brillouin zone boundary, exchange constant, etc. (see Table VIII).

1. Shape crossover

Due to the recent advances in high resolution neutron scattering techniques it became possible to resolve not only the width but also the shape of the spin correlation functions. This progress made it possible to test the predictions for the line shape from MC-theory [262,118] and RG-theory [61,22], which take into account solely the short-range exchange interaction. The latter theories for the critical dynamics were expected to fit the experimental data in an increasing quantitative way as one was able to measure the correlation functions at smaller and smaller wave vectors, since the influence of additional irrelevant interactions should diminish as one moves closer to criticality. It came as quite a surprise when Mezei found a nearly exponential decay of the Kubo relaxation function by spin echo experiments on *EuO* at $q = 0.024\text{\AA}^{-1}$ and $T = T_c$ [190], which was in drastic disagreement

with the bell-like shape predicted [262,118,61,22].

Actually – in contrast to the expectation – only at larger wave vectors the RG- and MC-calculations, taking into account exchange interaction only, were in accord with the experiment. This was shown by a comparison [77] of the shape of the RG-theory [61,22] with the heuristic shape of Ref. [77]. Also, a discrete version of the MC-theory gives quite reasonable an agreement with experiment for large wave vectors close to the Brillouin zone boundary [53,54].

In order to explain the anomalous exponential decay found by Mezei [190], it was asserted in Refs. [167,15] that neither MC- nor RG-theory is valid in the time regime probed by Mezei's [190] experiments. To fit the experimental results a “hybrid theory” [15] was proposed, which is a phenomenological interpolation scheme between the short and long time limits. In contrast it was shown on the basis of a mode coupling theory [82,85], which take into account the effects of the long-range dipolar interaction between the spins, that the experimental data can be explained quite naturally without any need of a special treatment of the short-time behavior. The results of this mode coupling analysis will be reviewed in this subsection.

We have seen in chapter III that the dynamic crossover in the *line width* sets in at wave vectors one order of magnitude smaller than found in the static susceptibility. Here we consider the *shape* crossover, i.e., changes in the functional form of the spin correlation function. From the solution of the dipolar MC-equations one finds the following scenario for the shape crossover.

- In the immediate vicinity of the critical temperature the *transverse* relaxation function shows a nearly *exponential decay* in time for wave vectors smaller than the dipolar wave vector q_D . Passing to wave vectors larger than q_D there is a shape crossover to a Hubbard-Wegner shape [118,262] corresponding to the isotropic Heisenberg fixed point (see chapter II). This shape crossover takes place close to the dipolar wave vector q_D in remarkable contrast to the crossover in the line width which sets in at wave vectors

almost one order of magnitude smaller.

- For wave vectors smaller than q_D and for temperatures in the intermediate vicinity of the critical temperature the *longitudinal* Kubo relaxation function exhibits a Gaussian decay at small times and damped oscillations for larger times. This shape is quite different from the exponential decay found for the transverse scaling function. Passing to larger wave vectors the shapes of the transverse and longitudinal relaxation functions become identical (Hubbard–Wegner shape).
- For temperatures well separated from the critical temperature (i.e. for temperatures where the correlation length becomes less than the typical dipolar length scale q_D^{-1} : $q_D \xi \leq 1$) the shape of the transverse and longitudinal relaxation becomes identical. Upon passing from small to large wave vectors both relaxation functions show a crossover from a hydrodynamic shape, which is nearly exponential, to the bell like Hubbard–Wegner shape.

In order to be specific and in view of spin echo experiments on *EuO* above T_c [192,193] we have displayed the Kubo relaxation function versus time for a set of wave vectors ($q = 0.018\text{\AA}^{-1}$, 0.025\AA^{-1} , 0.036\AA^{-1} , 0.071\AA^{-1} , 0.150\AA^{-1}) in Figs. 4.2-5. In Figs. 4.2 and 4.3 these are plotted versus the scaled time variables τ_α for a temperature in the immediate vicinity of T_c ($T = T_c + 0.25K$) and in Figs. 4.4 and 4.5 for a temperature $T = T_c + 8K$ well separated from T_c . For wave vectors $q \ll q_D = 0.147\text{\AA}^{-1}$ one can infer from Fig. 4.2 that the transverse scaling function decays nearly exponentially in time. This implies a Lorentzian like shape for the frequency dependent relaxation function for $q \ll q_D$ (solid line in Fig. 4.2). For larger wave vectors, $q \geq q_D$, the curves look similar to Gaussians for small times and oscillate for larger times, $\tau_T \geq 3$ (see point–dashed curve in Fig. 4.2). The oscillations of the longitudinal relaxation function (Fig. 4.3) leads to the side peaks in Fig. 4.9, where the longitudinal correlation function is plotted versus frequency for a fixed wave vector.

Further away from T_c the line shape crossover of the transverse relaxation function is much less pronounced and the shape resembles more a Gaussian even for wave vectors

much smaller than q_D . In Figs. 4.4 and 4.5 the transverse and longitudinal Kubo functions are shown for the same wave vectors as in Figs. 4.2 and 4.3 at $T = T_c + 8K$. For this temperature the shape of the longitudinal and transverse Kubo function is nearly the same (compare Figs. 4.4 and 4.5). This is precisely what one would have expected, because the influence of the dipolar forces decreases with separation from the critical point and then there is no difference any more between longitudinal and transverse modes.

To single out the line shape crossover the appropriate time scales are τ_α of Eq. 3.39 used in Figs. 4.2-5. On the other hand, for comparison with experiments it may be more convenient to present the transverse Kubo relaxation function versus the time scale $\tau' = \Lambda_{\text{lor}} q^{5/2} t$. Such plots are exhibited in Fig. 4.6 for $T = T_c$ and the wave vectors $q = 0.018 \text{\AA}^{-1}, 0.036 \text{\AA}^{-1}, 0.150 \text{\AA}^{-1}, 0.3 \text{\AA}^{-1}$ and in Fig. 4.7 for $T = T_c + 0.5K$ and $q = 0.018 \text{\AA}^{-1}, 0.025 \text{\AA}^{-1}, 0.036 \text{\AA}^{-1}, 0.071 \text{\AA}^{-1}$.

At $T = T_c$ triple-axis spectrometer scans at $q \geq 0.15 \text{\AA}^{-1}$ [193] show non-Lorentzian line shapes in agreement with predictions based on models with short range exchange interaction only and in agreement with the above MC result. Neutron Spin Echo (NSE) studies at much smaller wave vectors [190,193] lead to Lorentzian line shapes in agreement with the above crossover scenario for dipolar ferromagnets. In Fig. 4.8 data from NSE studies [190] on *EuO* right at the critical temperature are shown for the transverse Kubo relaxation function at the wave vector $q = 0.024 \text{\AA}^{-1}$ (solid line) versus time in *nsec*. We have used the theoretical value for the non universal scale $\Lambda = 7.1/5.1326 \text{ meV } \text{\AA}^{5/2}$ (see Table VIII). There is an excellent agreement with the experimental data for $t \leq 1 \text{ nsec}$. The experimental data are above the theoretical curve for $t \geq 1 \text{ nsec}$. This may be due to finite collimation effects in this time domain, as noted by Mezei [190]. To substantiate this point we have also plotted in Fig. 4.8 the relaxation function at $q = 0.028 \text{\AA}^{-1}$ (point-dashed curve), which is significantly higher than the curve for $q = 0.024 \text{\AA}^{-1}$ for $t \geq 1 \text{ nsec}$. The fairly large difference of the curves with $q = 0.024 \text{\AA}^{-1}$ and $q = 0.028 \text{\AA}^{-1}$ is implied by the close proximity to the crossover region.

In order to exhibit the difference from the MC theory including only short range exchange interaction the dashed curve in Fig. 4.8 shows the solution of Eqs. 3.40 and 3.41 for this

special case, i.e., $y = 0$, $x = 0$ and $\rho_{\text{cut}} = q_{\text{BZ}}/q$ with $q = 0.024 \text{ \AA}^{-1}$. The result differs drastically from the actual line shape including the long-range dipolar interaction. It is important to realize, that the crossover in the line shape starts nearly at q_D , whereas the line width still scales with the isotropic critical dynamic exponent $z = 5/2$ in this wave vector region.

Very recently the theoretical predictions concerning the line shape of the longitudinal relaxation function [82,85] have been verified experimentally [33,93]. Fig. 4.9 shows the longitudinal Kubo relaxation function for *EuS* at $T = 1.006T_c$ and $q = 0.19 \text{ \AA}^{-1}$. The normalized experimental data de-convoluted by a maximum entropy method agree quite well with the theoretical prediction (solid line). Especially the double peak structure corresponding to the over-damped oscillations in time are observed.

2. Line width crossover

From the frequency and wave vector dependent Kubo relaxation function one can define a characteristic line width by the half width at half maximum (HWHM)

$$\text{Re} [\Phi^\alpha(\omega = \Gamma_{\text{HW}}^\alpha)] = \frac{1}{2} \text{Re} [\Phi(\omega = 0)] , \quad (4.3)$$

which obeys the scaling law

$$\Gamma_{\text{HW}}^\alpha(q) = \Lambda_{\text{HW}} q^z \gamma_{\text{HW}}^\alpha(x, y) . \quad (4.4)$$

Let us start by comparing the theoretical and experimental line widths for *Fe*, *EuO* and *EuS* precisely at the critical temperature. Fig. 4.10 shows the scaling functions for the transverse and longitudinal line width in the Lorentzian approximation, normalized such that the line width approaches 1 for $q \gg q_D$. As already noted earlier, a remarkable result of mode coupling theory is that the dynamic dipolar crossover of the longitudinal line width starts near the dipolar wave vector $q \approx q_D$, whereas for the transverse line width it is shifted to a wave vector which is about one order of magnitude smaller than q_D . This explains

why no appreciable deviation from the exchange scaling prediction $\Gamma^T(q) \propto q^{5/2}$ in the wave vector range accessible up to now was found in Refs. [48,57], [188–192] and [264,28–30] in neutron scattering experiments right at the critical temperature. The experimental data in Fig. 4.10 are collected from Refs. [48,57], [188–192] and [264,28–30] and are normalized with respect to the theoretical value of the non-universal frequency scale $\Lambda_{\text{lor}} = 5.1326 \times \Lambda$. For a comparison the solid line in Fig. 4.10 shows the scaling function of the transverse line width as it has been obtained from the solution of the complete mode coupling equations [82,85]. Whereas the general functional form is quite similar to the scaling function obtained in the Lorentzian approximation, their asymptotic values at large values differ by a factor of approximately 1.2, which leads to an even better quantitative agreement between theory and experiment. It still needs experiments at smaller momentum transfer to detect the increasing of Γ because of the crossover to the dipolar regime.

In contrast to the data on the wave vector dependence right at the critical temperature, experiments on the scaling function above the critical temperature revealed huge deviations from the Resibois-Piette scaling function, as is evident from the neutron scattering data on *Fe* [188] shown in the scaling plot in Fig. 4.11, which become the more pronounced the closer to T_c .

This figure also shows a comparison of the HWHM (dashed-dotted line) of the transverse Kubo functions resulting from Eqs. 3.40 and 3.41 and the Lorentzian line width γ_{lor}^T (solid line) determined by Eq. 3.49. In the case of *Fe* curves a, b, c and d correspond to the temperatures $T - T_c = 1.4K, 5.8K, 21.0K, \text{ and } 51.0K$. All curves are normalized with respect to their value at criticality. This implies that the non universal frequency scale is then found to be $\Lambda_{\text{lor}} = 5.1326 \Lambda = 107.2 \text{ meV } \text{\AA}^{5/2}$ in the Lorentzian approximation and $\Lambda_{\text{HW}} = 1.37 \times \Lambda_{\text{lor}} = 147 \text{ meV } \text{\AA}^{5/2}$ for the HWHM. The latter value is in quite reasonable agreement with the experimental value $\Lambda_{\text{exp}} = 130 \text{ meV } \text{\AA}^{5/2}$. The Lorentzian line width and the HWHM have nearly the same $(q\xi)^{-1}$ -dependence. Especially for small wave vectors the difference comes about only because of the different non universal frequency scales. In

summary, the line width is affected by the line shape crossover only to a minor extent, since the former is only a coarse feature of the relaxation function. At small wave vectors only the non-universal scale is modified. This allows one to use the Lorentzian approximation for some later applications of the theory to NS, ESR, MR, and HFI experiments.

As can be inferred from Fig. 4.11 the complete solution of the mode coupling theory is in reasonable agreement with the experiment close to T_c ($T - T_c = 1.4K, 5.8K$) and gives an improvement over the Lorentzian approximation. The minor differences may be due to the following reasons. (i) As mentioned above the measured scaling functions of the transverse relaxation function were fitted to an exponential line, which is not the correct shape. (ii) Because the dipolar crossover temperature T_D of Fe is $8.6K$, static crossover effects not taken into account in the experiments may cause some changes. Furthermore the non universal scale of the correlation length ξ_0 is affected by experimental uncertainties. A change in ξ_0 would lead to a horizontal shift of the data points in Fig. 4.11.

Larger differences show up for temperatures further away from T_c ($T - T_c = 21K, 51K$), which cannot be accounted for by the shape crossover or static crossover effects. Here the measured line widths are larger than the theoretical. In order to explain this, it is necessary to take into account the van Hove terms and further relaxation mechanisms due to irrelevant interactions. Such irrelevant interactions are unimportant as concerns the critical behavior, but nevertheless may play an important role for temperatures well separated from T_c (see Ref. [85]). Pseudo-dipolar forces have been studied in Refs. [85] and Ref. [3]. Those additional interactions (crystal field interactions, the spin orbit interaction leading to pseudo-dipolar terms) are presumably less important in magnets with localized moments such as EuO and EuS . This can be seen from the comparison of the line width with the experimental data. Fig. 4.12 (Fig. 1 from Ref. [193], and Fig. 1 from Ref. [192]) shows a scaling plot of the transverse line width data for temperatures $T - T_c = 0.5K, 2K$, and $4K$ in EuO , which are in quantitative agreement with the mode coupling theory (solid lines).

Recently the transverse and for the first time the longitudinal spin fluctuations have been measured on EuS using inelastic scattering of polarized neutrons [33,93]. The observed re-

laxation rates follow rather precisely the *transverse* and *longitudinal* line width calculated from the dipolar mode coupling theory (see Figs. 4.13 and 4.14). Especially, these measurements confirm the behavior of the longitudinal line width predicted by mode coupling theory [80,81].

3. Constant energy scans

In this subsection we return to an analysis of the line shape and review results obtained by scans at constant frequency as opposed to constant wave vector in the previous sections. As will become clear in the following, certain features of the line shape of the correlation function can be accentuated by constant energy scans for the scattering function $S^T(q, \omega)$. Characteristic quantities in these scans are the peak position q_0 and the HWHM Δq . For an isotropic Heisenberg ferromagnet RG-theory predicts a flat curve for the reduced peak positions $q_0(\Lambda/\omega)^{2/5}$ plotted versus the scaled frequency $\omega\xi^{5/2}/\Lambda$ [123,78]. This theoretical result has been confirmed experimentally in certain energy and wave vector regions [29]. However, more recently Böni et al. [31] have found pronounced departures from the isotropic scaling law in *EuS* in a region, where according to Refs. [80,81] the dipolar interaction should have a considerable effect on the dynamics. This is quite similar to the situation in constant wave vector scans, where one finds deviations from the Resibois-Piette scaling function [188,189].

One of the most striking new features introduced by the dipolar interaction is the generalized dynamical scaling Eq. (3.31) with the additional scaling variable $y = q_D/q$. In conventional constant q scans plotted versus the scaling variable $x = 1/q\xi$ the line widths are not represented by a single scaling function but by a series of curves as exhibited in Figs. 3.1 and 3.2., where each curve corresponds to a fixed temperature. The failure of the isotropic scaling law in constant energy scans can also be attributed to the influence of the dipolar forces [82,85].

The generalized scaling law for the Kubo functions and characteristic frequencies leads

to the following scaling law for the peak position in constant energy scans [85]

$$q_0 \left(\frac{\Lambda}{\omega} \right)^{2/5} = \mathcal{Q} \left(\varphi, \frac{\omega}{\Lambda (\xi^{-2} + q_D^2)^{z/2}} \right). \quad (4.5)$$

From the above generalized scaling laws it becomes obvious that one obtains a set of curves parameterized by the scaling variable $\varphi = \arctan(q_D \xi)$, if Eq. (4.5) containing the two parameter scaling function \mathcal{Q} is plotted versus $\omega \xi^{5/2} / \Lambda$. In Fig. 4.15 the scaled peak position $q_0 (\Lambda_{\text{lor}} / \omega)^{2/5}$ is plotted versus $\hat{\omega} = \omega \xi^{5/2} / \Lambda_{\text{lor}}$ for the following set of scaling variables $\varphi =$ a) 1.490, b) 1.294, c) 0.970 and d) $\varphi = 0$. Case d) corresponds to an isotropic ferromagnet, i.e., $q_D = 0$. Λ_{lor} is related to Λ by $\Lambda_{\text{lor}} = 5.1326\Lambda$. The above values for φ correspond in the case of *EuS* ($q_D = 0.27\text{\AA}^{-1}$, $\xi_0 = 1.81\text{\AA}$) to the temperatures $T =$ a) $1.01T_c$, b) $1.06T_c$, and c) $1.21T_c$. Due to the generalized scaling law Eq. (4.5) the curves coincide with the isotropic theory for high frequency but deviate for small frequency. The frequency, where the deviation from the isotropic result sets in, increases upon approaching the critical temperature.

The steep drop off of the scaled peak positions at particular φ dependent values of $\hat{\omega}$ has been explained as follows [85]. The dipolar forces imply that the order parameter is no more conserved and the uniform relaxation rate Γ_0 becomes finite. Hence the scattering function $S^T(q, \omega)$ remains finite for vanishing wave vector

$$S^T(q = 0, \omega) \propto \frac{\Gamma_0 \xi^2}{\omega^2 + \Gamma_0^2} \quad \text{for } T \geq T_c \quad . \quad (4.6)$$

Since Γ_0 is proportional to ξ^{-2} Eq. (4.6) reduces to

$$S^T(q = 0, \omega) \propto \frac{1}{\omega^2} \quad \text{for } T = T_c \quad . \quad (4.7)$$

Therefore, the maximum of the constant energy scan at $q = 0$ increases strongly with decreasing frequency ω , whereas the local maximum at finite q is shifted to smaller q (see also the inset in Fig. 4.15). As a result of this competition only the maximum at $q = 0$ survives for low frequencies. In order to substantiate this, typical constant energy scans are shown in the inset of Fig. 4.15, where $S^T(q, \omega) / S^T(0, \omega)$ (in arbitrary units) is plotted versus $1/r$ for

$\varphi = 1.294$ and for a set of scaled frequencies ($\hat{\omega} = 10^{L/10}$ with $L = 8, 10, 12, 14, 16$ indicated in the graph). The corresponding scaled peak positions are indicated in the scaling plot by crosses. This behavior explains, why the scaled peak positions for dipolar ferromagnets show such a steep drop off at small frequencies.

Finally, it is important to note that the characteristic deviations from the isotropic theory exhibited in Fig. 4.15 result from the crossover in the time scale and not so much from the crossover in the shape function. This can be inferred from Fig. 4.16 where the scaled peak positions $q_0 \left(\frac{\Delta}{\omega}\right)^{2/5}$ in Lorentzian approximation is shown. Compared to Fig. 4.15 the maxima are overemphasized in Fig. 4.16, but the portions with the steep slope are nearly identical. The differences of the exact mode coupling theory and the Lorentzian approximation can also be seen in the insets of Figs. 4.15 and 4.16.

B. Electron spin resonance and magnetic relaxation

In electron spin resonance (ESR) and magnetic relaxation (MR) experiments one measures the electronic response function at zero wave vector and finite frequency

$$\chi^\alpha(\mathbf{q} = \mathbf{0}, \omega) = \frac{\Gamma^\alpha(\mathbf{q}, \omega)\chi^\alpha(\mathbf{q})}{i\omega + \Gamma^\alpha(\mathbf{q}, \omega)} \Big|_{\mathbf{q} \rightarrow 0}, \quad (4.8)$$

where $\Gamma^\alpha(\mathbf{q}, \omega)$ is the frequency dependent relaxation function in Eq. (3.19). Therefrom one determines the kinetic coefficient

$$L(\omega) = \Gamma^\alpha(\mathbf{q}, \omega)\chi^\alpha(\mathbf{q}) \Big|_{\mathbf{q} \rightarrow 0} \quad (4.9)$$

for the homogeneous magnetization dynamics. In Lorentzian approximation one finds for the kinetic coefficient at zero frequency

$$L_0(q_D, \xi) = \frac{g^2 J^2}{3\pi^2} k_B T \int_0^\infty dk k^2 \frac{\chi^L(k, q_D)\chi^T(k, q_D)}{\Gamma^L(k, q_D) + \Gamma^T(k, q_D)}, \quad (4.10)$$

where the dependence of the Onsager coefficient on the dipolar wave vector and the temperature is now indicated explicitly. Note that the kinetic coefficient for the homogeneous

relaxation is the same for the longitudinal and transverse spin fluctuations. Using the generalized dynamic scaling and introducing polar coordinates ($r = \sqrt{x^2 + y^2}$, $y/x = \tan \varphi$) one finds [81]

$$L_0(q_D, \xi) = BF(1/q_D \xi), \quad (4.11)$$

with the universal crossover function

$$F(1/q_D \xi) = \left(1 + \frac{1}{q_D^2 \xi^2}\right)^{-7/4} \int_0^\infty dr r^{5/2} \frac{\hat{\chi}^L(r, \varphi) \hat{\chi}^T(r, \varphi)}{\gamma^L(r, \varphi) + \gamma^T(r, \varphi)}, \quad (4.12)$$

and the non-universal constant

$$B = \frac{4\pi^2}{3} \Lambda q_D^{5/2}. \quad (4.13)$$

If there were no dipolar interaction ($g = 0$), one would simply find a vanishing Onsager coefficient due to the factor g^2 in equation (4.10). With regard to the crossover function F of Eq. (4.12) it is natural to define the reduced crossover temperature by

$$\tau_D = \frac{T_D - T_c}{T_c} = (q_D^2 \xi_0^2)^{1/\phi}, \quad (4.14)$$

where the crossover exponent ϕ equals the susceptibility exponent γ for a ferromagnet without dipolar interaction [4]. If one neglects the dipolar crossover of the correlation length, the scaling variable $q_D^2 \xi^2$ can be written as $q_D^2 \xi^2 = (\tau_{\text{cross}}/\tau)^\gamma$ and the crossover temperature in terms of the dipolar wave vector is given by

$$q_D \xi_D = 1. \quad (4.15)$$

The crossover temperatures T_D resulting from Eq. (4.15) can be found in Table IX.

The Onsager coefficient $L = \Gamma^\alpha \chi^\alpha$ does not depend on the sample shape [71] and is the same for the transverse and the longitudinal mode. The universal crossover function $F(\rho)$ with $\rho = 1/q_D \xi$ is plotted in Fig. 4.17 in units of its value at criticality $F(0)$. For temperatures larger than the dipolar crossover temperature $F(\rho)$ shows a $\xi^{7/2}$ power law behavior, which was first shown in Refs. [122,227]. In the strong dipolar limit, i.e., very close to the

transition temperature, the Onsager coefficient approaches a constant [72] reflecting the non conserved nature of the order parameter due to the presence of the dipolar interaction.

The kinetic Onsager coefficient at zero wave vector has been measured by magnetic relaxation experiments [147,98,148,64] and ESR experiments [148,147,149,150] for the Onsager coefficient in *EuS*, *EuO*, *CdCr₂S₄*, *CdCr₂Se₄* and *Ni* [236,238]. In order to extract the contribution of the critical fluctuations one has to subtract a non-critical background L_{bg} which in the critical region of all ferromagnets (except *Ni*) is very small, $L_{\text{bg}} \ll L_{\text{cr}}$ (see Table IX). The critical part of the Onsager coefficient

$$\hbar L_0(q_D, \xi) = L_d \frac{F(\rho)}{F(0)} = BF(\rho) \quad (4.16)$$

is compared with the crossover function F in Fig. 4.18 (Fig. 1 of Ref. [152]). The non-universal parameter $\hbar L_d = BF(0)$ was fixed by the data for the kinetic coefficient in the center of the critical region. There is an excellent agreement (except *Ni* and *EuO*) of the observed crossover with the results of the mode coupling theory. Especially, the data for *EuS* follow the theoretical function quite closely. The ESR-data on *Ni* [236], shown in Fig. 4.18, deviate from the mode coupling result. Spörel and Biller [238], however, find an increase in the electron paramagnetic resonance line width of *Ni* near T_c , in accord with mode coupling theory but opposite to what was found in Ref. [236]. It seems that the observation of the peaklike broadening depends critically on the quality of the sample. Recently Li et al. [165] have demonstrated that it is possible to observe the critical broadening of the linewidth in ultrathin *Ni* films. As further possible sources for the deviations in *Ni* and *EuO* from the dipolar crossover sample imperfections (e.g. oxygen vacancies in *EuO*, and internal stress in *Ni*) have been suggested [152].

The values of the fit-parameter L_d are listed in Table IX. But, even these values agree with the theoretical prediction as can be inferred from the inset in Fig. 4.18. The minor differences can be attributed to some uncertainties in the dipolar wave vector [152].

Because ESR experiments are performed in a magnetic field B there should be an effect on the relaxation rate starting at $\gamma B = \Gamma(q = \xi^{-1})$ [140]. Those data points are not given

in Fig. 4.18. The influence of the magnetic field on the relaxation rate at zero wave vector has recently been studied by Kötzer et al. [154]. In analyzing the effect of the magnetic field in terms of the internal isothermal susceptibility $\chi_{\text{int}} = \delta M / \delta H_{\text{int}}$ (H_{int} is the internal magnetic field related to the external magnetic field by demagnetization corrections) the data were found to collapse on a single curve. Hence, empirically, the field effect on the kinetic coefficient can be accounted for by using $q_D^2 \chi_{\text{int}}$ instead of $q_D^2 \xi^2$ as the scaling variable and the same scaling function F as for the case of zero magnetic field.

Up to now we have studied the behavior of the uniform relaxation at zero frequency only. Actually, the kinetic coefficient is frequency dependent, which was observed first by De Haas and Verstelle [98]. Measuring the uniform dynamic susceptibility in *EuO* they have found a deviation from a Debye spectrum (Lorentzian form), which according to Eqs. (4.8) and (4.9) is equivalent to a frequency dependent kinetic coefficient. Similar deviation from a Lorentzian have been found quite recently in *EuS* [97,59]. In order to study the frequency dependence of the kinetic coefficient one would have to solve the full frequency dependent mode coupling equations and therefrom deduce $L(q_D, \xi, \omega)$. As a first approximation one can use [155,59]

$$L(q_D, \xi, \omega) = \frac{g^2 J^2}{3\pi^2} k_B T \int_0^\infty dk k^2 \frac{\chi^L(k, q_D) \chi^T(k, q_D)}{\Gamma^L(k, q_D) + \Gamma^T(k, q_D) + i\omega}, \quad (4.17)$$

which is obtained as the first iteration step in a self consistent determination of the frequency dependent kinetic coefficient, starting with the damping coefficients $\Gamma^{L,T}(q, q_D, \xi)$ from the Lorentzian approximation. A scaling analysis of the frequency dependent kinetic coefficient gives

$$L(q_D, \xi, \omega) = BF(1/q_D \xi, \omega \xi^z / \Lambda), \quad (4.18)$$

with the scaling function

$$F(1/q_D \xi, \omega / \Lambda q_D^z) = \left(1 + \frac{1}{q_D^2 \xi^2}\right)^{-7/4} \int_0^\infty dr r^{5/2} \frac{\hat{\chi}^L(r, \varphi) \hat{\chi}^T(r, \varphi)}{\gamma^L(r, \varphi) + \gamma^T(r, \varphi) + i(\omega / \Lambda q_D^z) r^z \sin^z \varphi}. \quad (4.19)$$

The real and imaginary part of F is shown in Figs. 4.19a and 4.19b versus the scaled frequency $\hat{\omega} = \omega/\Lambda q_D^z$ for several values of $\varphi = \arctan(q_D \xi)$, indicated in the graphs. For small and large values of $\hat{\omega}$ the real part of the scaling function behaves asymptotically as

$$\text{Re}F(1/q_D \xi, \omega/\Lambda q_D^z) \approx F(1/q_D \xi) \begin{cases} 1 - (\hat{\omega}/\hat{\omega}_{c1}(1/q_D \xi))^2 & \text{for } \hat{\omega} \ll 1 \quad , \\ (\hat{\omega}/\hat{\omega}_{c2}(1/q_D \xi))^{-1-1/z} & \text{for } \hat{\omega} \gg 1 \quad . \end{cases} \quad (4.20)$$

The corresponding scaling functions for the Onsager coefficient at zero frequency $F(1/q_D \xi)$ and the scaling functions $\omega_{c2}(1/q_D \xi)$ and $\omega_{c1}(1/q_D \xi)$ characterizing the large and low frequency behavior, respectively, are shown in Figs. 4.20a,b,c. As can be inferred from these figures, the scaling function $\omega_{c1}(1/q_D \xi)$ is nearly constant. This finding is in accord with experiments by Dombrowski et al. [59]. The experiments have been analyzed assuming a Lorentzian shape for the kinetic coefficient [59]

$$L(q_D, \xi, \omega) \approx \frac{L(q_D, \xi)}{1 + i\omega/\omega_c}. \quad (4.21)$$

This shape differs from the theoretical results presented above, especially in the large frequency limit, i.e. for $\omega \gg \Lambda q_D^z$. At low frequencies the theoretical result has the same expansion as the Lorentzian approximation used in analyzing the experiments. It is found experimentally that the characteristic frequency ω_c is nearly independent on temperature. This is in accord with the above theoretical result, that the scaling function $\omega_{c1}(1/q_D \xi)$ is nearly constant over the whole temperature range. For a more detailed comparison with the experiment further analysis of the data on the basis of the results of the mode coupling theory for the frequency dependence of the Onsager coefficient seems to be necessary. It would be interesting to see, whether the experiment confirms the predicted large frequency behavior $L(\omega) \propto \omega^{-1-1/z}$.

Recently, the homogeneous magnetization dynamics has also been investigated in the ferromagnetic phase [59]. It is found that the scaling function for the kinetic coefficient below T_c agrees exactly with that observed earlier above T_c . Since a complete theory of the critical dynamics below T_c is still lacking, these results are not explained yet. However, those experimental findings are a clear indication of the importance of the dipolar interaction below the critical temperature.

C. Hyperfine Interactions

There are several nuclear, i.e., hyperfine interaction (HFI), methods commonly used to study critical fluctuations in magnets. These are nuclear magnetic resonance (NMR) [235], Mössbauer effect (ME) [143,144], perturbed angular correlations (PAC) [228,95,44,113] of gamma rays, and muon spin rotation (μ SR) (see also section IV C). The application of nuclear techniques to study critical phenomena in magnets has recently been reviewed by Hohenemser et al. [114]. For recent work on the application of μ -SR for the investigation of spin dynamics the reader may consult Refs. [239,52,104]. All of the hyperfine interaction methods are local probes which are related to a wave vector integral of the spin correlation functions. As such they offer a complement to neutron scattering. Dynamic studies, using hyperfine interaction probes, utilize the process of nuclear relaxation produced by time-dependent hyperfine interaction fields, which reflect fluctuations of the surrounding electronic magnetic moments.

The hyperfine interaction stems from the magnetic interaction of the electrons with the magnetic field produced by the nucleus. The hyperfine interaction of a nucleus with spin \mathbf{I} , g -factor g_N and mass m_N with one of the surrounding electrons with spin \mathbf{S} and orbital momentum \mathbf{L} can be written in the form [20,247]

$$H_{\text{hyp}} = \frac{Ze_0^2 g_N}{2m_N m c^2} \left[\frac{1}{r^3} \mathbf{I} \cdot \mathbf{L} + \frac{8\pi}{3} \delta^{(3)}(\mathbf{x}) \mathbf{I} \cdot \mathbf{S} - \frac{1}{r^3} \mathbf{I} \cdot \mathbf{S} + \frac{3(\mathbf{I} \cdot \mathbf{x})(\mathbf{S} \cdot \mathbf{x})}{r^5} \right]. \quad (4.22)$$

The first term represents the interaction of the orbital momentum of the electron with the nuclear magnetic moment of the nucleus. The second term is the Fermi contact interaction and the last two terms represent the dipolar interaction ⁸. The Fermi contact interaction

⁸Actually, also the Fermi contact interaction comes from the magnetic dipole interaction. In the evaluation of the matrix elements of the (residual) dipolar interaction, represented by the last two terms, an infinitesimal sphere around the origin has to be excluded. The singular part of the dipolar interaction coming from the interior of the sphere is represented by the Fermi contact term.

is finite only for electrons having a finite probability density at the nucleus, i.e. bound s -electrons or itinerant electrons.

For a substitutional nucleus the main contribution to the hyperfine field comes from the bound s -electrons [91], which are polarized by the magnetic ions. The large (and often negative) hyperfine field for transition–element ions comes from the polarization of the core s electrons by the spin density of the unpaired $3d$ electrons, which then contribute to the hyperfine field through the Fermi contact interaction [261]. The residual dipolar interaction is negligible in this case. Note also that this term is zero for cubic symmetry. The Hamiltonian, Eq. (4.22), can also be used for the analysis of spin resonance experiments with muons (μ SR). However, these do not have bound electrons and hence the Fermi contact term involves only conduction electrons and is of the same order of magnitude as the (residual) dipolar interaction [56,185] (see also section IV D). For instance in Pd , there is a dipolar contribution by the Pd f -electrons which also polarize the s -electrons which in turn contribute via the Fermi contact term to the hyperfine field at the muon site.

After the above general remarks, let us now return to those hyperfine interaction probes (ME, PAC, NMR), where the Fermi contact term gives the dominant contribution to the hyperfine field at the nucleus. Then the corresponding interaction Hamiltonian reduces to

$$\mathcal{H}(t) = A_{\text{contact}} \mathbf{I} \cdot \mathbf{S}(t). \quad (4.23)$$

If the spin auto–correlation time, τ_c , is much shorter than the Larmor period, $1/\omega_L$, and the nuclear lifetime, τ_N , (motional narrowing regime) the nuclear relaxation rate τ_R^{-1} is directly proportional to the (averaged) spin autocorrelation time τ_c

$$\tau_R^{-1} = C_{\text{hf}} \tau_c, \quad (4.24)$$

with a hyperfine coupling constant C_{hf} [113]. The nuclear relaxation rate equals the spin-spin relaxation rate $\tau_R^{-1} = T_2^{-1}$ in the case of NMR, is proportional to the relaxation induced excess line width $\Delta\Gamma$ for ME, and for PAC τ_R is given by the relaxation time of the perturbation factor.

The (averaged) spin autocorrelation time τ_c is defined by a time-integral

$$\tau_c = \frac{1}{2} \int_{-\infty}^{+\infty} dt \frac{1}{3} \sum_{\alpha} G^{\alpha\alpha}(\mathbf{r} = 0, t) = \frac{1}{6} \sum_{\alpha} \int_{\mathbf{q}} G^{\alpha\alpha}(\mathbf{q}, \omega = 0). \quad (4.25)$$

over the spin autocorrelation function $G^{\alpha\alpha}(\mathbf{r}, t) = \frac{1}{2} \langle \{S^{\alpha}(\mathbf{r}, t), S^{\alpha}(0, 0)\} \rangle$. Hence hyperfine interaction methods provide an integral property of the spin-spin correlation function. Upon using the fluctuation dissipation theorem (FDT), which in the special case $\omega = 0$ reduces to

$$G^{\alpha\alpha}(q, \omega = 0) = 2k_{\text{B}}T \frac{\chi^{\alpha}(\mathbf{q}, g)}{\Gamma^{\alpha}(\mathbf{q}, g)}, \quad (4.26)$$

one finds for the autocorrelation time

$$\tau_c = \frac{k_{\text{B}}T}{V_q} \int_{\text{BZ}} d^3q \frac{1}{3} \sum_{\alpha} \frac{\chi^{\alpha}(\mathbf{q}, g)}{\Gamma^{\alpha}(\mathbf{q}, g)}. \quad (4.27)$$

The \mathbf{q} -integration extends over the Brillouin zone (BZ), the volume of which is V_q .

Important information about the behavior of the auto-correlation time can be gained from a scaling analysis. Upon using the static and dynamic scaling laws Eq. (4.27) can be written as

$$\tau_c \propto 4\pi \int dq q^{-z} \frac{1}{3} \sum_{\alpha} \frac{\hat{\chi}^{\alpha}(q\xi, q/q_{\text{D}})}{\gamma^{\alpha}(q\xi, q/q_{\text{D}})}. \quad (4.28)$$

If there were no dipolar interaction, one could extract the temperature dependence from the integral in Eq. (4.28) with the result $\tau_c \propto \xi^{z-1}$. This expression can be used to define an effective dynamical exponent $z_{\text{eff}}(\tau)$, which depends on the correlation length by

$$\tau_c \propto \xi^{z_{\text{eff}}-1} \propto \left(\frac{T - T_c}{T_c} \right)^w. \quad (4.29)$$

In the presence of dipolar forces one finds after introducing polar coordinates as in section IV B

$$\tau_c = H \left(1 + \frac{1}{q_{\text{D}}^2 \xi^2} \right)^{(1-z)/2} \int_{r_0}^{\infty} dr r^{z-2} \frac{1}{3} \sum_{\alpha} \frac{\hat{\chi}^{\alpha}(r, \varphi)}{\gamma^{\alpha}(r, \varphi)}, \quad (4.30)$$

where $z = 5/2$ and the non universal constant H is given by [86]

$$H = \frac{(k_{\text{B}}T)^2}{32\pi^6 (\Lambda a^{-5/2})^3} (q_{\text{D}} a)^{3/2}. \quad (4.31)$$

The lower cutoff r_0 is

$$r_0 = \frac{q_D}{q_{\text{BZ}}} \sqrt{1 + \frac{1}{q_D^2 \xi^2}}, \quad (4.32)$$

where q_{BZ} is the boundary of the Brillouin zone. In the critical region it can be disregarded and replaced by $r_0 = 0$, since $q_{\text{BZ}} \gg q_D$ and the integrand in Eq. (4.30) is proportional to \sqrt{r} for small r . For very small ξ (outside the critical region) the cutoff reduces the autocorrelation time with respect to the critical value.

One should note, that the dominant wave vectors contributing to the relaxation time τ_c in Eq. (4.27) are close to the zone center. Quantitative estimates for the wave vector range probed by μ -SR experiments on *Fe* and *Ni*, which also apply for other hyperfine experiments, are given in Ref. [230].

The averaged autocorrelation time is a sum of two parts

$$\tau_c = \frac{1}{3}(\tau_L + 2\tau_T), \quad (4.33)$$

which we call longitudinal and transverse relaxation times

$$\tau_\alpha = H I_\alpha(\varphi), \quad (4.34)$$

where we have defined

$$I_\alpha(\varphi) = \left(1 + \frac{1}{q_D^2 \xi^2}\right)^{-3/4} \int_{r_0}^{\infty} dr \sqrt{r} \frac{\hat{\chi}^\alpha(r, \varphi)}{\gamma^\alpha(r, \varphi)}, \quad \alpha = L, T. \quad (4.35)$$

These two relaxation times are shown in Fig. 4.21 as functions of the scaling variable $1/q_D \xi$, where we have neglected the lower cutoff r_0 . Since the static longitudinal susceptibility does not diverge one finds that the longitudinal relaxation time is non-critical, whereas the transverse relaxation time diverges like $\tau_T \propto \xi$. This corresponds to an effective dynamical exponent $z_{\text{eff}} = 2$. When leaving the dipolar critical region there is a crossover to the isotropic Heisenberg region, where both curves join and the relaxation times $\tau_L = \tau_T = \tau_c$ are characterized by another power law $\tau_c \propto \xi^{3/2}$ corresponding to an effective dynamical exponent $z_{\text{eff}} = 5/2$.

Let us now compare with hyperfine experiments on *Fe* and *Ni*. Early PAC [228,95] and ME [143,144] were performed well in the dipolar region and an effective exponent $z = 2$ was found. The crossover in the dynamic exponent from $z = 2.5$ to $z = 2$ was first observed by Chow et al. [44,113]. The autocorrelation time τ_c is shown in Fig. 4.22 in units of the non universal constant H (see Table IX) versus the scaling variable $1/q_D\xi$. The data points in Fig. 4.22 are results of HFI experiments on *Fe* and *Ni* [228,95,44,113] for the autocorrelation time τ_c (in units of their non universal frequency scale H). As before there is no fit parameter for the scaling variable $1/q_D\xi$. So we conclude that our MC-theory accounts well for the experimental data demonstrating the universal crossover behavior from $z_{\text{eff}} = 5/2$ to $z_{\text{eff}} = 2$ as the critical temperature is approached.

Finally we would like to note that ME [45,46] and PAC [49] experiments on the dynamics of *Gd* show neither $z = 2.5$ nor $z = 2.0$ but $1.74 < z < 1.82$ depending on whether the system is assumed to have Heisenberg or Ising static exponents. Recent μ -SR experiments give similarly depressed values of the critical dynamic exponent z [259,260] (see section IV D). In Ref. [229] the μ -SR data [259,105] have been compared with the results from MC-theory for isotropic dipolar ferromagnets [81,86], and it is found that the available data are found to be in agreement with the MC-theory. *Gd* is supposed to have an uniaxial exchange anisotropy along the c -axis. Hence one expects that in the asymptotic region there is one critical mode along the c -axis with $z_{\text{eff}} = 2$ and two uncritical modes with $z_{\text{eff}} = 0$ perpendicular to the c -axis [72]. Since for polycrystalline probes τ_c is an average over the relaxation rates of these modes, it is possible that the experimental data in the crossover region yield effective exponents less than $z = 2$. Here more experimental work with single crystals and a more detailed mode coupling analysis beyond the scaling analysis in Ref. [72] would be needed to clarify the situation.

D. Muon Spin Relaxation (μ SR)

In muon spin relaxation (μ SR) experiments one observes the muon precession in an applied magnetic field or in a local magnetic field inside the sample⁹. For recent work on the application of μ SR to the investigation of spin dynamics we refer the interested reader to Refs. [239,52,104].

In analogy with other implanted probes¹⁰, like those discussed in section IV C, the muon spin will relax through interactions with fluctuating magnetic fields in its surroundings. However, in contrast the local magnetic field at the interstitial site of the muon has comparable contributions from the Fermi contact field *and* the dipolar field. In rare earth materials the residual dipolar field is high, and often the dominant field [135,103,136]. It has a reduced symmetry as compared to the Fermi contact coupling. Whereas the Fermi contact coupling is isotropic in space, the residual dipolar field has an anisotropy with respect to the wave vector. In the case of a hyperfine field dominated by the residual dipolar field this implies that the spin fluctuations transverse and longitudinal with respect to the wave vector contribute with different weights to the μ SR relaxation rate. Hence, one has a situation quite different from e.g. PAC and ME measurements where the interaction of the substitutional probe with the host atoms is mainly a contact hyperfine coupling. This feature of μ -SR offers the possibility to design experiments which allow to distinguish between spin fluctuations longitudinal and transverse to the wave vector \mathbf{q} [271,272,229].

Among the basic ferromagnets muon relaxation has been measured in *Fe* [108] and *Ni* [205], which have cubic crystal structure, and in *Gd* [259,260] which crystallizes in a hexagonal lattice. The data for the muon relaxation rate in *Fe* were interpreted by a dynamic exponent $z = 2.0$ [108] which would indicate that the data are taken in the dipolar

⁹Muon spin relaxation experiments are often performed in zero applied external field

¹⁰The positive muon ends up in interstitial sites in solids, and in metals the actual site is in most cases identical to that preferred by hydrogen.

region. Actually, the data cover both the dipolar and the isotropic region – the crossover temperature for iron is $T_D - T_c = 8.6K$ (see Table VIII) – with fairly large where the data error bars in the isotropic region, so that a crossover from $z = 2.5$ to $z = 2.0$ is not excluded by the data [69]. The observations in *Ni* [205] seemed to be conflicting with PAC [44] measurements, if one assumes that in both cases the contact field is the dominant contribution to the local magnetic field at the muon site. However, one has to take into account that the interaction of the muon with the surrounding is more complicated than for the other hyperfine probes, especially as already pointed out by Yushankhai [273] one has to take into account the classical dipolar interaction between the muon magnetic moment and the lattice ion magnetic moments. This has recently been done in Ref. [271,272], the results of which we will review next.

A zero-field μ SR measurement consists of measuring the depolarization function $P_z(t)$ [239],

$$P_z(t) = \frac{1}{2} Tr [\rho_m \sigma_z \sigma_z(t)] , \quad (4.36)$$

where ρ_m is the density operator of the magnet and σ_z the projection of the Pauli spin operator of the muon spin on the z -axis. $Tr[A]$ stands for the trace of A over the muon and magnet quantum states. Since the magnetic fluctuations are sufficiently rapid, the depolarization they induce can be treated in the motional narrowing limit. One finds [271]

$$P_z(t) = \exp[-\lambda_z t] , \quad (4.37)$$

with the damping rate

$$\lambda_z = \frac{\pi D}{V} \int \frac{d^3 q}{(2\pi)^3} \{ [\mathbf{G}(\mathbf{q}) \mathbf{C}(\mathbf{q}) \mathbf{G}(-\mathbf{q})]^{xx} + [\mathbf{G}(\mathbf{q}) \mathbf{C}(\mathbf{q}) \mathbf{G}(-\mathbf{q})]^{yy} \} , \quad (4.38)$$

where

$$C^{\alpha\beta}(\mathbf{q}) = \frac{1}{2} \left[\langle S_{\mathbf{q}}^{\alpha}(\omega) S_{-\mathbf{q}}^{\beta}(-\omega) \rangle + \langle S_{\mathbf{q}}^{\beta}(\omega) S_{-\mathbf{q}}^{\alpha}(-\omega) \rangle \right] |_{\omega=0} \quad (4.39)$$

is the symmetrized correlation function at zero frequency, and

$$\mathcal{D} = \left(\frac{\mu_0}{4\pi}\right)^2 \gamma_\mu^2 (g_L \mu_B)^2. \quad (4.40)$$

$\gamma_\mu = 851.6 \text{ Mrad s}^{-1} \text{ T}^{-1}$ is the gyro-magnetic ratio of the muon. The tensor \mathbf{G} characterizes the type of interactions by which the muon spin is coupled to the magnetic moments of the material considered. It is given by

$$G^{\alpha\beta}(\mathbf{q}) = r_\mu H \delta^{\alpha\beta} + D^{\alpha\beta}(\mathbf{q}). \quad (4.41)$$

The first term describes the Fermi contact coupling, where r_μ is the number of nearest-neighbor magnetic ions to the muon localization site and H measures the strength of the hyperfine coupling (see Table VIII). The simple form for the contact coupling is valid only if the muon site is a center of symmetry. The second term characterizes the dipolar coupling and can be calculated via Ewald's method [271]. To lowest order in the wave vector \mathbf{q} one finds

$$D^{\alpha\beta}(\mathbf{q}) = 4\pi \left[B^{\alpha\beta}(\mathbf{q} = 0) - \frac{q^\alpha q^\beta}{q^2} \right]. \quad (4.42)$$

The values of the tensor components $B^{\alpha\beta}(\mathbf{q} = 0)$ depend on the muon site. For muons in a tetrahedral or octahedral interstitial site in an *fcc* lattice one finds $B^{\alpha\beta}(\mathbf{q} = 0) = \frac{1}{3} \delta^{\alpha\beta}$ [156]. The situation is more complex for a *bcc* lattice [156].

For simplicity we confine ourselves to the case of an *fcc* lattice and refer the reader to Refs. [271,272,229] for a discussion of the more complicated cases of an *bcc* cubic crystal or a hexagonal lattice structure. For an *fcc* lattice the damping rate is found to be [271]

$$\lambda_z = \frac{8}{3} \frac{\mu_0}{4\pi} \gamma_\mu^2 \frac{k_B T}{v_a} \int_0^{q_{BZ}} dq q^2 \left[2p^2 \frac{\chi^T(q)}{\Gamma^T(q)} + (1-p)^2 \frac{\chi^L(q)}{\Gamma^L(q)} \right], \quad (4.43)$$

where we have defined

$$p = \frac{1}{3} + \frac{r_\mu H}{4\pi}. \quad (4.44)$$

When the Fermi contact interaction is large compared to the classical dipolar interaction, i.e., $|p| \gg 1$, Eq. 4.43 reduces to the result obtained in section IV C

$$\lambda_z^{\text{contact}} = \frac{1}{6\pi^2} \frac{\mu_0}{4\pi} (\gamma_\mu r_\mu H)^2 \frac{k_B T}{v_a} \int_0^{q_{BZ}} dq q^2 \left[2 \frac{\chi^T(q)}{\Gamma^T(q)} + \frac{\chi^L(q)}{\Gamma^L(q)} \right]. \quad (4.45)$$

On the other hand when the Fermi interaction is negligible, i.e. $p \simeq 1/3$, we get from Eq. 4.43

$$\lambda_z^{\text{dipolar}} = \frac{16}{27} \frac{\mu_0}{4\pi} \gamma_\mu^2 \frac{k_B T}{v_a} \int_0^{q_{BZ}} dq q^2 \left[\frac{\chi^T(q)}{\Gamma^T(q)} + 2 \frac{\chi^L(q)}{\Gamma^L(q)} \right]. \quad (4.46)$$

While Eq. (4.45) has been derived under the hypothesis that the muon spin interacts with the lattice spins through the isotropic hyperfine interaction, Eq. (4.46) has been obtained supposing that the coupling is only due to the classical dipolar interaction. One should note that the relative weight of the transverse and the longitudinal modes is reversed in going from a pure contact to a pure dipolar interaction of the muon with the lattice spins. Hence in combing PAC with μ -SR measurements it should be possible to distinguish between transverse and longitudinal relaxation rates.

Upon introducing polar coordinates as in section IV C one can write the damping rate in scaling form

$$\lambda_z = \mathcal{W} \left[2p^2 I_T(\varphi) + (1-p)^2 I_L(\varphi) \right], \quad (4.47)$$

where the non universal constant \mathcal{W} is given by

$$\mathcal{W} = \frac{8\pi^{3/2}}{3P} \sqrt{\frac{\mu_0}{4\pi}} \frac{\gamma_\mu^2 \hbar q_D^{3/2}}{g_L \mu_B} \sqrt{k_B T_C}. \quad (4.48)$$

The theoretical values of \mathcal{W} for the four magnets considered primarily in this section are listed in Table VIII. The scaling functions $I^{L,T}(\varphi)$ are defined in section IV C. Fig. 4.21 indicates that while $I_T(\varphi)$ exhibits a strong temperature dependence in the whole temperature range of the critical region, $I_L(\varphi)$ is practically temperature independent for $q_D \xi > 1$. Therefore, the temperature dependence of the μ SR damping rate λ_z depends on the relative weight of $I_T(\varphi)$ and $I_L(\varphi)$ which is controlled by the parameter p . As first noticed by Yushankhai [273], the transverse fluctuations do not contribute to λ_z if $r_\mu H/4\pi = -1/3$. In this case λ_z becomes temperature independent near T_c .

In Figs. 4.23 and 4.24 experimental data for Ni [205] and Fe [108] are compared with the results from MC-theory. One notices that most of the data have been recorded in the crossover temperature region where λ_z is not predominantly due to the transverse fluctuations. Again the MC-theory gives a quantitative explanation of the observed relaxation rates.

TABLE VIII. Material parameters for Ni , Fe , EuO and EuS . The parameter are defined in the main text.

	Ni	EuO	EuS	Fe
$a(\text{\AA})$	3.52 ⁽¹⁾	5.12 ⁽²⁾	5.95 ⁽²⁾	2.87 ⁽¹⁾
$T_C (K)$	627 ⁽¹⁾	69.1 ⁽²⁾	16.6 ⁽²⁾	1043 ⁽¹⁾
$q_D (\text{\AA}^{-1})$	0.013 ⁽³⁾	0.147 ^(3,4)	0.245 ^(1,35)	0.045 ⁽⁴⁾ (0.033) ⁽³⁾
$\xi_0 (\text{\AA})$	1.23 ⁽⁵⁾	1.57 ⁽⁶⁾	1.81 ⁽⁶⁾	0.95 ⁽⁷⁾ (0.82) ⁽⁸⁾
$r_\mu H/4\pi (T = 0 K)$	-0.11 ⁽⁹⁾	0 (?)	0 (?)	-0.51 ⁽⁹⁾
$\Upsilon (\text{\AA})$	0.00184	0.725	3.16	0.0239 (0.0129)
$\Lambda_{\text{exp}} (meV\text{\AA}^{5/2})$	350 ⁽⁵⁾	8.7 ⁽⁴⁾ (8.3) ⁽¹⁰⁾	2.1 ⁽¹¹⁾ (2.25) ⁽¹²⁾	130 ⁽¹³⁾
$\Lambda_{\text{lor}} (meV\text{\AA}^{5/2})$	241	7.09	2.08	90.0 (123)
$\mathcal{W}_{th} (MHz)$	0.358	5.35 (5.60)	6.87 (6.41)	2.98 (2.56)

The values have been taken from the references (1) [142], (2) [210], (3) [152], (4) [190], (5) [34], (6) [204], (7) [264], (8) [203], (9) [56], (10) [28], (11) [30], (12) [31], and (13) [188]. When no reference is indicated, the parameter has been computed from a formula given in the main text with parameters given in tables III.1 and IV.1.

TABLE IX. The dipolar wave vector q_D , the Curie temperature T_c , the experimental non universal constant for the Onsager coefficient L_d , L_{bg} and for the autocorrelation time H_{exp} .

	<i>EuS</i>	<i>EuO</i>	<i>CdCr₂S₄</i>	<i>CdCr₂Se₄</i>	<i>Fe</i>	<i>Ni</i>
$q_D[\text{\AA}^{-1}]$	0.245	0.147	0.058	0.034	0.045(0.033)	0.013
$T_c[K]$	16.6	69.1	84.4	127.8	1043	627
$\hbar L_d(\mu eV)$	38	24	5.9	4.4	–	3.0
$\hbar L_{bg}(\mu eV)$	1.8	0.64	0.01	0.01	–	–
$H_{exp}[10^{-13}sec]$	–	–	–	–	6.0	9.2

The values are taken from Refs. [152] and the references in Table VIII.

Captions to the figures:

Figure 4.1: Typical scattering geometry in neutron scattering experiments. The magnetic guide field \mathbf{H}_V is used to define the beam polarization \mathbf{P} . In order to measure the longitudinal spin fluctuations \mathbf{S}^L one has to go to a finite Bragg peak $\boldsymbol{\tau}$ with the wave vector \mathbf{q} perpendicular to the scattering vector $\mathbf{Q} = \boldsymbol{\tau} + \mathbf{q}$. For unpolarized neutrons only the transverse fluctuations can be measured in the forward direction, $\boldsymbol{\tau} = \mathbf{0}$.

Figure 4.2: Scaling function of the transverse Kubo relaxation function versus the scaled time variable τ_T at $T = T_c + 0.25K$ for $q = 0.018\text{\AA}^{-1}$ (solid), $q = 0.025\text{\AA}^{-1}$ (dotted), $q = 0.036\text{\AA}^{-1}$ (dashed), $q = 0.071\text{\AA}^{-1}$ (long dashed) and $q = 0.150\text{\AA}^{-1}$ (dot-dashed).

Figure 4.3: The same as in Fig. 4.2 for the longitudinal Kubo relaxation function.

Figure 4.4: Scaling function of the transverse Kubo relaxation function versus the scaled time variable τ_T at $T = T_c + 8.0K$ for the same set of wave vectors q as in Figs. 4.2 and 4.3.

Figure 4.5: The same as in Fig. 4.4 for the longitudinal Kubo relaxation function.

Figure 4.6: Scaling function of the transverse Kubo relaxation function versus $\tau' = \Lambda_{\text{lor}} q^z t$ at $T = T_c$ for $q = 0.025\text{\AA}^{-1}$ (solid), $q = 0.036\text{\AA}^{-1}$ (dotted), $q = 0.150\text{\AA}^{-1}$ (dashed) and $q = 0.300\text{\AA}^{-1}$ (long dashed).

Figure 4.7: Scaling function of the transverse Kubo relaxation function versus $\tau' = \Lambda_{\text{lor}} q^z t$ at $T = T_c + 0.5K$ for $q = 0.018\text{\AA}^{-1}$ (solid), $q = 0.025\text{\AA}^{-1}$ (dotted), $q = 0.036\text{\AA}^{-1}$ (dashed) and $q = 0.071\text{\AA}^{-1}$ (long dashed).

Figure 4.8: Transverse Kubo relaxation function $\Phi^T(q, g, t)$ at $q = 0.024\text{\AA}^{-1}$ (solid line) and $q = 0.028\text{\AA}^{-1}$ (dashed-dotted line) for dipolar ferromagnets versus time in *nsec*. The dashed line is the Kubo relaxation function for short range exchange interaction only at $q = 0.024\text{\AA}^{-1}$. Data points for $q = 0.024\text{\AA}^{-1}$ from Fig. 1 of Ref. [190].

Figure 4.9: Normalized experimental data deconvoluted by a maximum entropy method. The solid line shows the spectral shape function predicted by mode coupling theory. The full circles (dashed line) indicate(s) the deconvoluted data. Figure taken from Ref. [93].

Figure 4.10: Scaling functions versus $y^{-1} = q/q_D$ at T_c (in units of the theoretical non universal constant Λ) for (i) the HWHM of the complete solution of the MC equations for the transverse Kubo relaxation function (solid), (ii) transverse (point-dashed) and (iii) longitudinal line (dashed) width in Lorentzian approximation. Experimental data of the transverse line width for *EuO* (\square Ref. [28], \diamond Ref. [189]) and *Fe* (\triangle Ref. [188]).

Figure 4.11: Scaling function of the transverse line width in Lorentzian approximation (solid lines) and of the HWHM of the complete solution (dashed lines) versus the scaling variable $x = (q\xi)^{-1}$ for a set of temperatures ($T - T_c =$ a) 1.4K, b) 5.8K, c) 21K, d) 51K). The Resibois-Piette function (solid) and the HWHM from the complete solution of the MC equations (dashed) without dipolar interaction is also plotted e). Experimental results for *Fe* from Refs. [188,189] ($T - T_c =$ (\square) 1.4K, (\diamond) 5.8K, (\triangle) 21.0K, (\circ) 51.0K).

Figure 4.12: Scaling plot of the temperature dependence of the relaxation rate of critical fluctuations in *EuO* above the Curie temperature $T_c = 69.3K$. The solid lines represent the results from mode coupling theory [80]. The data were taken between $q = 0.018\text{\AA}^{-1}$ and $q = 0.15\text{\AA}^{-1}$. Taken from Ref. [192,193] ($\kappa_1 = 1/\xi$).

Figure 4.13: Comparison of the longitudinal linewidth of Lorentzian fits normalized to $\Lambda_{\text{exp}}q^{5/2}$ with $\Lambda_{\text{exp}} = 2.1\text{meV}\text{\AA}^{5/2}$ to the dipolar dynamic scaling function predicted by mode coupling theory for $q_D = 0.245\text{\AA}^{-1}$ for *EuS*. Figure taken from Ref. [33] ($\kappa = 1/\xi$).

Figure 4.14: The same as Fig. 4.13 for the transverse widths. Figure taken from Ref. [33].

Figure 4.15: Scaled peak positions $q_0(\Lambda_{\text{lor}}/\omega)^{2/5}$ for constant energy scans of the scattering function for the complete solution of the MC equations versus the scaling variable $\hat{\omega}$ for $\varphi =$

a) 1.490, b) 1.294, c) 0.970 and d) for the isotropic case, i.e., $\varphi = 0$. **Inset:** $S^T(q, \omega)/S^T(0, \omega)$ in arbitrary units versus $\frac{1}{r}$ for $\varphi = 1.294$ for some typical values of the scaled frequency ($\hat{\omega} = 10^{L/10}$ with $L = 8$ (solid), 10 (dashed), 12 (point dashed), 14 ($-\cdots-\cdots-$) and 16 ($-\cdots-\cdots-$) indicated in the graph by crosses).

Figure 4.16: The same as in Fig. 4.15 for the scattering function resulting from the Lorentzian approximation.

Figure 4.17: Universal crossover function $F(1/q_D \xi)/F(0)$ with $F(0) = 0.1956$ for the Onsager kinetic coefficient at zero frequency and zero wave vector versus the scaling variable $1/q_D \xi$.

Figure 4.18: Critical part of the Onsager kinetic coefficient for the homogeneous spin dynamics above T_c of $CdCr_2Se_4$ (Ref. [149]), $CdCr_2S_4$ (Ref. [150]), EuO (Ref. [148]), EuS (filled circles: Ref. [147], open circles: Ref. [152]), and Ni (Ref. [236]). The solid lines represent the result from mode coupling theory [81]. **Inset:** Nonuniversal amplitudes $\hbar L_d q_D^{-3/2}$ for the kinetic coefficient and the relaxation rate at the critical point $\hbar L_q q^{-1} q_D^{-1/2} = \Gamma^T(q, T = T_c)/q^{5/2} \approx 5.1326\Lambda$ for ferromagnets including Fe and Co . Figure taken from Ref. [152].

Figure 4.19: The real and imaginary parts of F are shown in a) and b) versus the scaled frequency $\hat{\omega} = \omega/\Lambda q_D^z$ for several values of $\varphi = \arctan(q_D \xi)$: $\varphi_1 = 0.99\frac{\pi}{2}$ (top curve), $\varphi_2 = 0.90\frac{\pi}{2}$, $\varphi_3 = \frac{\pi}{2}(1 - 10^{-0.5})$, $\varphi_4 = \frac{\pi}{2}(1 - 10^{-0.25})$, $\varphi_5 = \frac{\pi}{2}(1 - 10^{-0.1})$, $\varphi_6 = \frac{\pi}{2}(1 - 10^{-0.025})$ (bottom curve).

Figure 4.20: The scaling functions for the a) Onsager coefficient at zero frequency $F(1/q_D \xi)$ and b) the scaling functions $\omega_{c2}(1/q_D \xi)$ and c) $\omega_{c1}(1/q_D \xi)$ characterizing the large and low frequency behaviour, respectively.

Figure 4.21: Scaling functions $I_{L,T}(\varphi)$ for the transverse and longitudinal auto-correlation-time $\tau_{L,T}$ versus $1/q_D \xi$.

Figure 4.22: Auto correlation time τ_c/H (in units of the non universal constant H) versus the scaling variable $\frac{1}{q_D \xi}$ (solid line). Experimental results for the auto correlation time in units of H_{exp} for *Fe* (Ref. [113]: \sqcup) and *Ni* (Ref. [228]: \diamond , Ref. [95]: \triangle , Ref. [113]: \circ).

Figure 4.23: Temperature dependence of the μ SR damping rate for metallic *Ni*. The points are the experimental data of Nishiyama et al. [205]. The full line is the result of the model which takes the muon dipolar interaction into account. The dashed line gives the prediction when this latter interaction is neglected.

Figure 4.24: Temperature dependence of the μ SR damping rate for metallic *Fe*. The points are the experimental data of Herlach et al. [108]. The curves are the predictions of mode-coupling theory for different sets of material parameters. In Fig. 4.24a (Fig. 4.24b) the muon is supposed to diffuse between tetrahedral (octahedral) sites. The full and dashed lines are present the results obtained with (q_D, ξ_0) equal to $(0.033 \text{ \AA}^{-1}, 0.82 \text{ \AA})$ and to $(0.045 \text{ \AA}^{-1}, 0.95 \text{ \AA})$ respectively; see Table VIII.

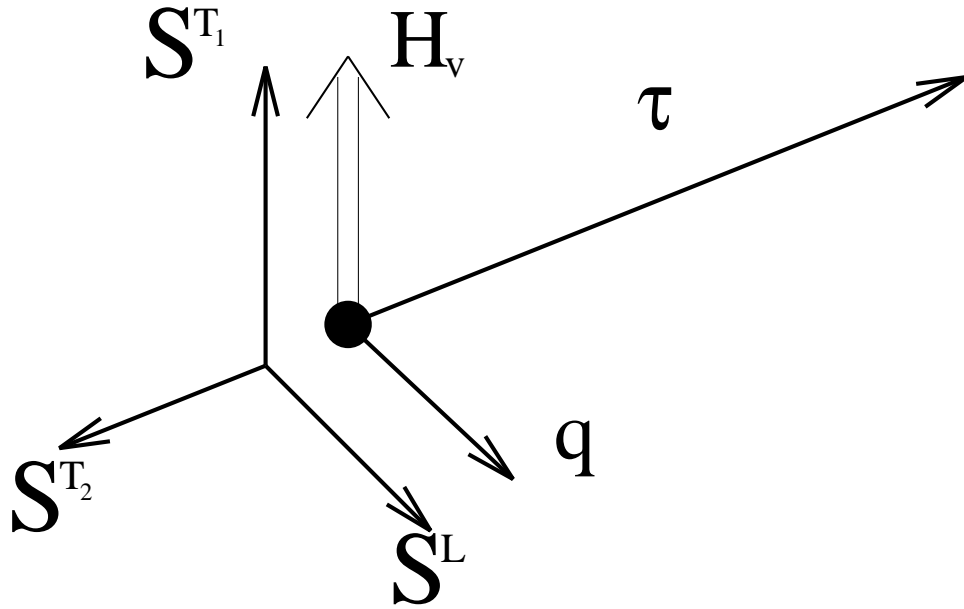


Figure 4.1: Typical scattering geometry in neutron scattering experiments. The magnetic guide field \mathbf{H}_v is used to define the beam polarization \mathbf{P} . In order to measure the longitudinal spin fluctuations \mathbf{S}^L one has to go to a finite Bragg peak $\boldsymbol{\tau}$ with the wave vector \mathbf{q} perpendicular to the scattering vector $\mathbf{Q} = \boldsymbol{\tau} + \mathbf{q}$. For unpolarized neutrons only the transverse fluctuations can be measured in the forward direction, $\boldsymbol{\tau} = 0$.

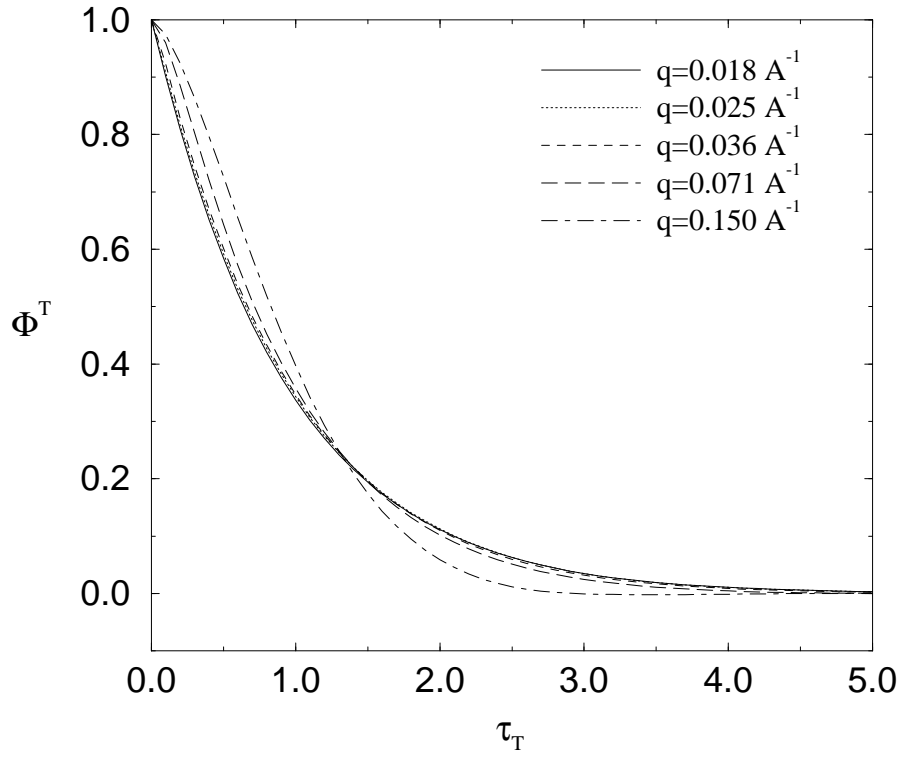


Figure 4.2: Scaling function of the transverse Kubo relaxation function versus the scaled time variable τ_T at $T = T_c + 0.25K$ for $q = 0.018\text{\AA}^{-1}$ (solid), $q = 0.025\text{\AA}^{-1}$ (dotted), $q = 0.036\text{\AA}^{-1}$ (dashed), $q = 0.071\text{\AA}^{-1}$ (long dashed) and $q = 0.150\text{\AA}^{-1}$ (dot-dashed).

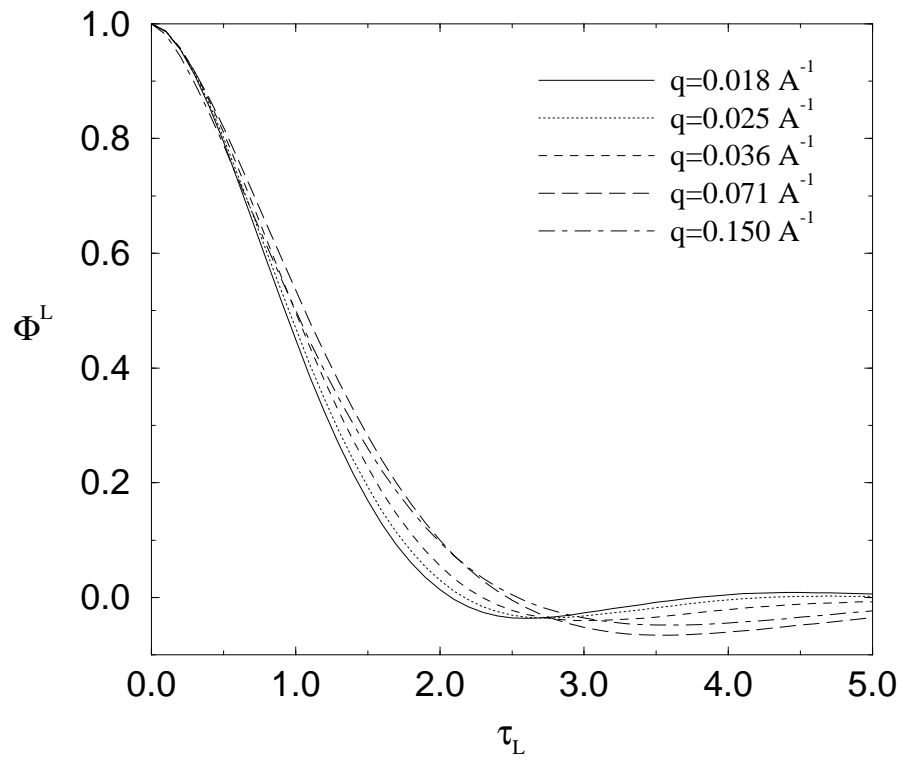


Figure 4.3: The same as in Fig. 4.2 for the longitudinal Kubo relaxation function.

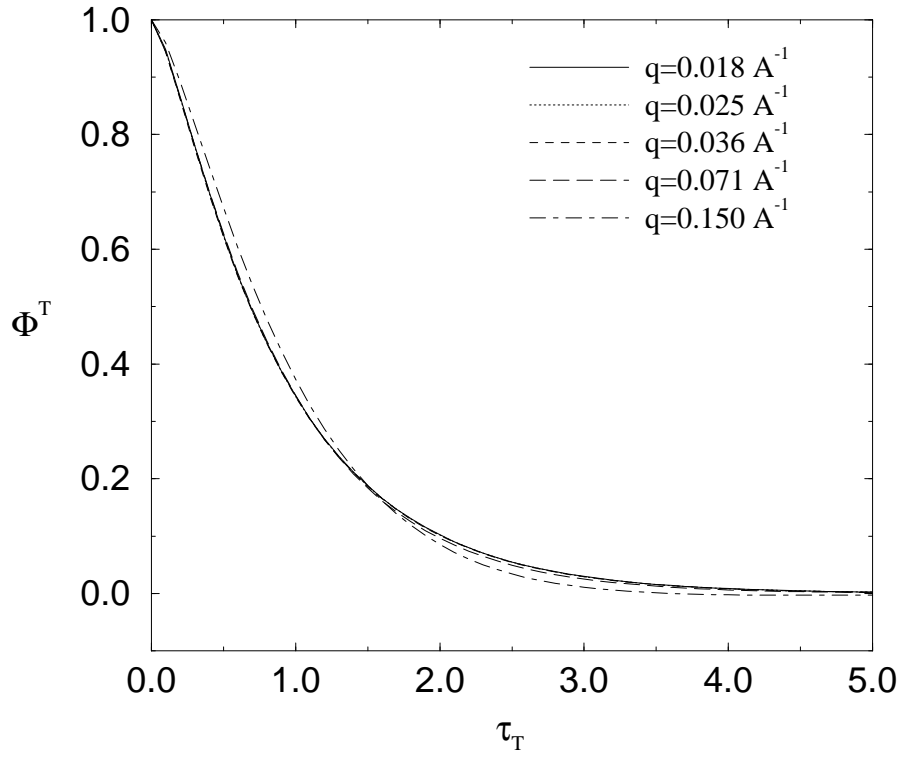


Figure 4.4: Scaling function of the transverse Kubo relaxation function versus the scaled time variable τ_T at $T = T_c + 8.0K$ for the same set of wave vectors q as in Figs. 4.2 and 4.3.

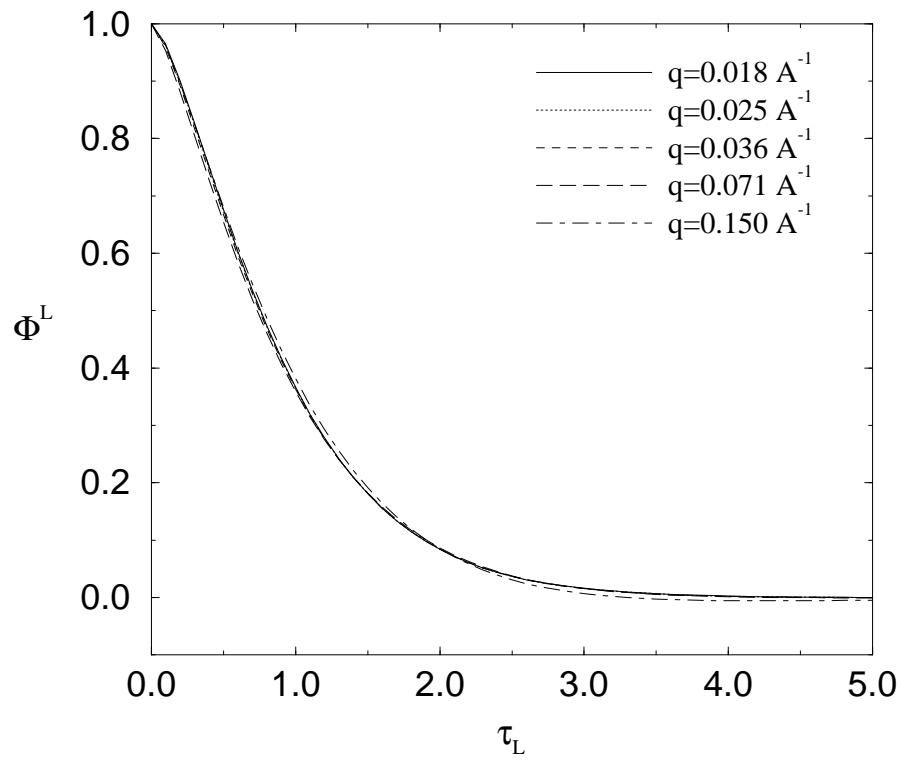


Figure 4.5: The same as in Fig. 4.4 for the longitudinal Kubo relaxation function.

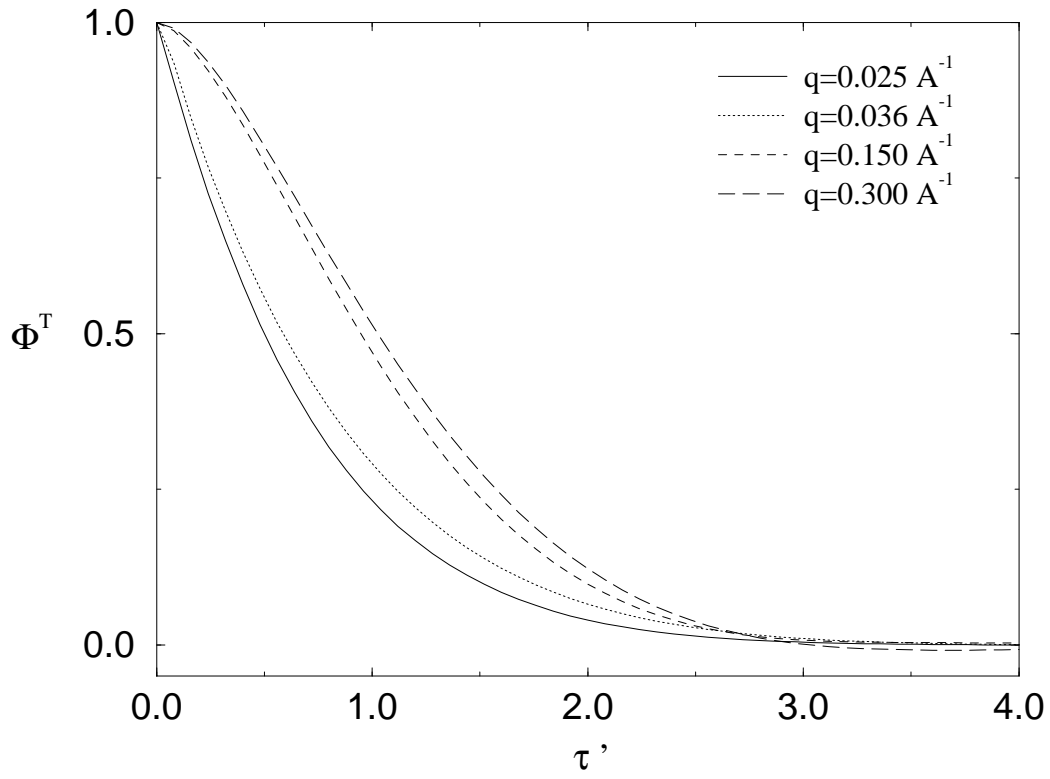


Figure 4.6: Scaling function of the transverse Kubo relaxation function versus $\tau' = \Lambda_{\text{lor}} q^z t$ at $T = T_c$ for $q = 0.025 \text{ \AA}^{-1}$ (solid), $q = 0.036 \text{ \AA}^{-1}$ (dotted), $q = 0.150 \text{ \AA}^{-1}$ (dashed) and $q = 0.300 \text{ \AA}^{-1}$ (long dashed).

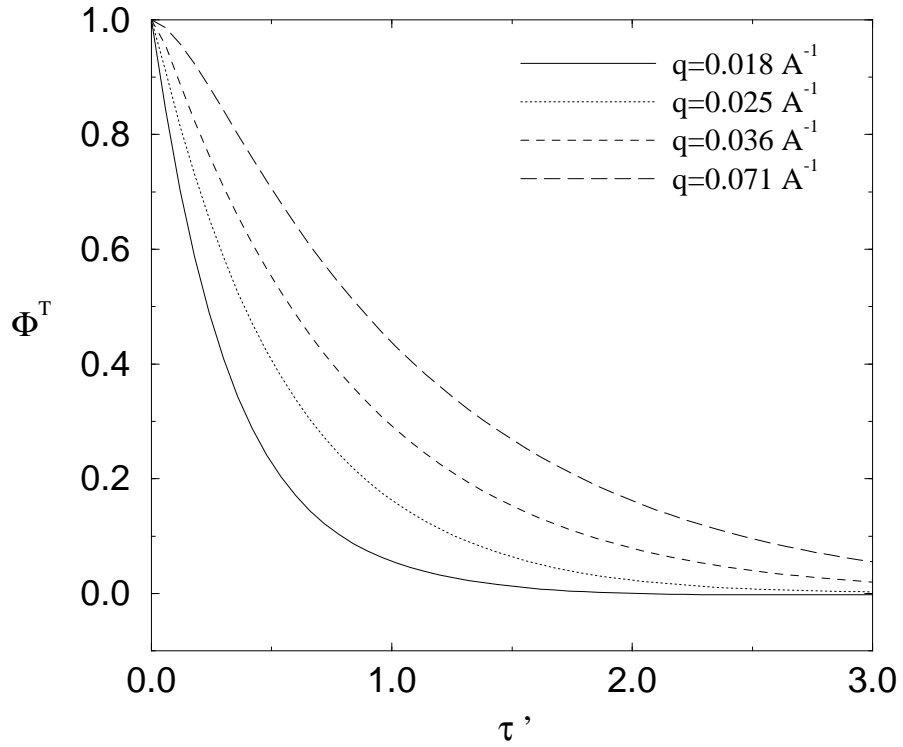


Figure 4.7: Scaling function of the transverse Kubo relaxation function versus $\tau' = \Lambda_{\text{lor}} q^z t$ at $T = T_c + 0.5K$ for $q = 0.018 \text{ \AA}^{-1}$ (solid), $q = 0.025 \text{ \AA}^{-1}$ (dotted), $q = 0.036 \text{ \AA}^{-1}$ (dashed) and $q = 0.071 \text{ \AA}^{-1}$ (long dashed).

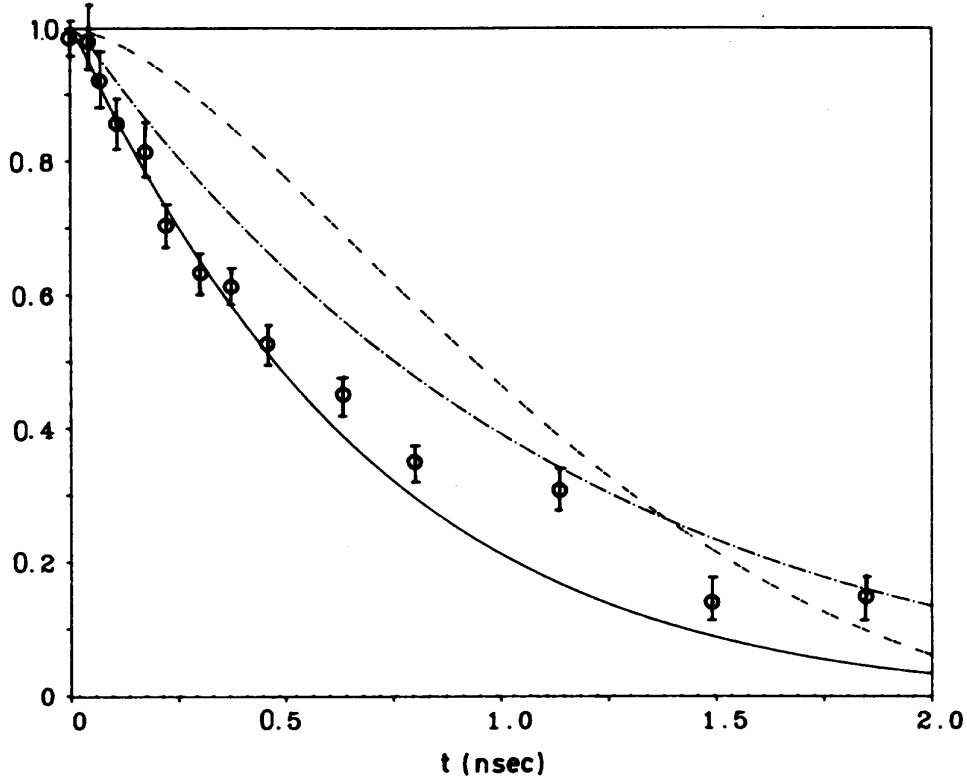


Figure 4.8: Transverse Kubo relaxation function $\Phi^T(q, g, t)$ at $q = 0.024\text{\AA}^{-1}$ (solid line) and $q = 0.028\text{\AA}^{-1}$ (dashed-dotted line) for dipolar ferromagnets versus time in *nsec*. The dashed line is the Kubo relaxation function for short range exchange interaction only at $q = 0.024\text{\AA}^{-1}$. Data points $q = 0.024\text{\AA}^{-1}$ from Fig. 1 of Ref. [190].

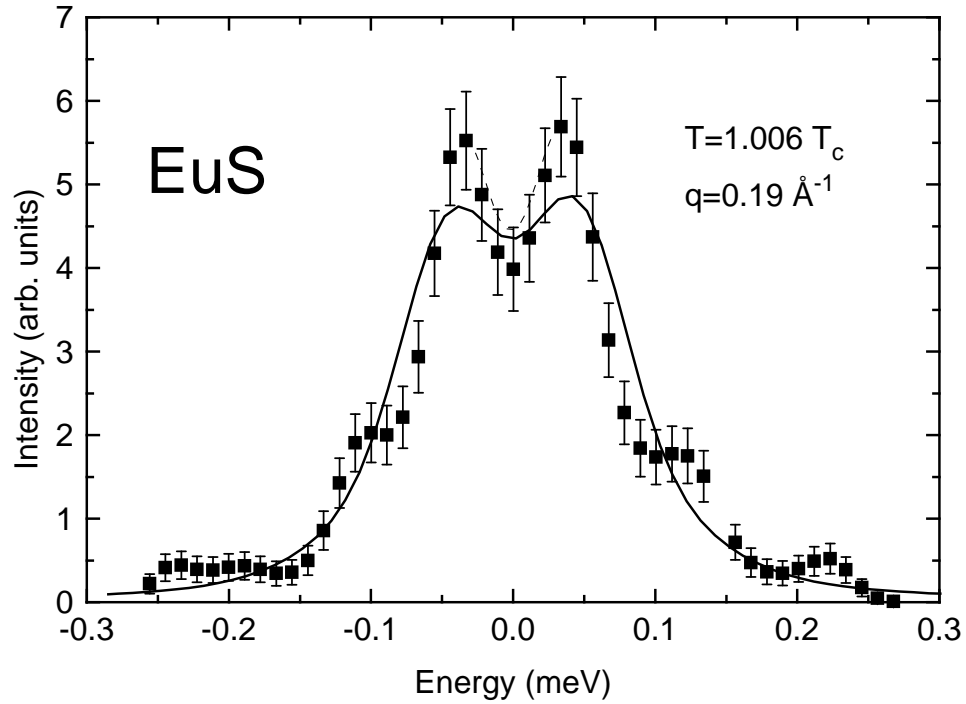


Figure 4.9: Normalized experimental data deconvoluted by a maximum entropy method. The solid line shows the spectral shape function predicted by mode coupling theory. The full circles (dashed line) indicate(s) the deconvoluted data. Taken from Ref. [93].

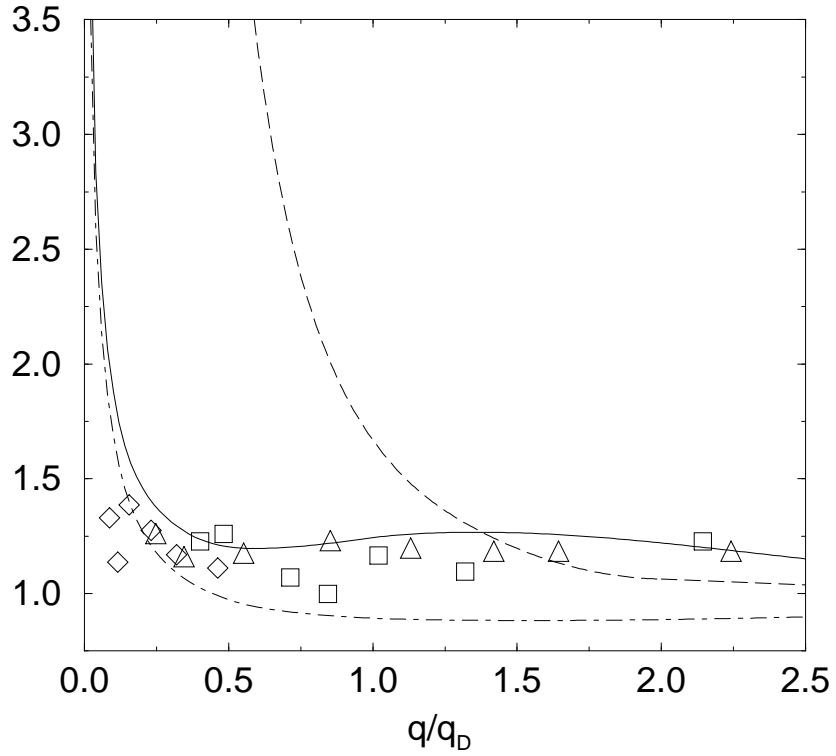


Figure 4.10: Scaling functions versus $y^{-1} = q/q_D$ at T_c (in units of the theoretical non universal constant Λ) for (i) the HWHM of the complete solution of the MC equations for the transverse Kubo relaxation function (solid), (ii) transverse (point-dashed) and (iii) longitudinal line (dashed) width in Lorentzian approximation. Experimental data of the transverse line width for *EuO* (\square Ref. [28], \diamond Ref. [189]) and *Fe* (\triangle Ref. [188]).

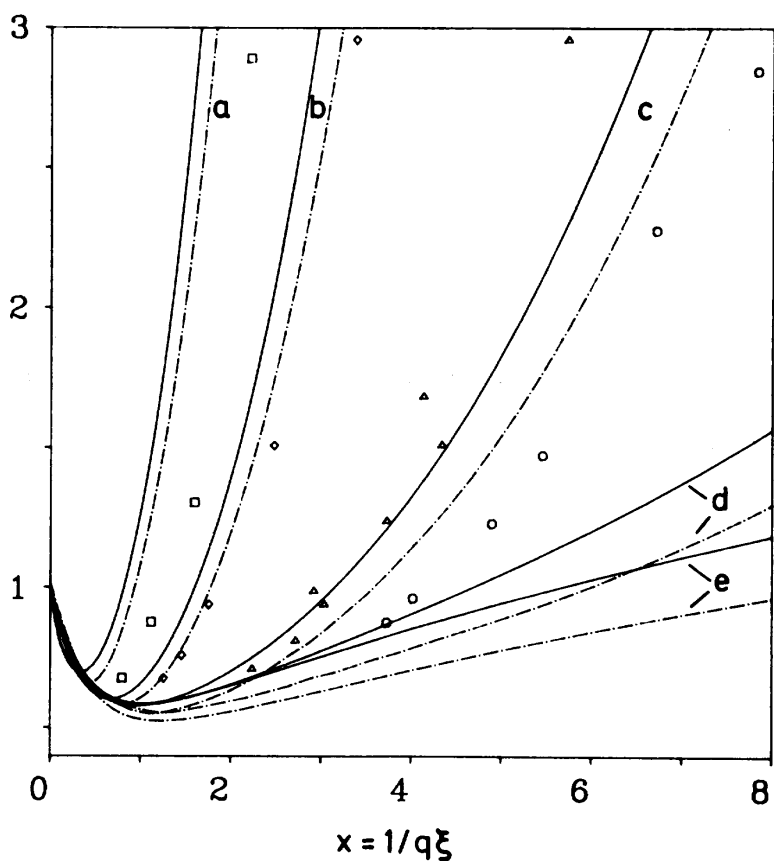


Figure 4.11: Scaling function of the transverse line width in Lorentzian approximation (solid lines) and of the HWHM of the complete solution (dashed lines) versus the scaling variable $x = (q\xi)^{-1}$ for a set of temperatures ($T - T_c =$ a) 1.4K, b) 5.8K, c) 21K, d) 51K). The Resibois-Piette function (solid) and the HWHM from the complete solution of the MC equations (dashed) without dipolar interaction is also plotted e). Experimental results for Fe from Refs. [188,189] ($T - T_c =$ (\square) 1.4K, (\diamond) 5.8K, (\triangle) 21.0K, (\circ) 51.0K).

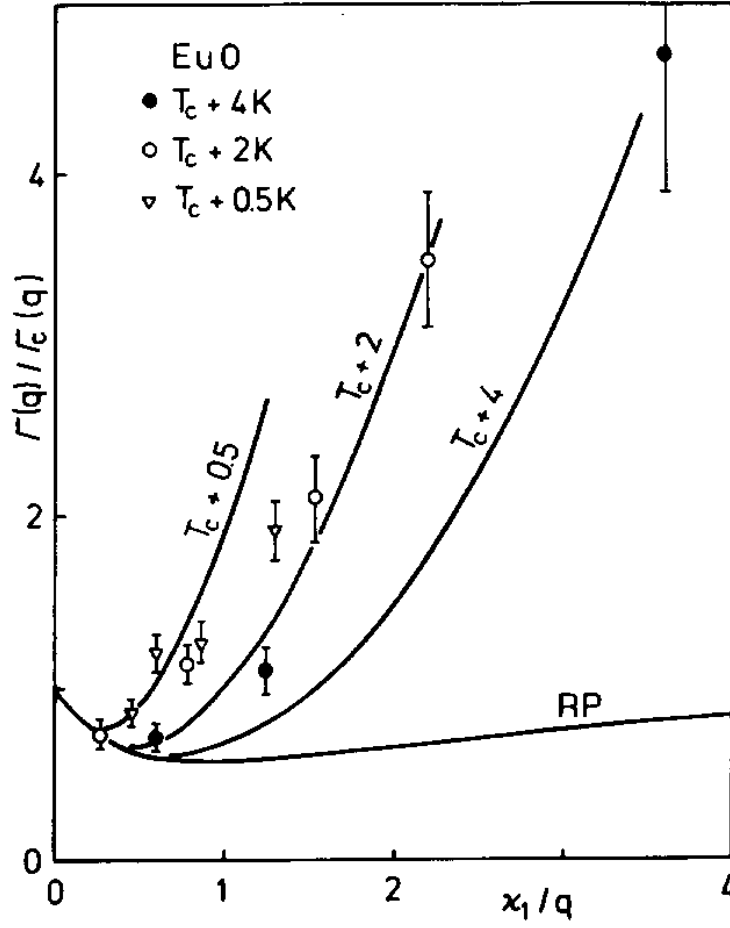


Figure 4.12: Scaling plot of the temperature dependence of the relaxation rate of critical fluctuations in *EuO* above the Curie temperature $T_c = 69.3K$. The solid lines represent the results from mode coupling theory [80]. The data were taken between $q = 0.018\text{\AA}^{-1}$ and $q = 0.15\text{\AA}^{-1}$. Taken from Ref. [192,193] ($\kappa_1 = 1/\xi$).

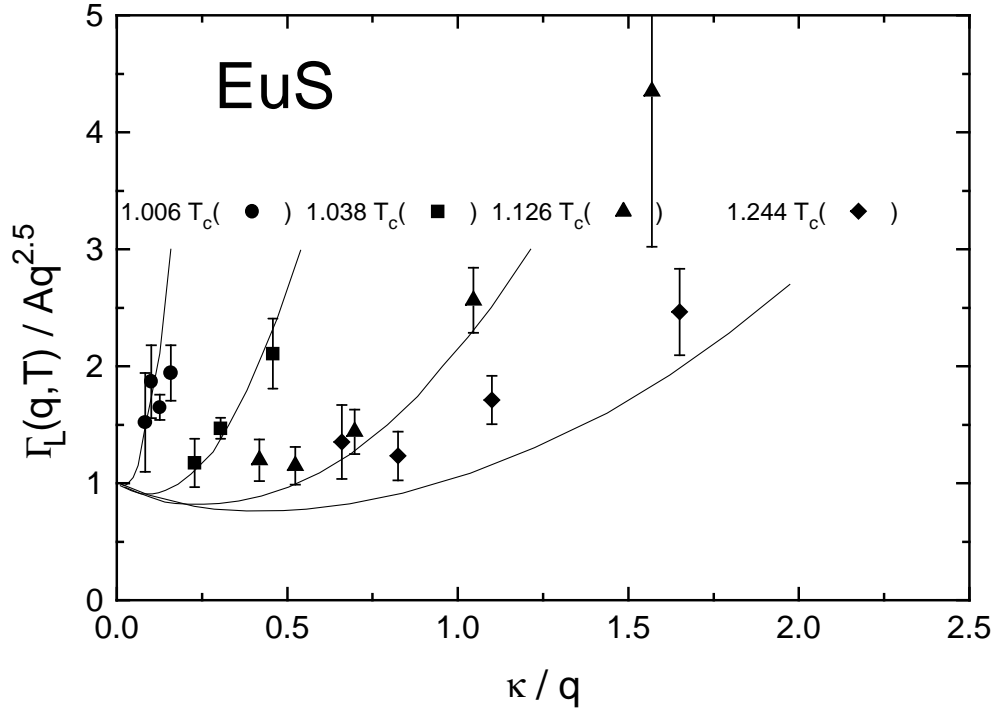


Figure 4.13: Comparison of the longitudinal linewidth of Lorentzian fits normalized to $\Lambda_{\text{exp}} q^{5/2}$ with $\Lambda_{\text{exp}} = 2.1 \text{meV} \text{\AA}^{5/2}$ to the dipolar dynamic scaling function predicted by mode coupling theory for $q_D = 0.245 \text{\AA}^{-1}$ for *EuS*. Figure taken from Ref. [33] ($\kappa = 1/\xi$).

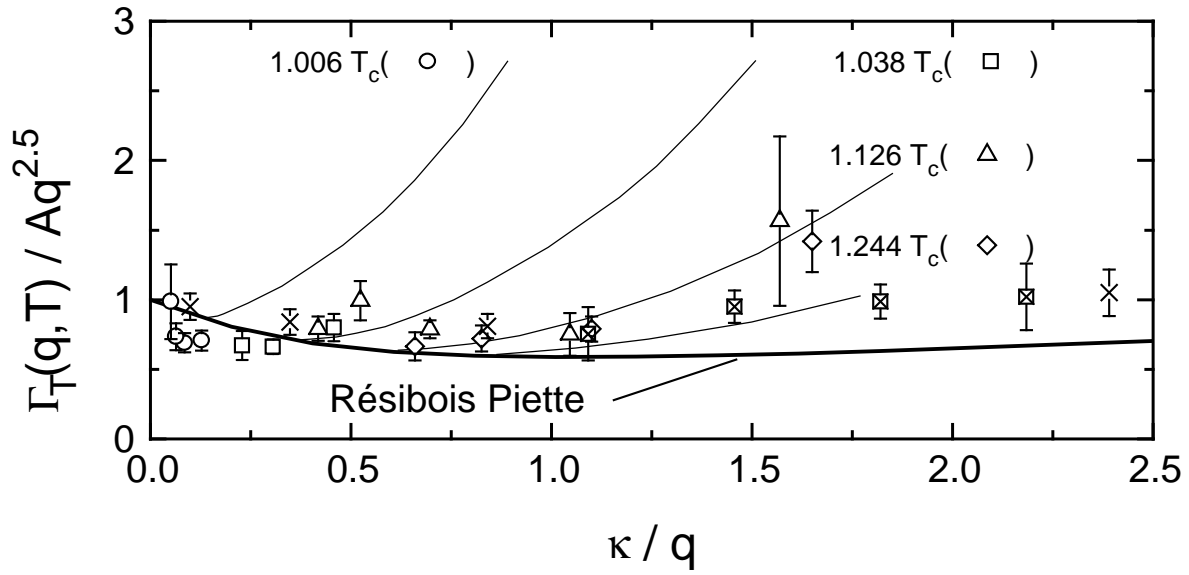


Figure 4.14: The same as Fig. 4.13 for the transverse widths. Figure taken from Ref. [33].

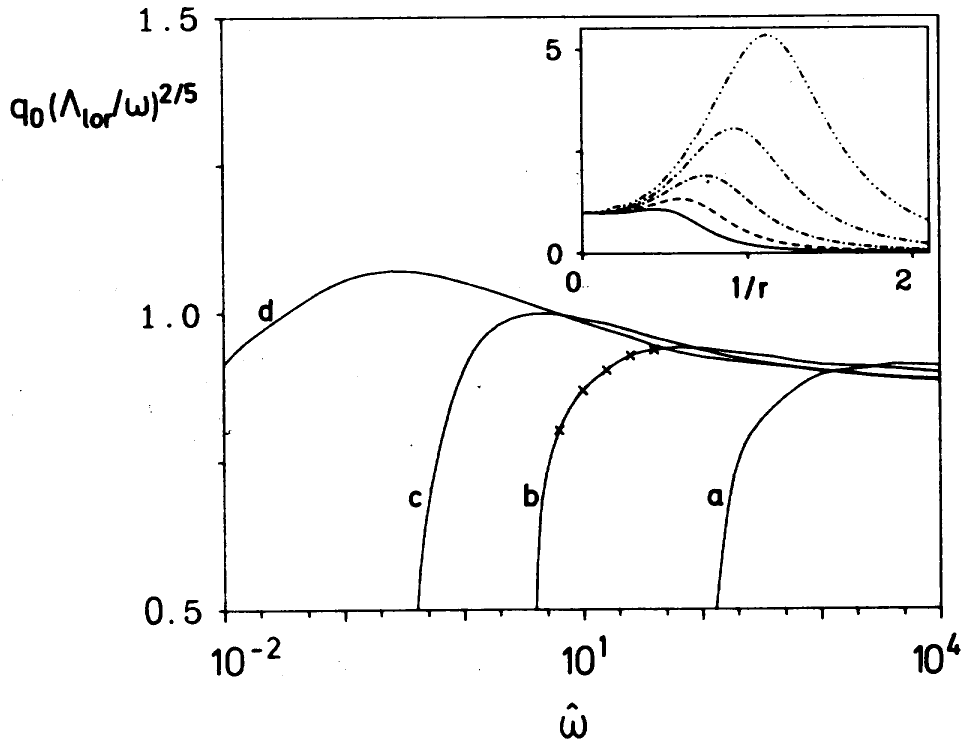


Figure 4.15: Scaled peak positions $q_0(\Lambda_{\text{lor}}/\omega)^{2/5}$ for constant energy scans of the scattering function for the complete solution of the MC equations versus the scaling variable $\hat{\omega}$ for $\varphi =$ a) 1.490, b) 1.294, c) 0.970 and d) for the isotropic case, i.e., $\varphi = 0$. **Inset:** $S^T(q, \omega)/S^T(0, \omega)$ in arbitrary units versus $\frac{1}{r}$ for $\varphi = 1.294$ for some typical values of the scaled frequency ($\hat{\omega} = 10^{L/10}$ with $L = 8$ (solid), 10 (dashed), 12 (point dashed), 14 ($-\dots-\dots-$) and 16 ($-\dots-\dots-$) indicated in the graph by crosses).

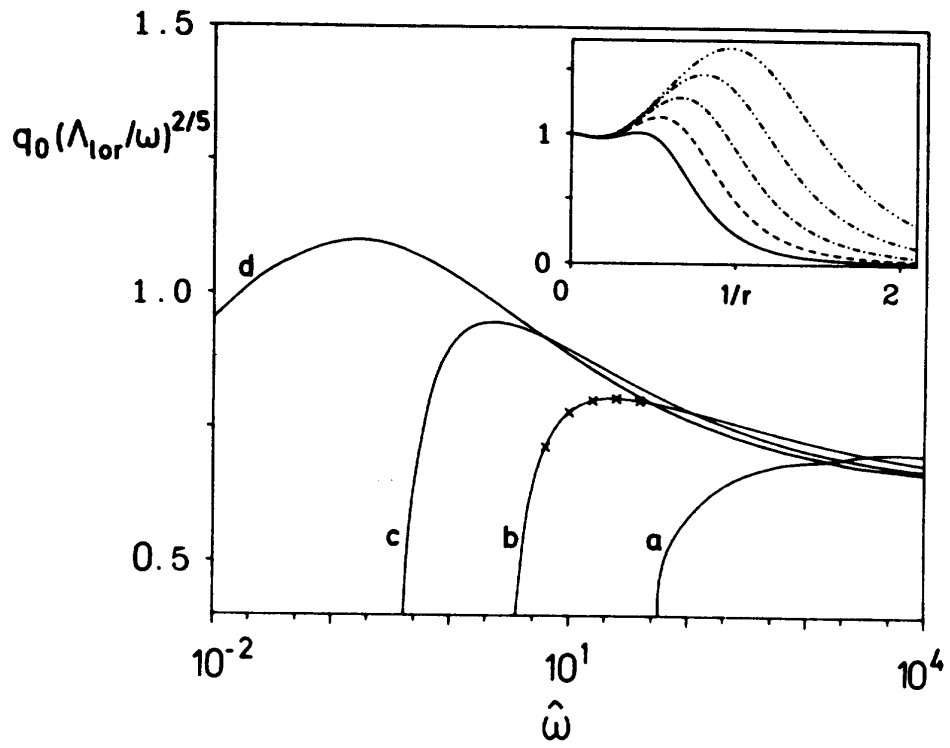


Figure 4.16: The same as in Fig. 4.15 for the scattering function resulting from the Lorentzian approximation.

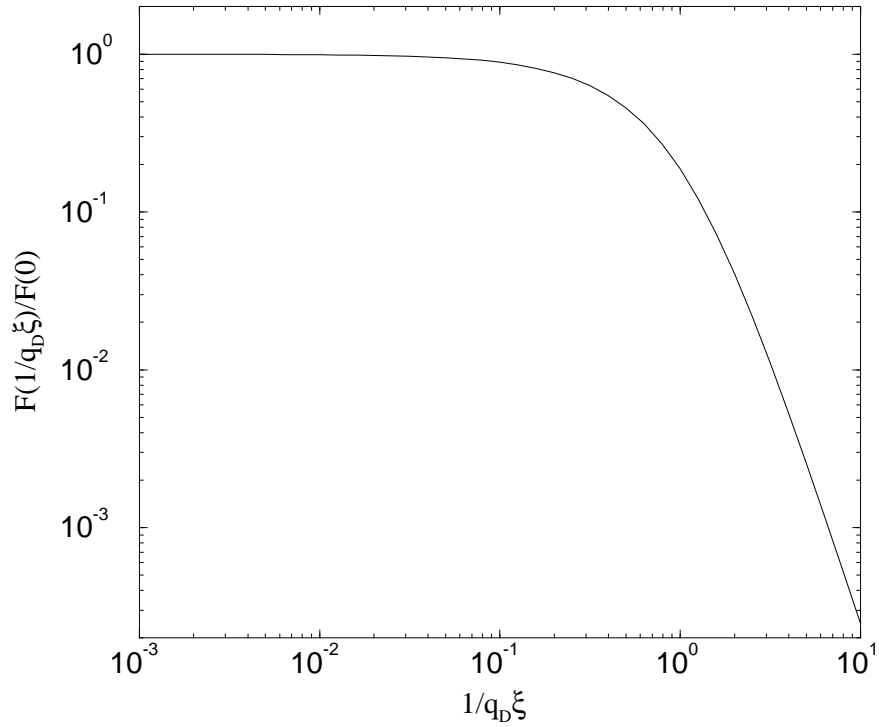


Figure 4.17: Universal crossover function $F(1/q_D \xi)/F(0)$ with $F(0) = 0.1956$ for the Onsager kinetic coefficient at zero frequency and zero wave vector versus the scaling variable $1/q_D \xi$.

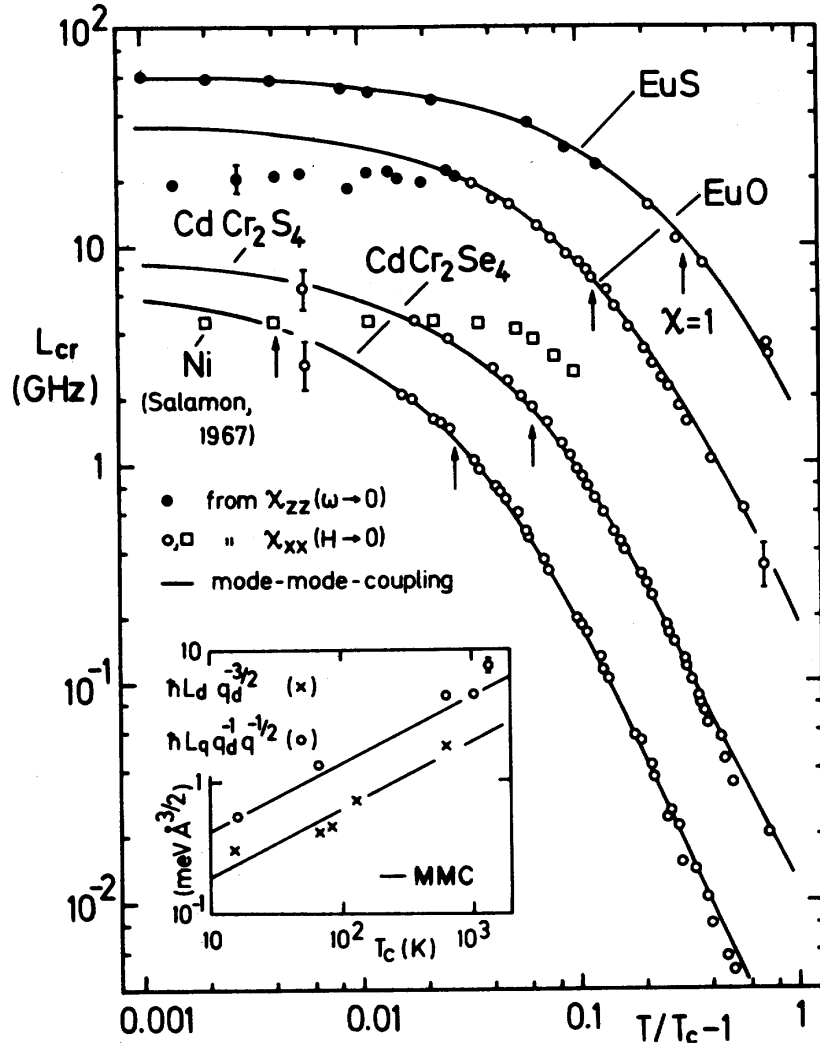


Figure 4.18: Critical part of the Onsager kinetic coefficient for the homogeneous spin dynamics above T_c of $CdCr_2Se_4$ (Ref. [149]), $CdCr_2S_4$ (Ref. [150]), EuO (Ref. [148]), EuS (filled circles: Ref. [147], open circles: Ref. [152]), and Ni (Ref. [236]). The solid lines represent the result from mode coupling theory [81]. **Inset:** Nonuniversal amplitudes $\hbar L_d q_d^{-3/2}$ for the kinetic coefficient and the relaxation rate at the critical point $\hbar L_q q_d^{-1/2} = \Gamma^T(q, T = T_c)/q^{5/2} \approx 5.1326\Lambda$ for ferromagnets including Fe and Co . Figure taken from Ref. [152].

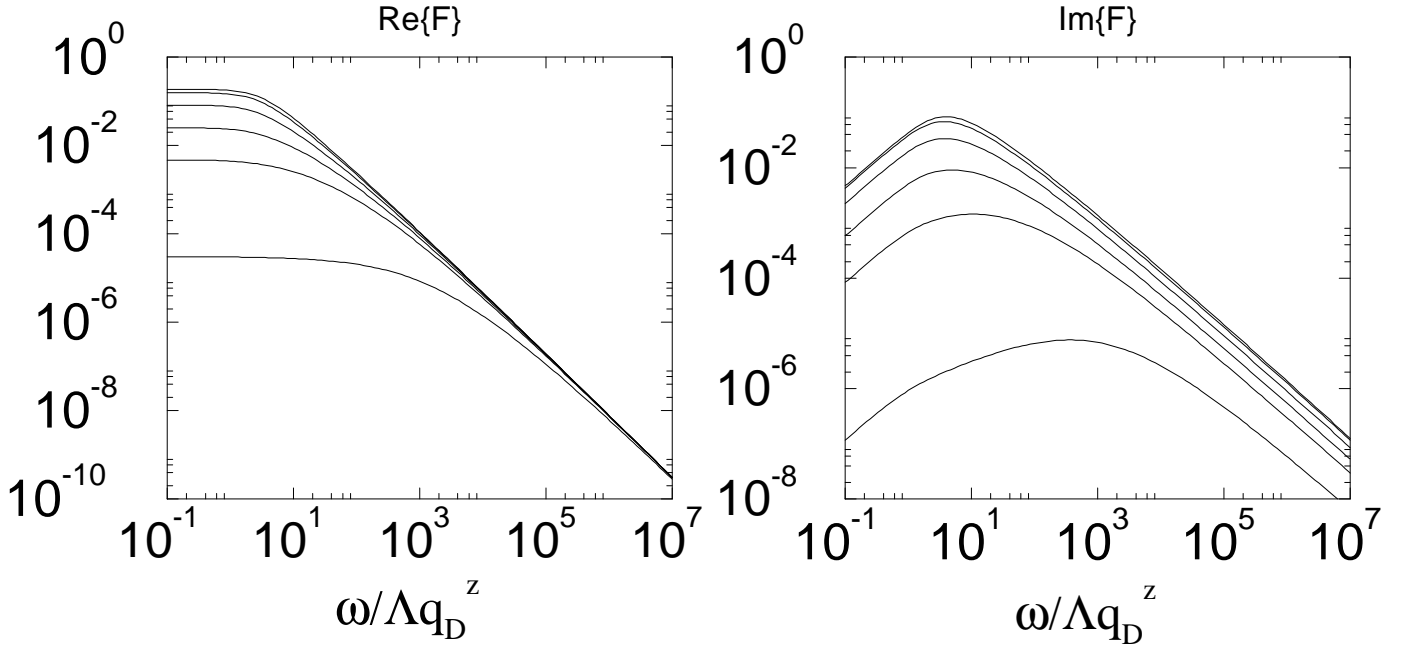


Figure 4.19: The real and imaginary parts of F are shown in a) and b) versus the scaled frequency $\hat{\omega} = \omega/\Lambda q_D^z$ for several values of $\varphi = \arctan(q_D \xi)$: $\varphi_1 = 0.99\frac{\pi}{2}$ (top curve), $\varphi_2 = 0.90\frac{\pi}{2}$, $\varphi_3 = \frac{\pi}{2}(1 - 10^{-0.5})$, $\varphi_4 = \frac{\pi}{2}(1 - 10^{-0.25})$, $\varphi_5 = \frac{\pi}{2}(1 - 10^{-0.1})$, $\varphi_6 = \frac{\pi}{2}(1 - 10^{-0.025})$ (bottom curve).

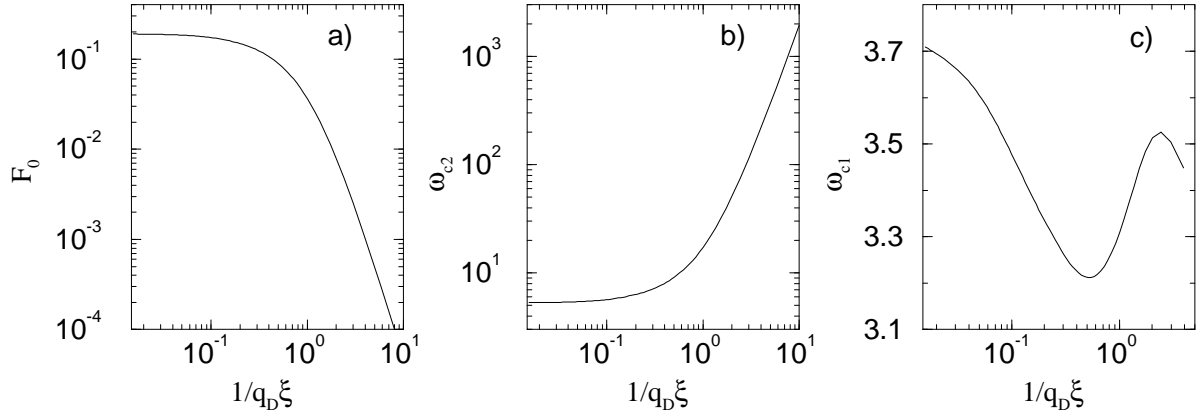


Figure 4.20: The scaling functions for the a) Onsager coefficient at zero frequency $F(1/q_D \xi)$ and b) the scaling functions $\omega_{c2}(1/q_D \xi)$ and c) $\omega_{c1}(1/q_D \xi)$ characterizing the large and low frequency behaviour, respectively.

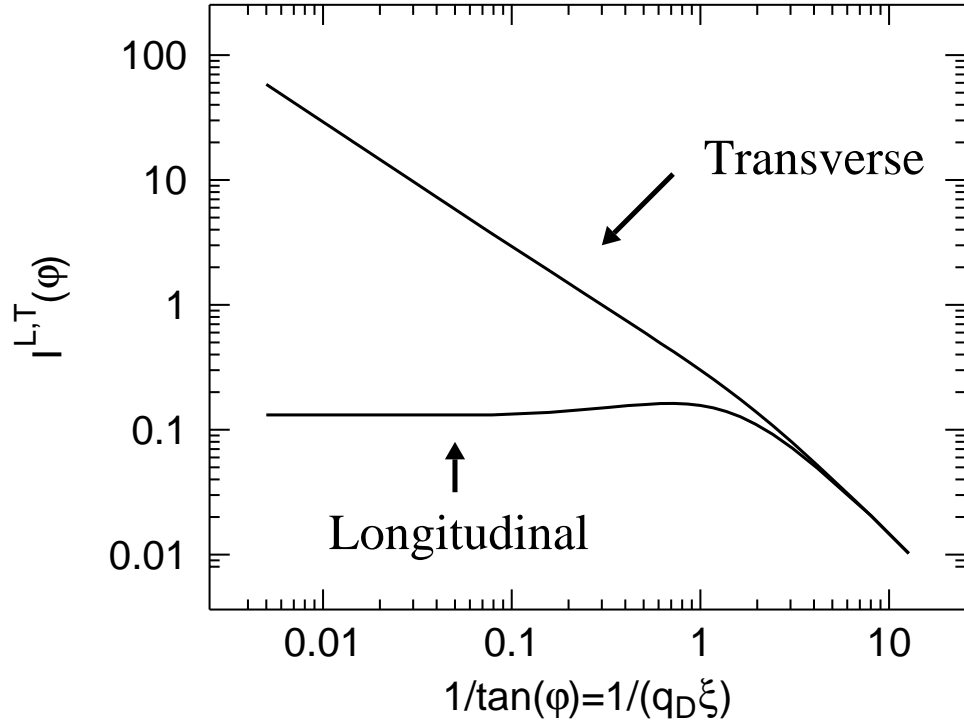


Figure 4.21: Scaling functions $I_{L,T}(\varphi)$ for the transverse and longitudinal auto-correlation-time $\tau_{L,T}$ versus $1/q_D \xi$.

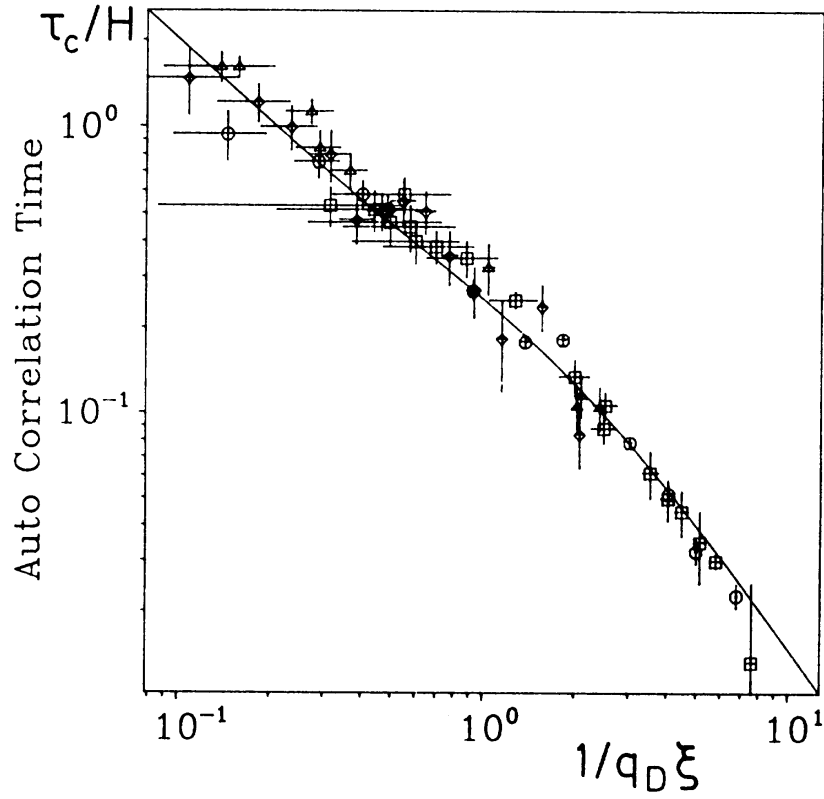


Figure 4.22: Auto correlation time τ_c/H (in units of the non universal constant H) versus the scaling variable $\frac{1}{q_D \xi}$ (solid line). Experimental results for the auto correlation time in units of H_{exp} for Fe (Ref. [113]: \square) and Ni (Ref. [228]: \diamond , Ref. [95]: \triangle , Ref. [113]: \circ).

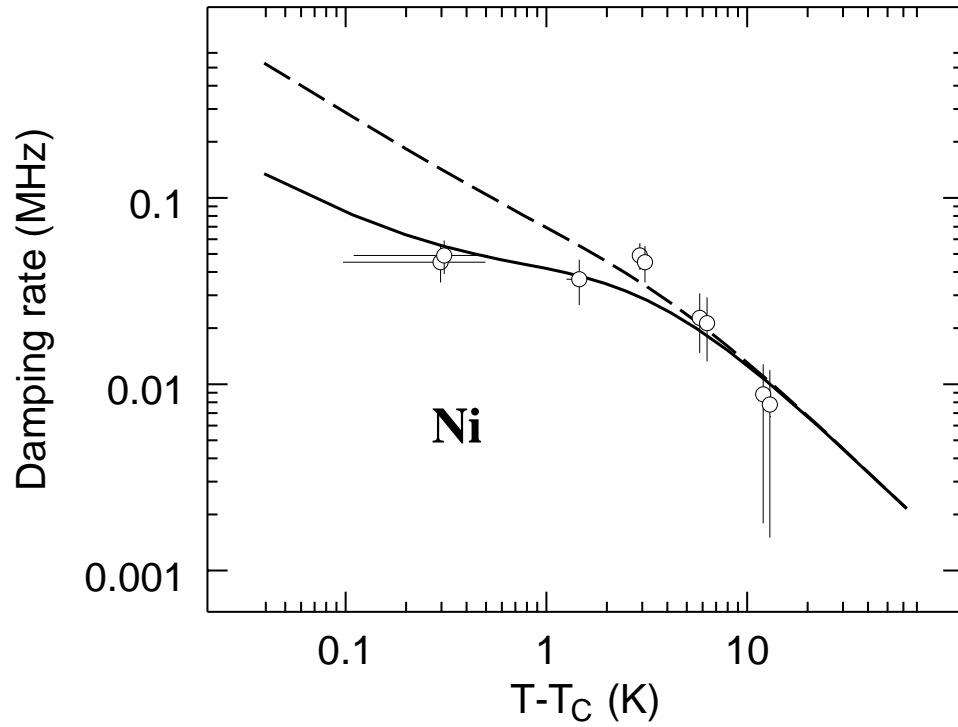


Figure 4.23: Temperature dependence of the μ SR damping rate for metallic *Ni*. The points are the experimental data of Nishiyama et al. [205]. The full line is the result of the model which takes the muon dipolar interaction into account. The dashed line gives the prediction when this latter interaction is neglected.

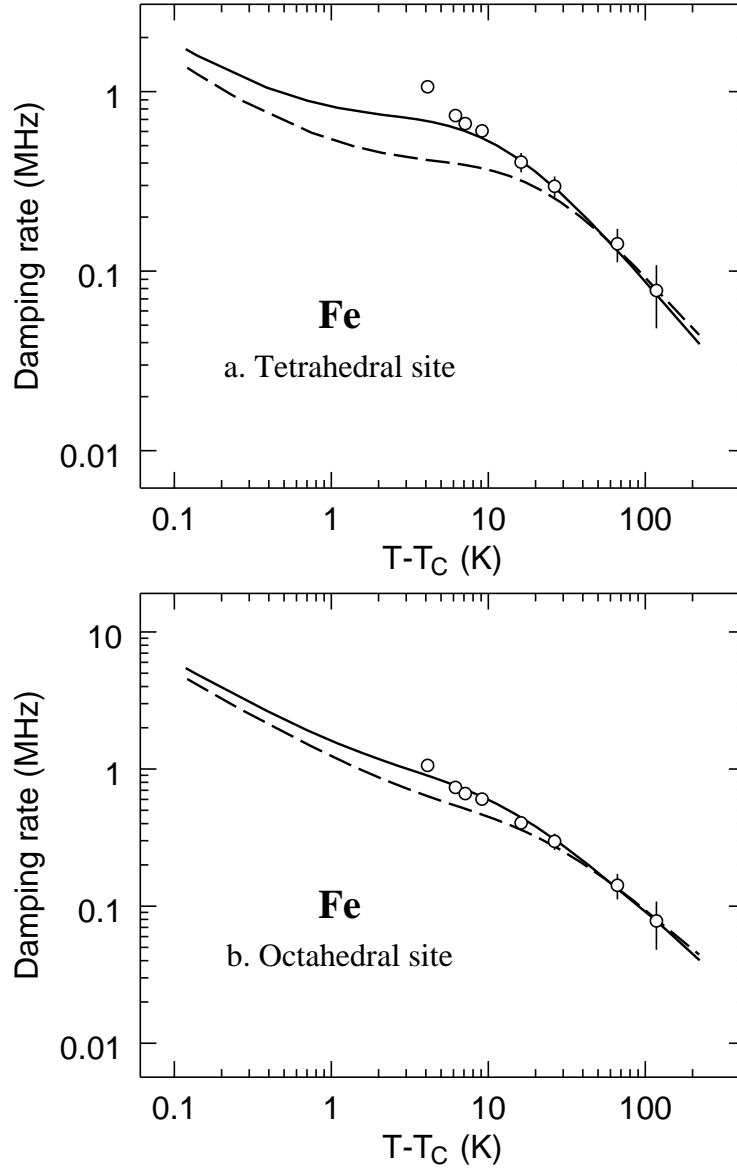


Figure 4.24: Temperature dependence of the μ SR damping rate for metallic *Fe*. The points are the experimental data of Herlach et al. [108]. The curves are the predictions of mode-coupling theory for different sets of material parameters. In Fig. 4.24a (Fig. 4.24b) the muon is supposed to diffuse between tetrahedral (octahedral) sites. The full and dashed lines present the results obtained with (q_D, ξ_0) equal to $(0.033 \text{ \AA}^{-1}, 0.82 \text{ \AA})$ and to $(0.045 \text{ \AA}^{-1}, 0.95 \text{ \AA})$ respectively; see Table VIII.

V. OTHER DIPOLAR SYSTEMS

Dipolar interactions are of importance not only for the critical behavior of three-dimensional isotropic ferromagnets, but also for other magnetic materials such as antiferromagnets, ferromagnets with an uniaxial or planar exchange anisotropy. Furthermore, dipolar interactions play an important role in two-dimensional systems, especially with regard to the existence of long-range order.

A. Dipolar Antiferromagnets

1. Hamiltonian and equation of Motion

The order parameter of an antiferromagnet is the staggered magnetization, i.e., in the case of two sublattices the difference of the magnetization on these. Due to the alternating nature of the order parameter one supposes that the effect of the dipolar interaction on the long-range order parameter fluctuations is averaged out and thus one expects no influence on the static critical behavior. Indeed in Ref. [5] it was shown that in contrast to the ferromagnetic case, the main parameters characterizing the dipolar interaction become irrelevant for the critical statics of antiferromagnets. Yet there is an important effect on the dynamics, since the dipolar forces lead to new damping processes in the long wave length dynamics of the magnetization, because they break conservation of the total magnetization. Since the magnetization and staggered magnetization are coupled dynamically, there should be a crossover in the dynamic critical exponents and related features in the dynamical scaling functions. This effect has been studied theoretically for temperatures above and at the Néel temperature T_N by means of mode-coupling theory [73].

The Hamiltonian of a dipolar antiferromagnet reads

$$H = - \sum_{l \neq l'} \sum_{\alpha\beta} \left(J_{ll'} \delta^{\alpha\beta} + A_{ll'}^{\alpha\beta} \right) S_l^\alpha S_{l'}^\beta, \quad (5.1)$$

with spins \mathbf{S}_l at lattice sites \mathbf{x}_l . The first term in brackets is the exchange interaction $J_{ll'}$ and the second the dipole-dipole interaction with the dipolar tensor given by

$$A_{ll'}^{\alpha\beta} = -\frac{1}{2}(g_L\mu_B)^2 \left(\frac{\delta^{\alpha\beta}}{|\mathbf{x}_l - \mathbf{x}_{l'}|^3} - \frac{3(\mathbf{x}_l - \mathbf{x}_{l'})^\alpha(\mathbf{x}_l - \mathbf{x}_{l'})^\beta}{|\mathbf{x}_l - \mathbf{x}_{l'}|^5} \right). \quad (5.2)$$

We define Fourier transformed quantities by

$$S_l^\alpha = \frac{1}{\sqrt{N}} \sum_{\mathbf{q}} e^{i\mathbf{q}\cdot\mathbf{x}} S_{\mathbf{q}}^\alpha, \quad (5.3)$$

$$J_{ll'} = \frac{1}{N} \sum_{\mathbf{q}} e^{i\mathbf{q}\cdot(\mathbf{x}_l - \mathbf{x}_{l'})} J_{\mathbf{q}}, \quad (5.4)$$

$$A_{ll'}^{\alpha\beta} = \frac{1}{N} \sum_{\mathbf{q}} e^{i\mathbf{q}\cdot(\mathbf{x}_l - \mathbf{x}_{l'})} A_{\mathbf{q}}^{\alpha\beta}, \quad (5.5)$$

and get

$$H = - \sum_{\mathbf{q}} \left(J_{\mathbf{q}} \delta^{\alpha\beta} + A_{\mathbf{q}}^{\alpha\beta} \right) S_{\mathbf{q}}^\alpha S_{-\mathbf{q}}^\beta \quad (5.6)$$

for the Hamiltonian in terms of Fourier components. In order to study the long-wavelength behavior of the model one needs to know the behavior of the dipole-dipole interaction tensor $A_{\mathbf{q}}^{\alpha\beta}$ at small wave vectors. The result depends on the lattice structure and the dimensionality of the system. For a three-dimensional system the expansion has been given in section III (see Eqs. (3.4)). In two dimensions the dipole-interaction tensor has been analyzed by Maleev [Maleev76]. He finds for small wave vectors

$$A_{\mathbf{q}}^{\alpha\beta} = A^{(0)} \left(\frac{1}{3} \delta^{\alpha\beta} - \hat{z}^\alpha \hat{z}^\beta \right) + A^{(1)} q \left(\hat{z}^\alpha \hat{z}^\beta - \frac{q^\alpha q^\beta}{q^2} \right), \quad (5.7)$$

where $\mathbf{q} = (q_x, q_y, 0)$ is an in-plane wave vector and z denotes the direction perpendicular to the plane $\mathbf{r} = (r_x, r_y, 0)$. The constants $A^{(0)}$ and $A^{(1)}$ depend on the lattice structure

$$A^{(0)} = \frac{3}{4} (g_L\mu_B)^2 \sum_{\mathbf{r} \neq 0} \frac{1}{r^3}, \quad (5.8)$$

$$A^{(1)} = \frac{\pi}{v_2} (g_L\mu_B)^2, \quad (5.9)$$

where v_2 is the volume of the 2D unit cell.

With the standard commutation relation for spin operators $[S_{\mathbf{k}}^\alpha, S_{\mathbf{q}}^\beta] = i\hbar \epsilon_{\alpha\beta\gamma} S_{\mathbf{k}+\mathbf{q}}^\gamma$ one gets the following equations of motion [217],

$$\begin{aligned}
\frac{d}{dt} S_{\mathbf{q}}^x = \sum_{\mathbf{k}} \bigg[& (A_{\mathbf{k}}^{yy} + J_{\mathbf{k}}) (S_{\mathbf{k}+\mathbf{q}}^z S_{-\mathbf{k}}^y + S_{\mathbf{k}}^y S_{\mathbf{q}-\mathbf{k}}^z) \\
& - (A_{\mathbf{k}}^{zz} + J_{\mathbf{k}}) (S_{\mathbf{k}}^z S_{\mathbf{q}-\mathbf{k}}^y + S_{\mathbf{q}+\mathbf{k}}^y S_{-\mathbf{k}}^z) \\
& + A_{\mathbf{k}}^{xy} (S_{\mathbf{k}}^x S_{\mathbf{q}-\mathbf{k}}^z + S_{\mathbf{q}+\mathbf{k}}^z S_{-\mathbf{k}}^x) \\
& - A_{\mathbf{k}}^{xz} (S_{\mathbf{k}}^x S_{\mathbf{q}-\mathbf{k}}^y + S_{\mathbf{q}+\mathbf{k}}^y S_{-\mathbf{k}}^x) \\
& + A_{\mathbf{k}}^{yz} (S_{\mathbf{q}+\mathbf{k}}^z S_{-\mathbf{k}}^z + S_{\mathbf{k}}^z S_{\mathbf{q}-\mathbf{k}}^z - S_{\mathbf{k}}^y S_{\mathbf{q}-\mathbf{k}}^y - S_{\mathbf{q}+\mathbf{k}}^y S_{-\mathbf{k}}^y) \bigg] \quad (5.10)
\end{aligned}$$

2. Critical Behavior of 3D Dipolar Antiferromagnets

Now we turn to the critical dynamics of dipolar antiferromagnets. Specializing to the three-dimensional isotropic case and retaining only those terms which are dominant in the long wavelength limit the Hamiltonian for a simple cubic lattice reduces to [73]

$$\begin{aligned}
H = J \int_{\mathbf{q}} \bigg[& ((qa)^2 - 6) \delta^{\alpha\beta} - g \frac{q^\alpha q^\beta}{q^2} \bigg] M_{\mathbf{q}}^\alpha M_{-\mathbf{q}}^\beta \\
& + J \int_{\mathbf{q}} (6 - (qa)^2) \delta^{\alpha\beta} N_{\mathbf{q}}^\alpha N_{-\mathbf{q}}^\beta, \quad (5.11)
\end{aligned}$$

where $M_{\mathbf{q}}^\alpha = S_{\mathbf{q}}^\alpha$ denotes the magnetization and $N_{\mathbf{q}}^\alpha = S_{\mathbf{q}+\mathbf{q}_0}^\alpha$ the staggered magnetization, and we have introduced the abbreviation $\int_{\mathbf{q}} = \int v_a \frac{d^3 q}{(2\pi)^3}$. The wave vector $\mathbf{q}_0 = \frac{\pi}{a}(1, 1, 1)$ characterizes the antiferromagnetic modulation.

Starting from this Hamiltonian mode coupling equations for the correlation functions of the magnetization and staggered magnetization have been derived and analyzed in Ref. [73]. For instance for the longitudinal magnetization mode one finds

$$\begin{aligned}
\Gamma_M^L(\mathbf{q}, t) = 4\Lambda_{\text{af}}^2 \int_0^{q_{BZ}} k^2 dk \int_{-1}^1 d(\cos \vartheta) \bigg[& \left(\frac{g}{12}\right)^2 \sin^2 \vartheta \Phi_M^T(\mathbf{k}_+, \xi, t) \Phi_M^L(\mathbf{k}, t) \\
& + \frac{(2\mathbf{q} \cdot \mathbf{k} + \mathbf{q}^2)^2}{(\mathbf{k}^2 + \xi^{-2})(\mathbf{k}_+^2 + \xi^{-2})} \left(\sin^2 \vartheta \Phi_N^T(\mathbf{k}_+, t) \Phi_N^L(\mathbf{k}, t) + \cos^2 \vartheta \Phi_N^T(\mathbf{k}_+, t) \Phi_N^T(\mathbf{k}, t) \right) \bigg], \quad (5.12)
\end{aligned}$$

where we have used the abbreviations $\mathbf{k}_+ = \mathbf{k} + \mathbf{q}$, $\Lambda_{\text{af}} = a^{3/2} \sqrt{\frac{Jk_B T}{8\pi^2}}$ and $q_{BZ} = \frac{2\pi}{2a} \sqrt{\frac{3}{4\pi}}$.

It is found that the memory kernels obey generalized scaling laws of the form

$$\Gamma_{M,N}^{L,T}(q, g, \xi, t) = \Lambda_{\text{af}}^2 q^{2z} \gamma_{M,N}^{L,T}(x, y, \tau), \quad (5.13)$$

$$\Phi_{M,N}^{L,T}(q, g, \xi, t) = \phi_{M,N}^{L,T}(x, y, \tau), \quad (5.14)$$

where the scaling variables are defined by $x = 1/q\xi$, $y = q_A/q$, and $\tau = \Lambda_{\text{af}} q^z t$ with the dynamic critical exponent $z = 3/2$. The characteristic wave vector q_A is related to the dipolar wave vector $q_D = \sqrt{g}/a$ by

$$q_A = \left(\frac{1}{12}\right)^{2/3} (q_D a)^{4/3} q_{BZ}. \quad (5.15)$$

The value $3/2$ is the dynamical critical exponent for isotropic antiferromagnets and any crossover to dipolar behavior is contained in the dynamic scaling function. In evaluating the transport coefficients $\Gamma_{M,N}^{L,T}$ only two mode decay processes have been considered (see Eq. (4.12)). Without dipolar interaction, i.e., for the isotropic exchange antiferromagnet, the magnetization modes can decay into staggered modes only [140,263,231,129].

The dipolar interaction leads in addition to a decay into two magnetization modes, dominating for small wave vectors. In the strong dipolar limit ($T \rightarrow T_N$ and $q \rightarrow 0$) the mode coupling equations for the magnetization modes can be solved exactly with the result

$$\Gamma_M^\lambda(q, \xi, t) = \frac{\Lambda_{\text{af}} g}{12 \sqrt{\frac{14}{9} + \frac{\pi^2}{8}}} q_{BZ}^{3/2} \left[\frac{16}{9} \delta^{\lambda L} + \left(\frac{\pi^2}{8} - \frac{2}{9} \right) \delta^{\lambda T} \right] \delta(t) \quad (5.16)$$

corresponding to a relaxation of the magnetization modes enforced by the dipolar interaction. The phase space for this decay is the full Brillouin zone, whereas the decay into staggered modes is weighted by the critical static susceptibilities. Therefore, with separation from the critical temperature and for larger wave vectors the decay of the magnetization mode into two staggered modes dominates the decay into two magnetization modes.

The mode coupling equations for dipolar antiferromagnets have been solved in the Lorentzian approximation in Ref. [73]. The results for the transverse scaling function for the magnetization and staggered magnetization $\gamma_{M,N}^T(x, \varphi)$ versus x for different values of $\varphi = N\pi/30$ with $N = 0, 1, \dots, 14$ are displayed in Figs. 5.1 and 5.2. The corresponding plots for the longitudinal scaling functions are very similar [73]. The curves with $N = 0$ correspond to the isotropic case. It is important to note, that the effect of the dipolar interaction

on the scaling functions of the magnetization and staggered magnetization modes is rather different. The scaled line width for the magnetization modes exceeds the isotropic curve by an amount which increases with T on approaching T_c (i.e. larger values of $\varphi = \arctan(q_D \xi)$). This reflects the crossover from a diffusive behavior $\Gamma_M \propto q^2 q_A^{-1/2}$ to a relaxational behavior $\Gamma_M \propto q_A^{3/2}$. The line width of the staggered magnetization at fixed scaling variable x decreases with T approaching T_c since the magnetization modes become uncritical. But, this change is much less pronounced than for the magnetization modes and more important, the asymptotic hydrodynamic dependence on the wave vector and correlation length is unmodified, i.e., the hydrodynamic behavior is always relaxational.

In the dipolar (D) and isotropic (I) critical (C) and hydrodynamical (H) limiting regions the mode coupling equations can be solved analytically. These regions are defined by DC: $y \gg 1, x \ll 1$; IC: $y \ll 1, x \ll 1$; DH: $y \gg x, x \gg 1$; IH: $y \ll x, x \gg 1$. The results are summarized in Table X, where we note that these asymptotic power laws are the same for the longitudinal and transverse fluctuations. In the immediate vicinity of $q = q_A$ there is a dynamic crossover from $z_{\text{eff}} = 3/2$ to $z_{\text{eff}} = 2$ for the staggered magnetization and from $z_{\text{eff}} = 3/2$ to an uncritical value $z_{\text{eff}} = 0$ for the magnetization modes.

$RbMnF_3$ is one of the most thoroughly studied isotropic antiferromagnets [255,51,162]. Taking the values for the exchange coupling and the static susceptibility of the magnetization from Refs. [255,270,121], the characteristic wave vector q_A is about 0.02 \AA^{-1} . Unfortunately the neutron scattering data [255,51,162] for the line width of the staggered magnetization modes are limited to the isotropic region and to our knowledge there are no data for the line widths of the magnetization modes.

The dipolar effects could be observed more readily in $EuSe$ and $EuTe$ because of their smaller transition temperatures $4.8K$ and $9.7K$ implying larger q_A . Experiments in the appropriate wave vector and temperature region are, however, still lacking.

B. Uniaxial Dipolar Ferromagnets

We have mainly concentrated on the influence of dipolar forces on otherwise isotropic ferromagnets. But, even in systems which are anisotropic to start with such as uniaxial ferromagnets, the dipolar interaction has a significant effect, because of its long-range nature.

The influence of the dipolar interactions on the critical statics of isotropic and uniaxial ferromagnets is quite different. Whereas for isotropic ferromagnets the dipolar interaction leads only to a slight modification of the critical exponents, Larkin and Khmel'nitskii [161] have discovered that uniaxial dipolar ferromagnets show classical behavior with logarithmic corrections in three dimensions. This system was then studied by Aharony [6] by means of the renormalization group method. Aharony employed an isotropic elimination procedure and calculated the critical exponents to first order in $(3 - d)$ as well as logarithmic corrections [7]. Note, that the dipolar interaction leads to a shift in the upper critical dimension from 4 to $d_c = 3$.

The existence of logarithmic corrections was verified experimentally for a number of uniaxial ferromagnetic substances [9,90]. However, these experiments were performed in regions of the reduced temperature, where departures from the asymptotic behavior are expected and are observed indeed. In particular, a maximum in the effective exponent of the susceptibility [90] has been found. On the basis of a generalized minimal subtraction scheme the latter crossover from Ising behavior with non classical exponents to asymptotic uniaxial dipolar behavior, which is characterized by classical exponents with logarithmic corrections, has been analyzed in Ref. [83,88]. The theoretical results for the specific heat and susceptibility are in quantitative agreement with measurements on $LiTbF_4$, where solely the strength of the dipolar coupling constant entered as an adjustable parameter [83,88].

The Landau-Ginzburg free energy functional for a n -component uniaxial spin system with an isotropic exchange coupling and dipolar interaction is given by [161,6]

$$\mathcal{H} = -\frac{1}{2} \int_k \left[r + k^2 + g^2 \frac{q^2}{k^2} \right] S^\alpha(\mathbf{k}) S^\alpha(-\mathbf{k})$$

$$-\frac{u_0}{4!} \int_{\{k_i\}} S^\alpha(\mathbf{k}_1) S^\alpha(\mathbf{k}_2) S^\beta(\mathbf{k}_3) S^\beta(-\mathbf{k}_1 - \mathbf{k}_2 - \mathbf{k}_3). \quad (5.17)$$

Here $S^\alpha(\mathbf{q})$ are the n components of the spin variables. The d -dimensional wave vector $\mathbf{k} = (\mathbf{p}, q)$ is decomposed into q , the component along the uniaxial direction, and \mathbf{p} , the remaining $(d-1)$ components. The bare reduced temperature is given by $r = (T - T_c^0)/T_c^0$ and g^2 is a measure of the relative strength of the dipolar interaction. The dipolar term $g^2 \frac{q^2}{k^2}$ suppresses the fluctuations in the z -direction.

In Ref. [76] the dynamics of uniaxial dipolar magnets was described in terms of a simple Time Dependent Ginzburg Landau Model (TDGL) with the equation of motion

$$\frac{\partial}{\partial t} S^\alpha(\mathbf{k}, t) = -\Gamma_0 \frac{\delta \mathcal{H}}{\delta S^\alpha(-\mathbf{k}, t)} + \eta(\mathbf{k}, t). \quad (5.18)$$

Since the order parameter is a non-conserved quantity in the presence of the dipolar interaction, the kinetic coefficient Γ_0 is wave vector independent. The random forces $\eta(\mathbf{k}, t)$ represent the uncritical degrees of freedom and are characterized by a Gaussian probability distribution. A renormalization group analysis for the above TDGL gives for the dynamic critical exponent [76]

$$z = 2 + c\eta, \quad \text{with } c = 0.92. \quad (5.19)$$

This may be compared with the value for the TDGL model for spin systems with short range exchange interaction [100,101], where $c = 0.73$ and the van Hove prediction $c = -1$.

Since for uniaxial dipolar magnets the fourth order coupling is marginal at $d = 3$, there are logarithmic corrections to the classical behavior. For the statics one finds [161,6] for the susceptibility χ and the specific heat C

$$\chi \propto \tau^{-1} |\ln \tau|^{1/3}, \quad C \propto |\ln \tau|^{1/3}, \quad (5.20)$$

where $\tau = (T - T_c)/T_c$ is the reduced temperature. The effect of the logarithmic corrections on the dynamics susceptibility can be approximated by [76]

$$\chi(\omega, \mathbf{p}, q, \tau) = \left[-\frac{i\omega}{\Gamma_0} + p^2 + g \frac{q^2}{p^2} + \mu_1(0) \left| \frac{1}{2l_0} \ln \mu_1(0) \right|^{-1/3} \right]^{-1}, \quad (5.21)$$

where $\mu_1(0)$ is proportional to the reduced temperature τ , and l_0 is some constant. In the hydrodynamic region $q \ll p \ll \xi^{-1}$ the relaxation coefficient implied by the latter result is

$$\Gamma \propto \tau (|\ln \tau| + \text{const.})^{-1/3} . \quad (5.22)$$

This result has also been found by Maleev [177] using mode coupling arguments. A detailed theoretical study of the dynamics of uniaxial dipolar ferromagnets, which takes into account not only the relaxational dynamics on the basis of TDGL model, but also includes nonlinear terms resulting from the Larmor precession in the local magnetic field is still lacking. A mode coupling analysis of this problem is in progress [107].

C. Two-dimensional Systems

Two-dimensional systems are interesting, because matter behaves qualitatively different as compared to three dimensions. We recall that the Bloch argument [25,211,158], which is proven on a rigorous basis by the Hohenberg–Mermin–Wagner theorem [111,186], excludes conventional long-range order in isotropic systems with a continuous symmetry and short-ranged interaction such as the Heisenberg ferromagnet, superfluid Helium films, and two-dimensional crystals [202]. Any hypothetical broken continuous magnetic or translational symmetry would be overwhelmed by long wavelength spin or phonon excitations, since the phase space for these Goldstone-like modes is enhanced in two dimensions. Two dimensions seem to be the borderline dimension where thermal fluctuations are just strong enough to prevent the appearance of a finite order parameter.

However, since the dipolar forces reduce the fluctuations longitudinal to the wave vector, related to the anisotropy of the dipolar interaction with respect to the separation of two spins one expects that a finite order parameter could exist in two-dimensional isotropic systems. In fact we will review in the following spin-wave theories, which show that the dipolar interaction leads to the existence of long-range order in two-dimensional ferromagnets and antiferromagnets and other systems which belong to the same universality class.

1. Ferromagnets

The possibility of a finite order parameter in two-dimensional ferromagnets was shown first by Maleev [178], who evaluated the low temperature properties, in particular the magnon excitation spectrum for Heisenberg ferromagnets in the presence of dipolar forces. Linear spin-wave theory [178] results in a magnon dispersion relation

$$E_{\mathbf{k}} = \sqrt{(Dk^2 + \Omega_0\alpha)(Dk^2 + \Omega_0ka \sin \varphi_{\mathbf{k}})}, \quad (5.23)$$

where $Dk^2 = 2S(J_0 - J_{\mathbf{k}})$ at $ka \ll 1$, $\Omega_0 = 2\pi S(g_L\mu_B)^2/v_2a \ll 2SJ_0$, $\alpha = SA_0/\Omega_0 \sim 1$, and $\varphi_{\mathbf{k}}$ is the angle between the wave vector \mathbf{k} and the magnetization \mathbf{M} . At sufficiently small k (and for \mathbf{k} not parallel to the magnetization) the energy of the spin-waves has the form

$$E_{\mathbf{k}} \propto \Omega_0 |\sin \varphi_{\mathbf{k}}| \sqrt{k}. \quad (5.24)$$

An analysis of the relative deviations of the magnetization from saturation (in the framework of linear spin-wave theory) results in an order of magnitude estimate for the transition temperature (for small dipolar couplings)

$$T_c \propto \frac{2J_0S^2}{\ln\left(\frac{2J_0S}{\Omega_0}\right)}. \quad (5.25)$$

It was also shown [109,63,16] that an exchange anisotropy leads to a suppression of thermal interaction and in turn to the existence of long-range order two-dimensional ferromagnets.

In two-dimensional ferromagnets, the dipolar interaction results in an easy-plane anisotropy [178,223]. This is due to the fact that the dipolar energy is minimized when all spins are aligned in plane. Thus the problem of a three-component Heisenberg ferromagnet with dipolar interaction is reduced to the problem of a two-component (planar) ferromagnet with renormalized values of the temperature and of the dipole-dipole interaction constant. The magnetic dipolar forces change fundamentally the nature of the low-temperature phase. This can be seen as follows. In the absence of dipolar interaction any long-range order is impossible since it gets destroyed by thermal fluctuations; the mean square of the spin fluctuations is given by $\langle |\delta S_{\mathbf{q}}|^2 \rangle \propto k_B T/q^2$. A planar (pure) exchange ferromagnet would

undergo a Kosterlitz–Thouless [145,146] transition. The Kosterlitz–Thouless phase is characterized by local but no long-range order and by bound vortex pairs. There is a divergent susceptibility throughout this phase. However, due to the dipolar interaction the spectrum of the spin fluctuations at small wave numbers is changed. Including the dipolar interaction, Eq. (5.7), one obtains the following reduced Hamiltonian

$$\mathcal{H} = -\frac{H}{k_B T} = -\frac{JS^2}{k_B T} v_2 a^2 \int \frac{d^2 q}{(2\pi)^2} \left[\left(q^2 - g_2 \frac{q_y^2}{|\mathbf{q}|} \right) \phi_{\mathbf{q}} \phi_{-\mathbf{q}} + \mathcal{O}(\phi^3) \right] \quad (5.26)$$

in terms of the azimuthal angle ϕ , where we have assumed a fixed length $\mathbf{S}^2 = 1$ and an ordering along the \hat{x} -direction. The relative strength of the dipolar interaction in two dimensions is characterized by the parameter $g_2 = A^{(1)}/Ja^2$. In the derivation of Eq. (5.26) the in-plane components of the dipolar interaction tensor have been used [214] $A_{\mathbf{q}}^{\alpha\beta} = \frac{A^{(0)}}{3} \delta^{\alpha\beta} - A^{(1)} \frac{q^\alpha q^\beta}{q} + \mathcal{O}(q^2)$ (A_0 and A_1 see Eqs. (5.8) and (5.9)). Neglecting all but the terms quadratic in $\phi_{\mathbf{q}}$, the mean square fluctuations about the local ordering are given by [214]

$$\langle \phi^2 \rangle \propto \frac{k_B T}{J} \int \frac{d^2 q}{(2\pi)^2} \frac{1}{q^2 + g_2 |\mathbf{q}| \sin^2 \varphi_{\mathbf{q}}}, \quad (5.27)$$

where $\varphi_{\mathbf{q}}$ is the angle between \mathbf{q} and the total magnetization. The above integral no longer diverges due to the presence of the dipolar interaction. Hence the dipolar interaction stabilizes ferromagnetic long-range order in more than one dimension [221,178]. Besides stabilizing the long-range order, the dipolar forces alter the vortex behavior [214]. Ref. [214] also contains an analysis of the static critical behavior. More recently the critical behavior has been reanalyzed in Ref. [18]. In passing we note that there are two reviews on excitations in low-dimensional systems by Pokrovsky et al. [222,224].

Actually the situation is more complicated in thin magnetic films. Mono- and two-layer iron orders perpendicularly to the planes for $T = 0K$, only for layer numbers above 3 the expected parallel orientation is observed [11]. This comes from the spin-orbit interaction, which effectively leads to a perpendicular anisotropy, which overcomes the dipolar interaction for the very thinnest layers. Upon raising the temperature a reorientation phase

transition [206] from a perpendicular to an in-plane orientation of the magnetization has been observed experimentally. It was argued by Pescia et al. [212,213] that this transition is driven by the competition between spin-orbit and dipolar interaction. The (classical) transition temperature has been estimated [225,213] to be of the order $T_R \approx (\lambda - \Omega) \frac{4cJa^3}{7(g_L\mu_B)^2}$, where c is the number of nearest neighbors, $\Omega = 2\pi(g_L\mu_B S)^2/a^3$ characterizes the strength of the dipolar interaction, and λ is the single-ion anisotropy constant favoring perpendicular orientation. Since the single-ion and the dipolar anisotropy parameters scale the same under a renormalization group transformation [213,225], it depends on the relative values of the single-ion anisotropy and the dipolar parameters, whether the transition temperature for the reorientation phase transition is smaller or larger than the Curie temperature. However, since the dipolar interaction parameter increases with the number of layers, the value of T_R is reduced for thicker films, as indeed observed experimentally [206]. Some of the above theoretical work is still rather controversial [164] and alternative mechanisms have been proposed for the experimentally observed reorientation phase transition [163]. Due to the combination of various anisotropies, dipole-dipole interaction, reduced dimensionality and enhanced importance of thermal fluctuations the phase diagram of thin magnetic films shows a variety of new and interesting phases [206,10,11] with properties still awaiting a theoretical explanation.

2. Antiferromagnets

Recently it has been shown [215] that long-range order is also possible in two-dimensional antiferromagnets due to the anisotropy of the dipolar interaction. The existence of the long-range order is a consequence of a subtle interplay between exchange and dipolar interaction. The classical ground state of an isotropic pure exchange antiferromagnet has a continuous degeneracy and hence no long-range order. The dipolar interaction lifts the continuous degeneracy of the ground state such that a spin alignment perpendicular to the plane is energetically favored (see Fig. 5.3). In other words, whereas the exchange interaction imposes

the antiferromagnetic order, the dipolar interaction prevents thermal fluctuations from its destruction. This can be seen most easily by considering the equations of motion at zero wave vector. Upon approximating the longitudinal spin components by their equilibrium expectation value $S_l^z \approx S e^{i\mathbf{q}_0 \cdot \mathbf{x}_l}$ the linearized form of Eqs. (5.10) (see Section 5.1) reads

$$\frac{d}{dt} S_0^x = 2S (A_{\mathbf{q}_0}^{zz} - A_{\mathbf{q}_0}^{yy}) S_{\mathbf{q}_0}^y, \quad (5.28)$$

$$\frac{d}{dt} S_{\mathbf{q}_0}^y = 2S [(J_{\mathbf{q}_0} - J_0) + (A_{\mathbf{q}_0}^{zz} - A_0^{xx})] S_0^x, \quad (5.29)$$

and an analogous set of equations for S_0^y and $S_{\mathbf{q}_0}^x$. The wave vector $\mathbf{q}_0 = \frac{\pi}{a}(1, 1, 0)$ characterizes the antiferromagnetic, staggered modulation of the ground state. The coefficient on the right hand side of Eq. (5.28) is nonzero due to the anisotropy of the dipolar interaction in 2D. The resulting energy gap at zero wave vector then is

$$E_0 = 2S \sqrt{A_{\mathbf{q}_0}^{zz} - A_{\mathbf{q}_0}^{xx}} \sqrt{(J_{\mathbf{q}_0} - J_0) - (A_0^{xx} - A_{\mathbf{q}_0}^{zz})}. \quad (5.30)$$

A more detailed information on the spin-wave spectrum can be obtained by linear spin-wave theory [215]. Introducing Bose operators by a Holstein-Primakoff transformation [141], given here only up to harmonic terms,

$$S_l^x = \sqrt{\frac{S}{2}}(a_l + a_l^\dagger), \quad S_l^y = \mp i \sqrt{\frac{S}{2}}(a_l - a_l^\dagger), \quad S_l^z = \pm(S - a_l^\dagger a_l), \quad (5.31)$$

where the upper (lower) sign refers to the first (second) sublattice, the Hamiltonian in the harmonic approximation is given by

$$H = \sum_{\mathbf{q}} \left\{ A_{\mathbf{q}} a_{\mathbf{q}}^\dagger a_{\mathbf{q}} + \frac{1}{2} B_{\mathbf{q}} (a_{\mathbf{q}} a_{-\mathbf{q}} + a_{\mathbf{q}}^\dagger a_{-\mathbf{q}}^\dagger) + C_{\mathbf{q}} a_{\mathbf{q}} a_{-\mathbf{q}-\mathbf{q}_0} + C_{\mathbf{q}}^* a_{\mathbf{q}}^\dagger a_{-\mathbf{q}-\mathbf{q}_0}^\dagger + C_{\mathbf{q}} a_{\mathbf{q}}^\dagger a_{\mathbf{q}+\mathbf{q}_0} + C_{\mathbf{q}}^* a_{\mathbf{q}+\mathbf{q}_0}^\dagger a_{\mathbf{q}} \right\} \quad (5.32)$$

with the coefficients

$$A_{\mathbf{q}} = S(2J_{\mathbf{q}_0} - J_{\mathbf{q}} - J_{\mathbf{q}+\mathbf{q}_0}) + S(2A_{\mathbf{q}_0}^{zz} - A_{\mathbf{q}}^{xx} - A_{\mathbf{q}+\mathbf{q}_0}^{yy}) \quad (5.33a)$$

$$B_{\mathbf{q}} = S(J_{\mathbf{q}+\mathbf{q}_0} - J_{\mathbf{q}}) + S(A_{\mathbf{q}+\mathbf{q}_0}^{yy} - A_{\mathbf{q}}^{xx}) \quad (5.33b)$$

$$C_{\mathbf{q}} = iS A_{\mathbf{q}}^{xy}. \quad (5.33c)$$

In this description the primitive cell is the crystallographic, which is half the magnetic. Diagonalization of the Hamiltonian, achieved by a Bogoliubov transformation, results in a spin-wave spectrum with two branches

$$E_{\mathbf{q}}^i = \sqrt{\frac{1}{2}(\Omega_1 \pm \Omega_2)} \quad (5.34)$$

where

$$\Omega_1 = A_{\mathbf{q}}^2 - B_{\mathbf{q}}^2 + A_{\mathbf{q}+\mathbf{q}_0}^2 - B_{\mathbf{q}+\mathbf{q}_0}^2 + 8C_{\mathbf{q}} C_{\mathbf{q}+\mathbf{q}_0}$$

and

$$\begin{aligned} \Omega_2^2 = & (A_{\mathbf{q}}^2 - B_{\mathbf{q}}^2 - A_{\mathbf{q}+\mathbf{q}_0}^2 + B_{\mathbf{q}+\mathbf{q}_0}^2)^2 + 16[C_{\mathbf{q}+\mathbf{q}_0}(A_{\mathbf{q}+\mathbf{q}_0} - B_{\mathbf{q}+\mathbf{q}_0}) - C_{\mathbf{q}}(A_{\mathbf{q}} - B_{\mathbf{q}})] \\ & \times [C_{\mathbf{q}}(A_{\mathbf{q}+\mathbf{q}_0} + B_{\mathbf{q}+\mathbf{q}_0}) - C_{\mathbf{q}+\mathbf{q}_0}(A_{\mathbf{q}} + B_{\mathbf{q}})]. \end{aligned}$$

In Fig. 5.4 the dispersion relation is shown for three values for the ratio of dipolar and exchange energy $\kappa = \frac{(g\mu_B)^2}{4|J|a^3}$ with isotropic nearest-neighbor exchange interaction ($J < 0$). The two branches can be resolved only for large values of κ .

In particular the gap is proportional to the square root of the difference of the magnetostatic energy between the configurations of in-plane and out-of-plane magnetization. In a three-dimensional simple cubic lattice the first root in Eq. (5.30) vanishes because of the symmetry, but in two-dimensional systems there is a finite gap for perpendicular antiferromagnetic order. We note that for sufficiently large exchange energy the gap is the geometric mean of dipole and exchange energy, which in turn implies that the gap is much larger than the dipolar energy for $\kappa \ll 1$.

The Néel temperature T_N has been determined via a high-temperature expansion, by employing Callen's method [215–217]. If the dipolar interaction is weak in comparison with the exchange interaction one can give an order of magnitude estimate for the transition temperature in the framework of linear spin-wave theory based on the Holstein–Primakoff transformation

$$T_N \propto \frac{|J|}{\ln\left(\frac{|J|}{E_0}\right)}. \quad (5.35)$$

This, however, gives an overestimate for the transition temperature, because it uses a temperature-independent dispersion relation. Actually, the magnon frequency softens with increasing temperature. Those effects have been accounted for in Ref. [216] by an extension of the Tyablikov decoupling scheme due to Callen [43]. In essence this leads to a replacement of the saturation magnetization of the spins S by the temperature-dependent order parameter σ . The resulting transition temperature is lowered with respect to the estimate from linear spin-wave theory. E_0 has been obtained by linear spin-wave theory and E_0^σ and T_N^{th} by the method of Callen. The results are summarized in Table XI and show a quite satisfactory agreement with experimental data. This theory has been extended to antiferromagnets on a honeycomb [218] and several other lattices [219].

Tables:

TABLE X. Behavior of the scaling functions of the line widths of an isotropic dipolar antiferromagnet in asymptotic regions.

	IC	DC	IH	DH
$\gamma_M^{L,T}$	1	$y^{3/2}$	$x^{-1/2}$	$r^{3/2}$
$\gamma_N^{L,T}$	1	$y^{-1/2}$	$x^{3/2}$	$r^{3/2}$

TABLE XI. Exchange energy $|J|$, lattice constant a , energy gap E_0 , spin-flop field H_{sf} , Néel temperature T_N and zero temperature order parameter σ_0 .

	$ J $ [K]	a [Å]	E_0^{exp} [K]	E_0^g [K]	E_0 [K]	T_N^{exp} [K]	T_N^{th} [K]	σ_0
K_2MnF_4	8.5 ^a	4.17 ^a	7.4 ^b	7.1	7.6	42 ^a	41	2.33
Rb_2MnF_4	7.4 ^c	4.20 ^g	7.3 ^b	6.5	7.0	38 ^g	36	2.33
Rb_2MnCl_4	11.2 ^f	5.05 ^e	7.5 ^f	6.1	6.6	56 ^f	48	2.32
$(CH_3NH_3)_2MnCl_4$	9.0 ^f	5.13 ^e		5.3	5.7	45 ^f	39	2.32

^a Reference [24], ^b Reference [265], ^c Reference [266], ^d Reference [267], ^e Reference [160], ^f Reference [243], ^g Reference [23].

Captions to the figures:

Figure 5.1: Scaling function for the line width of the transverse magnetization above T_N versus $x = 1/q\xi$ for different values of $\varphi = N\pi/30$ ($N=0,1,2,\dots,14$).

Figure 5.2: Scaling functions for the line width of the transverse and longitudinal staggered magnetization above T_N versus $x = 1/q\xi$ for different values of $\varphi = N\pi/30$ ($N=0,1,2,\dots,14$).

Figure 5.3: Classical ground state of a two-dimensional dipolar antiferromagnet with a dipolar interaction much smaller than the exchange interaction on a quadratic lattice. Taken from Ref. [217].

Figure 5.4: The spin-wave dispersion relation (Eq. (5.34)) of pure exchange antiferromagnets on a quadratic lattice with nearest-neighbor interaction (solid line) and with additional dipolar interaction ($S = 1/2$), for the ratios of dipolar energy to exchange energy $\kappa = \frac{(g\mu_B)^2}{4|J|a^3}$ along the $\frac{\pi}{a}[\xi, \xi, 0]$ direction: $\kappa = 0.1$ (long dashed), $\kappa = 0.01$ (dashed) and $\kappa = 0.001$ (dotted). The splitting of the two magnon branches is visible only for $\kappa = 0.1$.

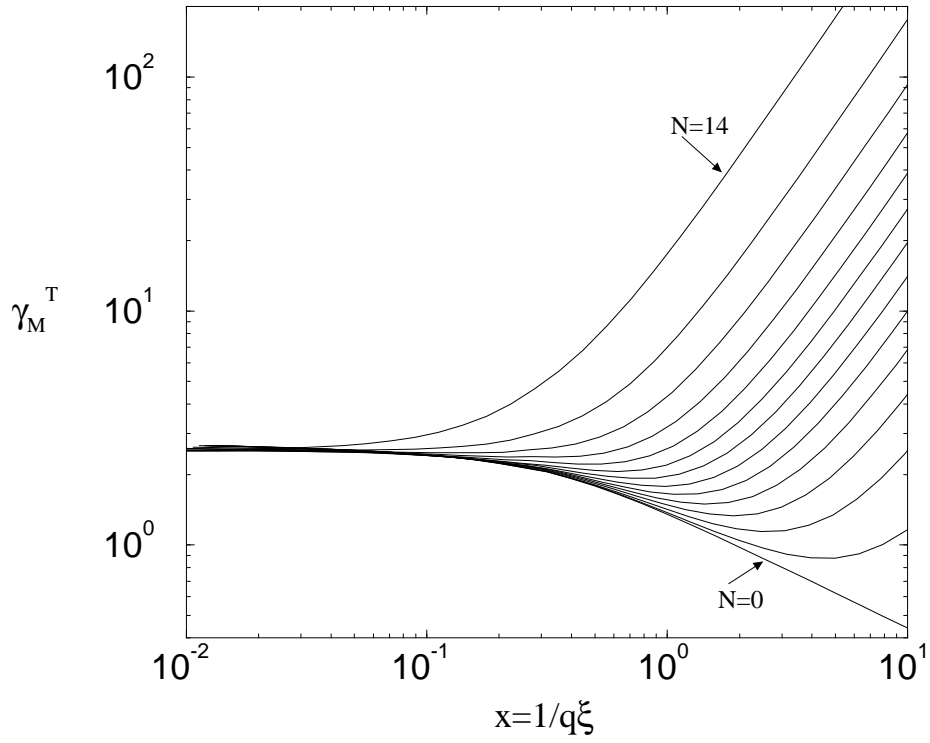


Figure 5.1: Scaling function for the line width of the transverse magnetization above T_N versus $x = 1/q\xi$ for different values of $\varphi = N\pi/30$ ($N=0,1,2,\dots,14$).

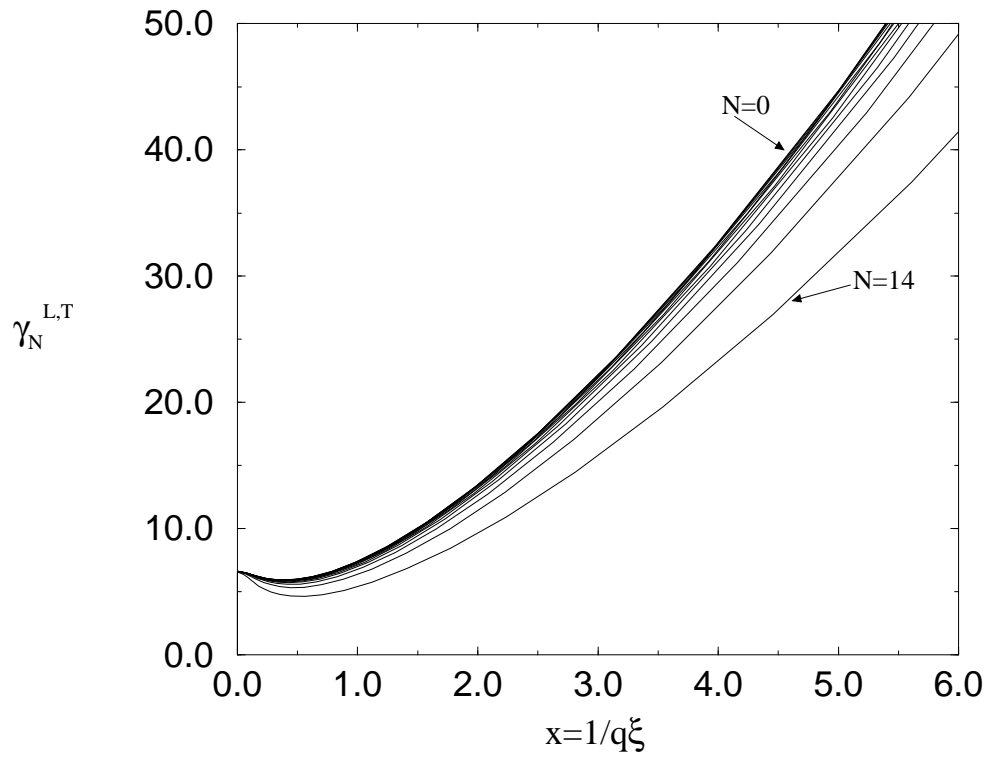


Figure 5.2: Scaling functions for the line width of the transverse and longitudinal staggered magnetization above T_N versus $x = 1/q\xi$ for different values of $\varphi = N\pi/30$ ($N=0,1,2,\dots,14$).

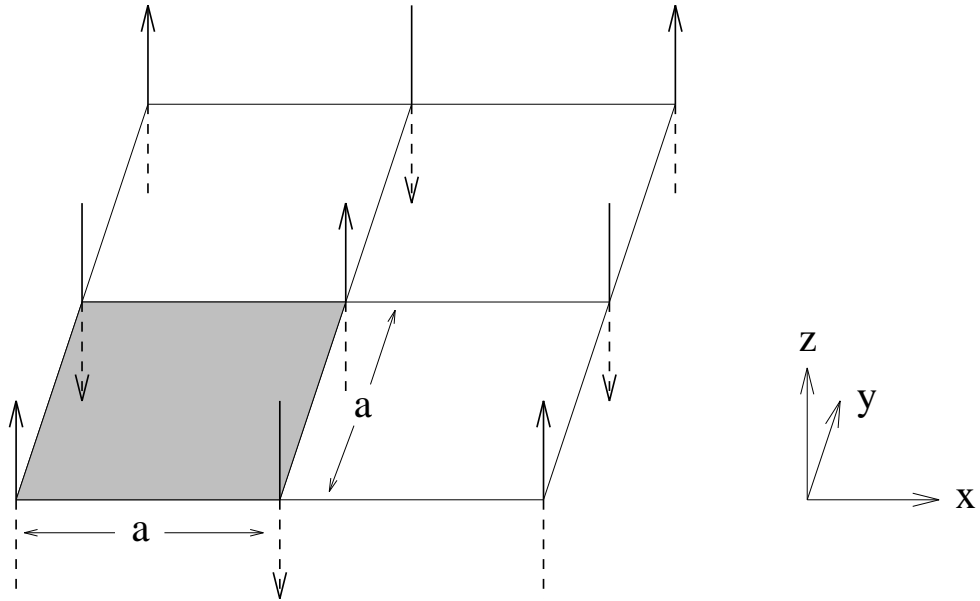


Figure 5.3: Classical ground state of a two-dimensional dipolar antiferromagnet with a dipolar interaction much smaller than the exchange interaction on a quadratic lattice. Taken from Ref. [217].

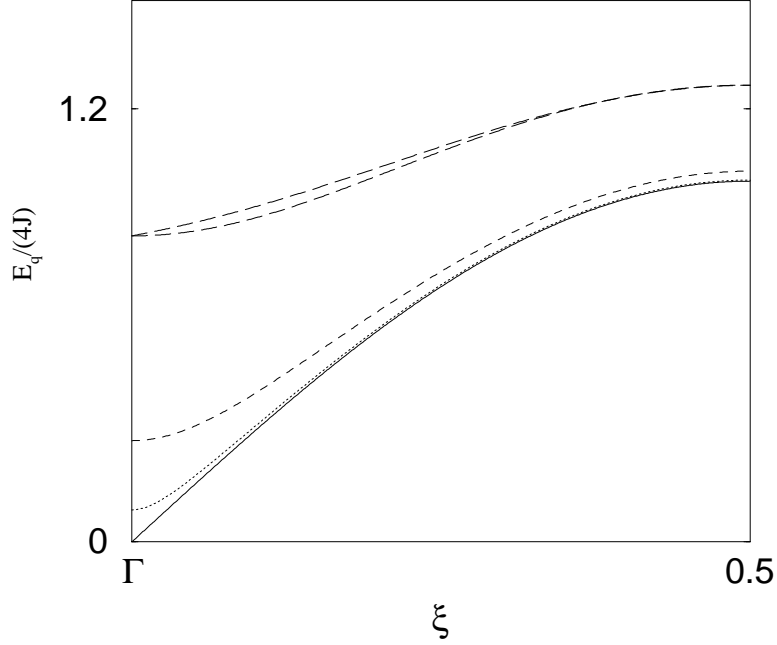


Figure 5.4: The spin-wave dispersion relation (Eq. (5.34)) of pure exchange anti-ferromagnets on a quadratic lattice with nearest-neighbor interaction (solid line) and with additional dipolar interaction ($S = 1/2$), for the ratios of dipolar energy to exchange energy $\kappa = \frac{(g\mu_B)^2}{4|J|a^3}$ along the $\frac{\pi}{a}[\xi, \xi, 0]$ direction: $\kappa = 0.1$ (long dashed), $\kappa = 0.01$ (dashed) and $\kappa = 0.001$ (dotted). The splitting of the two magnon branches is visible only for $\kappa = 0.1$.

VI. STOCHASTIC THEORY

A. Classical field theory and dynamic functional

If one tries to describe the critical dynamics of ferromagnets, one is in general not interested in the complete, highly complicated, microscopic time evolution. Rather, one is usually interested in the dynamics on time scales characteristic of its slowly varying dynamical quantities, such as those associated with hydrodynamic, order parameter or Goldstone modes.

A method to extract from the microscopic dynamics the equations of motion appropriate to these slowly varying quantities is the projection operator formalism of Zwanzig [276] and Mori [197]. Since the semi-phenomenological equations derived from this formalism form a common basis of mode coupling and dynamic renormalization group theories we briefly review the main ideas and results of this approach.

The idea is to eliminate the fast variables by introducing a projection operator \mathcal{P} , which projects onto the subspace of slowly varying modes. Descriptions of this formalism can be found in Refs. [139,198]. A short account is given in Appendix B. After having chosen an appropriate set of slow variables - which is crucial for the validity of the dynamics - one can derive formally exact non linear equations of motion for these modes (here these modes are denoted by $\{S_\alpha(t)\}$)

$$\begin{aligned} \frac{d}{dt}S_\alpha(t) = & v_\alpha(\{S(t)\}) \\ & + \sum_\beta \int_0^t d\tau P_{\text{eq}}^{-1}(\{S(t-\tau)\}) \frac{\partial M_{\alpha\beta}(\tau; \{S(t-\tau)\}) P_{\text{eq}}(\{S(t-\tau)\})}{\partial S_\beta^*(t-\tau)} + \zeta_\alpha(t), \end{aligned} \quad (6.1)$$

where

$$P_{\text{eq}}(\{S\}) = \exp \left[-\frac{1}{k_B T} \mathcal{H}(\{S\}) \right] \quad (6.2)$$

is the equilibrium probability distribution function. The first term in these equations,

$$v_\alpha(\{S(t)\}) = \langle i\mathcal{L}S_\alpha; \{S(t)\} \rangle, \quad (6.3)$$

is called the streaming term and describes the systematic part of the driving forces. This term can be expressed in terms of Poisson brackets. (The conditional average $\langle X; \{a\} \rangle$ is defined by $\langle X; \{a\} \rangle = \langle X \delta(S - a) \rangle / P_{\text{eq}}(\{S(t)\})$ where the average is taken in the microcanonical ensemble [140].) The second term contains the memory kernel

$$M_{\alpha\beta}(t; \{S(t)\}) = \langle \zeta_\alpha(t) \zeta_\beta^*(0); \{S(t)\} \rangle, \quad (6.4)$$

and characterizes the damping of this adiabatic motion by frictional effects arising from the “random” forces. The “random” forces are given in terms of the projection operator $\mathcal{Q} = 1 - \mathcal{P}$ and the Liouville operator \mathcal{L}

$$\zeta_\alpha(t) = \exp[it\mathcal{Q}\mathcal{L}] i\mathcal{Q}\mathcal{L}S. \quad (6.5)$$

Whether this force can be regarded as random or not depends crucially on the choice of the projection operator, i.e., whether \mathcal{P} contains all the slowly varying quantities of the system under consideration.

The semi-phenomenological equations of motion are obtained from the above exact equations by making the following basic, and at least plausible assumptions. First one assumes that one can neglect memory effects in $M_{\alpha\beta}$ and makes the Markovian approximation

$$M_{\alpha\beta}(t; \{S(t)\}) \approx 2L_{\alpha\beta}(\{S(t)\})\delta(t). \quad (6.6)$$

Second one takes the kinetic coefficients to be independent of the slow variables

$$L_{\alpha\beta}(\{a\}) \approx L_{\alpha\beta}, \quad (6.7)$$

and third one assumes that all slowly varying variables are contained in the choice of the projection operator so that the forces f_α are really random and have a Gaussian probability distribution

$$w(\{\zeta\} | t_0 \leq t \leq t_1) \sim \exp \left[-\frac{1}{4} \int_{t_0}^{t_1} dt \zeta_\alpha(t) L_{\alpha\beta}^{-1} \zeta_\beta(t) \right]. \quad (6.8)$$

Then the exact equations reduce to the following semi-phenomenological equations of the Langevin form

$$\frac{d}{dt}S_\alpha(t) = v_\alpha(\{S(t)\}) - \sum_\beta L_{\alpha\beta}^0 \frac{\delta\mathcal{H}(\{S(t)\})}{\delta S_\beta^*(t)} + \zeta_\alpha(t), \quad (6.9)$$

where the streaming term,

$$v_\alpha(\{S(t)\}) = -\lambda f \sum_\beta \left[\frac{\delta}{\delta S_\beta} Q_{\alpha\beta}(\{S\}) - Q_{\alpha\beta}(\{S\}) \frac{\delta\mathcal{H}(\{S\})}{\delta S_\beta^*(t)} \right], \quad (6.10)$$

can be expressed in terms of Poisson brackets

$$Q_{\alpha\beta}(\{S\}) = \{S_\alpha, S_\beta\}_P = -Q_{\beta\alpha}(\{S\}). \quad (6.11)$$

The equilibrium distribution does not determine the driving force in the Langevin equations uniquely. Only the dissipative couplings which are generated by the derivative of the effective Hamiltonian \mathcal{H} are related to the static properties of the system. As a direct consequence with each static universality class are associated several dynamic universality classes depending on the structure of the Poisson brackets.

After these general preliminaries we can now start to set up a stochastic equation of motion for the dynamics of dipolar ferromagnets. If the interaction between the spins in an isotropic Heisenberg ferromagnet is solely given by the short range exchange interaction the dynamics are described by precession of the spins in a local magnetic field generated by the surrounding spins. The rotation invariance of the Heisenberg Hamiltonian implies that the total spin is conserved. As shown explicitly in chapter III A this is no longer the case if one takes into account the long-ranged dipole-dipole interaction. Hence the spin dynamics of a isotropic dipolar ferromagnet are described by the following semi-phenomenological Langevin equations

$$\frac{\partial \mathbf{S}(\mathbf{x}, t)}{\partial t} = \lambda f \mathbf{S}(\mathbf{x}, t) \times \frac{\delta \mathcal{H}([S])}{\delta \mathbf{S}(\mathbf{x}, t)} - \hat{L} \frac{\delta \mathcal{H}([S])}{\delta \mathbf{S}(\mathbf{x}, t)} + \boldsymbol{\zeta}(\mathbf{x}, t), \quad (6.12)$$

where $\mathbf{S}(\mathbf{x}, t)$ is the local spin density. The local magnetic field is determined by the functional derivative of the Landau-Ginzburg functional $\mathcal{H}[S]$ with respect to the spin density.

For the present case the Landau-Ginzburg functional is given by

$$\begin{aligned} \mathcal{H}[S] = & -\frac{1}{2} \int_q \left[(r + q^2) \delta^{\alpha\beta} + g \frac{q^\alpha q^\beta}{q^2} \right] S^\alpha(\mathbf{q}) S^\beta(-\mathbf{q}) \\ & - \frac{u}{4!} \int \int \int_{\mathbf{q}_1 \mathbf{q}_2 \mathbf{q}_3} S^\alpha(\mathbf{q}_1) S^\alpha(\mathbf{q}_2) S^\beta(\mathbf{q}_3) S^\beta(-\mathbf{q}_1 - \mathbf{q}_2 - \mathbf{q}_3). \end{aligned} \quad (6.13)$$

$S^\alpha(\mathbf{q})$ ($\alpha=1,2,\dots,n$) are the components of the bare spin variable with n equal to the space dimensionality d . We further used the abbreviation $\int_q = \int d^d q / (2\pi)^d$, r is the reduced temperature-deviation and g denotes the relative strength of the dipolar interaction.

The dipolar interaction in Eq.(6.13) breaks the symmetry of the spin fluctuations transverse and longitudinal to the wave vector \mathbf{q} , which is reflected in the free propagator

$$G^{\alpha\beta} = \frac{q^\alpha q^\beta}{q^2} G^L + \left(\delta^{\alpha\beta} - \frac{q^\alpha q^\beta}{q^2} \right) G^T, \quad (6.14)$$

where $G^L(r, g, q) = (r + g + q^2)^{-1}$ and $G^T(r, q) = (r + q^2)^{-1}$.

The time scale is characterized by the quantity λ . The mode coupling coefficient f determines the strength of the coupling of the spin density to the local magnetic field. Since the order parameter is a non conserved quantity the leading term in the Onsager operator

$$\hat{L} = \lambda(\gamma - \nabla^2) \quad (6.15)$$

is wave vector independent, $\lambda\gamma$, and not $-\lambda\nabla^2$ as for a conserved order parameter. The quantity γ characterizes - like g in statics - the relative strength of the dipolar interaction. The random forces $\zeta(\mathbf{x}, t)$ have a Gaussian probability distribution

$$w_\zeta([\zeta_i(\mathbf{x}, t)] | t_0 \leq t \leq t_1) \sim \exp \left(-\frac{1}{4} \sum_i \int_{t_0}^{t_1} dt \int d^d x \zeta_i(\mathbf{x}, t) \hat{L}^{-1} \zeta_i(\mathbf{x}, t) \right), \quad (6.16)$$

which is uniquely determined by the lowest moments

$$\langle \zeta(\mathbf{x}, t) \rangle = 0, \quad (6.17a)$$

$$\langle \zeta_i(\mathbf{x}, t) \zeta_j(\mathbf{x}', t') \rangle = 2\hat{L} \delta(\mathbf{x} - \mathbf{x}') \delta(t - t') \delta_{ij}. \quad (6.17b)$$

Note that we have set $\beta = 1/k_B T = 1$.

In particular for the implementation of the dynamic renormalization group theory in a way analogous to static critical phenomena it is convenient to introduce a functional which generates the perturbation expansion for the frequency dependent correlation and response functions, which is equivalent to the equations of motion. We shall use the functional integral formulation [127,17], which converts the Langevin equations into a dynamic functional with

one additional field [182]. The idea is that, instead of solving the Langevin equations (6.12) for the stochastic spin fields $\mathbf{S}(\mathbf{k}, t)$ in terms of the random forces $\boldsymbol{\zeta}(\mathbf{k}, t)$ and then averaging over the Gaussian weight, one can eliminate the random forces in favor of the spin variables by introducing a path probability density $W(\{S\})$ via

$$W(\{S\})\mathcal{D}[S] = w(\{\zeta\})\mathcal{D}[\zeta]. \quad (6.18)$$

Furthermore, it is convenient to perform a Gaussian transformation in order to "linearize" the dynamic functional. This is accomplished by introducing response fields \tilde{S} [127,182] by

$$W(\{S\}) = \int \mathcal{D}[i\tilde{S}] \exp \left\{ \mathcal{J}[S, \tilde{S}] \right\}. \quad (6.19)$$

For more details on the general formalism we refer the reader to Refs. [127,61,17,182]. The generating functional for the correlation functions is

$$Z[h, \tilde{h}] = \frac{1}{\mathcal{N}} \int \mathcal{D}[S] \mathcal{D}[i\tilde{S}] \exp \left[\mathcal{J}_{t_0}^{t_1}[S, \tilde{S}] + \sum_i \int d^d x \int_{t_0}^{t_1} dt (h_i S_i + \tilde{h}_i \tilde{S}_i) \right], \quad (6.20)$$

where the normalization factor \mathcal{N} is chosen such that $Z[h = 0, \tilde{h} = 0] = 1$. The symbols $\mathcal{D}[S]$ and $\mathcal{D}[i\tilde{S}]$ denote functional measures of the path integral. The Janssen-Dominicis functional is given by

$$\mathcal{J}_{t_0}^{t_1}[S, \tilde{S}] = \sum_i \int_{t_0}^{t_1} dt \int d^d x \left[\tilde{S}_i \hat{L} \tilde{S}_i - \tilde{S}_i \left(\frac{\partial S_i}{\partial t} - K_i[S] \right) - \frac{1}{2} \frac{\delta K_i[S]}{\delta S_i} \right], \quad (6.21)$$

where the functional of the forces is

$$\mathbf{K}[S] = \lambda f \mathbf{S}(\mathbf{x}, t) \times \frac{\delta \mathcal{H}([S])}{\delta \mathbf{S}(\mathbf{x}, t)} - \hat{L} \frac{\delta \mathcal{H}([S])}{\delta \mathbf{S}(\mathbf{x}, t)}. \quad (6.22)$$

In formulating the perturbation theory one splits the functional, Eqs. (6.21) and (6.22), into a harmonic part

$$\begin{aligned} \mathcal{J}_{\text{harm}}[S, \tilde{S}] = & \int_k \int_\omega \left[\lambda(\gamma + k^2) \tilde{S}^\alpha(\mathbf{k}, \omega) \tilde{S}^\alpha(-\mathbf{k}, -\omega) + \right. \\ & \left. - \tilde{S}^\alpha(\mathbf{k}, \omega) \left[i\omega \delta^{\alpha\beta} + \lambda(\gamma + k^2) G^{\alpha\beta}(r, g, \mathbf{k})^{-1} \right] S^\alpha(\mathbf{k}, \omega) \right], \end{aligned} \quad (6.23)$$

which is bilinear in the stochastic spin fields S and \tilde{S} and a part $\mathcal{J}_{\text{int}}[S, \tilde{S}]$ containing the interaction terms. Here $G^{\alpha\beta}(r, g, \mathbf{k})$ denotes the static propagator, Eq. (6.14). Furthermore we have introduced the short hand notations $\int_k = \int d^d k / (2\pi)^d$, $\int_\omega = \int d\omega / 2\pi$. The

Fourier transform of the spin density is defined by $\mathbf{S}(\mathbf{x}, t) = \int_k \int_\omega \mathbf{S}(\mathbf{k}, \omega) e^{i(\mathbf{k}\cdot\mathbf{x} - \omega t)}$. Hence the generating functional can be written as

$$Z[h, \tilde{h}] = \frac{1}{\mathcal{N}} \exp \left[\mathcal{J}_{\text{int}} \left(\frac{\delta}{\delta h}, \frac{\delta}{\delta \tilde{h}} \right) \right] \times \int \mathcal{D}[S] \mathcal{D}[\tilde{S}] \exp \left[\mathcal{J}_{\text{harm}}[S, \tilde{S}] + \sum_i \int d^d x \int_{t_0}^{t_1} dt (h_i S_i + \tilde{h}_i \tilde{S}_i) \right], \quad (6.24)$$

We start with the discussion of the harmonic part, Eq. (6.23). It can be written in matrix notation as

$$\mathcal{J}_{\text{harm}}[S, \tilde{S}] = -\frac{1}{2} \int_k \int_\omega (\tilde{S}^\alpha(\mathbf{k}, \omega), S^\alpha(\mathbf{k}, \omega)) \mathbf{A}^{\alpha\beta}(\mathbf{k}, \omega) (\tilde{S}^\beta(-\mathbf{k}, -\omega), S^\beta(-\mathbf{k}, -\omega))^T. \quad (6.25)$$

The matrix $\mathbf{A}^{\alpha\beta}(\mathbf{k}, \omega)$ is given by

$$\mathbf{A}^{\alpha\beta}(\mathbf{k}, \omega) = \begin{pmatrix} -2L(k) & i\omega - A^{\alpha\beta}(\mathbf{k}) \\ -i\omega - A^{\alpha\beta}(\mathbf{k}) & 0 \end{pmatrix}, \quad (6.26)$$

where we have defined

$$A^{\alpha\beta}(\mathbf{k}) = -L(k)[G^{\alpha\beta}(r, g, \mathbf{k})]^{-1}, \quad (6.27)$$

$$L(k) = \lambda(\gamma + k^2). \quad (6.28)$$

The harmonic part of the partition function

$$Z_0[h, \tilde{h}] = \int \mathcal{D}[S] \mathcal{D}[\tilde{S}] \exp \left[\mathcal{J}_{\text{harm}}[S, \tilde{S}] + \sum_i \int d^d x \int_{t_0}^{t_1} dt (h_i S_i + \tilde{h}_i \tilde{S}_i) \right], \quad (6.29)$$

can be calculated explicitly with the result

$$Z_0[h, \tilde{h}] = \exp \left[\frac{1}{2} \int_k \int_\omega (\tilde{h}^\alpha(\mathbf{k}, \omega), h^\alpha(\mathbf{k}, \omega)) (\mathbf{A}^{\alpha\beta}(\mathbf{k}, \omega))^{-1} (\tilde{h}^\beta(-\mathbf{k}, -\omega), h^\beta(-\mathbf{k}, -\omega))^T \right]. \quad (6.30)$$

Hence the free propagators are found to be

$$\begin{pmatrix} \langle \tilde{S}^\alpha(\mathbf{k}, \omega) \tilde{S}^\beta(\mathbf{k}', \omega') \rangle_0 & \langle \tilde{S}^\alpha(\mathbf{k}, \omega) S^\beta(\mathbf{k}', \omega') \rangle_0 \\ \langle S^\alpha(\mathbf{k}, \omega) \tilde{S}^\beta(\mathbf{k}', \omega') \rangle_0 & \langle S^\alpha(\mathbf{k}, \omega) S^\beta(\mathbf{k}', \omega') \rangle_0 \end{pmatrix} = \delta(\omega + \omega') \delta(\mathbf{k} + \mathbf{k}') (\mathbf{A}^{\alpha\beta}(-\mathbf{k}, -\omega))^{-1}, \quad (6.31)$$

where

$$\left(\mathbf{A}^{\alpha\beta}(\mathbf{k}, \omega)\right)^{-1} = \mathbf{A}_L^{-1}(\mathbf{k}, \omega)P_L^{\alpha\beta}(\mathbf{k}) + \mathbf{A}_T^{-1}(\mathbf{k}, \omega)P_T^{\alpha\beta}(\mathbf{k}). \quad (6.32)$$

Hence the longitudinal and transverse propagators are given by

$$\mathbf{A}_\alpha^{-1}(\mathbf{k}, \omega) = \begin{pmatrix} 0 & 1/[-i\omega - A_\alpha(k)] \\ 1/[i\omega - A_\alpha(k)] & 2L(k)/[\omega^2 + A_\alpha(k)^2] \end{pmatrix}, \quad (6.33)$$

where

$$A_{L,T}(k) = -L(k) \begin{cases} r + k^2 & \text{for } \alpha = T, \\ r + g + k^2 & \text{for } \alpha = L. \end{cases} \quad (6.34)$$

In summary, one gets for the response propagators

$$R^{\alpha\beta}(\mathbf{k}, \omega) = \langle \tilde{S}^\alpha(\mathbf{k}, \omega)S^\beta(-\mathbf{k}, -\omega) \rangle_0 = R^T(k, \omega)P_T^{\alpha\beta}(\mathbf{k}) + R^L(k, \omega)P_L^{\alpha\beta}(\mathbf{k}), \quad (6.35)$$

where the transverse and the longitudinal parts are given by

$$R^{L,T}(k, \omega) \equiv \frac{1}{-i\omega - A_{L,T}(k)}, \quad (6.36)$$

and the projection operators are defined by $P_T^{\alpha\beta} = \delta^{\alpha\beta} - q^\alpha q^\beta / q^2$ and $P_L^{\alpha\beta} = q^\alpha q^\beta / q^2$. For the correlation propagators one obtains

$$C^{\alpha\beta}(\mathbf{k}, \omega) = \langle S^\alpha(\mathbf{k}, \omega)S^\beta(-\mathbf{k}, -\omega) \rangle_0 = C^T(k, \omega)P_T^{\alpha\beta}(\mathbf{k}) + C^L(k, \omega)P_L^{\alpha\beta}(\mathbf{k}), \quad (6.37)$$

where

$$C^{L,T}(k, \omega) \equiv \frac{2L(k)}{\omega^2 + A_{L,T}(k)^2}. \quad (6.38)$$

The diagrammatic representations are depicted in Figs.6.1.a.

The interaction part of the dynamic functional

$$\mathcal{J}_{\text{int}}[S, \tilde{S}] = \mathcal{J}_{\text{MC}}[S, \tilde{S}] + \mathcal{J}_{\text{RE}}[S, \tilde{S}], \quad (6.39)$$

consists of a mode coupling vertex $\mathcal{J}_{\text{MC}}[S, \tilde{S}]$, originating from the Larmor term $\mathbf{S} \times \frac{\delta \mathcal{H}}{\delta \mathbf{S}}$ in Eq. (6.12), and relaxation vertices $\mathcal{J}_{\text{RE}}[S, \tilde{S}]$, originating from the nonlinear terms of the static Hamiltonian, $\hat{L} \frac{\delta \mathcal{H}}{\delta \mathbf{S}}$. The mode coupling vertex is given by

$$\begin{aligned} \mathcal{J}_{\text{MC}}[S, \tilde{S}] &= \lambda f \epsilon_{\alpha\beta\gamma} \int_{\mathbf{k}} \int_{\omega} \int_{\mathbf{p}} \int_{\nu} \left[\left(\mathbf{p} + \frac{\mathbf{k}}{2} \right)^2 \delta^{\gamma\mu} + g \frac{(p^\mu + \frac{k^\mu}{2})(p^\gamma + \frac{k^\gamma}{2})}{(\mathbf{p} + \frac{\mathbf{k}}{2})^2} \right] \\ &\quad \times \tilde{S}^\alpha(\mathbf{k}, \omega) S^\beta(\mathbf{p} - \frac{\mathbf{k}}{2}, \nu - \frac{\omega}{2}) S^\mu(-\mathbf{p} - \frac{\mathbf{k}}{2}, -\nu - \frac{\omega}{2}). \end{aligned} \quad (6.40)$$

It consists of an isotropic part

$$\mathcal{J}_{\text{MCI}}[S, \tilde{S}] = \lambda f \epsilon_{\alpha\beta\gamma} \int_{\mathbf{k}} \int_{\omega} \int_{\mathbf{p}} \int_{\nu} (\mathbf{p} \cdot \mathbf{k}) \tilde{S}^\alpha(\mathbf{k}, \omega) S^\beta(\mathbf{p}_-, \nu_-) S^\gamma(\mathbf{p}_+, \nu_+), \quad (6.41)$$

and a dipolar part

$$\mathcal{J}_{\text{MCD}}[S, \tilde{S}] = \lambda f g \epsilon_{\alpha\beta\gamma} \int_{\mathbf{k}} \int_{\omega} \int_{\mathbf{p}} \int_{\nu} \frac{p_+^\mu p_+^\gamma}{p_+^2} \tilde{S}^\alpha(\mathbf{k}, \omega) S^\beta(\mathbf{p}_-, \nu_-) S^\mu(\mathbf{p}_+, \nu_+), \quad (6.42)$$

whose graphical representations are shown in Figs.6.1.b-c. We have used the short hand notations $\mathbf{p}_\pm = \mp(\mathbf{p} \pm \mathbf{k}/2)$ and $\nu_\pm = \mp(\nu \pm \omega/2)$.

The dipolar mode coupling vertex can be symmetrized by the substitution $\mathbf{p} \rightarrow -\mathbf{p}$ in Eq. (6.41) leading to

$$\begin{aligned} \mathcal{J}_{\text{MCD}}[S, \tilde{S}] &= \frac{1}{2} \lambda f g \epsilon_{\alpha\beta\gamma} \int_{\mathbf{k}} \int_{\omega} \int_{\mathbf{p}} \int_{\nu} \left[\frac{p_+^\mu p_+^\gamma}{p_+^2} \tilde{S}^\alpha(\mathbf{k}, \omega) S^\beta(\mathbf{p}_-, \nu_-) S^\mu(\mathbf{p}_+, \nu_+) + \right. \\ &\quad \left. - \frac{p_-^\mu p_-^\beta}{p_-^2} \tilde{S}^\alpha(\mathbf{k}, \omega) S^\mu(\mathbf{p}_-, \nu_-) S^\gamma(\mathbf{p}_+, \nu_+) \right]. \end{aligned} \quad (6.43)$$

The relaxation vertex is given by

$$\begin{aligned} \mathcal{J}_{\text{RE}}[S, \tilde{S}] &= -\frac{u}{3!} F^{\alpha\beta\gamma\delta} \int_{\mathbf{k}_1} \int_{\mathbf{k}_2} \int_{\mathbf{k}_3} \int_{\omega_1} \int_{\omega_2} \int_{\omega_3} \lambda \left[\gamma + (\sum_i \mathbf{k}_i)^2 \right] \\ &\quad \times \tilde{S}^\alpha(\sum_i \mathbf{k}_i, \sum_i \omega_i) S^\beta(-\mathbf{k}_1, -\omega_1) S^\gamma(-\mathbf{k}_2, -\omega_2) S^\delta(-\mathbf{k}_3, -\omega_3). \end{aligned} \quad (6.44)$$

It contains a diffusive part

$$\begin{aligned} \mathcal{J}_{\text{Diff}}[S, \tilde{S}] &= -\frac{u}{3!} \lambda F^{\alpha\beta\gamma\delta} \int_{\mathbf{k}_1} \int_{\mathbf{k}_2} \int_{\mathbf{k}_3} \int_{\omega_1} \int_{\omega_2} \int_{\omega_3} (\sum_i \mathbf{k}_i)^2 \\ &\quad \times \tilde{S}^\alpha(\sum_i \mathbf{k}_i, \sum_i \omega_i) S^\beta(-\mathbf{k}_1, -\omega_1) S^\gamma(-\mathbf{k}_2, -\omega_2) S^\delta(-\mathbf{k}_3, -\omega_3), \end{aligned} \quad (6.45)$$

and a relaxational part

$$\begin{aligned} \mathcal{J}_{\text{Rel}}[S, \tilde{S}] &= -\frac{u}{3!} \lambda F^{\alpha\beta\gamma\delta} \int_{\mathbf{k}_1} \int_{\mathbf{k}_2} \int_{\mathbf{k}_3} \int_{\omega_1} \int_{\omega_2} \int_{\omega_3} \gamma \\ &\quad \times \tilde{S}^\alpha(\sum_i \mathbf{k}_i, \sum_i \omega_i) S^\beta(-\mathbf{k}_1, -\omega_1) S^\gamma(-\mathbf{k}_2, -\omega_2) S^\delta(-\mathbf{k}_3, -\omega_3), \end{aligned} \quad (6.46)$$

whose diagrammatic representations are given in Figs. 6.1.d-e. This decomposition is not important from a technical point of view, since both terms have the same tensorial structure. But, it emphasizes that the relaxational vertices due to the exchange interaction and dipolar interaction are diffusive and relaxational, respectively.

With the above perturbation theory at hand, we can now calculate the Greens functions defined by

$$\begin{aligned}
G_{N,\tilde{N}}^{\alpha_1,\dots,\alpha_N,\beta_1,\dots,\beta_{\tilde{N}}}(\mathbf{k}_1, \omega_1; \dots; \mathbf{k}_N, \omega_N; \mathbf{k}_{N+1}, \omega_{N+1}; \dots; \mathbf{k}_{N+\tilde{N}}, \omega_{N+\tilde{N}}) &= \\
= \langle S^{\alpha_1}(\mathbf{k}_1, \omega_1) \dots S^{\alpha_N}(\mathbf{k}_N, \omega_N) \tilde{S}^{\beta_1}(\mathbf{k}_{N+1}, \omega_{N+1}) \dots \tilde{S}^{\beta_{\tilde{N}}}(\mathbf{k}_{N+\tilde{N}}, \omega_{N+\tilde{N}}) \rangle &= \\
= \frac{\delta^{N+\tilde{N}}}{\delta h^{\alpha_1}(\mathbf{k}_1, \omega_1) \cdot \dots \cdot \delta \tilde{h}^{\beta_{\tilde{N}}}(\mathbf{k}_{N+\tilde{N}}, \omega_{N+\tilde{N}})} Z[h, \tilde{h}] \Big|_{h, \tilde{h}=0} . & \quad (6.47)
\end{aligned}$$

It is convenient to consider the vertex functions

$$\Gamma_{N,\tilde{N}}^{\alpha_1,\dots,\alpha_N,\beta_1,\dots,\beta_{\tilde{N}}}(\mathbf{k}_1, \omega_1; \dots; \mathbf{k}_N, \omega_N; \mathbf{k}_{N+1}, \omega_{N+1}; \dots; \mathbf{k}_{N+\tilde{N}}, \omega_{N+\tilde{N}}), \quad (6.48)$$

which can be obtained from the cummulants by a Legendre transformation [17].

B. Self consistent one loop theory

In the preceding sections we have derived a path integral representation of the dynamics starting from semi-phenomenological Langevin equations. Within this method a perturbation theory for the correlation and response functions could be formulated which is similar to the usual field theoretic procedure for static critical phenomena. In each finite order of perturbation theory infrared divergences arise reflecting the infrared divergences in the second derivatives of the free energy close to a critical point. In order to remove these divergences (which appear combined with the ultraviolet divergencies at the upper critical dimension of the model) and to have a perturbation theory with a small parameter one can use the concepts of renormalized field theories, i.e., upon introducing renormalization factors and expanding around the upper critical dimension.

Instead we follow here a alternative route, which consists in the resummation of certain classes of diagrams to infinite order in perturbation theory. Such methods are frequently

used in condensed matter physics quite successfully. These methods are characterized by the fact that they lead to self consistent equations for the correlation functions.

In this section we formulate such a self consistent procedure for critical dynamics. It will turn out that the resulting equations are equivalent to mode coupling theory.

1. Self consistent determination of the line width in Lorentzian approximation

As we have already seen in the discussion of the mode coupling theory one can obtain quite reasonable results for the line width by assuming that the line shape is given by a Lorentzian. In the above formulation in terms of a dynamical functional the line width is given by [17]

$$\Gamma_{\text{lor}}^{\alpha} = -2 \frac{[\Gamma_{11}^{\alpha}(q, 0)]^2}{\Gamma_2^{\alpha}(q)\Gamma_{02}^{\alpha}(q, 0)} \quad (6.49)$$

where $\Gamma_2^{\alpha}(q)$ is the inverse static susceptibility ($\alpha = L, T$). Upon using the Fluctuation Dissipation Theorem (FDT)

$$\Gamma_{11}^{\alpha}(q, 0) = [\lambda(\gamma + q^2) + \lambda f \Gamma_{X,10}^{\alpha}(q, 0)] \Gamma_2^{\alpha}(q) \quad (6.50)$$

one obtains to one loop order $-2\Gamma_{11}^{\alpha}(q, 0) = \Gamma_2^{\alpha}(q)\Gamma_{02}^{\alpha}(q, 0)$ and consequently $\Gamma_{\text{lor}}^{\alpha} = \Gamma_{11}^{\alpha}(q, 0) = -\frac{1}{2}\Gamma_2^{\alpha}(q)\Gamma_{02}^{\alpha}(q, 0)$. To zeroth order we have $\Gamma_{02}^{\alpha}(q, 0) = -2\lambda(\gamma + q^2)$. The one loop contributions to $\Gamma_{02}^{\alpha\beta}(q, 0)$ are shown in Fig. 6.2. The transverse and longitudinal Lorentzian line width is found to be

$$\begin{aligned} \Gamma_{\text{lor}}^T(q)\chi^T(q) &= \lambda(\gamma + q^2) + 2(\lambda f)^2 \int_p \int_{\omega} \left[v_{TT}^T(g, \mathbf{p}, \mathbf{q}) C^T(\mathbf{p}_-, \omega) C^T(\mathbf{p}_+, \omega) + \right. \\ &\quad \left. + v_{TL}^T(g, \mathbf{p}, \mathbf{q}) C^T(\mathbf{p}_-, \omega) C^L(\mathbf{p}_+, \omega) + \right. \\ &\quad \left. + v_{LL}^T(g, \mathbf{p}, \mathbf{q}) C^L(\mathbf{p}_-, \omega) C^L(\mathbf{p}_+, \omega) \right], \end{aligned} \quad (6.51)$$

and

$$\begin{aligned} \Gamma_{\text{lor}}^L(q)\chi^L(q) &= \lambda(\gamma + q^2) + 2(\lambda f)^2 \int_p \int_{\omega} \left[v_{TT}^L(g, \mathbf{p}, \mathbf{q}) C^T(\mathbf{p}_-, \omega) C^T(\mathbf{p}_+, \omega) + \right. \\ &\quad \left. + v_{TL}^L(g, \mathbf{p}, \mathbf{q}) C^T(\mathbf{p}_-, \omega) C^L(\mathbf{p}_+, \omega) \right], \end{aligned} \quad (6.52)$$

where we have introduced the notation $\mathbf{p}_\pm = \mathbf{p} \pm \frac{\mathbf{q}}{2}$. The vertex functions $v_{\alpha\beta}^\sigma(g, \mathbf{p}, \mathbf{q})$ are given by

$$v_{TT}^T(g, \mathbf{p}, \mathbf{q}) = \frac{1}{d-1} \left[d^2 - 4d + 6 - \frac{(\mathbf{p}_+ \cdot \mathbf{p}_-)^2}{p_+^2 p_-^2} - 2 \frac{(\mathbf{p}_+ \mathbf{q})^2}{p_+^2 q^2} \right] (\mathbf{p} \cdot \mathbf{q})^2 \quad (6.53a)$$

$$v_{TL}^T(g, \mathbf{p}, \mathbf{q}) = \frac{4}{d-1} \left[d - 3 + \frac{(\mathbf{p}_+ \cdot \mathbf{p}_-)^2}{p_+^2 p_-^2} + \frac{(\mathbf{p}_+ \cdot \mathbf{q})^2}{p_+^2 q^2} \right] (\mathbf{p} \cdot \mathbf{q} + \frac{g}{2})^2 \quad (6.53b)$$

$$v_{LL}^T(g, \mathbf{p}, \mathbf{q}) = \frac{1}{d-1} \left[1 - \frac{(\mathbf{p}_+ \cdot \mathbf{p}_-)^2}{p_+^2 p_-^2} \right] (\mathbf{p} \cdot \mathbf{q})^2 \quad (6.53c)$$

$$v_{TT}^L(g, \mathbf{p}, \mathbf{q}) = \left[d - 3 + 2 \frac{(\mathbf{p}_+ \cdot \mathbf{q})^2}{p_+^2 q^2} \right] (\mathbf{p} \cdot \mathbf{q})^2 \quad (6.53d)$$

$$v_{TL}^L(g, \mathbf{p}, \mathbf{q}) = 4 \left[1 - \frac{(\mathbf{p}_+ \cdot \mathbf{q})^2}{p_+^2 q^2} \right] (\mathbf{p} \cdot \mathbf{q} + \frac{g}{2})^2 \quad (6.53e)$$

Upon substituting in the integrals (6.51) and (6.52) $\mathbf{p}_+ = \mathbf{p} + \frac{\mathbf{q}}{2} \rightarrow \mathbf{p}$ the above vertex functions are identical to the vertex functions in section III, Eqs. (3.20)-(3.24). The frequency integration can readily be done leading to

$$\int_\omega C^\alpha(\mathbf{p}_-, \omega) C^\beta(\mathbf{p}_+, \omega) = \frac{\chi^\alpha(\mathbf{p}_-) \chi^\beta(\mathbf{p}_+)}{\lambda [(\gamma + p_-^2)/\chi^\alpha(\mathbf{p}_-) + (\gamma + p_+^2)/\chi^\beta(\mathbf{p}_+)]}, \quad (6.54)$$

i.e., the product of the static susceptibilities divided by the sum of the line width to zeroth order. This structure corresponds to the first step in an iteration procedure and suggests to define a self-consistent approximation by replacing the bare line width by the full line width.

$$\frac{\chi^\alpha(\mathbf{p}_-) \chi^\beta(\mathbf{p}_+)}{\lambda [(\gamma + p_-^2)/\chi^\alpha(\mathbf{p}_-) + (\gamma + p_+^2)/\chi^\beta(\mathbf{p}_+)]} \rightarrow \frac{\chi^\alpha(\mathbf{p}_-) \chi^\beta(\mathbf{p}_+)}{[\Gamma_{\text{lor}}^\alpha(\mathbf{p}_-) + \Gamma_{\text{lor}}^\beta(\mathbf{p}_+)]} \quad (6.55)$$

This self consistent approach corresponds to a partial resummation of the perturbation series as shown in Fig. 6.3. The resulting equations are identically with the mode coupling equations in Lorentzian approximation found by the conventional derivation in section III. The factorization approximation (two mode approximation) in the conventional derivation corresponds to the structure of the one loop diagrams here.

2. Self consistent equation for the Kubo relaxation function

In the preceding section we derived for the sake of simplicity the mode coupling equations in the so called Lorentzian approximation for the line shape. Here we go beyond this approximation and derive a self consistent theory for the full wave vector and frequency dependent relaxation functions. The dynamic susceptibility can be written as [17] ($\alpha = L, T$)

$$\chi^\alpha(q, \omega) = \frac{\lambda(\gamma + q^2) + \lambda f \Gamma_{X,10}^\alpha(q, \omega)}{\Gamma_{11}^\alpha(-q, -\omega)}. \quad (6.56)$$

The X-insertion is defined by [17]

$$X^\alpha(\vec{q}, \omega) = \epsilon_{\alpha\beta\gamma} \int_{\mathbf{k}} \int_{\nu} \tilde{S}^\beta(\vec{k} - \vec{q}/2, \nu - \omega/2) S^\gamma(-\vec{k} - \vec{q}/2, -\nu - \omega/2). \quad (6.57)$$

Upon using the (explicit) structure of the dynamic propagators $C^\alpha(q, t)\Theta(t) = \chi^\alpha(q)R^\alpha(q, t)$ one can show that the relation

$$\Gamma_{11}^\alpha(-q, -\omega) = -i\omega + [\lambda(\gamma + q^2) + \lambda f \Gamma_{X,10}^\alpha(q, \omega)] \Gamma_2^\alpha(q) \quad (6.58)$$

holds to one loop order. This implies for the Kubo relaxation function $\Phi^\alpha(q, \omega)$, which is related to the dynamic susceptibility by

$$\Phi^\alpha(q, \omega) = \frac{1}{i\omega} [\chi^\alpha(q, \omega) - \chi^\alpha(q)], \quad (6.59)$$

a structure analogous to Eq. (3.25)

$$\Phi^\alpha(q, \omega) = \frac{\chi^\alpha(q)}{\Gamma_{11}^\alpha(-q, -\omega)} = \frac{\chi^\alpha(q)}{-i\omega + [\lambda(\gamma + q^2) + \lambda f \Gamma_{X,10}^\alpha(q, \omega)] \Gamma_2^\alpha(q)}. \quad (6.60)$$

To one loop order one obtains for $\Gamma_{X,10}^\alpha(q, t)$

$$\begin{aligned} \Gamma_{X,10}^T(q, t) = 2\lambda f \int_p \Theta(t) & \left[v_{TT}^T(g, \mathbf{p}, \mathbf{q}) C^T(\mathbf{p}_-, t) C^T(\mathbf{p}_+, t) + \right. \\ & + v_{TL}^T(g, \mathbf{p}, \mathbf{q}) C^T(\mathbf{p}_-, t) C^L(\mathbf{p}_+, t) + \\ & \left. + v_{LL}^T(g, \mathbf{p}, \mathbf{q}) C^L(\mathbf{p}_-, t) C^L(\mathbf{p}_+, t) \right], \end{aligned} \quad (6.61a)$$

$$\begin{aligned} \Gamma_{X,10}^L(q, t) = 2\lambda f \int_p \Theta(t) & \left[v_{TT}^L(g, \mathbf{p}, \mathbf{q}) C^T(\mathbf{p}_-, t) C^T(\mathbf{p}_+, t) + \right. \\ & \left. + v_{TL}^L(g, \mathbf{p}, \mathbf{q}) C^T(\mathbf{p}_-, t) C^L(\mathbf{p}_+, t) \right], \end{aligned} \quad (6.61b)$$

where the vertex functions are identical to Eqs. (6.53a-6.53e). We have $C^\alpha(q, t)\Theta(t) = \chi^\alpha(q)R^\alpha(q, t)$. Eqs. (6.60-6.61b) can be written in a self-consistent form by replacing the propagator $C^\alpha(q, t)$ by the full Kubo relaxation function $\Phi^\alpha(q, t)$ on the right hand side of Eqs. (6.61a,6.61b). This corresponds, as in the preceding section, to a partial resummation of the perturbation series. The resulting equations are identical with the mode coupling equations Eqs. (3.19)-(3.25) in section III . Hence we have shown that mode coupling theory is equivalent to a self consistent one loop theory. The factorization approximation in the conventional derivation of mode coupling theories is here a direct consequence of the structure of the one loop theory. Furthermore the present procedure has the advantage to be extendible to a self consistent formulation of higher loop order. In order to justify the validity of the mode coupling approach one has to ask in what sense higher order terms are small compared with the self consistent one loop theory. This question will be addressed in Appendix C, where we restrict ourselves to the isotropic case (in order to simplify the discussion).

Captions to the figures:

Figure 6.1: Basic elements of the dynamical perturbation theory. a) Correlation and response propagators, b) isotropic mode coupling vertex, c) dipolar mode coupling vertex, d) isotropic relaxational vertex, and e) dipolar relaxational vertex.

Figure 6.2: One-loop diagrams for the vertex function $\Gamma_{02}^{\alpha\beta}(\mathbf{q}, \omega)$.

Figure 6.3: Partial summation of the perturbation theory for $\Gamma_{02}^{\alpha\beta}(\mathbf{q}, \omega)$, where vertex corrections are neglected. This resummation leads to the mode coupling equations.

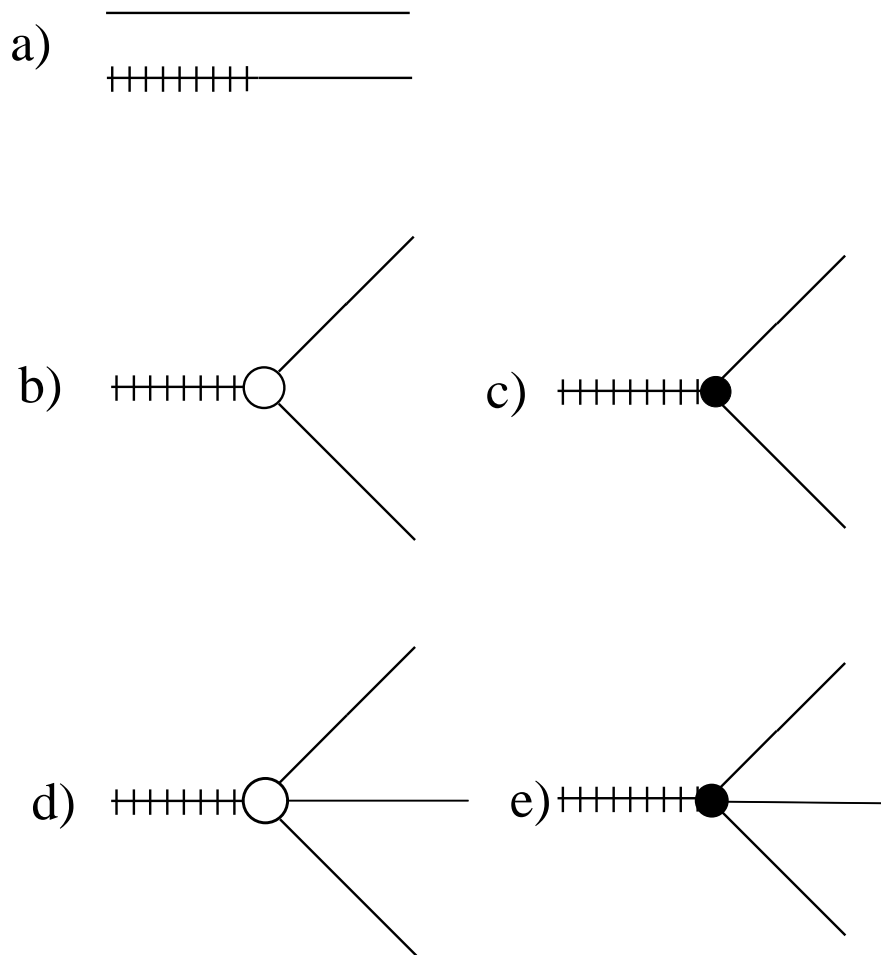


Figure 6.1: Basic elements of the dynamical perturbation theory. a) Correlation and response propagators, b) isotropic mode coupling vertex, c) dipolar mode coupling vertex, d) isotropic relaxational vertex, and e) dipolar relaxational vertex.

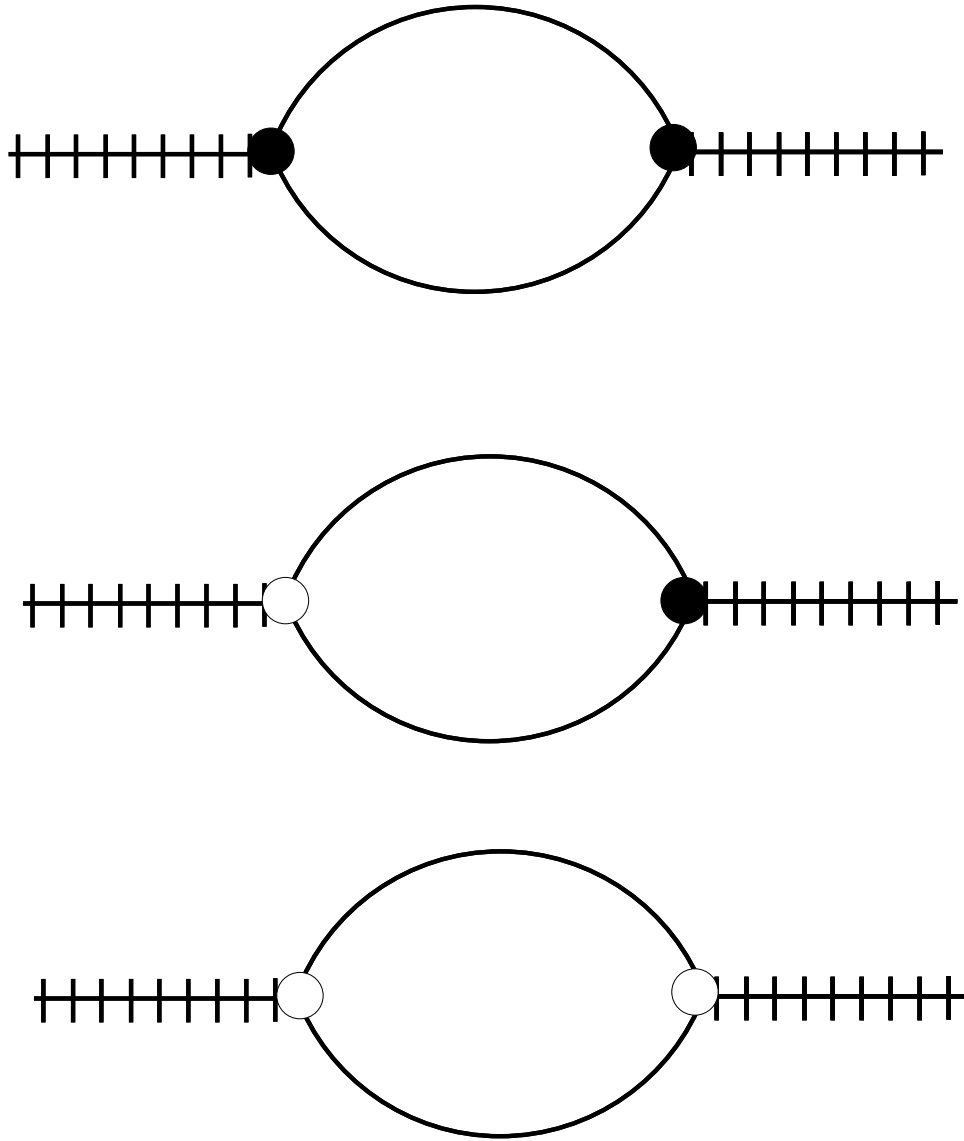


Figure 6.2: One-loop diagrams for the vertex function $\Gamma_{02}^{\alpha\beta}(\mathbf{q}, \omega)$.

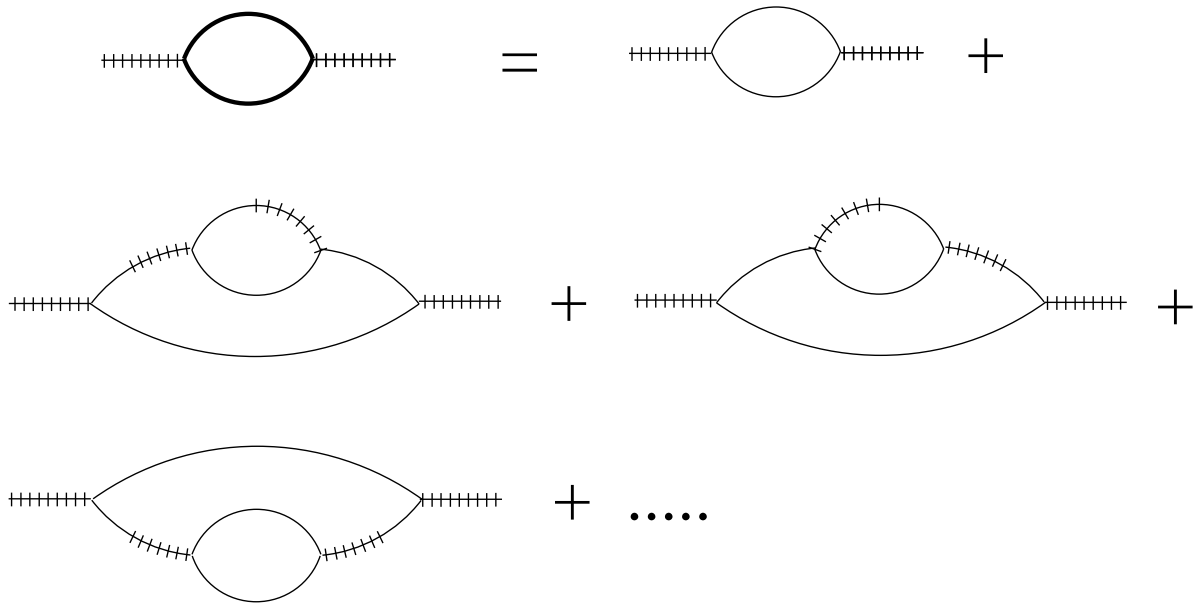


Figure 6.3: Partial summation of the perturbation theory for $\Gamma_{02}^{\alpha\beta}(\mathbf{q}, \omega)$, where vertex corrections are neglected. This resummation leads to the mode coupling equations.

VII. CONCLUSIONS AND OUTLOOK

The past decade has witnessed substantial progress in understanding the critical dynamics of real ferromagnets, both on the experimental and the theoretical side. In this review we have concentrated on the interplay between exchange and dipole–dipole interaction. We have presented theoretical and experimental evidence that many aspects of the critical dynamics of ferromagnets such as *Fe*, *Ni*, *EuO*, *EuS*, and many other magnetic materials are now fairly well understood on the basis of a mode coupling theory which takes into account exchange as well as the dipole–dipole interaction. In this final section we conclude our overview by summarizing some of the main theoretical and experimental achievements and by briefly discussing a number of open problems in the field of critical dynamics of magnets.

One of the most important theoretical advances towards our understanding of the critical dynamics of real ferromagnets was the realization that additional interactions such as the dipole–dipole interaction can lead to a qualitatively new behavior of the frequency and wave vector dependence of the spin–spin correlation functions [79,80]. A description of a mode coupling theory, which on top of the exchange interaction takes into account the dipole–dipole interaction, has been given in section III. The main results of this mode coupling analysis can be summarized as follows. The dipolar interaction leads to an anisotropy of the spin fluctuations with respect to the direction of the wave vector and introduces a second length scale q_D^{-1} besides the correlation length ξ . The presence of a second length scale leads to generalized dynamic scaling laws, containing two scaling variables, $x = 1/q\xi$ and $y = q_D/q$ for the length scale and one scaling variable $\tau_\alpha = \Lambda q^z \Omega^\alpha(x, y)t$ for the time scale. Due to the dipolar anisotropy the characteristic time scales $1/[\Lambda q^z \Omega^\alpha(x, y)]$ are different for the longitudinal and transverse modes ($\alpha = L, T$). This is mainly due to the non critical longitudinal static susceptibility implying that the longitudinal characteristic frequency $\Lambda q^z \Omega^L(x, y)$ shows no critical slowing down asymptotically. Furthermore, the dipolar interaction leads to a quite interesting crossover in the line width and line shape of the spin-spin correlation functions.

Line width crossover. Precisely at the critical temperature the dynamic critical exponent for the transverse line width undergoes a crossover from $z = 5/2$ to $z = 2$, which is displaced with respect to the static crossover to wave vectors smaller by almost one order of magnitude. This explains why up to now this crossover escaped detection by neutron scattering experiments right at T_c . For the longitudinal line width the crossover is predicted to be from $z = 5/2$ to an uncritical behavior $z = 0$ and, in contrast to the transverse width, it occurs in the immediate vicinity of the static crossover, characterized by q_D . If the line shapes are approximated by Lorentzians the concomitant Lorentzian line widths obey the scaling law $\Gamma^\alpha(q, \xi, g) = \Lambda q^z \gamma^\alpha(x, y)$. For vanishing dipolar coupling g , the scaling functions coincide with the Resibois-Piette scaling function. If the strength of the dipolar interaction g is finite, the curves approach the Resibois-Piette scaling function for small values of the scaling variable x and deviate therefrom with increasing x . Since the dipolar interaction leads to a non conserved order parameter, the line width in the hydrodynamic limit is given by $\Gamma \propto q^0$ instead of $\Gamma \propto q^2$ as for an isotropic exchange ferromagnet.

Line shape crossover. Close to T_c the line shapes of the longitudinal and transverse relaxation function coincide in the isotropic Heisenberg limit, i.e., for large values of the wave vector q ($q \gg q_D$). In this limit the dipolar interaction becomes negligible and the shape is of the Hubbard-Wegner type as discussed in section II. Upon increasing the value of the scaling variable $r = \sqrt{(1/q\xi)^2 + (q_D/q)^2}$, the line shapes of the transverse and longitudinal relaxation function become drastically different. Whereas the transverse relaxation function shows a nearly exponential temporal decay, over-damped oscillations show up for the longitudinal relaxation function. The line shape crossover sets in in the vicinity of the dipolar wave vector q_D in contrast to the line width crossover, which starts at a wave vector almost one order of magnitude smaller. The situation is quite different for temperatures well separated from the critical temperature. Then, the difference in the shape crossover of the longitudinal and transverse relaxation function diminishes with decreasing $q_D \xi$. For $q_D \xi \ll 1$ the shape crossover as a function of r corresponds to the crossover from the critical (Hubbard-Wegner) shape to the hydrodynamic shape as discussed in section II.

On the experimental side, an important development began with the observation that the data for the line widths above the transition temperature [188,189,31] in magnetic materials such as *EuO* and *Fe* could not be described by the Resibois-Piette scaling function resulting from a mode coupling theory [231] as well as a renormalization group theory [174,123], which take into account the short range exchange interaction only. Even more, the data could not be collapsed onto any other single scaling function. Those experimental results were explained quantitatively on the basis of the mode coupling theory [79–81] described in section III. Clear indications of the importance of the dipolar interaction have also been observed in hyperfine interaction experiments on *Fe* and *Ni*, where one found a crossover in the dynamical critical exponent from $z = 5/2$ to $z = 2$ [228,95,113,114], and with electron spin resonance and magnetic relaxation experiments [147–149] [150,64,152], where a non vanishing Onsager coefficient at zero wave vector was found. For all these data now there exists a quantitative theoretical description (see section IV).

With advances in the neutron scattering technique subsequent experiments investigated the line shape of the spin-spin correlation function. This progress made it possible to test the predictions for the line shape from MC–theory [262,118] and RG–theory [61,22], which take into account solely the short–range exchange interaction. Originally those theories for the critical dynamics were expected to fit the experimental data in an increasing quantitative way as one was able to measure the correlation functions at smaller and smaller wave vectors, since the influence of additional irrelevant interactions should diminish as one moves closer to criticality. It came as quite a surprise when Mezei found a nearly exponential decay of the Kubo relaxation function by spin echo experiments on *EuO* at $q = 0.024\text{\AA}^{-1}$ and $T = T_c$ [190], which was in drastic disagreement with the bell–like shape predicted [262,118,61,22]. The anomalous exponential decay found by Mezei [190], was shown again to be a dipolar effect [82,85]. Recently, significant experiments have been performed using polarized neutrons [33,93], which allowed for the first time to measure the longitudinal and transverse spin-spin correlation functions separately. The results confirmed the theoretical predictions concerning the line width [80] as well as the line shape of the lon-

gitudinal relaxation function [82,85]. The experimental data, de-convoluted by a maximum entropy method, agree quite well with the theoretical predictions, especially the double peak structure corresponding to the over-damped oscillations in time have been observed. This can be regarded as a success of the mode coupling theory.

For the critical dynamics below T_c experimental investigations are scarce. In contrast to the very satisfactory situation above T_c , where quantitative agreement between experiment and theory has been achieved, the situation in the ferromagnetic phase is by far less clear. Theoretical investigations so far have concentrated on the dynamics of isotropic exchange ferromagnets, neglecting dipolar effects [81,240]. In this context it has been shown within the framework of mode coupling theory that the amplitude of the scaling function for the spin-wave frequency of the isotropic Heisenberg Hamiltonian is universal [240]. A comparison of the theory [81], taking into account the so determined universal amplitude [240], with recent measurements of the longitudinal line width on *Ni* [34] below and not too close to the critical point gives quantitative agreement.

But also in the ferromagnetic phase profound effects of the dipolar interaction on the spin dynamics have been revealed in recent experiments. Using polarized neutron scattering the spin excitations in *EuS* and *Pd₂MnSn* have been investigated below T_c by Böni et al. [37,38]. These investigations indicate that there are deviations from the theoretical correlation functions of isotropic exchange ferromagnets. Especially, an anisotropy of the spin fluctuations with respect to the polarization relative to the wave vector \mathbf{q} has been observed. Still further experimental and theoretical progress is needed in order to reach a thorough understanding of the spin dynamics in the ferromagnetic phase. The most convincing experimental indication for the importance of the dipolar interaction below T_c has been obtained recently in a measurement of the homogeneous magnetization dynamics [59]. It is found that the scaling function for the kinetic coefficient below T_c coincides with the one observed earlier above T_c . Up to now, there is no theoretical explanation for these interesting experimental findings, but work in the framework of mode coupling theory is in progress [241].

Besides three-dimensional ferromagnetic materials with isotropic exchange interaction there are other magnetic systems, where the dipole-dipole interaction influences the critical behavior, such as antiferromagnets or ferromagnets with a uniaxial or planar exchange anisotropy. The critical dynamics of isotropic dipolar antiferromagnets is affected by the dipolar interaction featuring a crossover from diffusive to relaxational dynamics of the magnetization and a crossover in the dynamic exponent [5]. The effect on the staggered magnetization is much less pronounced than for the corresponding order parameter modes in the ferromagnetic case. For ferromagnets with a uniaxial exchange anisotropy the dipolar interaction leads first of all to a reduction of the upper critical dimension from $d_c = 4$ to $d_c = 3$. As a consequence the critical statics is described by mean field theory with logarithmic corrections [161]. A time dependent Ginzburg Landau model [76] for the dynamics results in logarithmic corrections to the conventional van Hove theory of critical dynamics.

We conclude with some comments on two-dimensional (2D) magnetic systems. These are interesting because the Hohenberg-Mermin-Wagner theorem [111,186] excludes conventional long-range order in isotropic systems with a continuous symmetry and short-ranged interaction. Two dimensions seem to be the borderline dimension where thermal fluctuations are just strong enough to prevent the appearance of a finite order parameter. However, the anisotropy of the dipolar interaction with respect to the separation of two spins leads to a suppression of the longitudinal fluctuations and thus a finite order parameter may exist in two dimensions (see section V). The dipolar interaction is responsible for the existence of long range order in both ferromagnetic [177] and antiferromagnetic thin films [215,216]. There is quite an interesting phase diagram with various spin flop and intermediate phases for two-dimensional dipolar antiferromagnets in a finite external magnetic field [217].

Two-dimensional ferromagnets are interesting for practical reasons as magnetic storage devices as well as from a fundamental point of view. With the recent advances in thin film technology it becomes possible to study the critical behavior of two-dimensional magnetic systems [11]. Due to the combined effect of anisotropy, dipole-dipole interaction, and increased importance of thermal fluctuations in two dimensions, the phase diagram of fer-

romagnetic thin films shows a variety of new phases [206,10,11]. The theoretical predictions in this field are still rather controversial [212,213,164,134]. A still open and very interesting question is the critical dynamics of all those phases.

ACKNOWLEDGMENTS

It is a pleasure to acknowledge helpful discussions with P. Böni, D. Görlitz, J. Kötzler, F. Mezei, C. Pich, H. Schinz, U.C. Täuber, and A. Yaouanc. The work of E.F. has been supported by the Deutsche Forschungsgemeinschaft (DFG) under Contracts No. Fr. 850/2-1,2. This work has also been supported by the German Federal Ministry for Research and Technology (BMFT) under the contract number 03-SC3TUM.

APPENDIX A: FLUCTUATION-DISSIPATION RELATIONS

In this appendix we collect several fluctuation dissipation theorems, which are of importance for the dynamics of systems described by nonlinear Langevin equations.

Let \mathcal{T} be the time reversal operation: $t \rightarrow -t$. Then detailed balance (time reversal symmetry) implies [128] that

$$\mathcal{T} \exp \left[\mathcal{J}_{t_1}^{t_2} - \mathcal{H}_{t_1} \right] = \exp \left[\mathcal{J}_{-t_2}^{-t_1} - \mathcal{H}_{-t_2} \right], \quad (\text{A1})$$

where $\mathcal{H}_t = \mathcal{H}(S(t))$ is the stationary probability distribution function and $\mathcal{J}_{t_1}^{t_2}[S, \tilde{S}]$ the dynamic functional. For simplicity we have assumed a one-component field S . Without loss of generality one can assume that the field $S(x, t)$ is even or odd under time reversal, i.e.

$$\mathcal{T}S = \epsilon S, \quad \epsilon = \pm 1. \quad (\text{A2})$$

In the case of spins S is odd under time reversal. The stationary distribution $P_{\text{st}}[S] = e^{-\mathcal{H}[S]}$ is characterized by the “free energy” $\mathcal{H}[S]$. The time reversal symmetry implies that

$$\mathcal{T}\tilde{S}(t) = -\epsilon \left(\tilde{S}(-t) - \frac{\delta \mathcal{H}[S(-t)]}{\delta S(-t)} \right). \quad (\text{A3})$$

Now one uses the causality property of the response functions

$$\langle S(t_1)S(t_2)\dots S(t_k)\tilde{S}(\tilde{t}_1)\tilde{S}(\tilde{t}_2)\dots\tilde{S}(\tilde{t}_k) \rangle = 0, \quad \text{if one } \tilde{t}_j > \text{ all } t_i. \quad (\text{A4})$$

Then for example

$$\langle S(t)\tilde{S}(0) \rangle = 0 \text{ for } t < 0. \quad (\text{A5})$$

With the time reversal operation and Eq. (A3) it then follows from Eq. (A5) for $t < 0$

$$\langle S(-t) \left(\tilde{S}(0) - \frac{\delta \mathcal{H}[S(0)]}{\delta S(0)} \right) \rangle = 0. \quad (\text{A6})$$

Upon redefining $t = -t$ one obtains for $t > 0$

$$\langle S(t)\tilde{S}(0) \rangle = \Theta(t) \langle S(t) \frac{\delta \mathcal{H}[S(0)]}{\delta S(0)} \rangle \quad (\text{A7})$$

The same arguments can be repeated for $\langle S(t_1)S(t_2)\dots S(t_k)\tilde{S}(\tilde{t}_1) \rangle$ with $\tilde{t}_1 > \text{all } t_j$. The result is

$$\langle S(t_1)S(t_2)\dots S(t_k)\tilde{S}(\tilde{t}_1) \rangle = \Theta(\tilde{t}_1, \{t_j\}) \langle S(t_1)S(t_2)\dots S(t_k) \frac{\delta \mathcal{H}[S(\tilde{t}_1)]}{\delta S(\tilde{t}_1)} \rangle . \quad (\text{A8})$$

where $\Theta(\tilde{t}_1, \{t_j\})$ is an obvious generalization of the Θ -function. Note that these generalized FDT's hold for the cummulants and not for the vertex functions. In particular we get

$$G_{11}(k, t) = \Theta(t) \frac{\nu k^2}{D} G_{02}(k, t) . \quad (\text{A9})$$

In a completely analogous way one can derive the following identities [17,128]

$$\chi_{\alpha\beta}(x - x', t - t') = -\Theta(t - t') \frac{d}{dt} \langle S^\alpha(x, t) S^\beta(x', t') \rangle \quad (\text{A10a})$$

$$C_{\alpha\beta}(k, \omega) = \frac{2k_B T}{\omega} \text{Im}[\chi_{\alpha\beta}(k, \omega)] \quad (\text{A10b})$$

$$-\Theta(t - t') \frac{d}{dt} \langle S^\alpha(x, t) S^\beta(x', t') \rangle = L_{\gamma\beta} \langle S^\alpha(x, t) \tilde{S}^\gamma(x', t') \rangle - \lambda f \langle S^\alpha(x, t) X^\beta(x', t') \rangle \quad (\text{A10c})$$

with $X^\beta = \epsilon_{\beta\mu\nu} \tilde{S}^\mu S^\nu$. Therefrom one can deduce the following identities for the vertex functions

$$\Gamma_{11}^{\alpha\beta}(q, \omega = 0) = [\lambda q^a \delta^{\alpha\gamma} + \lambda f \Gamma_{X,10}^{\alpha\gamma}(q, \omega = 0)] \Gamma_2^{\gamma\beta}(q) , \quad (\text{A11a})$$

$$\begin{aligned} -i\omega \Gamma_{20}^{\alpha\beta}(q, \omega) &= \lambda q^a [\Gamma_{11}^{\alpha\beta}(q, \omega) - \Gamma_{11}^{\alpha\beta}(-q, -\omega)] \\ &+ \lambda f [\Gamma_{11}^{\alpha\gamma}(q, \omega) \Gamma_{X,10}^{\gamma\beta}(q, \omega) - \Gamma_{11}^{\alpha\gamma}(-q, -\omega) \Gamma_{X,10}^{\gamma\beta}(-q, -\omega)] , \end{aligned} \quad (\text{A11b})$$

where $\Gamma_2^{\alpha\beta}(q) = \langle S^\alpha(-q) S^\beta(q) \rangle^{-1}$ is the static two-point vertex function, and $\Gamma_{X,\tilde{N}}^{\alpha\beta}$ denotes a vertex function with one X -insertion. If the Hamiltonian is quadratic in the fields $\{S\}$, i.e., $\mathcal{H} = \frac{1}{2} \int d^d x c_{\alpha\beta} S^\alpha S^\beta$ then one has a further identity

$$\langle S^\alpha(t) \tilde{S}^\beta(t') \rangle = \Theta(t - t') c_{\alpha\beta} \langle S^\alpha(t) S^\beta(t') \rangle . \quad (\text{A12})$$

APPENDIX B: DERIVATION OF NON-LINEAR LANGEVIN EQUATIONS

In this Appendix we give a short derivation of non-linear Langevin equations based on the projector formalism of Mori [197] and Zwanzig [276]. In our presentation we follow closely the papers by Kawasaki [139] and Mori et al. [198,199].

As a first step in deriving non-linear Langevin equations for a particular physical system, one has to choose the relevant slow variables. This choice is in general dictated by the conservation laws and spontaneously broken symmetries in the system under consideration. Let us assume that we have found an appropriate set of slowly varying variables $\{S\} = (S_1, S_2, \dots, S_n)$. Then, the next step consists in separating an arbitrary dynamical variable X into a part that is associated with the slow variables $\{S\}$ and the rest. This is accomplished by introducing an projection operator by

$$\mathcal{P}X(t) = \sum_j (X, \Psi_j) \Phi_j(\{S\}), \quad (\text{B1})$$

where one defines the inner product as the value of the Kubo relaxation function at $t = 0$

$$(A, B) = \Phi_{AB}(t=0) = i \lim_{\epsilon \rightarrow 0} \int_t^\infty d\tau e^{-\epsilon\tau} \langle [A, B^\dagger] \rangle |_{t=0}, \quad (\text{B2})$$

which is identical with the static susceptibility. The functions $\Phi_j(\{S\})$ and $\Psi_j(\{S\})$ are two suitable sets of functions which are orthonormal with respect to the inner product defined in Eq. (B2)

$$(\Phi_i, \Psi_j) = \delta_{ij}. \quad (\text{B3})$$

The microscopic dynamics of an arbitrary dynamic variable X following from the Heisenberg equations of motion can formally be presented by the Liouville equation

$$\frac{d}{dt}X(t) = i\mathcal{L}X(t). \quad (\text{B4})$$

It was shown in Ref. [139] that with the aid of the operator identity,

$$\begin{aligned} \frac{d}{dt}e^{it\mathcal{L}} &= e^{it\mathcal{L}}i\mathcal{L}_0 + \int_0^t ds e^{i(t-s)\mathcal{L}}i\mathcal{L}_0 e^{it(\mathcal{L}-\mathcal{L}_0)}i(\mathcal{L}-\mathcal{L}_0) \\ &+ e^{it(\mathcal{L}-\mathcal{L}_0)}i(\mathcal{L}-\mathcal{L}_0), \end{aligned} \quad (\text{B5})$$

one can derive a formally exact non-linear Langevin equation

$$\begin{aligned} \frac{d}{dt}X(t) &= \sum_{\beta} (i\mathcal{L}X, \Psi_{\beta}) \Phi_{\beta}(\{S(t)\}) \\ &\quad - \sum_{\beta} \int_0^t d\tau (f_X(\tau), \tilde{f}_{\beta}) \Phi_{\beta}(\{S(t-\tau)\}) + f_X(t), \end{aligned} \quad (\text{B6})$$

with the “random” forces

$$f_X(t) = e^{it\mathcal{Q}\mathcal{L}} i\mathcal{Q}\mathcal{L}X, \quad (\text{B7a})$$

$$\tilde{f}_{\alpha} = \tilde{\mathcal{Q}}i\tilde{\mathcal{L}}\Psi_{\alpha}(\{S(t)\}), \quad (\text{B7b})$$

where $\mathcal{Q} = 1 - \mathcal{P}$. Note that the adjoint operators of \mathcal{L} and \mathcal{P} are denoted by $\tilde{\mathcal{L}}$ and $\tilde{\mathcal{P}}$.

The first term in Eq. (B6) is the so called “adiabatic” term, and it describes the time variation of the dynamic variable X which follows adiabatically the changes in the slow variables $\{S(t)\}$. The second term represents the damping of this adiabatic motion. The last term is the stochastic force acting upon the dynamical variable X . Note, however, that this interpretation depends on the appropriate choice of the slow variables and the sets of functions $\Phi_{\alpha}(\{S(t)\})$ and $\Psi_{\alpha}(\{S(t)\})$. Upon choosing (we assume that the statics is diagonal in the variables S^{α})

$$\Phi_{\alpha}(\{S(t)\}) = \chi_{\alpha}^{-1/2} S_{\alpha}, \quad (\text{B8a})$$

$$\Psi_{\alpha}(\{S(t)\}) = \chi_{\alpha}^{-1/2} S_{\alpha}, \quad (\text{B8b})$$

with $(S_{\alpha}, S_{\beta}) = \delta_{\alpha\beta}\chi_{\alpha}$ one obtains Mori’s generalized Langevin equations [197]

$$\frac{d}{dt}S_{\alpha}(t) = \sum_{\beta} i\omega_{\alpha\beta} S_{\beta}(t) - \sum_{\beta} \int_0^t d\tau (f_{\alpha}(\tau), f_{\beta}) S_{\beta}(t-\tau) + f_{\alpha}(t), \quad (\text{B9})$$

where

$$i\omega_{\alpha\beta} = (i\mathcal{L}S_{\alpha}, S_{\beta})\chi_{\alpha}^{-1}, \quad (\text{B10a})$$

$$f_{\alpha}(t) = e^{it\mathcal{Q}\mathcal{L}} \mathcal{Q}i\mathcal{L}S_{\alpha}. \quad (\text{B10b})$$

The latter equations are the basis for the mode coupling theory discussed in sections II and III. However, with the above choice of a linear projection operator the “random”

forces are orthogonal with respect to the slow variables S_α only. It has been shown in Refs. [138,140,277] that the “random” forces may not be really random since they contain products of the slow variables S_α . Another choice for the projection operator is to include all the suitable symmetrized polynomials of $\{S\}$ among the sets of functions $\{\Psi\}$ and $\{\Phi\}$. Now we restrict ourselves to the case of classical mechanics, where one has $\{\Psi\} = \{\Phi\}$. This choice corresponds to the projection operator introduced by Zwanzig [275,276]. The completeness relation for the Zwanzig projection operator reads

$$\sum_{\alpha} \Phi_{\alpha}(\{S\})\Phi_{\alpha}^*(\{S'\}) = \frac{\delta(S - S')}{P_{eq}(\{S\})} \quad (\text{B11})$$

with the equilibrium probability distribution function

$$P_{eq}(\{S\}) = \exp \left[-\frac{1}{k_B T} \mathcal{H}(\{S\}) \right]. \quad (\text{B12})$$

The resulting generalized Langevin equation takes the form

$$\begin{aligned} \frac{d}{dt} S_{\alpha}(t) = & v_{\alpha}(\{S(t)\}) \\ & + \sum_{\beta} \int_0^t d\tau P_{eq}^{-1}(\{S(t-\tau)\}) \frac{\partial M_{\alpha\beta}(\tau; \{S(t-\tau)\}) P_{eq}(\{S(t-\tau)\})}{\partial S_{\beta}^*(t-\tau)} + \zeta_{\alpha}(t), \end{aligned} \quad (\text{B13})$$

with the so called mode coupling term

$$v_{\alpha}(\{S(t)\}) = \langle i\mathcal{L}S_{\alpha}; \{a\} \rangle, \quad (\text{B14a})$$

and the memory kernel

$$M_{\alpha\beta}(t; \{a\}) = \langle f_{\alpha}(t) f_{\beta}^*(0); \{a\} \rangle, \quad (\text{B14b})$$

where we have introduced the notation $\langle X; \{a\} \rangle = \langle X \delta(S - a) \rangle / P_{eq}(\{a\})$ for the conditional average.

The semi-phenomenological equations of motion are obtained from the above exact equations by making three basic, plausible assumptions. (i) First one makes a Markovian approximation for the kinetic coefficients. This is justified by the fact that one has included all suitable symmetrized polynomials of the slow variables in the projection operator.

$$M_{\alpha\beta}(t; \{a\}) \approx 2L_{\alpha\beta}(\{a\})\delta(t). \quad (\text{B15a})$$

(ii) Second one assumes that all kinetic coefficients are independent of the slow variables

$$L_{\alpha\beta}(\{a\}) \approx L_{\alpha\beta}. \quad (\text{B15b})$$

(iii) Third one takes the random forces ζ as Gaussian white noise

$$w(\{\zeta\}|t_0 \leq t \leq t_1) \sim \exp\left[-\frac{1}{4} \int_{t_0}^{t_1} dt \zeta_\alpha(t) L_{\alpha\beta}^{-1} \zeta_\beta(t)\right] \quad (\text{B15c})$$

Then the generalized Langevin equations reduce to

$$\frac{d}{dt} S_\alpha(t) = v_\alpha(\{S(t)\}) - \sum_\beta L_{\alpha\beta}^0 \frac{\delta \mathcal{H}(\{S(t)\})}{\delta S_\beta^*(t)} + \zeta_\alpha(t), \quad (\text{B16})$$

where

$$\mathcal{H}(\{S\}) = -k_B T \ln(P_{\text{eq}}(\{S\})), \quad (\text{B17a})$$

$$v_\alpha(\{S(t)\}) = -\lambda f \sum_\beta \left[\frac{\delta}{\delta S_\beta} Q_{\alpha\beta}(\{S\}) - Q_{\alpha\beta}(\{S\}) \frac{\delta H(\{S\})}{\delta S_\beta^*(t)} \right]. \quad (\text{B17b})$$

The Poisson brackets are defined by

$$Q_{\alpha\beta}(\{S\}) = \{S_\alpha, S_\beta\}_P = -Q_{\beta\alpha}(\{S\}). \quad (\text{B18})$$

We close this appendix by presenting the generalized Langevin equation for the example of an isotropic ferromagnet

$$\mathcal{H} = \frac{1}{2} \int d^d x [r S^2(\mathbf{x}, t) + (\nabla S(\mathbf{x}, t))^2] + \frac{u}{4!} \int d^d x (S^2(\mathbf{x}, t))^2. \quad (\text{B19})$$

The Poisson brackets are given by

$$Q_{\alpha\beta}(\mathbf{k}, \mathbf{k}') = \epsilon_{\alpha\beta\gamma} S^\gamma(\mathbf{k} + \mathbf{k}'). \quad (\text{B20})$$

Since the order parameter is conserved the kinetic coefficient is

$$L(\mathbf{k}) = \lambda k^2, \quad (\text{B21})$$

(in general $L(\mathbf{k}) = \lambda k^a$). Hence one obtains the following generalized Langevin equation for isotropic ferromagnets

$$\frac{d}{dt}\mathbf{S}(\mathbf{x}, t) = \lambda f \mathbf{S} \times \frac{\delta \mathcal{H}}{\delta \mathbf{S}(\mathbf{x}, t)} - \lambda (i \nabla)^a \frac{\delta \mathcal{H}}{\delta \mathbf{S}(\mathbf{x}, t)} + \boldsymbol{\zeta}(\mathbf{x}, t). \quad (\text{B22})$$

Note that the conventional (van Hove) theory of critical dynamics is obtained by making the following additional assumptions: (i) The Onsager coefficient L remains finite at the critical point. (ii) The mode coupling term is ignored: $f = 0$. (iii) A quadratic approximation is made for the free energy functional $\mathcal{H} = \frac{1}{2} \int_k \chi^{-1}(\mathbf{k}) \mathbf{S}(\mathbf{k}, t) \mathbf{S}(-\mathbf{k}, t)$, where $\chi(\mathbf{k})$ is the static susceptibility.

One should also note that in mode coupling theory solely the latter approximation is made (and further additional approximations like two-mode approximation and neglecting the vertex corrections).

APPENDIX C: VALIDITY OF MODE COUPLING THEORY, HIGHER ORDERS IN PERTURBATION THEORY

In this section we analyze how higher orders in perturbation theory can be incorporated in the self consistent approach. For the sake of simplicity and clarity we restrict ourselves to the case of isotropic ferromagnets with exchange interaction only. The extension to dipolar ferromagnets is straightforward.

First we consider the corrections from two-loop contributions to the vertex functions Γ_{02} and Γ_{11} shown in Figs. A.1 and A.2. Due to the tensorial structure of the relaxation and mode coupling vertices they can not be contracted ($F^{\alpha\beta\gamma\delta} \epsilon_{\alpha'\gamma\delta} = 0$).

The 2-loop diagrams of Γ_{11} and Γ_{02} can be divided into two categories. The first category consists of “true” 2-loop diagrams connecting two relaxation vertices. The second type consists of diagrams whose structure is - up to vertex corrections - identical to the one-loop diagrams. Upon defining a renormalized mode coupling vertex, as shown in Fig. A.3, the 2-loop contributions to the vertex functions Γ_{11} and Γ_{02} are given by the diagrams in Figs. A.4 and A.5.

The modifications of the self consistent equations resulting from these types of two-loop diagrams are now discussed separately.

(I) The vertex corrections in Fig. A.3 correspond to the vertex function $\Gamma_{12}(q, p, \nu = 0, \omega)$. Since all diagrams have a bare mode coupling vertex with an external response line (see e.g. [55]), the one-loop contribution to $\Gamma_{12}(q, p, \nu = 0, \omega)$ is proportional to $\mathbf{p} \cdot \mathbf{q}$, i.e., it has the same wave vector dependence as the original bare mode coupling vertex. The remaining frequency integral is a function $f(\omega)$ of the external frequency ω . Because only the long time behavior is of importance for the critical dynamics the limit $\omega \rightarrow 0$ merely leads to a renormalization of the amplitude, λf , of the mode coupling vertex and not to a change in its wave vector dependence. (But, see the discussion of higher order vertex corrections later)

(II) The two-loop diagram connecting two relaxation vertices Γ_{02}^{RR} is proportional to

$$\Gamma_{02}^{RR} \sim \lambda^2 q^4 \int_p \int_k \int_\omega C(\mathbf{p}, \omega) C(\mathbf{k}, \omega) C(\mathbf{q} - \mathbf{p} - \mathbf{k}, \omega). \quad (\text{C1})$$

Upon introducing the dimensionless wave vector variables $\hat{\mathbf{p}} = \mathbf{p}/q$ and $\hat{\mathbf{k}} = \mathbf{k}/q$, carrying out the frequency integrals, and replacing the correlation propagators according to Eqs. (6.55) one finds

$$\Gamma_{02}^{RR} \sim q^{4-z}. \quad (\text{C2})$$

In comparing this result with the wave vector dependence, q^{3-z} , of the one-loop diagram, connecting two mode coupling vertices, one recognizes that the contribution of Γ_{02}^{RR} can be neglected in the long wave length limit. Hence this two-loop diagram does not change the self-consistent equations as well.

The above discussion shows that in a self consistent theory the two-loop diagrams are small compared to the one-loop diagrams in the long time and long wave length limit.

Now we discuss higher order vertex corrections, where an internal line of a one-loop vertex correction is decorated with a static insertion. It can be shown that the renormalization of the mode coupling vertex is of purely static origin [87]. This is due to an exact relation between the renormalization factor of the mode coupling vertex and the time scale and field renormalization. To lowest order the mode coupling vertex is given by

$$\Gamma_{12}^{(0)}(\mathbf{p}, \mathbf{q}) = v_3(\mathbf{p}, \mathbf{q}) = \lambda_0 f_0 \epsilon_{\alpha\beta\gamma} \mathbf{p} \cdot \mathbf{q}. \quad (\text{C3})$$

This expression can also be written in terms of the bare static susceptibilities as

$$v_3(\mathbf{p}, \mathbf{q}) = \frac{\lambda_0 f_0}{2} \epsilon_{\alpha\beta\gamma} [\chi_B^{-1}(\mathbf{p} + \mathbf{q}/2) - \chi_B^{-1}(\mathbf{p} - \mathbf{q}/2)] \quad (\text{C4})$$

showing that the wave vector dependence of the mode coupling vertex is determined by the static susceptibilities. In order to take into account the static IR divergences correctly, one way to proceed is to replace the bare static susceptibilities by the fully renormalized static susceptibilities

$$\lambda_0 f_0 \mathbf{p} \cdot \mathbf{q} \rightarrow \frac{\lambda f}{2} [\chi^{-1}(\mathbf{p} + \mathbf{q}/2) - \chi^{-1}(\mathbf{p} - \mathbf{q}/2)] \quad (\text{C5})$$

in the mode coupling vertex. This replacement is suggested by the exact relation between the renormalization factors. It is also equivalent to replacing the nonlinear Landau-Ginzburg functional by

$$\mathcal{H}_{eff} = \int_k \chi^{-1}(\mathbf{k}) \mathbf{S}(\mathbf{k}) \cdot \mathbf{S}(-\mathbf{k}) \quad (\text{C6})$$

where $\chi^{-1}(\mathbf{k})$ is the fully renormalized static susceptibility. This approximation is often used in mode coupling theories without any justification. Here it is a consequence of the exact relation between the renormalization factors.

Besides these static vertex renormalizations (due to the non linearity in the Landau-Ginzburg functional) there could also be dynamic vertex renormalizations. But this is not the case here as we will show next. This can be seen from the diagrammatic representation of the dynamic vertex renormalization (see Fig. A.3. Any diagram contributing to the vertex corrections starts with a bare mode coupling vertex. Therefore to leading order in the wave number one can replace the remaining wave vectors (in the integrals of the corresponding diagrams) by their values at $\mathbf{p} = \mathbf{q} = 0$. This leads then only to changes of the amplitude. Hence we have

$$v_3(\mathbf{p}, \mathbf{q}) = \frac{\lambda f}{2} [\chi^{-1}(\mathbf{p} + \mathbf{q}/2) - \chi^{-1}(\mathbf{p} - \mathbf{q}/2)] + O(\omega, p). \quad (\text{C7})$$

This gives a precise specification of the approximations involved by neglecting the vertex corrections.

As we have seen above, the effects of the four point coupling can be taken into account by a static renormalization of the mode coupling vertex, Eq. (C7). Then one is left with a dynamic theory with a harmonic (effective) Landau-Ginzburg functional and a mode coupling vertex. In this case the fluctuation-dissipation relation (A12) applies (see Appendix A), which in the case of a purely quadratic Landau-Ginzburg functional reduces to

$$G_{11}(\mathbf{k}, t) = \Theta(t)\chi^{-1}(\mathbf{k})G_{02}(\mathbf{k}, t) \quad (\text{C8})$$

This implies for the Fourier transform $G_{11}(\omega) + G_{11}(-\omega) = \chi^{-1}G_{02}(\omega)$ and consequently

$$2\text{Re}[G_{11}(\omega)] = \chi^{-1}G_{02}(\omega) \quad (\text{C9})$$

By using the generalized FDT's in Appendix A we find

$$\Phi(\mathbf{q}, \omega) = \frac{1}{i\omega}[\chi(\mathbf{q}, \omega) - \chi(\mathbf{q})] = \frac{\chi(\mathbf{q})}{-i\omega + [\lambda q^2 + \lambda f \Gamma_{X,10}(\mathbf{q}, \omega)]/\chi(\mathbf{q})}. \quad (\text{C10})$$

This is exactly the same structure as the non linear Langevin equations (with the linear projection operator) (see section III) with the memory kernel

$$M(\mathbf{q}, \omega) = \frac{\lambda q^2 + \lambda f \Gamma_{X,10}(\mathbf{q}, \omega)}{\chi(\mathbf{q})} \quad (\text{C11})$$

Neglecting the mode coupling contribution ($f = 0$) leads immediately to the conventional theory (van Hove theory) of critical dynamics. The mode coupling contribution to the memory function is given by

$$\Gamma_{X,10}(\mathbf{q}, t) = \lambda f \int_k \left[\frac{1}{\chi(\mathbf{q} + \mathbf{k}/2)} - \frac{1}{\chi(\mathbf{q} - \mathbf{k}/2)} \right] \frac{1}{\chi(\mathbf{q} + \mathbf{k}/2)} \Phi(\mathbf{q} + \mathbf{k}/2, t) \Phi(\mathbf{q} - \mathbf{k}/2, t). \quad (\text{C12})$$

In the strong coupling limit, where the van Hove term λq^2 (in general there will be a crossover from van Hove to strong coupling) can be neglected, a scaling analysis of the above self consistent equations shows that the dynamic exponent is given by

$$z = \frac{1}{2}(d + 2 - \eta) \tag{C13}$$

i.e., with this generalized mode coupling theory we find the correct dynamic exponent. This resolves a long standing problem with the conventional derivation of the mode coupling theory, which gives a dynamic exponent with the wrong sign of η . The correct expression, Eq. (C13), is a consequence of the fact that we have correctly taken into account the vertex renormalizations of the mode coupling vertex by static decorations of internal lines.

The above analysis is not a rigorous derivation of a self consistent theory. It shows, however, that the neglected terms are small in the long time and long wave length limit. Furthermore, taking into account static corrections of the mode coupling vertex - suggested by an exact relation between the renormalization factors of the mode coupling vertex and the static field renormalization - we could show that the self consistent theory (generalized mode coupling theory) is capable of giving the exact result for the dynamic critical exponent with the correct sign of η .

Captions to the figures:

Figure A.1: One-loop and two-loop diagrams contributing to the vertex function Γ_{11} .

Figure A.2: One-loop and two-loop diagrams contributing to the vertex function Γ_{02} (the self energy).

Figure A.3: Diagrams contributing to the one-loop vertex correction.

Figure A.4: One-loop and two-loop diagrams contributing to the vertex function Γ_{11} , drawn in terms of the renormalized vertex.

Figure A.5: One-loop and two-loop diagrams contributing to the vertex function Γ_{02} , drawn in terms of the renormalized vertex.

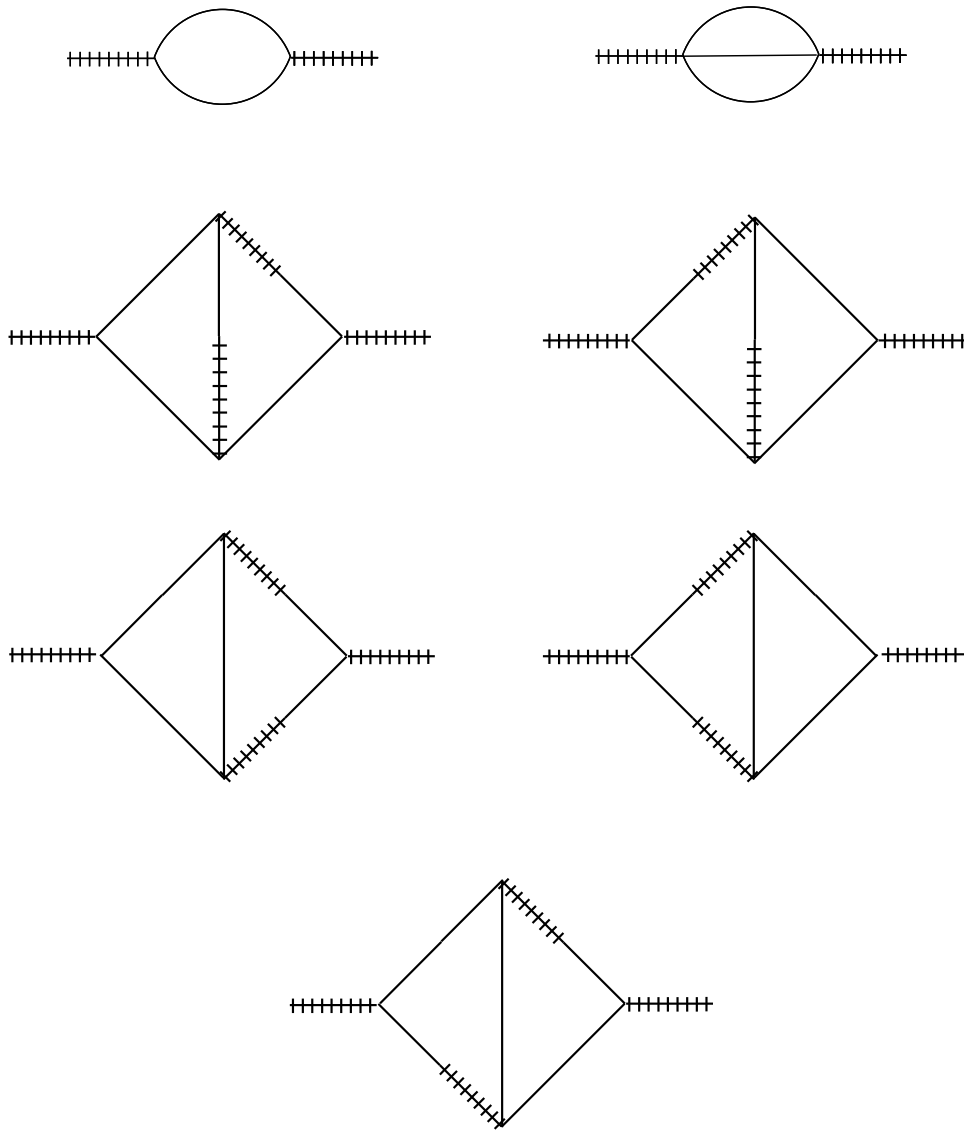


Figure A.1: One-loop and two-loop diagrams contributing to the vertex function Γ_{11} .

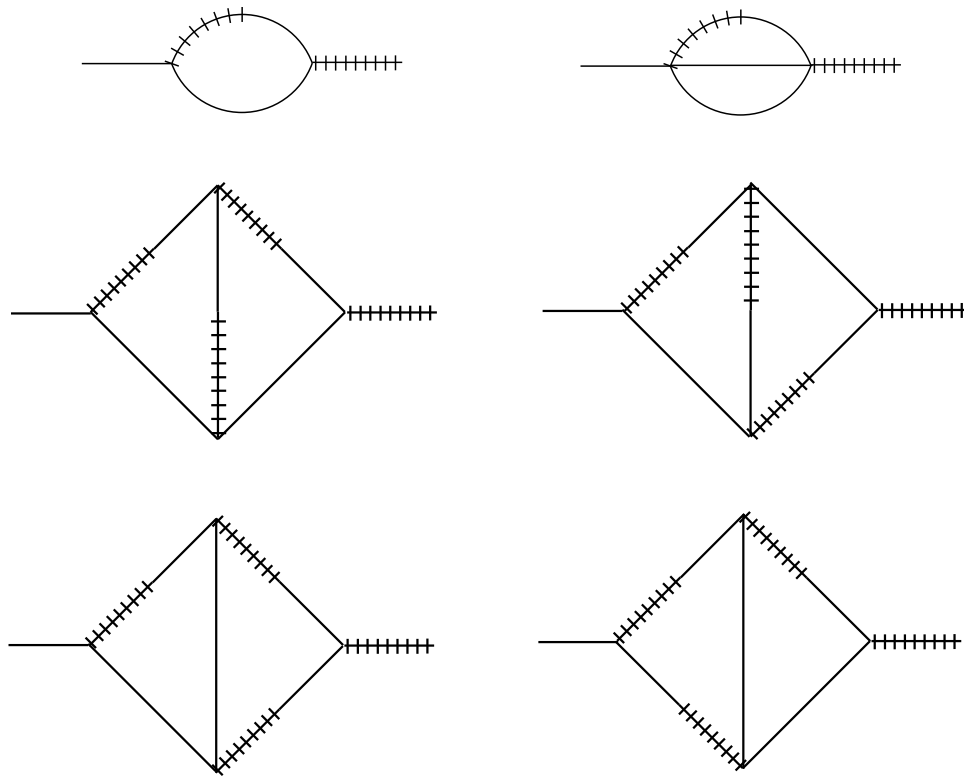


Figure A.2: One-loop and two-loop diagrams contributing to the vertex function Γ_{02} (the self energy).

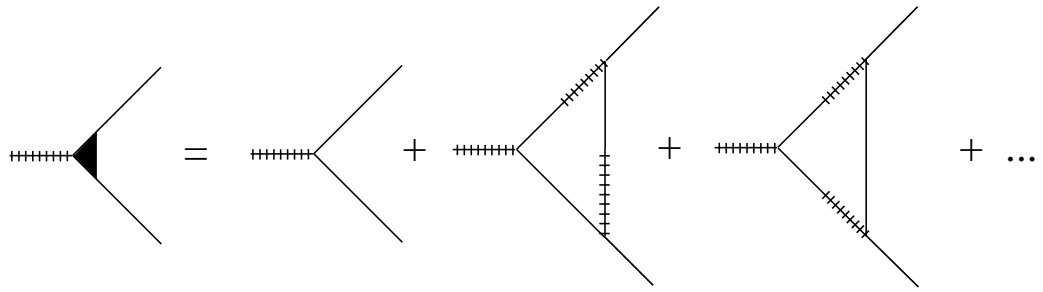


Figure A.3: Diagrams contributing to the one-loop vertex correction.



Figure A.4: One-loop and two-loop diagrams contributing to the vertex function Γ_{11} , drawn in terms of the renormalized vertex.



Figure A.5: One-loop and two-loop diagrams contributing to the vertex function Γ_{02} , drawn in terms of the renormalized vertex.

REFERENCES

- 1 C. Aberger, and R. Folk, Phys. Rev. **B 38**, 6693 (1988).
- 2 C. Aberger, and R. Folk, Phys. Rev. **B 38**, 7207 (1988).
- 3 C. Aberger, and R. Folk, Physica **B 156 & 157**, 229 (1989).
- 4 A. Aharony, and M.E. Fisher, Phys. Rev. **B 8**, 3323 (1973); A. Aharony, Phys. Rev. **B 8**, 3342 (1973).
- 5 A. Aharony, Phys. Rev. **B 8**, 3349 (1973).
- 6 A. Aharony, Phys. Rev. **B8**, 3363 (1973); Phys. Lett. **44 A**, 313 (1973).
- 7 A. Aharony, and B.I. Halperin, Phys. Rev. Lett. **35**, 1308 (1975).
- 8 A. Aharony, in *Phase Transitions and Critical Phenomena*, ed. by C.Domb, and M.S. Green, Vol. 6 (Academic Press, New York, 1976).
- 9 G. Ahlers, A. Kornblit and H.J. Guggenheim, Phys. Rev. Lett. **34**, 1227 (1975).
- 10 R. Allensbach, and A. Bischof, Phys. Rev. Lett. **69**, 3385 (1992).
- 11 See e.g. the review article R. Allensbach, J. Magn. Magn. Mat. **129**, 160 (1994), and the references cited therein.
- 12 D.J. Amit, and Y.Y. Goldschmidt, Ann. of Phys. **114**, 356 (1978).
- 13 D.J. Amit, *Field Theory, the Renormalization Group, and Critical Phenomena* (World Scientific, 1984).
- 14 P.W. Anderson, and H. Suhl, Phys. Rev. **100**, 1788 (1955).
- 15 U. Balucani, M.G. Pini, P. Carra, S.W. Lovesey, and V. Tognetti, J. Phys. **C20**, 3953 (1987).
- 16 M. Bander, and D.L. Mills, Phys. Rev. **B 38**, 12015 (1988).
- 17 R. Bausch, H.K. Janssen, and H. Wagner, Z. Phys. **B 24**, 113 (1976).

- 18 K. De'Bell and D.J.W. Geldart, Phys. Rev. **B 39**, 743 (1989).
- 19 H.S. Bennett, and P.C. Martin, Phys. Rev. **138**, A608 (1965).
- 20 H.A. Bethe, and E.E. Salpeter, *Quantum Mechanics of One- and Two-Electron Atoms*,
(Springer, Berlin, 1957).
- 21 J.K. Bhattacharjee, and R.A. Ferrell, Phys. Rev. **B 24**, 6480 (1981).
- 22 J.K. Bhattacharjee, and R.A. Ferrell, J. Stat. Phys. **41**, 899 (1985).
- 23 J.R. Birgeneau, H.J. Guggenheim, G. Shirane, Phys. Rev. B **1**, 2211 (1970).
- 24 J.R. Birgeneau, H.J. Guggenheim, and G. Shirane, Phys. Rev. B **8**, 304 (1973).
- 25 F. Bloch, Z. Phys. **61**, 206 (1930).
- 26 H.G. Bohn, A. Kollmar, and W. Zinn, Phys. Rev. **B 30**, 6504 (1984).
- 27 P. Borckmans, D. Walgraef, and G. Dewel, Physica **A 91**, 411 (1977).
- 28 P. Böni, and G. Shirane, Phys. Rev. **B 33**, 3012 (1986).
- 29 P. Böni, M.E. Chen, and G. Shirane, Phys. Rev. **B 35**, 8449 (1987).
- 30 P. Böni, G. Shirane, H.G. Bohn, and W. Zinn, J. Appl. Phys. **61**, 3397 (1987).
- 31 P. Böni, G. Shirane, H.G. Bohn, and W. Zinn, J. Appl. Phys. **63**, 3089 (1988).
- 32 P. Böni, and S.M. Shapiro, J. Phys. - Cond. Matter **1**, 6123 (1989).
- 33 P. Böni, D. Görlitz, J. Kötzler, and J.L. Martinez, Phys. Rev. **B 43**, 8755 (1991).
- 34 P. Böni, J.L. Martinez, and J.M. Tranquada, Phys. Rev. **B 43**, 575 (1991).
- 35 P. Böni, G. Shirane, J.L. Martinez, and M.A. Mook, Physica **B 180**, 219 (1992).
- 36 P. Böni, H.A. Mook, J.L. Martinez, and G. Shirane, Phys. Rev. **B 47**, 3171 (1993).
- 37 P. Böni, Physica **B 192**, 94 (1993).

- 38 P. Böni, Y. Endoh, H.A. Graf, M. Hennion, J.L. Martínez, and G. Shirane, *Dipolar anisotropy of spin waves in isotropic ferromagnets EuS and Pd₂MnSn*, preprint (1994).
- 39 P. Borckmans, D. Walgraef and G. Dewel, *Physica* **91A**, 411 (1978).
- 40 E. Brezin and J. Zinn-Justin, *Phys. Rev.* **B 13**, 251 (1976).
- 41 A.D. Bruce, J.M. Kosterlitz, and D.R. Nelson, *J. Phys.* **C 9**, 825 (1976).
- 42 A.D. Bruce, *J. Phys.* **C 10**, 419 (1977).
- 43 H.B. Callen, *Phys. Rev.* **130**, 890 (1963).
- 44 L. Chow, C. Hohenemser, and R.M. Suter, *Phys. Rev. Lett.* **45**, 908 (1980).
- 45 A.R. Chowdhury, G.S. Collins, and C. Hohenemser, *Phys. Rev.* **B 30**, 6277 (1984).
- 46 A.R. Chowdhury, G.S. Collins, and C. Hohenemser, *Phys. Rev.* **B 33**, 5070, 6231 (1986).
- 47 M.H. Cohen, and F. Keffer, *Phys. Rev.* **99**, 1135 (1955).
- 48 M.F. Collins, V.J. Minkiewicz, R. Nathans, L. Passell and G. Shirane, *Phys. Rev.* **179**, 417 (1969)
- 49 G.S. Collins, A.R. Chowdhury, and C. Hohenemser, *Phys. Rev.* **B 33**, 4747 (1986).
- 50 M.F. Collins, *Magnetic Critical Scattering* (Oxford University Press, Oxford, 1989).
- 51 L.M. Corliss, A. Delapalme, J.M. Hastings, R. Nathans, and A. Tucciarone, *J. Appl. Phys.* **41**, 1384 (1970).
- 52 S.F. Cox, *J. Phys.* **C 20**, 3187 (1987).
- 53 A. Cuccoli, V. Tognetti, S.W. Lovesey and R. Vaia, *Phys. Lett.* **A 131**, 57 (1988); *J. Phys.:* *Condens. Mat.* **2**, 3339 (1991).
- 54 A. Cuccoli, V. Tognetti and S.W. Lovesey, *Phys. Rev.* **B 39**, 2619 (1989).
- 55 U. Decker, and F. Haake, *Phys. Rev.* **A 11**, 2043 (1974).

- 56 A.B. Denison, H. Graf, W. Kündig, and P.F. Meier, *Helv. Phys. Acta* **52**, 460 (1979).
- 57 O.W. Dietrich, J. Als-Nielsen and L. Passell, *Phys. Rev.* **B 14**, 4923 (1976).
- 58 V. Dohm, *Solid State Comm.* **20**, 659 (1976)
- 59 R. Dombrowski, D. Görlitz, J. Kötzler, and Chr. Marx, *J. Appl. Phys.* **75**, 6054 (1994).
- 60 C. de Dominicis, *Nuovo Cim. Lett.* **12**, 567(1975); C. de Dominicis, E. Brezin and J. Zinn-Justin, *Phys. Rev.* **B 12**, 4945 (1975); E. Brezin and C. de Dominicis, *Phys. Rev.* **B 12**, 4954 (1975).
- 61 C. de Dominicis, *J. Phys. (Paris)* **37**, Colloque C-247 (1976).
- 62 C. de Dominicis and L. Peliti, *Phys. Rev. Lett.* **38**, 505 (1977); *Phys. Rev.* **B 18**, 353 (1978).
- 63 W. Döring, *Z. Naturforschung a* **16**, 1008, 1146 (1961).
- 64 R.A. Dunlap and A.M. Gottlieb, *Phys. Rev.* **B 22**, 3422 (1980).
- 65 F.J. Dyson, *Phys. Rev.* **102**, 1217 (1956); *ibid* **102**, 1230 (1956).
- 66 K. Elk and W. Gasser, *Die Methode der Greenschen Funktionen in der Festkörperphysik*, (Akademie-Verlag, Berlin, 1979).
- 67 R.J. Elliott, and R.D. Lowde, *Proc. Roy. Soc. (London)* **A230**, 46 (1955).
- 68 P.P. Ewald. *Ann. Phys. (Leipzig)* **54**, 519 (1917); **54**, 57 (1917); **64**, 253 (1921).
- 69 M. Fähnle, private communication (1991).
- 70 R.A. Ferrell, N. Menyhárd, H. Schmidt, F. Schwabl, P. Szépfalusy, *Phys. Rev. Lett.* **18**, 891 (1967); *Phys. Rev. Lett.* **24 A**, 493 (1967); *Ann. Phys. (N.Y.)* **47**, 565 (1968).
- 71 W. Finger, *Physica* **B 90**, 251 (1977).
- 72 W. Finger, *Phys. Lett.* **A 60**, 165 (1977).
- 73 T.M. Fischer, E. Frey, and F. Schwabl, *Phys. Lett.* **A 146**, 457 (1990); *J. Magn. Magn.*

- Mat. **104-107**, 201 (1992); T.M. Fischer, Diploma Thesis, Technische Universität München (1989);
- 74 M.E. Fisher, and A. Aharony, Phys. Rev. Lett. **30**, 559 (1973).
- 75 M.J. Fixman, J. Chem. Phys. **33**, 1363 (1960); **36**, 1961 (1962).
- 76 R. Folk, H. Iro, and F. Schwabl, Z. Phys. **B 27**, 169 (1977).
- 77 R. Folk, and H. Iro, Phys. Rev. **B 32**, 1880 (1985).
- 78 R. Folk, and H. Iro, Phys. Rev. **B 34**, 6571 (1986).
- 79 E. Frey, Diploma Thesis, Technische Universität München, unpublished (1986).
- 80 E. Frey, and F. Schwabl, Phys. Lett. **A 123**, 49 (1987).
- 81 E. Frey, and F. Schwabl, Z. Phys. **B 71**, 355 (1988); *ibid* **B 76**, 139 (1989).
- 82 E. Frey, F. Schwabl, and S. Thoma, Phys. Lett. **A 129**, 343 (1988).
- 83 E. Frey, and F. Schwabl, J. de Phys. Coll. **C 8**, 1569 (1988).
- 84 E. Frey, and F. Schwabl, J. de Phys. Coll. **C 8**, 1531 (1988).
- 85 E. Frey, F. Schwabl, and S. Thoma, Phys. Rev. **B 40**, 7199 (1989).
- 86 E. Frey, and F. Schwabl, Hyp. Int. **50**, 767 (1989).
- 87 E. Frey, Doctoral Thesis, Technische Universität München, unpublished (1989).
- 88 E. Frey, and F. Schwabl, Phys. Rev. **B 42**, 8261 (1990).
- 89 E. Frey, and F. Schwabl, Phys. Rev. **B 43**, 833 (1991).
- 90 R. Frowein, J. Kötzler, B. Schaub and H.G. Schuster, Phys. Rev. **B 25**, 4905 (1982).
- 91 *Chemical Applications of Mössbauer Spectroscopy*, edited by V.I. Goldanski, and R.H. Herber, (Academic Press, 1968).

- 92 J. Goldstone, *Nuovo Cimento* **19**, 154 (1961).
- 93 D. Görnitz, J. Kötzler, F.J. Bermejo, P. Böni, and J.L. Martinez, *Physica* **B 180**, 214 (1992).
- 94 D. Görnitz, J. Kötzler, and T. Lange, *J. Magn. Magn. Mat.* **104**, 339 (1992).
- 95 A.M. Gottlieb, and C. Hohenemser, *Phys. Rev. Lett.* **31**, 1222 (1973).
- 96 R. Graham, in *Springer Tracts in Modern Physics*, (Springer, Berlin, 1973), Vol. 66.
- 97 M. Grahl, D. Görnitz, J. Kötzler, T. Lange, and I. Sessler, *J. Appl. Phys.* **69**, 6179 (1991).
- 98 L.J. De Haas, and J.C. Verstelle, *Physica* **86-88B**, 1291 (1977).
- 99 B.I. Halperin and P.C. Hohenberg, *Phys. Rev. Lett.* **19**, 700 (1967); *Phys. Rev.* **177**, 952 (1969).
- 100 B.I. Halperin, P.C. Hohenberg, and S. Ma, *Phys. Rev. Lett.* **29**, 1548 (1972); *Phys. Rev. B* **10**, 139 (1974).
- 101 B.I. Halperin, P.C. Hohenberg, and S. Ma, *Phys. Rev. B* **13**, 4119 (1976).
- 102 A.B. Harris, *Phys. Rev.* **175**, 674 (1968).
- 103 O. Hartmann, E. Karlsson, R. Wäppling, J. Chappert, A. Yaouanc, L. Asch, and G.M. Kalvius, *J. Phys.* **F 16**, 1593 (1986).
- 104 O. Hartmann, *Hyp. Int.* **49**, 61 (1989)
- 105 O. Hartmann, R. Wäppling, E. Karlsson, G.M. Kalvius, L. Asch, F.J. Litterst, K. Aggarwal, K.H. Münch, F.N. Gyax, and A. Schenk, *Hyperfine Interact.* **64**, 369 (1990).
- 106 W. Heisenberg, *Z. Physik* **49**, 619 (1928).
- 107 S. Henneberger, E. Frey, and F. Schwabl, unpublished (1994).
- 108 D. Herlach, K. Fürderer, M. Fähnle, and L. Schimmele, *Hyp. Int.* **31**, 287 (1986).
- 109 C. Herring, and C. Kittel, *Phys. Rev.* **81**, 869 (1951).

- 110 J.A. Hertz, Int. J. Magn. **1**, 253, 307, 313 (1971).
- 111 P.C. Hohenberg, Phys. Rev. **158**, 383 (1967).
- 112 P.C. Hohenberg and B.I. Halperin, Rev. Mod. Phys. **49**, 435 (1977).
- 113 C. Hohenemser, L. Chow, and R.M. Suter, Phys. Rev. **B 26**, 5056 (1982).
- 114 C. Hohenemser, N. Rosov, and A. Kleinhammes, Hyp. Int. **49**, 267 (1989), and references cited therein.
- 115 T. Holstein, and H. Primakoff, Phys. Rev. **58**, 1098 (1940).
- 116 G. t' Hooft, and M. Veltman, Nucl. Phys. **B 44**, 189 (1972).
- 117 L. van Hove, Phys. Rev. **93**, 1374 (1954).
- 118 J. Hubbard, J. Phys. **C4**, 53 (1971).
- 119 J. Hubbard, J. of Appl. Phys. **42**, 1390 (1971).
- 120 J. Hubbard, Phys. Rev. **B 19**, 2626 (1979); *ibid* **B 20**, 4584 (1979).
- 121 D.L. Huber, and D.A. Krüger, Phys. Rev. Lett. **24**, 111 (1970).
- 122 D.L. Huber, J. Phys. Chem. Solids **32**, 2145 (1971).
- 123 H. Iro, Z. Phys. **B 68**, 485 (1987).
- 124 H. Iro, J. Magn. Magn. Mat. **73**, 175 (1988).
- 125 H. Iro, Physica **B 156 & 157**, 232 (1989).
- 126 E. Ising, Z. Physik **31**, 253 (1925).
- 127 H.K. Janssen, Z. Phys. **B 23**, 377 (1976).
- 128 see H.K. Janssen in Lecture Notes in Physics 104, *Dynamic Critical Phenomena and Related Topics*, ed. by C.P. Enz, (Springer Verlag, Berlin, 1979).

- 129 C. Joukoff-Piette, and P. Resibois, Phys. Lett. **42**, 531 (1973).
- 130 L.P. Kadanoff, and J. Swift, Phys. Rev. **166**, 89 (1968).
- 131 V.P. Kalashnikov, and S.V. Tret'jakov, Phys. Lett. A **146**, 463 (1990); Phys. Lett. **A 156**, 239 (1991).
- 132 V.P. Kalashnikov, and S.V. Tret'jakov, Physica B **162**, 265 (1990).
- 133 V.N. Kashcheev, and M.A. Krivoglaz, Fiz. Tverd. Tela (Leningrad) **3**, 1541 (1961) [Sov. Phys. Solid State **3**, 1117 (1961)].
- 134 A. Kashuba, and V.L. Pokrovsky, Phys. Rev. Lett. **70**, 3155 (1993); Phys. Rev **B 48**, 10335 (1993).
- 135 E.B. Karlsson, Phys. Rep. **82**, 272 (1982).
- 136 E.B. Karlsson, Hyp. Int. **64**, 331 (1990).
- 137 K. Kawasaki, J. Chem. Sol. **28**, 1277 (1967).
- 138 K. Kawasaki, Ann. of Phys. **61**, 1 (1970).
- 139 K. Kawasaki, J. Phys. **A 6**, 1289 (1973).
- 140 K. Kawasaki, in *Phase Transitions and Critical Phenomena* , Vol.5a, ed. by C. Domb and M.S. Green, (Academic Press, 1976), and references therein.
- 141 F. Keffer, in *Encyclopedia of Physics*, edited by S. Flügge (Springer Verlag, Heidelberg, 1966), Vol. XVIII/2, p. 37ff.
- 142 C. Kittel, *Introduction to Solid State Physics*, 4th ed. (Wiley, New York, 1971).
- 143 M.A. Kobeissi, R. Suter, A.M. Gottlieb, and C. Hohenemser, Phys. Rev. **B 11**, 2455 (1976).
- 144 M.A. Kobeissi, and C. Hohenemser, Hyp. Int. **4**, 480 (1978).
- 145 J.M. Kosterlitz, and D.J. Thouless, J. Phys. **C 5**, L124 (1972).

- 146 J.M. Kosterlitz, and D.J. Thouless, J. Phys. **C 6**, 1181 (1973).
- 147 J. Kötzler, G. Kamleiter, and G. Weber, J. Phys. **C 9**, L361 (1976).
- 148 J. Kötzler, W. Scheithe, R. Blickhan, and E. Kaldis, Solid State Comm. **26**, 641 (1978).
- 149 J. Kötzler and H. von Philipsborn, Phys. Rev. Lett. **40**, 790 (1978).
- 150 J. Kötzler, and W. Scheithe, J. of Magn. and Magn. Mat. **9**, 4 (1978).
- 151 J. Kötzler, J. of Magn. Magn. Mat. **54**, 649 (1986).
- 152 J. Kötzler, Phys. Rev. B **38**, 12027 (1988).
- 153 J. Kötzler, D. Görlitz, F. Mezei, and B. Farago, Europhys. Lett. **1**, 675 (1986).
- 154 J. Kötzler, E. Kaldis, G. Kamleiter, and G. Weber, Phys. Rev. **B 43**, 11280 (1991).
- 155 J. Kötzler, D. Görlitz, M. Hartl, and Chr. Marz, IEEE Trans. Magn. **30**, 828 (1994).
- 156 H. Kronmüller, H.-R. Hilzinger, P. Monachesi, and A. Seeger, Appl. Phys. **18**, 183 (1979).
- 157 R. Kubo, J. Phys. Soc. Jpn. **12**, 570 (1957).
- 158 L.D. Landau, Zh. Eksp. Teor. Fiz. **7**, 627 (1937).
- 159 L.D. Landau, and I.M. Khalatnikov, Dokl. Acad. Nauk. SSSR **96**, 469 (1954).
- 160 Landolt-Börnstein, *Numerical Data and Functional Relationship in Science and Technology*, Vol. **12** (Springer-Verlag, Berlin, 1978).
- 161 A.I. Larkin, and D.E. Khmel'nitskii, Sov. Phys. JETP **29**, 1123 (1969).
- 162 H.Y. Lau, L.M. Corliss, A. Delapalme, J.M. Hastings, R. Nathans, and A. Tucciarone, Phys. Rev. Lett. **23**, 1225 (1969).
- 163 A.P. Levanyuk, and N. Garcia, J. Phys. Condens. Matter **4**, 10277 (1992).
- 164 A.P. Levanyuk, and N. Garcia, Phys. Rev. Lett. **70**, 1184 (1993).

- 165 Yi Li, M. Farle, and K. Baberschke, Phys. Rev. **B 41**, 9596 (1990). Yi Li, K. Baberschke, and M. Farle, J. Appl. Phys. **69**, 4992 (1991).
- 166 S.W. Lovesey, *Theory of Neutron Scattering from Condensed Matter, Vol. I & II*, Clarendon Press, Oxford (1984).
- 167 S.W. Lovesey, and R.D. Williams, J. Phys. **C 19**, L253 (1986).
- 168 S.W. Lovesey, and K.N. Trohidou, J. Phys.: Condens. Matter **3**, 1827 (1991); Erratum J. Phys.: Condens. Matter **3**, 5255 (1991)
- 169 S.W. Lovesey, J. Phys.: Condens. Matter **5**, L251 (1993).
- 170 R.D. Lowde, J. Appl. Phys. **36**, 884 (1965).
- 171 J.W. Lynn, Phys. Rev. **B 11**, 2624 (1975).
- 172 J.W. Lynn, Phys. Rev. **B 28**, 6550 (1983).
- 173 J.W. Lynn, Phys. Rev. Lett. **52**, 775 (1984).
- 174 S. Ma, and G.F. Mazenko, Phys. Rev. **B 11**, 4077 (1975).
- 175 See e.g. the excellent book by S.-K. Ma, *Modern Theory of Critical Phenomena*, (Benjamin/Cummings Publ. Comp., 1976).
- 176 S.V. Maleev, Zh. Eksp. Teor. Fiz. **66**, 1809 (1974) [Sov. Phys. JETP **39**, 889 (1974)].
- 177 S.V. Maleev, Zh. Eksp. Teor. Fiz. **69**, 1398 (1975) [Sov. Phys. JETP **42**, 713 (1976)].
- 178 S.V. Maleev, Zh. Eksp. Teor. Fiz. **70**, 2374 (1976) [Sov. Phys.-JETP **43**, 1240 (1976)].
- 179 S.V. Maleev, Soc. Sci. Rev. A. Phys. **8**, 323 (1987).
- 180 M. Månson, J. Phys. C **7**, 4073 (1974).
- 181 W. Marshall, and S.W. Lovesey, *Theory of thermal neutron scattering*, (Clarendon, Oxford, 1971).

- 182 P.C. Martin, E.D. Siggia, and H.A. Rose, Phys. Rev. **A 8**, 423 (1973).
- 183 J.L. Martinez, P. Böni, and G. Shirane, Phys. Rev. **B 32**, 7037 (1985).
- 184 G.F. Mazenko, Phys. Rev. **B 14**, 3933 (1976).
- 185 P.F. Meier, Hperf. Int. **8**, 591 (1981).
- 186 N.D. Mermin and H.Wagner, Phys. Rev. Lett. **17**, 1133 (1966).
- 187 F. Mezei, Z. Phys. **255**, 146 (1972); see also the review articles in Lecture Notes in Physics 128, *Neutron Spin Echo*, edited by F. Mezei, Springer Verlag (1980).
- 188 F. Mezei, Phys. Rev. Lett. **49**, 1096 (1982); *ibid* **49**, 1537 (1982) (E).
- 189 F. Mezei, J. of Magn. and Magn. Mat. **45**, 67 (1984).
- 190 F. Mezei, Physica **B 136**, 417 (1986).
- 191 F. Mezei, in *Magnetic Excitations and Fluctuations II*, ed. by U. Balucani, S.W. Lovesey, M. Rasetti, and V. Tognetti, Springer Proceedings in Physics (Springer Verlag, Berlin, 1987).
- 192 F. Mezei, J. de Phys. Coll. **C 8**, 1537 (1988).
- 193 F. Mezei, B. Farago, S.M. Hayden, and W.G. Stirling, Physica **B 156&157**, 226 (1989).
- 194 V.J. Minkiewicz, M.F. Collins, R. Nathans, and G. Shirane, Phys. Rev. **182**, 624 (1969).
- 195 P.W. Mitchell, R.A. Cowley, and R. Pynn, J. Phys. **C 17**, L875 (1984).
- 196 H.A. Mook, J.W. Lynn, and R.M. Nicklow, Phys. Rev. Lett. **30**, 556 (1973).
- 197 H. Mori, Progr. Theor. Phys. **33**, 423 (1965).
- 198 H. Mori, and H. Fujisaka, Progr. Theor. Phys. **49**, 764 (1973).
- 199 H. Mori, and H. Fujisaka, and H. Shigematsu, Progr. Theor. Phys. **51**, 109 (1974).
- 200 A.H. Morrish, *The Physical Principles of Magnetism*, (John Wiley & Sons, New York, 1965).

- 201 T. Nattermann, and S. Trimper, *J. Phys.* **C 9**, 825 (1976).
- 202 D.R. Nelson, in *Phase Transitions and Critical Phenomena*, Vol.7, ed. by C. Domb and J.L. Lebowitz, (Academic Press, 1983).
- 203 J. Als-Nielsen, in *Phase Transitions and Critical Phenomena*, Vol.5a, ed. by C. Domb and M.S. Green, Academic Press (1976) and references therein.
- 204 J. Als-Nielsen, O.W. Dietrich, and L. Passell, *Phys. Rev.* **B 14**, 4908 (1976).
- 205 K. Nishiyama, E. Yagi, K. Ishida, T. Matsuzaki, K. Nagamine, and T. Yamazaki, *Hyp. Int.* **17-19**, 473 (1984).
- 206 D.P. Pappas, K.P. Kamper, and H. Hopster, *Phys. Rev. Lett.* **64**, 3179 (1990).
- 207 L. Passell, J. Als-Nielsen, and O.W. Dietrich, *Proceedings of the Fifth IAEA Symposium on Neutron Inelastic Scattering* (IAEA, Vienna, 1972), p. 619.
- 208 G. Parette, and R. Kahn, *J. de Phys. (Paris)* **32**, 447 (1971).
- 209 G. Parette, *Ann. Phys.* **7**, 313 (1972).
- 210 L. Passell, O.W. Dietrich, and J. Als-Nielsen, *Phys. Rev.* **B 14**, 4897, 4908, 4923 (1976), and references therein.
- 211 R. Peierls, *Helv. Phys. Acta* VII, Suppl. 2, 81 (1936).
- 212 D. Pescia, and V.L. Pokrovsky, *Phys. Rev. Lett.* **65**, 2599 (1990).
- 213 D. Pescia, and V.L. Pokrovsky, *Phys. Rev. Lett.* **70**, 1185 (1993).
- 214 R.A. Pelcovits, and B.I. Halperin, *Phys. Rev.* **B 19**, 4614 (1979).
- 215 C. Pich and F. Schwabl, *Phys. Rev.* **B 47**, 7957 (1993).
- 216 C. Pich and F. Schwabl, *Phys. Rev.* **B 49**, 413 (1994).
- 217 C. Pich, Doctoral Thesis, Technische Universität München (1994).

- 218 C. Pich, and F. Schwabl, *J. Magn. Magn. Mat.* **140-144**, ??? (1994).
- 219 C. Pich, and F. Schwabl, unpublished (1994).
- 220 M.W. Pieper, J. Kötzler, and K. Nehrke, *Phys. Rev.* **B 47**, 11962 (1993).
- 221 V.L. Pokrovsky, and M.V. Feigelman, *Zh. Eksp. Teor. Fiz.* **72**, 557 (1977) [*Sov. Phys.-JETP* **45**, 291 (1977)].
- 222 V.L. Pokrovsky, *Adv. Phys.* **28**, 595 (1979).
- 223 V.L. Pokrovsky, and M.V. Feigelman, *Zh. Eksp. Teor. Fiz.* **76**, 784 (1979) [*Sov. Phys.-JETP* **49**, 395 (1979)].
- 224 V.L. Pokrovsky, M.V. Feigelman, and A.M. Tsvelik, in *Spin Waves and Excitations II*, ed. by A.S. Borovik–Roamov, and S.K. Sinha, (Elsevier Publ., 1988).
- 225 P. Politi, A. Rettori, and M.G. Pini, *Phys. Rev. Lett.* **70**, 1183 (1993).
- 226 V. Privman, P.C. Hohenberg, and A. Aharony, in *Phase Transitions and Critical Phenomena*, Vol. 14, edited by C. Domb and J.L. Lebowitz, (Academic Press, 1991).
- 227 R. Raghavan, and D.L Huber, *Phys. Rev.* **B 14**, 1185 (1976).
- 228 R.C. Reno, and C. Hohenemser, *Proc. 7th Ann. Conf. on Magnetism and Magnetic Materials*, ed. D.C. Graham, and J.J. Rhyne (AIP, New York, 1972).
- 229 P. Dalmas de Réotier, and A. Yaouanc *Phys. Rev. Lett.* **72**, 290 (1994).
- 230 P. Dalmas de Réotier, A. Yaouanc, and E. Frey, *Phys. Rev.* **B 50**, 3033 (1994).
- 231 P. Résibois, and C. Piette, *Phys. Rev. Lett.* **24**, 514 (1970).
- 232 P. Résibois, and M. De Leener, *Phs. Rev. Lett.* **25 A**, 65 (1967).
- 233 P. Résibois, and M. De Leener, *Phs. Rev.* **178**, 806, 819 (1969).
- 234 E. Riedel, and F. Wegner, *Phys. Rev. Lett.* **24**, 730 (1970).

- 235 M. Saham, J. Barak, U. El-Hanany, and W.W. Warren, Phys. Rev. **B 22**, 5400 (1980).
- 236 M.B. Salamon, Phys. Rev. **155**, 24 (1967).
- 237 L. Sasvári, J. Phys. **C 10**, L633 (1977).
- 238 F. Spörel, and E. Biller, Solid State Comm. **17**, 833 (1975).
- 239 A. Schenk, *Muon Spin Rotation Spectroscopy, Principles and Applications in Solid State Physics* (Adam Hilger Ltd., Bristol and Boston, 1985).
- 240 H. Schinz, and F. Schwabl, J. Magn. Magn. Mat. **140-144**, ???? (1994).
- 241 H. Schinz, Doctoral Thesis, Technische Universität München, unpublished (1994).
- 242 H. Schinz, private communication (1994).
- 243 B. Schröder, V. Wagner, N. Lehner, K.M. Kesharwani, and R. Geick, Phys. stat. sol. (b) **97**, 501 (1980).
- 244 F. Schwabl, and K.H. Michel, Phys. Rev. **B 2**, 89 (1970).
- 245 F. Schwabl, Z. Phys. **246**, 13 (1971).
- 246 F. Schwabl, J. Appl. Phys. **64**, 5867 (1988).
- 247 F. Schwabl, *Quantum Mechanics*, (Springer, Heidelberg, 1991).
- 248 G. Shirane, P. Böni, and J.L. Martinez, Phys. Rev. **B 36**, 881 (1987).
- 249 O. Steinsvoll, C.F. Majkrzak, G. Shirane, and J.P. Wicksted, Phys. Rev. Lett. **51**, 300 (1983); Phys. Rev. **B 30**, 2377 (1984).
- 250 U.C. Täuber, and F. Schwabl, Phys. Rev. **B 46**, 3337 (1992).
- 251 U.C. Täuber, and F. Schwabl, Phys. Rev. **B 48**, 186 (1993).
- 252 H.S. Toh, and G.A. Gehring, J. Phys.: Condens. Matter **2**, 7511 (1990).

- 253 B.P. Toperverg, and A.G. Yashenkin, Phys. Rev. **B 48**, 16505 (1993).
- 254 K.N. Trohidou, and S.W. Lovesey, J. Phys.: Condens. Matter **5**, 1109 (1993).
- 255 A. Tucciarone, H.Y. Lau, L.M. Corliss, A. Delapalme, and A. Hastings, Phys. Rev. **B 4** 3206 (1971).
- 256 E.A. Turov, *Physical Properties of Magnetically Ordered Crystals*, (Academic Press, New York, 1965).
- 257 V.G. Vaks, A.I. Larkin, and S.A. Pikin, Zh. Eksp. Theor. Fiz. **53**, 281 (1967) [Soviet Phys. - JETP **26**, 188 (1968)]; V.G. Vaks, A.I. Larkin, and S.A. Pikin, Zh. Eksp. Theor. Fiz. **53**, 1089 (1967) [Soviet Phys. - JETP **26**, 647 (1968)].
- 258 J.H. van Vleck, Phys. Rev. **52**, 1137 (1937).
- 259 E. Wäckelgard, O. Hartmann, E. Karlsson, R. Wäppling, L. Asch, G.M. Kalvius, J. Chappert, and A. Yaouanc, Hyp. Int. **31**, 325 (1986).
- 260 E. Wäckelgard, O. Hartmann, E. Karlsson, R. Wäppling, L. Asch, G.M. Kalvius, J. Chappert, and A. Yaouanc, Hyp. Int. **50**, 781 (1989).
- 261 R.E. Watson, and A.J. Freeman, Phys. Rev. **123**, 2027 (1961).
- 262 F. Wegner, Z. Phys. **216**, 433 (1968).
- 263 F. Wegner, Z. Phys. **218**, 260 (1969).
- 264 J.P. Wicksted, P. Böni and G. Shirane, Phys. Rev. **B 30**, 3655 (1984).
- 265 H.W. De Wijn, L.R. Walker, S. Geschwind, and H.J. Guggenheim, Phys. Rev. **8**, 299 (1973).
- 266 H.W. De Wijn, L.R. Walker, and R.E. Walstedt, Phys. Rev. **8**, 285 (1973).
- 267 A.F.M. Arts and H.W. De Wijn, *Magnetic Properties Of Layered Transition Metal Compounds* ed. by L.J. De Jongh, (Kluwer Academic Publishers, 1990), p. 191ff.

- 268 W.G. Williams, *Polarized Neutrons*, (Clarendon Press, Oxford, 1988).
- 269 K.G. Wilson and J. Kogut, *Physics Reports* **12 C**, 76 (1974).
- 270 C.G. Windsor and R.W.H. Stevenson, *Proc. Phys. Soc. (London)* **87**, 501 (1966).
- 271 A. Yaouanc, P. Dalmas de Réotier, and E. Frey, *Phys. Rev.* **B 47**, 796 (1993).
- 272 A. Yaouanc, P. Dalmas de Réotier, and E. Frey, *Europhys. Lett.* **21**, 93 (1993).
- 273 V.Yu. Yushankhai, *Hyp. Int.* **50**, 775 (1989).
- 274 Markus Zobel, Diploma Thesis, Technische Universität München, unpublished (1991).
- 275 R. Zwanzig, *J. Chem. Phys.* **33**, 1388, (1960).
- 276 R. Zwanzig, *Phys. Rev.* **124**, 983 (1961).
- 277 R. Zwanzig, in *Statistical Mechanics*, ed. by S. Rice, K. Freed, and J. Light, (University Press, Chicago, 1972).

